LASER PHOTOFRAGMENT KINETICS

A thesis
submitted in partial fulfilment of the requirements for the degree
of

Doctor of Philosophy in Chemistry

in the

University of Canterbury

by

Andrew Robert Whyte

University of Canterbury

1988

To the memory of

Anne Jean Whyte (d. 1987)

and

Robert William (Bob) Whyte (d. 1984),

much-loved Mum and Dad and my two best friends.

"If you can't take a joke, you should never have joined."

ACKNOWLEDGEMENTS

During the period of this work there have been many people whose assistance I have greatly appreciated. First and foremost I wish to thank my supervisor, Professor L. F. Phillips, for his continued interest in and enthusiasm for this work, for much valuable advice, for his considerable patience, and for occasional diversions on the ski slopes and the water. I am very grateful to Dr. G. A. Rodley for many wide-ranging and illuminating discussions and for his encouragement and support at a difficult time. For similar support through a second, similarly difficult time I am much indebted to Dr. R. G. A. R. Maclagan and to Associate Professor R. G. Gilbert of the University of Sydney. My thanks go also to Professor M. P. Hartshorn for encouragement and advice over the last five years.

I am grateful to the Chemistry Department for the award of a Teaching Fellowship for three years.

Several members of the Department's technical staff have given freely of their time and expertise during the course of this work. In particular I wish to thank to Messrs. R. W. Gillard, K. Gillard, A. M. Fergusson, R. M. McGregor, D. J. Macdonald and D. Morrison for their patience and assistance.

For many valuable discussions and moments of light relief, both in and out of the lab., I am grateful to Mike Bird, John Harrison, Sean Smith and Drs. Chris Nokes and Bryce Williamson. Thanks also to new friends at Sydney University, particularly Kieran Lim, Greg Russell, Ian Maxwell and Dr. Gunnar Nyman.

Finally, I wish to thank my family and friends outside Chemistry Departments and, most of all, Joanne for her continuing love and patience under a variety of trying circumstances.

A. R. Whyte
1988

TABLE OF CONTENTS

Wordprocessing, typesetting and laserprinting by ***JMV* Computer Services Pty. Ltd.**
26 Boronia St., Kyle Bay, NSW, 2221. Ph. 546 3882

LIST OF FIGURES

(List of figures con'd.)

LIST OF TABLES

ABSTRACT

We report here several studies of the kinetics of reactions of free radical species in the gas phase. The radicals were produced by ultraviolet laser photolysis of stable precursor molecules in the presence of various reactant gases together with an excess of inert bath gas. The ensuing reactions were followed by means of either time-resolved laser-induced fluorescence (LIF) measurements of relative radical concentrations, or time-resolved resonance fluorescence measurements of the relative concentrations of product atoms. From the LIF measurements, bimolecular rate coefficients have been obtained at room temperature for the reactions

$CN + N \rightarrow N_2 + C$ [$(1.00 \pm 0.13) \times 10^{-10}$ cm^3s^{-1}],
$CN + O_2 \rightarrow$ products [$(1.27 \pm 0.23) \times 10^{-11}$ cm^3s^{-1}],
$NH_2 + N \rightarrow$ products [$(1.21 \pm 0.14) \times 10^{-10}$ cm^3s^{-1}],
$NH_2 + NO \rightarrow$ products [$(1.81 \pm 0.12) \times 10^{-11}$ cm^3s^{-1}],
$NH_2 + NO_2 \rightarrow$ products [$(2.11 \pm 0.18) \times 10^{-11}$ cm^3s^{-1}],
$NH + NO \rightarrow$ products [$(5.78 \pm 0.64) \times 10^{-11}$ cm^3s^{-1}],
$NH + NO_2 \rightarrow$ products [$(1.61 \pm 0.14) \times 10^{-11}$ cm^3s^{-1}].

The rate coefficients for the reactions of NH have also been determined over the temperature range 269 - 377 K, yielding activation energies of 0 ± 2 kJ mol^{-1} (NH + NO) and - 9.5 $\pm$3.2 kJ mol^{-1} (NH + NO_2). In addition to the rate coefficient measurements the nature of the products of the NH_2 + N reaction has been investigated by measuring the relative yields of product hydrogen atoms via resonance fluorescence. The time dependence of the H atom concentration is consistent with production of H by the reaction $NH_2 + N \rightarrow N_2 + H + H$. The same method has been used to establish that H atoms are not produced in the reaction between NH_2 + NO.

These results have been interpreted in relation to the mechanisms of the reactions concerned. In particular, the nature of the primary products of the NH_2 + NO reaction is still uncertain; the present results on the NH_2 + NO and NH + NO systems indicate that OH is not a primary product of the former reaction, contrary to previous suggestions. This uncertainty and the results of a recent theoretical study of the kinetics of the NH_2 + NO reaction have raised questions about the nature of the reaction potential energy surface. Using the methods of *ab initio* molecular orbital theory we have determined the structures, relative energies and vibrational frequencies of a range of species which occur along the reaction coordinates leading to several alternative sets of products. The results of this investigation have been compared to those of earlier experimental and theoretical studies of the NH_2 + NO reaction.

NOTE ON UNITS AND SYMBOLS

The following symbols are used in this work:

Symbol	Quantity	Note
k_i	rate coefficient for the reaction or process (i)	(a)
k_{ia}	rate coefficient for the a-th channel of reaction (i) if more than one possible channel	(a)
k_i	general i-th order rate coefficient	(a)
ν_i	i-th vibrational mode of a given molecule	
υ_i	number of vibrational quanta in mode ν_i	
ΔH_f	heat of formation at 298 K i.e. $\Delta H_f = \Delta H_f^0$ (298 K)	(b,c)
ΔH_r	heat of reaction at 298 K calculated from ΔH_f values *via* Hess's law	(b,c)

Notes

(a) Rate coefficients are expressed in 'per molecule' units, $cm^3 s^{-1}$ (= cm^3 $molecule^{-1}$ s^{-1}) for a bimolecular rate coefficient k_2. Rate coefficients on a per mol basis may be obtained by multiplying by Avogadro's number. Unimolecular rate coefficients have units of s^{-1}.

(b) Energies are given in units of either kJ mol^{-1} or cm^{-1} as appropriate. In Chapter 7 the calculated total energies of H-N-O species are given in atomic units (hartrees, 1 hartree = 2625.5 kJ mol^{-1} [7.40]).

(c) Unless otherwise stated all heats of formation are drawn from the JANAF Thermochemical Tables and subsequent Supplements [2.9].

Standard symbols for physical constants are used throughout. These include:

h (Planck's constant = 6.626×10^{-34} J s),
c (speed of light *in vacuo* = 2.998×10^{10} cm s^{-1}),
e (electronic charge, 1.602×10^{-19} C),
k_B (Boltzmann constant = 1.381×10^{-23} J K^{-1}) and
R (Gas constant = 8.314 J K^{-1} mol^{-1}) .

CHAPTER 1

INTRODUCTION

1.1 General Introduction

The field of gas phase kinetics is one of the largest and most rapidly developing areas of modern physical chemistry. One of the main reasons for the continued interest in gas phase chemical systems, as distinct from those existing in condensed phases, is the fact that in such systems the fine details of elementary processes, both physical and chemical, may be studied in an environment which is relatively free from interference from the background medium. For example, the wealth of detailed information on the energetics and dynamics of elementary reactions which is obtainable under the essentially collisionless conditions prevailing in molecular beam experiments may be contrasted with the perennial problems of distinguishing, characterising and controlling solvent effects in liquid phase systems.

In general the processes studied within the domain of gas phase kinetics may be divided into two classes, namely intramolecular and intermolecular processes. Each of these classes may be further subdivided according to the precise nature of the process in question. Into the first category fall the processes by which atoms and molecules interact with radiation (absorption, emission and photon scattering processes); non-radiative transitions, such as internal conversion, intersystem crossing, predissociation and intramolecular vibrational and rotational relaxation; and chemical reactions, including unimolecular dissociations and isomerisations. Intermolecular interactions also include both reactive and non-reactive processes. The latter group contains such processes as rotational, vibrational and electronic quenching, which are examples of the larger class of collisional energy transfer processes, while the former group includes various types of chemical reaction, notably bimolecular association and metathesis reactions and termolecular recombinations, all of which are influenced by both the amount and the distribution of energy in the reactants. Studies of the rates of any of these processes generally involve significant overlap between purely kinetic considerations and those relating to other fields, especially experimental disciplines such as photochemistry and spectroscopy, and the theoretical domains of classical, quantum and statistical mechanics and thermodynamics.

A major impetus for the recent, rapid expansion in gas phase kinetics has been the advent of commercially available lasers of various types [1.1 - 4]. Lasers possess a

number of properties which make them extremely useful in studies of processes such as those mentioned above. The most important of these properties are the very high source brightness and narrow bandwidth (monochromaticity) of lasers and the existence of various techniques for both discrete shifting and continuous tuning of the wavelength of laser radiation over significant portions of the infrared, visible and ultraviolet regions of the electromagnetic spectrum. Important among these techniques are the tuning methods which exploit the intense broad-bandwidth fluorescence obtainable from various classes of organic dyes [1.5 - 7], and a range of non-linear optical processes such as harmonic generation (frequency doubling or tripling), frequency summation and differencing and higher-order wave-mixing techniques including stimulated Raman scattering, optical parametric oscillation and coherent Raman scattering [1.1, 1.8 - 10]. These non-linear processes occur as a result of the interaction of the source laser radiation with an active material, typically a crystal or a gas under high pressure, *via* the second- or higher-order components of its electric susceptibility tensor [1.1, 1.8, 1.11, 1.12]. Since these components are typically much smaller than the linear ones, non-linear effects become significant only at relatively high incident electric field strengths i.e. at high radiation intensities. Hence they could not be observed in the optical region prior to the advent of lasers, whose high brightness and strong directionality result in intensities which are commonly several orders of magnitude greater than those available from conventional light sources.

New methods for obtaining variable-wavelength laser radiation are continually being developed; thus it is currently possible to obtain virtually complete coverage of the 1100 - 200 nm spectral region, while high power outputs are available at discrete wavelengths in and below this range through the use of pulsed rare-gas and rare-gas halide excimer lasers [a)] [1.1, 1.2, 1.13] or the second or higher harmonics of solid-state lasers e.g. ruby, neodymium-doped yttrium aluminium garnet (Nd:YAG) or Nd:glass systems [1.14 - 16]. Continuously tunable radiation in both the vacuum- and extreme ultraviolet regions can also be achieved using various combinations of the non-linear techniques mentioned above [1.17], however applications of these techniques in experimental chemical kinetics have not yet become routine.

The attributes of lasers just described make them ideal sources both for the controlled production of reactive species, including ground-state and excited atoms, molecules, radicals and ions, by laser photolysis of stable precursor molecules, and for the study of subsequent chemical processes involving these photofragment species. The

a) The rare-gas halide lasers should correctly be referred to as exciplex lasers. However the generic term excimer is widely used in the literature for lasers of this type and this convention will be followed hereafter.

field of laser-induced chemistry, in which such processes may be grouped, is already very large and is growing rapidly as laser and instrumentation technology continues to advance. Several reviews of various aspects of laser-induced chemistry have recently been given [1.18 - 22] which augment earlier compilations of papers in this field [1.3, 1.23 - 25].

As far as kinetic studies of gas phase chemical reactions are concerned, an important advantage of the laser photolysis technique over conventional methods for the production of such excited or reactive species lies in its comparative cleanness. By this is meant the capacity for generation of large, localised concentrations of a desired species without co-production of others which could interfere with the process under study through reaction, quenching or other interactions with the target species. The latter problem can be a major source of difficulty in interpreting the results of experiments using the traditional discharge flow [1.26 - 28] and pulse radiolysis [1.29] techniques, as well as those of shock tube [1.30] and flame [1.31] studies where extensive numerical simulations based on a complex model mechanism are usually required in order to extract kinetic parameters from the raw data. The use of an optical filter to limit the excitation bandwidth in a conventional flash photolysis experiment [1.32] partly eliminates this problem but at the cost of a diminished yield of the species in question due to the associated reduction in flash intensity. These concerns may be largely avoided in a well-designed laser photolysis experiment, which allows kinetic measurements to be made in a comparatively simple chemical environment which may be closely monitored and controlled and whose effects on the process under study may be readily characterised.[a)]

Lasers have also proven to be extremely valuable tools for the detection of reactive species and a large number of powerful techniques have recently been developed which complement the traditional methods of atomic and molecular absorption, emission and fluorescence spectroscopy [1.17, 1.33], electron spin resonance spectroscopy [1.34, 1.35] and mass spectrometry [1.34]. The most widely used of the laser-based techniques is laser-induced fluorescence (LIF) [1.1, 1.33, 1.36] in which fluorescence is excited from one or more selected rovibronic transitions in the target species by a narrow-bandwidth tunable dye laser operating in the U.V.- visible region, or from rovibrational levels if an infrared laser is used. This simple technique, when used in conjunction with signal-averaging or photon-counting techniques, is very sensitive. For example, Fairbank and co-workers [1.37] have used LIF excited by a frequency-modulated continuous-wave dye laser to detect sodium atoms at concentrations as low as 10^2 cm^{-3}. This limit

a) A useful review of both the laser- and flash photolysis techniques has been given recently by West [1.40].

represents an average of only two atoms in the viewing region! LIF is also very selective, particularly for small molecules, such as OH, CH_2 and NH_2, whose electronic spectra are relatively uncongested. For larger species the increased probability of electronic quenching limits the range of pressures over which the technique may be applied. Other laser-based detection methods have been developed which are useful in situations where LIF is not viable, e.g. where the fluorescence yield in a convenient detection region is very low due to predissociation of the upper state of the absorbing transition. Important among these are infrared and UV-visible laser absorption [1.19], laser magnetic resonance [1.1, 1.38, 1.39], multiphoton ionisation [1.1, 1.20, 1.21] and coherent anti-Stokes Raman spectrometry (CARS) [1.1, 1.9, 1.10]. Demtröder [1.1] has given a very useful survey of these and numerous other spectroscopic detection methods involving the use of lasers. Applications of several of these methods in kinetic studies of elementary reactions of atoms and radicals have been reviewed by Baggott and Pilling [1.36].

1.2 Scope of the Present Work

The work described in this thesis consisted of five studies, four experimental and one theoretical, of the reactions of the cyanogen (CN), amidogen (NH_2) and imidogen (NH) radicals with atomic and molecular species. The reactions of such small free radicals with atoms, in particular, are of considerable practical interest due to their importance in the chemistry of atmospheric and combustion processes. On the other hand, the relative simplicity of such reactions makes them important test systems for new developments in theories of chemical dynamics and kinetics and molecular energy transfer, as well as rendering them amenable to study by the methods of *ab initio* quantum chemistry. Each of the studies reported in this thesis was intended to make a contribution in one or more of these areas.

In each of the experimental studies, laser photolysis of a stable precursor molecule was used to generate the radical in question in the presence of an excess of reactant gas and reactions were followed by monitoring either LIF from the radicals or resonance fluorescence from product atoms. (The basic experimental methods common to all of these studies are described in Chapter 2.) The laser photolysis/LIF (hereafter LP/LIF) technique is now very widely used, to the extent that virtually any volume of any of the leading journals in physical chemistry or chemical physics, published since 1980, is likely to contain several reports of studies based on this method for production and detection of reactive species. It would therefore be virtually impossible to give a general review of even recent applications of the LP/LIF method and this will not be attempted here.[a)] Instead, each experimental study is described in a separate and essentially self-

contained chapter (Chapters 3 - 6) comprising (a) an introduction, in which previous studies of the reactions in question are briefly reviewed; (b) an experimental section, containing details of the experimental method specific to that study including any modifications to the basic methods outlined in Chapter 2; and (c) a discussion of the results obtained, followed by a summary and an epilogue in which developments which have occurred since the completion of the present study are briefly described.

From the experiments using the LP/LIF technique (Chapters 3, 4 and 6), bimolecular rate coefficients have been measured for the following reactions:

(a)	$CN(X^2\Sigma^+,\upsilon''= 0,1) + O_2$	$\rightarrow$	products	(Ch. 3)
(b)	$CN(X^2\Sigma^+,\upsilon''= 0,1) + N$	$\rightarrow$	products	(Ch. 3)
(c)	$NH_2(\tilde{X}^2B_1) + NO$	$\rightarrow$	products	(Ch. 4)
(d)	$NH_2 + NO_2$	$\rightarrow$	products	(Ch. 4)
(e)	$NH_2 + N$	$\rightarrow$	products	(Ch. 4)
(f)	$NH(X^3\Sigma^-) + NO$	$\rightarrow$	products	(Ch. 6)
(g)	$NH + NO_2$	$\rightarrow$	products	(Ch. 6)

In Chapter 5, experiments using time-resolved Lyman-α resonance fluorescence measurements to established the nature of the products of the $NH_2 + N$ reaction (e) are described.

Reactions (a) - (e) were studied at ambient temperature; reactions (f) and (g) were examined at temperatures in the range 269 - 377 K. All studies were carried out at pressures between 1 and 3 Torr. The results of these studies have been compared to those of earlier workers, where applicable, and conclusions regarding the various reaction mechanisms have been drawn.

As will be seen in the introductions to the relevant chapters, all of the reactions (a) - (g) have previously been shown to be important in combustion systems. In particular there has been considerable interest and some debate over the last fifteen years regarding the nature of both the mechanism and the primary products of the $NH_2 + NO$ reaction (c). Discussions of various aspects of these problems appear in each of Chapters 4, 5 and 6 since the areas covered in these studies overlap to a certain extent.

In Chapter 7 are presented the results of a theoretical study of reaction (c) by the methods of *ab initio* molecular orbital theory . This study was motivated by previous attempts to model the experimentally observed features of the $NH_2 + NO$ reaction system by means of statistical rate theories, as described in the introduction to Chapter 7,

---

a) Partial reviews of the literature up to 1980 have been given, e.g. references [1.18] and [1.21].

and was also intended to shed light on the relative importance of several possible product channels which have been proposed. From the result of the *ab initio* calculations and those of the experimental studies reported in Chapters 4 - 6, a simple and consistent explanation has been derived which accounts for apparent discrepancies between the results of previous experimental studies of reaction (c).

In Chapter 8 some general conclusions are drawn from the results presented in the preceding chapters and areas for potential future study suggested by those results are discussed.

CHAPTER 2

EXPERIMENTAL

In this chapter equipment and techniques common to all or most of the present kinetics experiments are described. Details of apparatus or procedures peculiar to an individual study will be discussed in the experimental section of the appropriate chapter; in particular, a full description of the NH_2 + N product-analysis experiment will be given in Chapter 5.

The kinetic studies of the reactions of the CN, NH_2 and NH radicals were made in a fast-flow system by means of the laser photolysis/laser-induced fluorescence (LP/LIF) technique. A simple delayed-probe method was employed which involved measurements of the rate of decay of the intensity of the LIF from the radical under study in the presence of an excess of reactant R (i.e. under the conditions of pseudo-first-order kinetics) as a function of time. The radicals were generated at time $t = 0$ by excimer laser photolysis of a flowing gas mixture containing a stable precursor species together with a fixed concentration of reactant in a large excess of an inert carrier gas. The reactant concentration could be controlled by varying the flow rate of R in the mixture.The radical concentration was probed at some later time Δt, the delay time Δt being the independent variable in the experiment. A complete set of experiments then consisted in measuring the first-order LIF decay rate k_1' over a range of reactant concentrations (i.e. flow rates) including [R] = 0, at constant temperature and pressure.

2.1 Apparatus

A. Excimer Laser

The photolysis light source used in this work was a LUMONICS Inc. Model TE861T thyratron-switched, multigas, excimer laser. The principles of operation of excimer lasers are well documented [2.1, 2.2] and will not be discussed here. They are well suited to the present applications because of the high energies and short durations of the pulses they produce, and their ability to operate at high repetition rates, typically up to 200 pps (pulses per second). The LUMONICS system is capable of operation with a variety of gas mixtures, allowing operation at selected output wavelengths ranging from the vacuum ultraviolet (F_2 emission at 157 nm) through the visible to the infrared (CO_2, 10.6 μm). In these studies both the 193.3 nm argon fluoride (ArF) and the 248.5 nm krypton fluoride (KrF) emissions were used. Typical operating conditions and performance figures are given in Table 2-1. Pulse energies were measured with a SCIENTECH model 364 power/energy meter. The output beam had a rectangular

(*ca.* 2 x 1 cm^2) cross-section but was usually subject to some spatial filtering, either by deliberate use of apertures or accidentally as a result of cell design, so that the measured energies provided upper limits to the effective energies. Except in the case of the NH_2 + N product study (Chapter 5), the absolute values of pulse energies were not significant provided that a sufficient yield of radicals or atoms was achieved. The spectral profiles of the ArF and KrF emissions were measured using a McPHERSON Model 218 0.3 m monochromator (Section 2.1 G).

TABLE 2-1: Excimer laser operating characteristics.

Parameter	Lasing species	
	ArF	KrF
Wavelength , nm	193.3	248.5
Pulse width, ns	10	10
Range of pulse energies, mJ	0.5 - 100	75 - 100
Repetition rate, Hz	18 - 30	40
Bandwidth, cm-1	~100	~100
Beam dimensions	2 x 0.6	2 x 0.7

B. Probe Dye Laser

The probe source used for kinetic studies was an AVCO model C5000/4000 Hantsch-type nitrogen-pumped dye laser. The thyratron-switched nitrogen laser produced short (*ca.* 10 ns) pulses at 337.1 nm with energies around 1 mJ. Several different dye solutions were required to provide appropriate probe beams for the detection of CN, NH_2, NH and OH radicals, the latter being a possible product of the NH + NO and NH + NO_2 reactions. The dye laser wavelength could be varied either manually or by a synchronous motor coupled to the diffraction grating drive through a reduction gear-box which allowed very slow scanning over the dye's fluorescence band. Wavelengths used ranged from visible (598 nm, NH_2, Chapter 4) to the ultraviolet (306.4 nm, OH, Chapter 6). For measurements in the ultraviolet it was necessary to frequency-double the dye laser output, using either an angle-tuned potassium dihydrogen phosphate (KDP) second harmonic generation (SHG) crystal, or a temperature phase-matched (TPM) ammonium dihydrogen arsenate (ADA) SHG crystal. These crystals were supplied by INRAD (Interactive Radiation, Inc.). The ADA crystal was tuned using an INRAD 5-1 TPM SHG system temperature controller with a bandwidth of ± 0.1 °C, corresponding to a maximum wavelength uncertainty of ± 0.1 nm. The spectral bandwidth of the dye laser output depended on the wavelength region in use. Using the 0.3 m monochromator the absolute value in the ultraviolet (295 - 460 nm) was found to be 0.1 nm full width at half-

maximum (fwhm), decreasing to 0.05 nm near λ = 598 nm. The properties of the various probe radiations are summarised in Table 2-2.

TABLE 2-2: Dye laser operating characteristics.

Fluorescer	Wavelength (nm)	Dye [a]	Concentration (10^{-3} mol L^{-1})	Solvent	Bandwidth (cm^{-1})	Frequency doubling method [b]
OH	306.4 (612.8)	R590	5.3	ethanol	11	TPM ADA
NH	336.1 (672.2)	CV670/R590	3.3/2.5	ethanol	9	Angle-tuned KDP
CN (υ" = 0)	388.3	BBQ	2.5	1:1 toluene/ ethanol	7	-
CN (υ" = 1)	421.6	S420	2.1	1:4 ethanol/ water	6	-
CN (υ" = 2)	460.6	C460	3.5	ethanol	5	-
NH_2	597.7	R590	5.3	ethanol	1.4	-

a) Dyes supplied by EXCITON CHEMICAL CO. INC.

b) TPM ADA, temperature phase-matched ammonium dihydrogen arsenate crystal; KDP, potassium dihydrogen phosphate crystal.

The energies of undoubled dye laser pulses were estimated to be of the order of a few microjoules after allowance for the conversion efficiencies of the different dyes. To allow high pulse repetition rates (up to 500 Hz) the AVCO laser is fitted with a continuous-circulation cassette for dye solutions.

C. Photolysis Cell Design

All photolysis cells used in this work were made from SCHOTT 'Duran' glass (similar to Pyrex) in the glassblowing workshop of the Chemistry Department. A number of different cells were used, with successive models arising from attempts to obtain a design in which the cell's performance was optimised with respect to different parameters. These included a low internal scattering profile and high stray-light suppression, rejection of fluorescence excited from windows, short residence time for atomic species (especially N atoms), and capacity for variable-temperature operation. The use of glass made construction and subsequent modification of cells relatively easy. Some general features of a typical cell are described below. Diagrams and additional details relating to individual cells (or deviations from the present description) will be found in the appropriate chapters.

The cell was constructed so that the counter-propagating photolysis and probe beams entered collinearly to obtain a maximum active volume. Windows for the admission of laser beams were made of either SUPRASIL quartz or magnesium fluoride and were attached to the cell using TORR-SEAL epoxy resin. The windows were usually inclined at an angle to the optical axis to inhibit internal reflection of the laser beams. In some cells glass versions of the light baffle described by Butler [2.3] were incorporated in the window arms to improve stray light rejection and cut down internal scattering. In these cells the internal surfaces of the sidearms were coated with AQUADAG colloidal carbon (ACHESON COLLOIDS CO.). However these baffles could not be used when the excimer laser was operated unfocussed due to the large losses which would have occurred, since the baffle aperture was usually less than 5 mm in diameter. A further problem was the phenomenon of window luminescence, presumably due to a combination of factors including nonlinear optical processes resulting from the high photon flux of the excimer laser and defects or impurities in the window material. This luminescence appeared as a red emission at the window surface. When quartz windows were used this was accompanied by a blue-white fluorescence observable at the window edge. To offset these effects the windows were usually placed upwards of 10 cm from the viewing region and either glass colour filters (CORNING) or interference filters were used to isolate the fluorescence under study. The success of these measures was demonstrated by the observation of very low background light levels (typically $<< 1$ % of peak fluorescence intensity measurements) in 'empty-cell' experiments using both lasers together.

In experiments using LIF or resonance fluorescence detection the fluorescent emission was viewed by a photomultiplier mounted vertically above the optical axis of the cell. The photomultiplier housing was screwed onto a circular aluminium flange to which was glued a B34 standard-taper ground-glass cone, which in turn fitted into a B34 socket built into the cell, with lubrication by APIEZON 'N' or 'H' grade vacuum grease.

Gas mixtures for photolysis entered the cell close to the excimer laser window to reduce the possibility of window burning. Despite this precaution a gradual build-up of photolysis products was occasionally observed as a dark deposit on the window; normally this could be removed by heating the window with the cell under vacuum.

The cell was evacuated, *via* a large liquid nitrogen trap, by a two-stage rotary pump (WELCH Duoseal Model 1397B, pumping speed *ca.* 450 litre/minute). Flow velocities within the cell were estimated to be in the range 150 - 600 cm s^{-1} at typical working pressures between 1 and 3 Torr; plug flow was assumed in these calculations.

Total pressure measurements were made *via* a glass line opening into the cell close to the viewing region. The minimum pressure obtainable was usually 5 - 10 mTorr.

With the exception of the study of imidogen (NH) radical reactions (Chapter 6), all measurements were carried out at ambient temperature which was determined to within ±2 °C using mercury-in-glass thermometers mounted on the gas handling manifold framework and, occasionally, pre-calibrated thermistors or copper-Constantan thermocouples taped to the cell. The agreement between the ambient temperature determined in this way and that of the gas stream was confirmed in experiments in which the stream temperature was measured by a thermocouple just downstream from the viewing region. The effects of laser heating of gases within the viewing region by the excimer beam were assumed to be minimal in view of the large excess of carrier gas used in all experiments with the flow system ($p_{\text{carrier}} : p_{\text{absorber}} > 100 : 1$, typically).

The cell and the surrounding glass lines were usually given several coats of a matt black vinyl paint to exclude room light. This measure was successful to the extent that under typical operating conditions no effect of switching off the laboratory's fluorescent lights could be detected in background experiments.

D. Vacuum Line

Gas handling procedures, such as purification of reactants or radical precursors and preparation of flowing mixtures for photolysis, were carried out in a conventional glass vacuum line (see Fig. 2.1) using standard techniques,e.g. freeze-pump-thaw cycling and trap-to-trap distillation. The line was pumped by a combination of rotary and oil-diffusion pumps. All pumps were isolated by cold traps (liquid nitrogen or dry ice/ethanol). Stopcocks used were of the greaseless type (J. Young, Scientific Glassware Ltd.).

Gas pressure in the line and/or photolysis vessel were read using either an MKS BARATRON type 170 M capacitance manometer with a 0 - 1000 Torr sensor, for pressures above 10 Torr, or a TEXAS INSTRUMENT (TI) Model 144 quartz-spiral (Bourdon) gauge for lower pressures. Reference vacuums for both instruments, provided by two-stage oil-diffusion pumps and monitored using EDWARDS Pirani-type gauges, were always at least a factor of 10^3 below the pressures measured. From a check of the TI gauge against the manufacturer's calibration data, the uncertainty in measurements of total pressure in the cell was determined to be less than 1 %.

Individual gas flows were monitored directly using HASTINGS mass flowmeters coupled to a digital voltmeter (DVM). The flowmeters, ranging in capacity

from 5 to 1000 standard cubic centimetres per minute (sccm), were each adjusted to provide a 1.5 V d.c. output at full-scale deflection; the linearity of the meters was guaranteed to within 1% up to full scale. Flows were controlled by means of EDWARDS needle valves placed downstream from each meters, except in the case of the 10 sccm meter in the reactant line, for which a GRANVILLE-PHILLIPS variable leak valve was used.

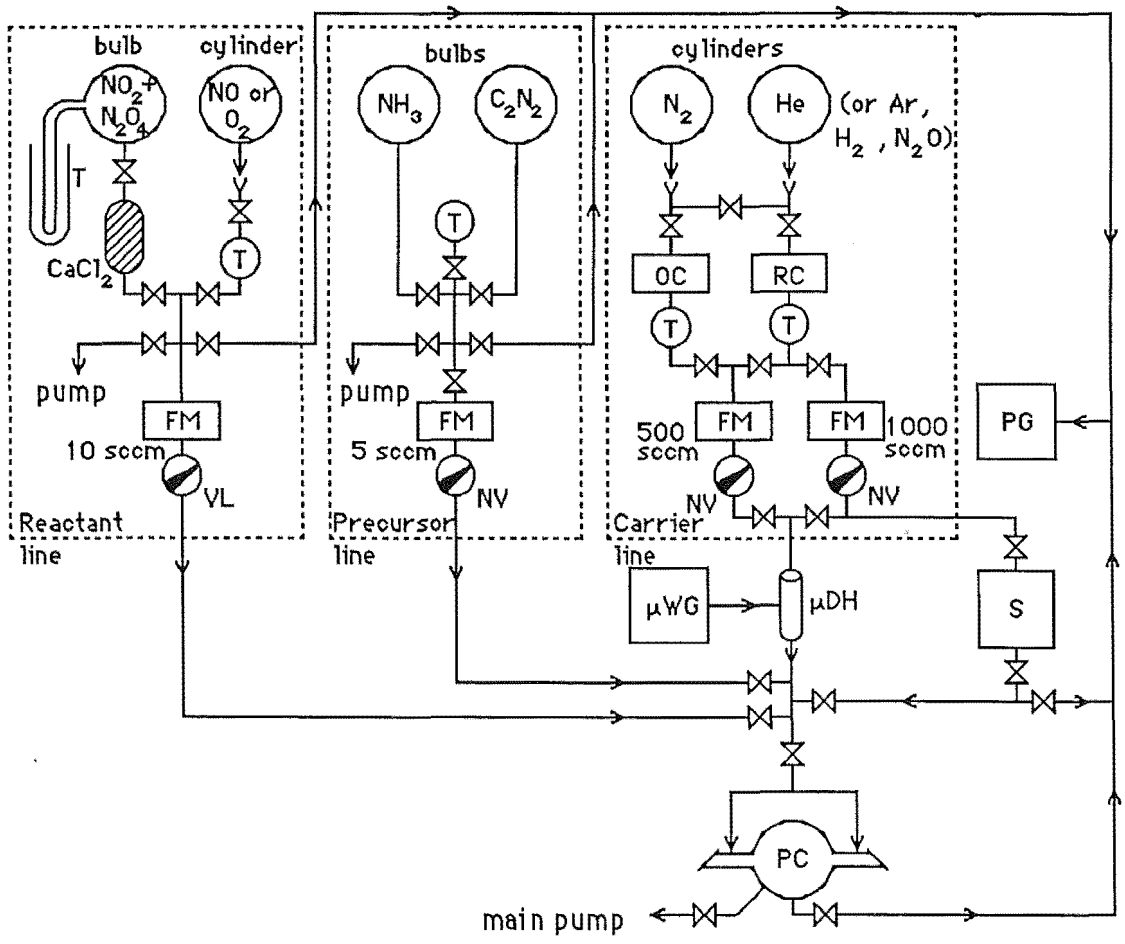

FIGURE 2.1: Schematic diagram of glass vacuum line.

Key: –⋈– = greaseless stopcock; T = cold trap; FM = flowmeter (sccm = std. cubic cm min^{-1}); OC = oxidised BTS catalyst; RC = reduced BTS catalyst; PG = pressure gauges; VL = variable leak valve; N = needle valve; μWG = microwave generator; μDH = microwave discharge head; S = N_2H_4 saturator; PC = photolysis cell.

Each flowmeter was calibrated over its entire range using standard wet-test methods. In all cases but one this calibration gave a flowmeter calibration factor which was constant over the full range of meter. For the 500 sccm meter generally used to

measure carrier gas flow, the calibration factor was flow-dependent. In this case a linear least-squares analysis of the calibration data yielded a calibration equation, quadratic in indicated flow, which was precise to within 0.3 % over the meter's range. The flowmeters were spot-checked for variation of their calibrations throughout the period of this work; no significant changes were observed. The calculation of gas mixture parameters is described in Section 2.4.

E. Atom Source and Photometric Titration Procedure

In experiments on nitrogen atom/radical reactions, the atoms were generated by a microwave discharge (EMS Microtron 200) either in a stream of pure nitrogen or, more commonly, through a trace of N_2 added to the main carrier flow upstream from the photolysis cell. In the former case the atom concentration [N] was controlled by varying the discharge power and turning off the discharge for experiments at zero [N]; when the N_2/carrier system was used, the discharge ran continuously at a low power and [N] was controlled by varying N_2 flow rate.

Nitrogen atom concentrations were determined by means of a photometric titration method [2.4] as follows. The intensity of the nitrogen afterglow due to the reactions

$$N + N + M \rightarrow N_2^* + M$$

$$N_2^* \rightarrow N_2 + h\nu \quad \text{(yellow Lewis-Rayleigh afterglow)}$$

was monitored at a viewport a short distance downstream from the cell with an unfiltered EMI 9781B photomultiplier and a KEITHLEY Model 417 high-speed picoammeter. The atoms were titrated both before and after a given experiment by addition of nitric oxide. The NO flow rate was varied to obtain a minimum photocurrent which occurred at the end-point of the titration, as indicated by the following reaction scheme:

$$N + NO \rightarrow N_2 + O \quad \text{(fast)}$$

Excess N : $N + O + M \rightarrow NO^* + M \rightarrow NO + h\nu$ (blue) + M

Excess NO : $NO + O + M \rightarrow NO_2^* + M \rightarrow NO_2 + h\nu$ (greenish) + M

End-point : $O + O + M \rightarrow O_2^* + M \rightarrow O_2 + h\nu$ (i.r.) + M

(The infrared O_2 emission was not seen by the photomultiplier.) The concentration of NO (= [N]) could then be calculated as described in Section 2.4.

In the earlier experiments on kinetics of the CN and NH_2 radical reactions (Chapters 3 and 4) the NO could be added through either of two jets, one just upstream and the other just downstream from the cell. Preliminary measurements had indicated that wall removal of the atoms caused significant decay of [N] during passage through the cell. To minimise this effect cells were soaked in a 10 % solution of analytical grade phosphoric acid and allowed to dry slowly in air prior to installation in the vacuum line. By comparison of the end-point NO flows at the two jets for titrations performed in the absence of radicals, the loss of N atoms in the 'poisoned' cells was determined to be less than 5 % and the mean of the two flow rates was used in the calculation of [N]. Atom concentrations generated by this method were typically in the 10^{12} - 10^{14} cm^{-3} range. The overall uncertainty in [N] was estimated to be 6 - 8 %. In the later NH_2 + N product study (Chapter 5) only a single upstream titration inlet was used.

F. Light Detection Systems

In all the experiments described here the detectors used were photomultipliers. Several different photomultipliers were employed in a number of applications including fluorescence measurements, photometric titration of nitrogen atoms, determination of laser spectral profiles and tuning of the probe laser by either direct or indirect methods.

In the LIF and resonance fluorescence experiments the total fluorescence was observed by a photomultiplier mounted as close as possible to the viewing region, as described in Section 2.1C. This arrangement eliminated the need for collection optics. In general the total emission was filtered, either by suitably chosen glass colour filters or by interference filters, to minimise the effects of scattered light from the photolysis pulse. (An exception to this case is described in Section 5.2).

G. The 0.3 m Monochromator

In all situations such as tuning of the probe laser, location of a spectral feature and measurement of laser spectral profiles, a McPHERSON Model 218 0.3 m scanning monochromator was used to provide the required wavelength resolution of the radiation. This instrument was fitted with a 1200 groove/mm diffraction grating blazed at 300.0 nm, with a nominal efficiency of 75 % at 296.0 nm falling to 58 % at 404.6 nm. The indicated wavelength scale was calibrated against the Hg emission spectrum. The theoretical resolution available using 10 μm entrance and exit slits was 0.06 nm in first order; the reciprocal linear dispersion of the instrument was 2.65 nm/mm. In practice the resolution was typically about 0.08 nm. The monochromator could be evacuated if required; in this work it was purged with nitrogen for experiments below 200 nm.

H. Instrumentation

Discussion of the boxcar integrator used for signal averaging and of the various elements of the timing control system is deferred to Section 2.3 of this chapter. The corresponding description of the waveform eductor used in the NH_2 + N product study is contained in Section 5.2.

Many diagnostic procedures throughout these experiments were facilitated by the use of a TEKTRONIX Model 7904 500 MHz oscilloscope. This instrument was fitted with dual-channel and differential vertical amplifiers and provided a wide range of display modes and timebase options. Of these the 7B85 Delaying Timebase unit was particularly valuable in such applications as calibration of the boxcar integrator timebase to nanosecond accuracy, delicate adjustment of sub-microsecond time delays, dye laser tuning and visual monitoring of experimental signals.

I. Microcomputer and Software

In the first two studies (kinetics of the reactions of CN and NH_2 , Chapters 3 and 4) data acquisition and subsequent analysis were performed by a RADIO SHACK TRS-80 microcomputer (8-bit Z80 processor), *via* a DATEL MDAS-16 interface unit having sixteen 12-bit analog-to-digital (A/D) inputs and four 8-bit D/A outputs. In the later work this system was replaced by a DIGITAL EQUIPMENT CORPORATION (DEC) LSI 11/23 system fitted with a DEC AXV11C A/D-D/A (both 12-bit) interface. Both computer systems incorporated twin floppy-disk drives for data storage.

The programs used were of three basic types, namely data acquisition, data processing and ancillary routines. The data acquisition and processing groups were further subdivided according to the signal processing technique used. Thus for experiments using the boxcar integrator, the sampling rate and input gate delay were controlled by the program BOXCAR and data analysis was performed using BOXFIT and LSQFIT, while for measurements made with the waveform eductor the stored waveform was read by program EDUCTR and the resulting files processed using EDPROC. A brief description of each of these programs is given in Table 2-3. The third group of programs contained the routines used for calculation of flowmeter calibration and heat capacity correction factors, and gas mixture parameters. Most of these programs were written in BASIC and were based on existing routines written by Professor L. F. Phillips.

TABLE 2-3: Computer programs for data acquisition and analysis.

Program name	Description
BOXCAR	Active input/output routine for use with boxcar integrator *via* A/D interface. User-defined sampling regime. Generates BCI gate delay control voltage and reads timebase voltage, i.e. actual gate delay (X), and BCI output signal (Y). Stores (X,Y) data and sampling parameters on disk.
EDUCTR	Passive input routine for use with waveform eductor *via* A/D interface. Reads stored digitised waveform at the end of experiment and converts to analog form. Stores (X,Y) data and user-entered instrument parameters on disk.
BOXFIT	Interactive program for analysis of first-order kinetic data obtained using BCI. Reads data files generated by BOXCAR, performs background corrections, converts (X,Y) voltages to *ln* (intensity) - *vs* - time format, extracts first-order decay constant.
EDPROC	General data file manipulation program. Allows a variety of operations to be performed including scaling, pointwise file subtraction or division, linear extrapolation near a discontinuity and least-squares analysis. Used especially for analysis of waveform eductor data from measurements of H atom yields from NH_2 + N reaction (Chapter 5).
LSQFIT	General least-squares regression program, used especially for extraction of bimolecular rate coefficients from k_2 - *vs* - [R] data (Section 2.4). Student's *t*-test available for linear fit.

2.2 Purification of Materials

The chemicals used throughout these experiments may be grouped into three classes, namely carrier or bath gases, radical precursors, and reactant gases. The purification procedures applied to each of these materials are outlined below. The treatments of a few ancillary reagents not listed here are described at appropriate points through the text.

A. Carrier Gases: He, Ar, N_2, H_2, N_2O

Helium (New Zealand Industrial Gases Scientific grade, supplied at nominal purity ≥ 99.993 %), argon (NZIG Welding gd., n.p. >99.99 %), nitrogen (NZIG Industrial gd., n.p. > 99.9 % or NZIG Oxygen-free gd., n.p. > 99.995 %), hydrogen (NZIG Industrial gd., n.p. >99.7 %) and nitrous oxide (NZIG Medical gd., n.p. > 99 %)

were further purified by passage through a bed of either reduced copper turnings at around 400 °C [a] or reduced BASF BTS catalyst at 150 - 180 °C (100 °C, N_2O) [b], followed by trapping over silica gel at either -196 °C (liquid nitrogen); He, H_2) or -78 °C (dry ice/ethanol; Ar, N_2, N_2O).

B. Radical Precursors: C_2N_2, NH_3, N_2H_4

Dicyanogen (MATHESON/INTERNATIONAL, n. p. ≥ 99 %) and ammonia (CHRISTCHURCH GAS, COAL AND COKE CO., n. p. > 99.9 %) were purified by the same method.The gas was initially subjected to trap-to-trap distillation, the middle fraction from which was stored in a blackened 10 litre glass bulb and subsequently repurified by freeze-pump-thaw cycling over analytical grade potassium hydroxide. In some experiments involving C_2N_2, the initial distillation was omitted; this made no significant difference to the derived results.

Liquid hydrazine (FLUKA AG, *purum*) was used as supplied in a room-temperature saturator to provide N_2H_4 in the gas phase for experiments on NH radical reactions (see Section 6.2).

C. Reactant Gases: NO, NO_2, O_2

Nitric oxide (MATHESON/INTERNATIONAL c.p. gd., n. p. > 99.2 %) for use both as a reactant and in photometric titration of nitrogen atoms, and oxygen (NZIG Industrial gd., n.p. > 99.5 %) were passed through silica gel traps at -78 °C.

Nitrogen dioxide was prepared in a blackened 10 litre bulb by overnight reaction of excess O_2 with NO and purified by freeze-pump-thawing over either anhydrous calcium sulphate or calcium chloride. The final product was stored over calcium chloride. Samples of NO_2 prepared in this way remained free from NO for up to a week, as shown by the absence of any blue or green colouration of the frozen solid.

2.3 Experimental Configuration and Procedures

A. Instrumentation

The experimental configuration used for LP/LIF measurements is shown schematically in Fig. 2.2. A 10 V pulse produced by the variable-frequency square-wave

---

[a] CN experiments (He, Ar, N_2) only.
[b] All other experiments

generator simultaneously triggered the excimer laser and initiated the timebase ramp of a PRINCETON APPLIED RESEARCH (PAR) model 160 boxcar integrator (hereafter simply "boxcar").[a] The delay between the photolysis and probe pulses was produced by the delayed trigger circuitry of the boxcar as follows. With the delayed trigger switch set to scan mode, the boxcar produces a 5 V output pulse which is essentially synchronous with the opening of the input gate and can be used to trigger another instrument, in this case the probe dye laser. Thus with the gate delay under external (microcomputer) control, using the D/A output to provide the control voltage, the timing of the probe laser pulse could be varied with respect to the excimer laser pulse and the LIF decay profile could be recovered by sampling the boxcar output as a function of Δt.

Additional flexibility in the optimisation of the timing of the experiment was obtained by provision of an additional variable delay between the opening of the boxcar gate and the probe pulse. This was done by inserting a monostable multivibrator having a variable mark/space ratio between the delayed trigger output of the boxcar and the dye laser control unit, and triggering the dye laser with the trailing edge of the monostable pulse.

The LIF emission was isolated by a suitable filter or filters and detected by the photomultiplier, the output of which was amplified by a fast preamplifier (rise-time = 3 ns) and taken to the 100 kΩ input of the boxcar. The averaged signal and the timebase voltage were sampled by the microcomputer via the A/D interface, the data being stored in the processor's memory during the experiment and subsequently transferred to disk for storage pending later analysis.

B. Experimental Procedure

Initial preparation for a typical series of kinetics measurements involved an extended period of pumping of the cell and vacuum line. At the same time, the excimer laser cavity was 'passivated' with fluorine atoms produced by a 1 kHz, 15 kV discharge in a mixture of F_2 and He [2.7], and the radical precursor and reactant gases were repurified if necessary. The excimer laser was then charged with the appropriate operating mixture and optimisation of the boxcar parameters and tuning of the dye laser were carried out as follows.

---

a) Nearly all of the present kinetic experiments made use of the PAR 160 boxcar. Since boxcars are ubiquitous in kinetic studies using photophysical techniques and the detailed principles of their operation are well-documented [2.5, 2.6], only immediately relevant details of the use of this instrument will be given here.

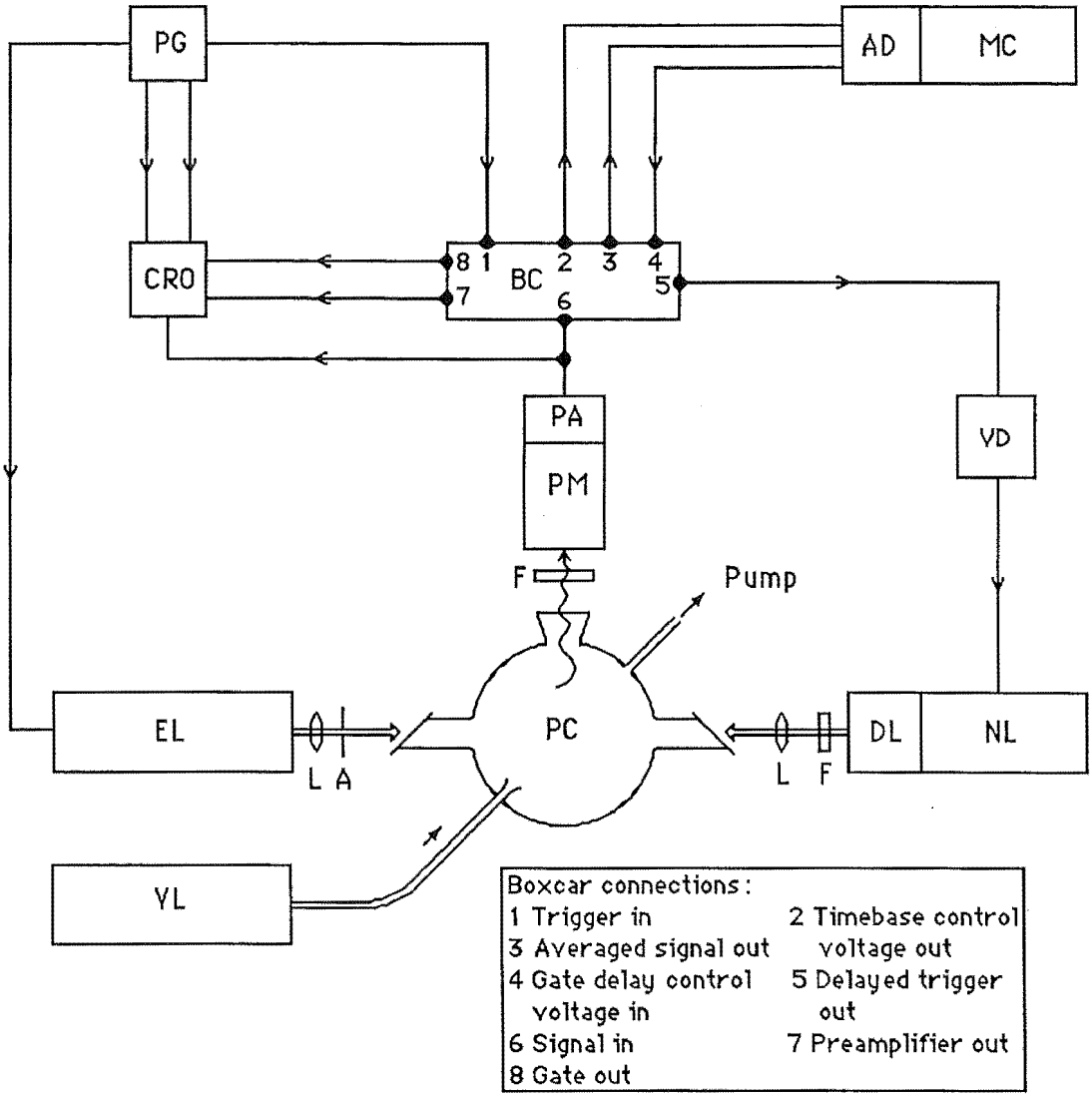

FIGURE 2.2: Experimental configuration for LIF measurements.

Key: PG = pulse generator; AD = analog/digital interface; MC = micro-computer; CRO = oscilloscope; BC = boxcar integrator; PA = preamplifier; PM = photomultiplier tube; VD = variable delay; EL = excimer laser; PC = photolysis cell; DL = dye laser; NL = nitrogen laser; VL = vacuum line; L = quartz lens; F = filter; A = aperture.

The boxcar timebase was selected on the basis of an estimate of the pseudo-first-order reaction lifetime τ. With the reactant concentrations available under fast-flow conditions and for bimolecular rate coefficients k_2 in the 10^{-11} to 10^{-10} cm^3 s^{-1} range, $\tau = (k_2[R])^{-1}$ was generally of the order of 0.1 to 1 ms, so that the timebase (TB) values used were typically in the 0.1 to 0.5 ms range. This choice of timescale allowed measurements to be made within a 'scan window' which began sufficiently long after the excimer laser pulse to avoid interference from the prompt emission generated in the photolysis process, and ended before the signal became too small.

The choice of the repetition rate f for the experiment involved a compromise between duty-factor considerations and the need to extend the lifetime of the excimer laser gas mixture. The boxcar's duty factor, defined by the relation DF = AT x f where AT is the aperture time, governs the real-time response of the instrument *via* the observed time-constant (OTC) [a], which is given by OTC = TC/DF where TC is the selected normal resolution mode time-constant. Hence, increasing the repetition rate results in a faster real-time response, i.e. a shorter experiment. Unfortunately, however, the lifetime of the excimer laser gas mixture falls off with increasing repetition rate. Balancing of these two factors lead to the use of repetition rates between 10 and 70 Hz, with the minimum available time-constant (TC = 0.01 ms) being selected to reduce the boxcar's response time, and subsequent noise-reduction being effected by computer averaging of multiple scans.

Preliminary adjustment of the dye laser was made by coarse-tuning to the desired wavelength using the 0.3 m monochromator with narrowed slits. At this point a typical flowing mixture of carrier and radical precursor gases was set up, the excimer laser started, and the dye laser wavelength carefully varied until a maximum fluorescence signal was obtained. Next, adjustments were made to the dye laser optics and the probe beam path to ensure accurate alignment with the photolysis beam and minimise scattering inside the cell. Finally, the timing of the dye laser pulse relative to the opening of the boxcar gate was optimised. This involved variation of the aperture time, to which the observed signal was found to be rather sensitive, and fine adjustment of the variable delay in the dye laser control line. It was often necessary to repeat the later steps in this procedure several times in order to maximise the observed signal. Both the wavelengthtuning and the alignment of the dye laser were checked and adjusted as necessary throughout a set of experiments.

The initial preparation having been thus completed, the first step in a single experiment was the setting up of the desired gas mixture. A finite period of time was always necessary for the individual gas flows to settle down to the required values, during which the data-collection program (BOXCAR) was initialised with appropriate values of the parameters governing the data acquisition and boxcar gate control processes. These included the boxcar timebase and the fractions of this value which defined the scan window, the number of scans to be made, the number of data points per scan and the number of individual samples of the boxcar output to be averaged at each point. In

---

a) The OTC is the time taken for the boxcar output to reach 63 % (1 - e^{-1}) of its final value.

measurements involving nitrogen atoms as the reactant species, the initial photometric titration to determine [N] was carried out at this point, as described in Section 2.1 E.

The initial step in the data collection was a measurement of the baseline signal obtained with the cell dark, i.e. with the excimer laser off and the probe beam blocked. For this measurement the boxcar gate was set to the end of the scan window. The value stored was usually the average of 50 - 100 individual samples of the boxcar output, this number being sufficient to guarantee a standard deviation s less than 10 % of the measured value, which was in turn set at 0.5 - 1 % of the peak experimental signal using the boxcar's zero-adjust control. A similar measurement was made at the end of the experiment as a check on the baseline stability. The baseline drifts observed in this way were typically comparable to s.

Following the baseline measurement, the excimer laser was switched on and the intensity - *vs* - time data collected. During the experiment, gas flows, total pressure and temperatures were noted for subsequent use in calculations of reactant concentration. When the data collection was completed, the excimer laser was switched off, the dye laser beam blocked and the second baseline measurement made. In the case of the atom reactions, the photometric titration was repeated at this point. The data could then be viewed in both tabular and graphical form; provided no obvious anomalies were present the data-set was transferred to a disk file for later analysis. After this final step the flow conditions were altered ready for the start of the next experiment.

A complete set of kinetics experiments at a given temperature and pressure, for which the carrier gas flow was maintained constant throughout, usually involved 20 to 40 individual experiments of the type described above. The first and last runs in such a set were performed with only the carrier gas present. These measurements enabled account to be taken of any residual effect of the photolysis pulse, e.g. reflective scattering of the window luminescence discussed in Section 2.1 C, and of the small effect of Rayleigh scattering of the probe laser beam. The remaining runs were carried out with the radical precursor present at a constant flow rate, while the reactant concentration [R] was varied over as large a range as possible, from [R] = 0 to an upper limit occurring where either the pseudo-first-order lifetime $\tau = (k_2[R])^{-1}$ became small compared to the minimum delay time necessary to avoid interference by the photolysis pulse, or quenching of fluorescence reduced the LIF signal to an unacceptably low level. Typically this limit was reached at flow rates corresponding to $[R] \approx 10^{15}$ cm^{-3}.

For every two experiments at non-zero [R], at least one was made with reactant absent to allow corrections to be made for [R]-independent processes, such as

pumpout and diffusion out of the exciting beam, causing depletion of the radical concentration.

2.4 Data Reduction Procedures

This section contains a discussion of the methods used to analyse the results of the LP/LIF experiments conducted using the boxcar (Chapters 3, 4, 6). The procedures used for the analysis of the results of the hydrogen atom resonance-fluorescence measurements in the NH_2 + N system will be discussed in Chapter 5.

The analysis of data obtained from a set of LP/LIF experiments involved the following steps:

(i) Evaluation of the pseudo-first-order rate coefficients k_1' for each individual experiment using program BOXFIT. Data files (*ex* BOXCAR) for different reactant concentrations (including zero) were corrected for background effects and converted to the $ln\ (I_f)$ - *vs* - time format. Linear least-squares regression analysis was then used to obtain the exponential decay constant k_1'. The quality of the fit obtained was indicated by the ratio of the RMS deviation to the peak $ln\ (I_f)$ value. For experiments yielding large slopes, i.e. with large [R], this ratio was generally less than 1 %, rising to about 5 % for experiments with [R] = 0.

(ii) Calculation of [R] for each experiment. The concentrations (number densities) of the components of the pre-mixed gas streams were calculated from the observed flow rates, the total pressure in the cell and the stream temperature. A simple computer program incorporated these data together with correction factors (supplied by HASTINGS) based on the specific heats (C_p) of the gases present, the above-mentioned flowmeter calibration factors and observed zero corrections for each meter, to provide the corrected flow rate, partial pressure and number density of each component.

When NO_2 was used as a reactant it was necessary to calculate the specific heat correction factor, taking account of the strongly temperature-dependent equilibrium

$$2\ NO_2 \rightleftharpoons N_2O_4.$$

This was achieved using formulae supplied by HASTINGS, the equilibrium constant data of Baulch *et al.* [2.8] and heat capacity data from the JANAF thermochemical tables [2.9], and allowing for a nominal temperature rise in the body of the flowmeter of 10 °C. Because $C_p(N_2O_4) \approx 2\ C_p(NO_2)$, the correction factor, in terms of final flow, does not vary greatly with the total pressure of $NO_2 + N_2O_4$.

A conservative analysis of the sources of uncertainty in these calculations resulted in an estimate of 5 - 8 % for the typical total uncertainty in values of reactant concentrations [R] derived from this program. A list of estimated systematic uncertainties used throughout this work is given in the Appendix.

(iii) Linear least-squares regression analysis of the k_1' - *vs* - [R] data (using program LSQFIT) to obtain the uncorrected bimolecular rate coefficients k_2'. In treating the results of a set of experiments at constant pressure, the least-squares regression line was fitted to the expression

$$k_1' = k_2' [R] + k_1''$$

where k_1'' is the rate of disappearance of the radicals at [R] = 0. The observation of an approximately inverse dependence of the values of k_1'' on the total pressure and the buffer gas molecular weight indicated that diffusion away from the viewing region was the main process for radical removal in the absence of the reactant R, although a small component due to the reaction with the parent molecules would also be expected.

When k_2' was found to be independent of pressure (which was the case for all the reactions studied by this method) a global fit using all the available data was used to obtain a final value for k_2'. In this case however the pressure dependence of k_1'' required a slight modification of the analysis used. As was noted in Section 2.3 B, a measurement of k_1'', i.e. a run with R absent, was made either immediately before or after each experiment with non-zero [R]. For the global fit each value of k_1' was first corrected by subtraction of the associated k_1'' to give k_1, i.e. $k_1 = k_1' - k_1''$. The overall k_2' was then obtained from the equation

$$k_1 = k_2' [R]$$

where the regression was constrained by the inclusion of points at the origin corresponding to runs having [R] = 0.

(iv) Correction of k_2' for systematic uncertainties to yield the final result $k_2' \pm \Delta k_2$ where the uncertainty Δk_2 includes both systematic and statistical contributions. The latter usually represented either 90 % or 95 % (2σ) confidence limits obtained from the application of Student's t-test to the least-squares regression determination of k_2'. The systematic contribution to Δk_2 was estimated from a consideration of the probable sources of error present in the particular experimental configuration used to measure k_2'.

CHAPTER 3

REACTIONS OF CN WITH N ATOMS AND O_2

3.1 Introduction

The cyanogen radical (CN) is known to be an important species in a wide range of chemical systems. It is one of the most abundant and ubiquitous extraterrestrial molecules, having been observed in a large number of stars with a frequency approaching those of CH and CH^+ [3.1]. More recently, CN rotational and hyperfine as well as optical lines have been reported in numerous interstellar sources [3.2]. These include both dust and molecular clouds, in which CN is believed to play a vital role in the synthesis of larger interstellar molecules, many of which contain the CN moiety [3.3]. CN is also a commonly observed transient species in combustion processes. Recent studies have demonstrated its role in the formation of so-called "prompt" nitric oxide in fuel-rich flames [3.4, 3.5] and its importance in determining the fate of other nitrogen species in flames containing hydrocarbons [3.6] or nitrogenous fuels [3.7]. In the numerical studies by Phillips of the breakdown of C_2N_2 in $H_2/N_2/O_2$ flames [3.8, 3.9], some 50 % of the reactions included in the proposed mechanism involved CN radicals.

The modelling of such complex systems requires detailed knowledge of the rate coefficients (and the temperature dependences thereof) of the component elementary reactions. Toward this end, many kinetic studies have been made of the reactions of CN with a variety of small molecules likely to be important in combustion processes (see Table 3-1). A number of these studies have focussed attention on the effects of vibrational excitation of the CN radical on the rate of reaction (see e.g. references [3.10 - 12]). However, although such effects are likely to be significant under the conditions obtaining in combustion systems, relatively little quantitative data yet exists. Furthermore, the interpretation of the results of these experiments is complicated due to the difficulty of separating the effects of vibrational quenching from those of chemical reaction and the possibility of repopulation of the state under study by cascade processes (i.e. vibrational relaxation and internal conversion) or by regeneration in secondary reactions. These issues will be considered further in Section 3.3.

The reactions of CN with atomic species constitute another little known area of CN chemistry. This is in spite of the fact that large atom concentrations are known to be present in many H - C - N - O combustion systems. Again, technical considerations mainly related to the clean generation and determination of sufficient yields of atoms and the potential complexity of the resulting reaction mechanism have, until recently, made very difficult the extraction of quantitative results from studies of H - C - N - O systems.

TABLE 3-1: Rate coefficients for reactions of $CN(X^2\Sigma^+,\upsilon'')$.

Reactant	T (K)	k [a] ($cm^3\ s^{-1}$)	Method [b]	Reference
C	4400 - 13000	5±2.5(-10)exp(-151/RT) [c]	ST/ES	[3.23]
O	298	2.1 (-11) (0 - 6) 1.05 (-10) (7)	FP/AS	[3.10]
H_2	300	1.6±0.3 (-14) (0) 3.0±0.4 (-14) (1)	LP/LIF	[3.11]
N_2	300	No reaction (0) 1.5±0.6 (-15) (1)	LP/LIF	[3.11]
CO	300	No reaction (0) 1.3±0.4 (-12) (1)	LP/LIF	[3.11]
NO	300	1.6±0.3 (-13) (0) 5.6±0.8 (-11) (1) 6.2±1.0 (-11) (2)	LP/LIF	[3.12]
H_2O	296	5 (-13)	FP/AS	[3.35]
HCN	300	1.8±0.6 (-14) (0) 4.0±0.5 (-13) (1)	LP/LIF	[3.11]
CO_2	300	2.3±0.4 (-14) (0) 4.0±0.4 (-14) (1)	LP/LIF	[3.11]
CNCl	296	2.5 (-15)	FP/AS	[3.35]
C_2H_2	294	2.3±0.1 (-10)	LP/LIF	[3.31]
C_2N_2	301 300	3.6 (-15) (0) 1.1±0.1 (-13) (1)	FP/AS LP/LIF	[3.35] [3.11]
CH_4	300	5.6±0.3 (-13) (0) 8.4±0.3 (-13) (1)	LP/LIF	[3.11]
C_2H_4	294	2.7±0.1 (-10)	LP/LIF	[3.31]
C_2H_6	294	2.9±0.1 (-11)	LP/LIF	[3.31]
C_3H_6	294	2.3±0.3 (-10)	LP/LIF	[3.31]
C_4H_6	300	2.8 (-10)	PR/AS	[3.36]
C_6H_6	300	4.3 (-10)	PR/AS	[3.36]

a) First parenthetical figure is base ten exponent. Second parenthetical figure, if present, is value of υ''; $\upsilon'' = 0$ otherwise.

b) FP - flash photolysis; LP - laser photolysis; PR - pulse radiolysis; ST - shock tube; AS - absorption spectroscopy; ES - emission spectroscopy; LIF - laser-induced fluorescence.

c) Activation energy E_A (kJ mol^{-1}) estimated semi-empirically. $R = 8.314 \times 10^{-3}$ kJ K^{-1} mol^{-1}.

Prior to the present work, the only reaction of CN with atoms which had been studied in detail is that with ground-state atomic oxygen

$$CN\ (v'')\ +\ O(^3P)\ \rightarrow\ CO\ (v')\ +\ N\ (^4S,^2D) \qquad (1)$$

Following the initial work of Boden and Thrush [3.13], Wolfrum and co-workers have reported several studies of reaction (1) [3.10, 3.14 - 16] including measurements of k_1 based on the disappearance of CN (v'') [3.10] as well as on the formation of both CO(v') and N [3.16], using kinetic absorption spectroscopy. Energy distributions in the CO product were also studied using a CO laser to probe the individual vibrational levels, and branching ratios for the formation of ground- and excited-state N atoms were determined [3.15]. No effect of vibrational excitation upon k_1 ($= 2 \times 10^{-11}$ cm^3 s^{-1}) was observed for $v'' = 0$ to 6, but a marked increase occurred at $v'' = 7$ ($k_1 = 1 \times 10^{-10}$ cm^3 s^{-1}) [3.10]. This result was interpreted in terms of a late barrier for the alternative endothermic channel

$$CN\ (v''\ =7)\ +\ O\ \rightarrow\ NO\ (v')\ +\ C\ (^3P),\ \Delta H_r = +138\ \text{kJ mol}^{-1} \qquad (1a)$$

The analogous reaction of ground-state CN with nitrogen atoms

$$CN\ +\ N(^4S)\ \rightarrow\ \text{products}, \qquad (2)$$

has been proposed as an important step in the decomposition of organic compounds in the presence of active nitrogen. Early workers [3.17, 3.18] postulated a variety of mechanisms to account for the behaviour of the CN emission which was found to be the major component in the characteristic flames observed in such mixtures. This emission was proposed to arise from electronically excited CN formed either directly by reaction of N atoms with CN_2 [a)] [3.17]:

$$N\ +\ CN_2\ \rightarrow\ CN^*\ +\ N_2,$$

or by collision of ground-state CN with an excited nitrogen molecule [3.18]:

$$N\ +\ CN_2\ \rightarrow\ CN\ +\ N_2^*$$

$$N_2^*\ +\ CN\ \rightarrow\ CN^*\ +\ N_2$$

In each case the CN_2 was assumed to be formed by the reaction

$$CN\ +\ N\ (+\ M)\ \rightarrow\ CN_2\ (+\ M)$$

---

a) formulated as either CNN or NCN

More recently Safrany and Jaster have made a detailed study of the reactions of organic molecules with active nitrogen [3.19, 3.20] in which they found that a branched chain mechanism based around the steps

$$CN + N \rightarrow N_2 + C, \qquad \Delta H_r = -191 \pm 11 \text{ kJ mol}^{-1} \qquad (2b)$$

$$C + C_2N_2 \rightarrow C_2N + CN, \qquad -35 \pm 140 \text{ kJ mol}^{-1} \qquad (3)$$

$$N + C_2N \rightarrow 2CN, \qquad -159 \pm 148 \text{ kJ mol}^{-1} \qquad (4)$$

could account for their observations on the decomposition of hydrogen-deficient species such as C_2H_2 and HCN, as well as C_2N_2 itself. In this mechanism CN_2 was considered to be unimportant, the chain carriers being CN, C atoms and C_2N. The presence of C_2N was inferred from the observation of its dimer dicyanoacetylene $C_2(CN)_2$, among the reaction products, along with a carbon-rich polymer. Indirect evidence for the presence of C atoms generated by reaction (2b) was also obtained from inhibition and quenching experiments using additives such as O_2 and N_2O, the results of which could be explained in terms of reactions of the additive with C atoms competing effectively with reaction (3).

In a subsequent study by Kley *et al.* [3.21] of the reactions of HCN, C_2N_2 and several hydrocarbons with active nitrogen, C atoms were detected directly using vacuum ultraviolet absorption spectroscopy, and their concentration was shown to be large relative to those of other reactive species. These observations strongly support the operation of reaction (2b) in the active nitrogen/organic system.

Both reaction (2b) and its carbon atom analogue

$$CN + C \rightarrow C_2 + N \qquad (5)$$

have been included in a chain mechanism for the dissociation of CN formed in shock-tube experiments on mixtures of BrCN or C_2N_2 with argon. Fairbairn [3.22] detected emission from C, CN and C_2, while in a more detailed investigation Slack [3.23] observed the C_2 and CN emissions and derived semi-empirical Arrhenius parameters for the rate coefficients k_{2b} and k_5 in the temperature range 4400 - 13000 K. The initial aim of the present work was to measure the rate coefficient of reaction (2b) at room temperature and to determine the effect, if any, of vibrational excitation of the CN radical on this parameter.

In the absence of a previous measurement of k_{2b} at this temperature the reaction

$$CN + O_2 \rightarrow \text{products} \qquad (6)$$

was also studied to check the reliability of the LP/LIF experiment. Five previous measurements of k_6 near 300 K have been reported. These are summarised in Table 3-2 together with two results obtained at higher temperatures. Two of the room temperature studies [3.10, 3.24] included measurements of k_6 as a function of the CN vibrational state, but the results obtained were conflicting. However, the overall agreement among the various k_6 values is reasonably good in view of the variety of experimental methods used. In this work the value of k_6 was determined for the $v'' = 0$ and $v'' = 1$ levels of ground-state CN. This work has been previously reported as reference [3.0].

3.2 Experimental

The photolysis cell, shown in Fig. 3.1, was made from a 250 cm^3 bulb as described in Section 2.1 C. A Woods horn was incorporated to reduce internal scattering. The windows used were of magnesium fluoride.

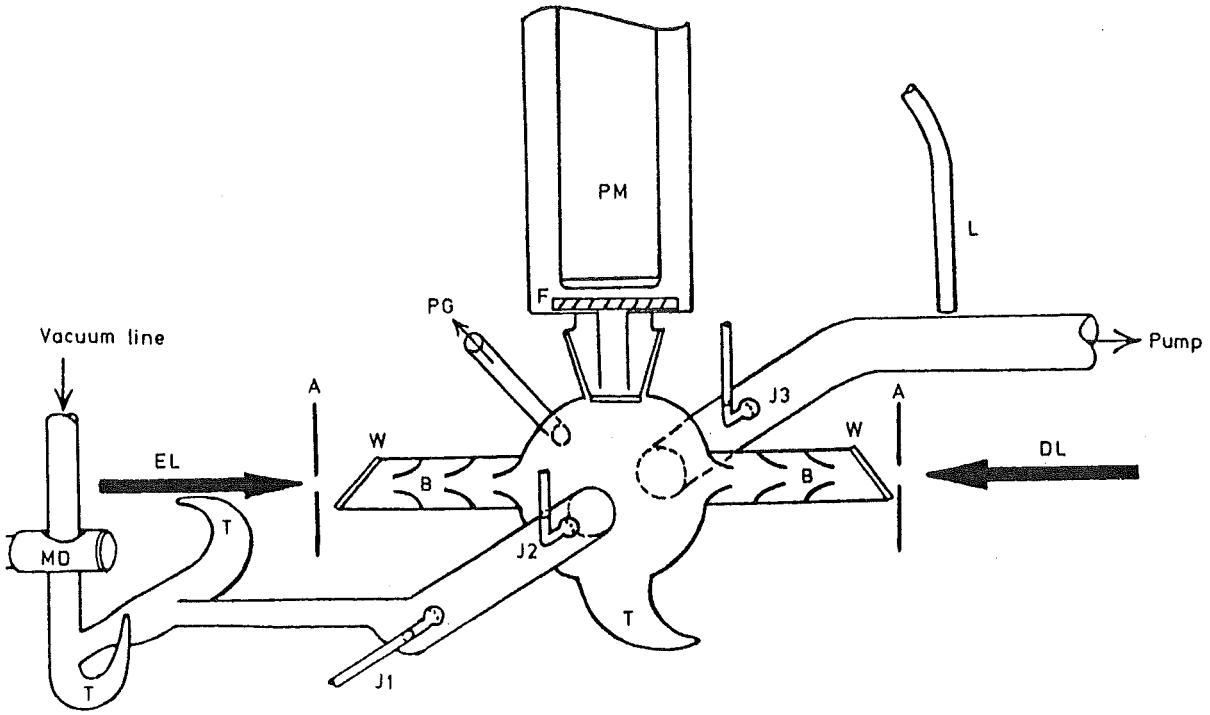

FIGURE 3.1: Schematic diagram of the photolysis cell.

Key: A - aperture; B - stray-light baffle; DL - dye laser beam; EL - excimer laser beam; F - filter; J1 and J3 - NO inlet jets; J2 - C_2N_2 inlet jet; L - light pipe for photometric titrations; MD - microwave discharge head; PG - pressure gauge; PM - photomultiplier in housing; T - light traps; W- MgF_2 windows.

CN radicals were generated by 193 (ArF) excimer laser photolysis of mixtures containing C_2N_2, an inert carrier gas and either O_2 or nitrogen atoms, produced as described in Section 2.1 E. At a repetition rate of 28 Hz, the effective pulse energy after spatial filtering of the focussed beam was estimated to be around 50 mJ. Helium, argon and nitrogen carriers were used, the total pressure varying between 1.2 and 3.5 Torr. Reactant concentrations were determined as described in Section 2.4. All measurements were made at ambient temperature (300 ± 2 K).

Probe wavelengths corresponding to the (0,0), (0,1) and (0,2) vibrational bands of the CN violet ($B^2\Sigma^+$) - ($X^2\Sigma^+$) system were obtained from the dye laser using BBQ, S420 and C460 dye solutions, respectively (see Table 2-2). Fig. 3.2 shows representative laser excitation spectra of these three bands produced by scanning the dye laser wavelength using the synchronous motor, and monitoring the total fluorescence

TABLE 3-2: Kinetic data for the reaction CN(v'') + O_2 → products.

Year	T (K)	A (10^{-11} cm^3s^{-1})	E_A (kJ mol^{-1})	k (rt) [a] ($10^{-11}cm^3s^{-1}$)	Method [b]	Reference
1962	296	-	-	0.91	FP/AS	[3.35]
1965	rt	-	-	0.76	FP/AS	[3.37]
1968	687	-	~0 [c]	0.73	DF/AS	[3.13]
1972	303,375	-	~0.75	1.12±0.03 incr. to 1.9 ±0.6 (4)	PR/AS	[3.24]
1973	298	-	-	1.05 (0) decr. to 0.26 (7)	FP/AS	[3.10]
1975	275-398	5.31	4.2±1.2	1.00	FP/AS	[3.16]
1975	~1500	10 [d]	~7 [e]	0.6	Fl./MS	[3.8]
1983	300±2	-	-	1.27±0.23 (0,1)	LP/LIF	This work
1984	~2400	-	0 [f]	0.80+0.68,-0.31	ST/AS	[3.30]
1984	300	-	5.9 [g]	2.0±0.1 (0); 2.4±0.1 (1)	LP/LIF	[3.11]
1985	294	-	-	2.5±0.2	LP/LIF	[3.31]
1986	rt	-	-	1.9±0.1	LP/LIF	[3.32]

a) Parenthical figure, if present, is value of v'' ; v'' = 0 otherwise. rt - room temperature.

b) FP - flash photolysis; DF - discharge-flow; PR - pulse radiolysis; Fl. - flame; LP - laser photolysis; ST - shock tube; AS - absorption spectroscopy; LIF - laser-induced fluorescence; MS - mass spectrometry. c) Estimated by comparison with [3.37]. d) Estimated.

e) Chosen to agree with [3.24] at 375 K. g) Estimated assuming gas-kinetic A factor.

f) Recommended T -independent value for T = 300 - 2400 K from consideration of earlier work.

intensity, with a minimum delay between the photolysis and probe pulses. The band origin and head wavelengths were assigned using the data of Pearse and Gaydon [3.25] and LeBlanc [3.26]. The rotational distribution in each violet-degraded band is essentially thermal, as expected for the 20 μs probe delay period and high pressure (*ca.* 1 Torr C_2N_2) used. As a result of the low population of the $v'' = 2$ state at room temperature, a C_2N_2 pressure of around 0.2 Torr was required for observation of the (0,2) band. However for kinetic measurements on the CN(v'') + N reaction, an upper limit of *ca.* 5×10^{-4} Torr was imposed on the C_2N_2 pressure by the need to avoid depletion of the N atoms by reaction with C_2N_2, which was found to become significant at N atom concentrations greater than 10^{14} cm^{-3}. Thus the kinetic studies were restricted to the reactions of CN($v'' = 0, 1$). For these experiments the dye laser was tuned to the intensity maximum in the unresolved P-branch of the appropriate band.

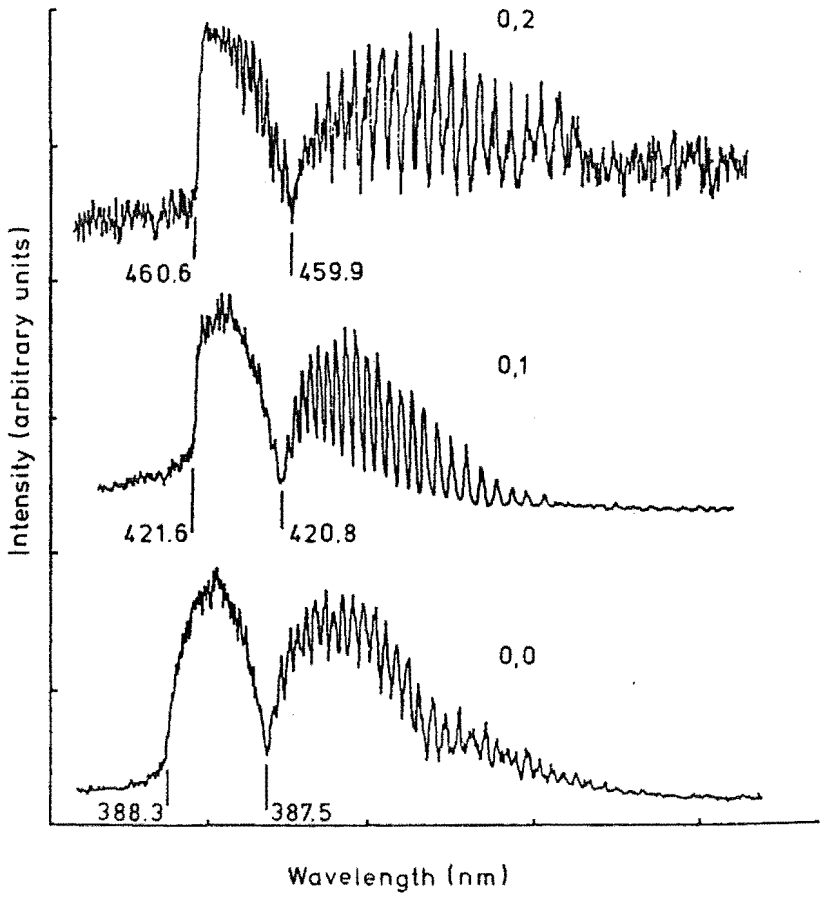

FIGURE 3.2: Fluorescence excitation spectra of the CN($B^2\Sigma^+ \leftrightarrow X^2\Sigma^+$) band system. The first three bands in the (0,υ") series are shown.

The CN fluorescence was isolated by a CORNING CS5-58 filter and observed with an EMI 9813QB photomultiplier whose preamplified output was taken to the boxcar. The timebase used varied from 0.1 to 0.5 ms, the scan window beginning at Δt = 20 μs to avoid the intense prompt emission following the photolysis pulse. A typical experiment consisted of 4 scans over the timebase window, each scan comprising 20 data points with 4 individual samples of the boxcar output being taken at each point.

3.3 Results and Discussion

A. The Reaction CN (v'' = 0) + O_2 → products

Representative semilogarithmic plots of CN fluorescence intensity against probe laser delay time, obtained for CN (v'' = 0) in the presence of varying O_2 concentrations, are shown in Fig. 3.3. The linearity of these plots confirms that radical removal occurs by a first-order process. In Fig. 3.4 the corrected pseudo-first-order rate

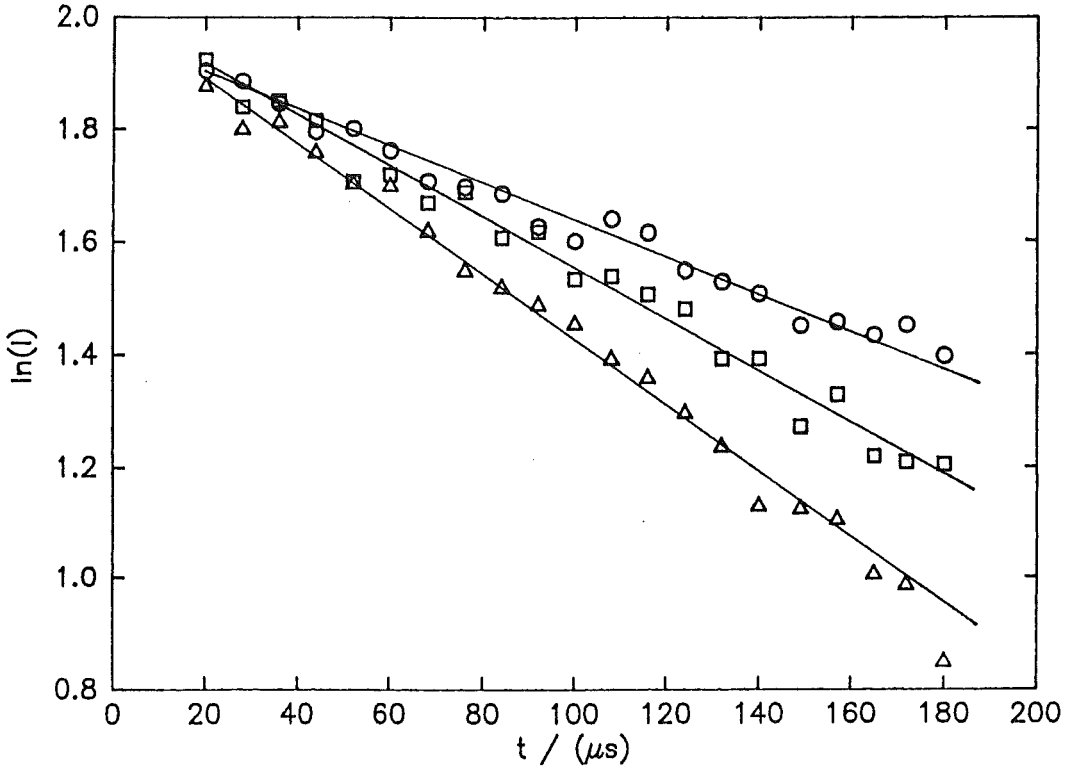

FIGURE 3.3: CN + O_2 → products: representative first-order decays of CN LIF intensity with time.

Circles, [O_2] = 0 cm^{-3}; squares, [O_2] = 1.68 x 10^{14} cm^{-3}; triangles [O_2] = 3.32 x 10^{14} cm^{-3}.

coefficients k_1 (see Section 2.4) are plotted as a function of the O_2 concentration for both the $v'' = 0$ and $v'' = 1$ levels of CN. A least-squares regression analysis applied to the data for each level separately gave k_6 ($v'' = 0$) = $(1.35 \pm 0.20) \times 10^{-11}$ cm^3 s^{-1} and k_6 ($v'' = 1$) = $(1.25 \pm 0.32) \times 10^{-11}$ cm^3 s^{-1}, where the uncertainties represent the sum of 90 % confidence limits from Student's t -testing of the regression results and experimental uncertainties amounting to *ca.* ± 5 %. A global fit to all the data gave k_6 ($v'' = 0,1$) = $(1.27 \pm 0.23) \times 10^{-11}$ cm^3 s^{-1}.

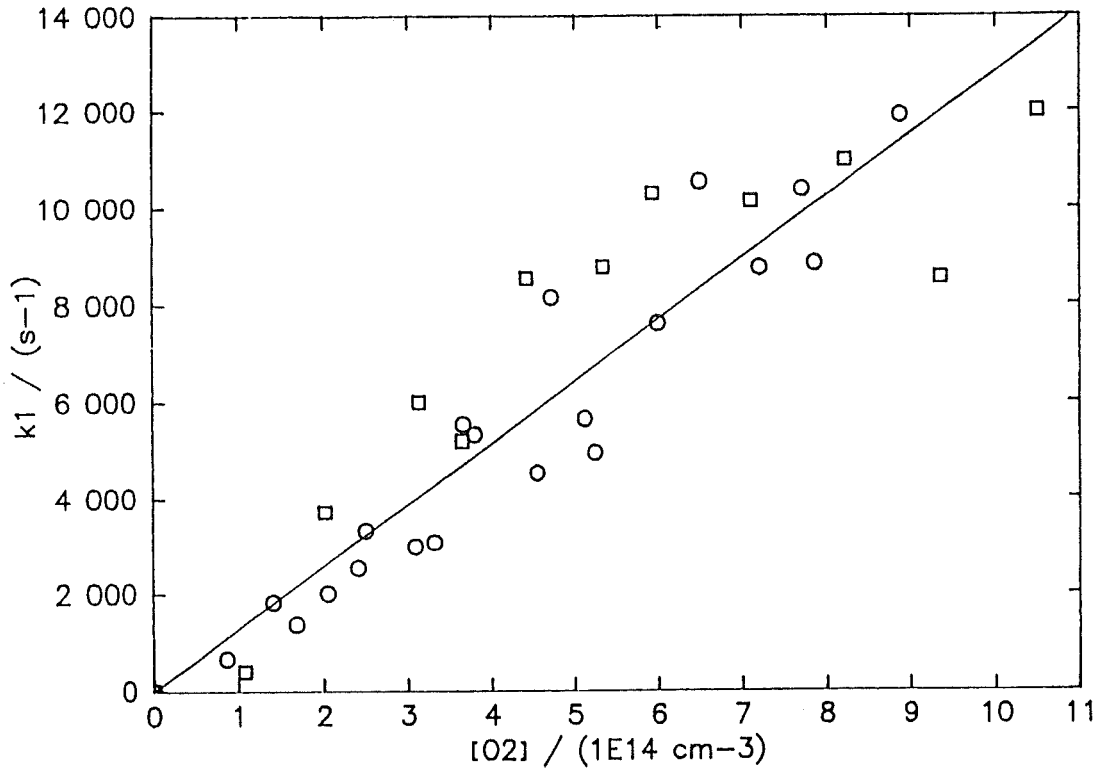

FIGURE 3.4: CN(υ'') + O_2 → products: plot of pseudo-first-order decay rates k_1 *vs.* [O_2] to determine k_6.

Circles, υ'' = 0 data; squares, υ'' = 1 data. Solid line is least-squares regression line for υ''=(0,1) data.

These results are in good agreement with those obtained by previous workers (see Table 3-2) and although the values of k_6 for $v'' = 0$ and $v'' = 1$ overlap within their combined error limits, there is at least a suggestion of a decrease in k_6 with increasing v''. This is in accord with the findings of Wolfrum *et al.* [3.10] who found that k_6 decreased monotonically from k_6 ($v'' = 0$) = 1.05×10^{-11} to k_6 ($v'' = 7$) =

2.6×10^{-12} cm^3 s^{-1}, with $k_6 (v'' = 1) \approx 9 \times 10^{-12}$ cm^3 s^{-1}, although they did not provide uncertainty limits for these results, while in an earlier study Boden and Thrush [3.13] failed to find evidence for any effect of vibrational excitation. In contrast, Bullock and Cooper [3.24], using pulse radiolysis to generate the radicals, observed an increase in k_6 by a factor of about two over the range $v'' = 0$ to $v'' = 4$. This result was explained in terms of the formation of an NC-OO collision complex in which vibrational energy transfer from the C-N to the O-O band increased the efficiency of formation of the products OCN + O [a]. Arguments based on the effective use of vibrational energy in overcoming the activation barrier, or an additional depletion of states having $v'' > 0$ by vibrational quenching, were rejected in view of the known low E_A (4.2 ± 1.4 kJ mol^{-1} [3.16]) for reaction (6) and the large (488 cm^{-1}) difference between the vibrational frequencies of CN and O_2. The effect of vibrational energy on the A factor for reaction (6) could also be discounted.

The observation of a decrease in k_6 with increasing v'' can be explained most simply in terms of repopulation of the vibrational level in question by cascade processes occurring on a time scale similar to that of the reaction. Jackson and Halpern [3.24] have demonstrated that two-photon absorption by C_2N_2 at 193 nm can be expected with focussed pulses at energies as low as 25 mJ and that the resulting CN radicals are formed in a range of electronic and vibrational excited states.Thus under the conditions used in these experiments cascade processes are likely to have been significant. A similar argument may be applied to the results of Wolfrum *et al.* in view of the broad bandwidth of their argon photolysis lamp, while those of Boden and Thrush may have been affected by optical pumping of CN by the continuous source used for absorption measurements. It should be noted that the effect of such processes will be greater for states having high v'' due to their much smaller initial populations. At the much higher pressures used in pulse radiolysis experiments, thermalisation of the CN vibrational distribution would occur on a much shorter time scale (< 50 ns [3.24]) so that no effect of cascading would be observed.

B. <u>The Reaction CN + N → N_2 + C</u>

Initial experiments on this system using a 0.5 ms time scale yielded $ln (I_f)$ - *vs* - time plots such as those shown in Fig. 3.5 for the CN ($v'' = 0$) state. These plots exhibit an upward curvature at long times. In the case of runs with [N] = 0 the deviation

---

[a] Two exothermic product channels exist for reaction (6). The branching factors ϕ have been measured by Wolfrum *et al.* [3.15] who found $\phi = 0.94 \pm 0.02$ for reaction leading to OCN + O ($\Delta H_f = -27 \pm 21$ kJ mol^{-1}), and $\phi = 0.06 \pm 0.02$ for CO + NO products ($\Delta H_f = -455 \pm 11$ kJ mol^{-1}).

from linearity may be due to contributions from higher order CN removal processes. However in experiments with N atoms present the curvature is much more pronounced and may be attributed to repopulation of the CN ground state. Since for the $v'' = 0$ level the effect of cascading will be small, this repopulation must be due to regeneration of CN by secondary reactions such as reactions (3) and (4). To avoid errors arising from this effect a 0.1 ms time scale was used in all subsequent experiments to measure k_{2b}, from which linear $ln\,(I_f)$ - *vs* - t plots were obtained, e.g. Fig. 3.6.

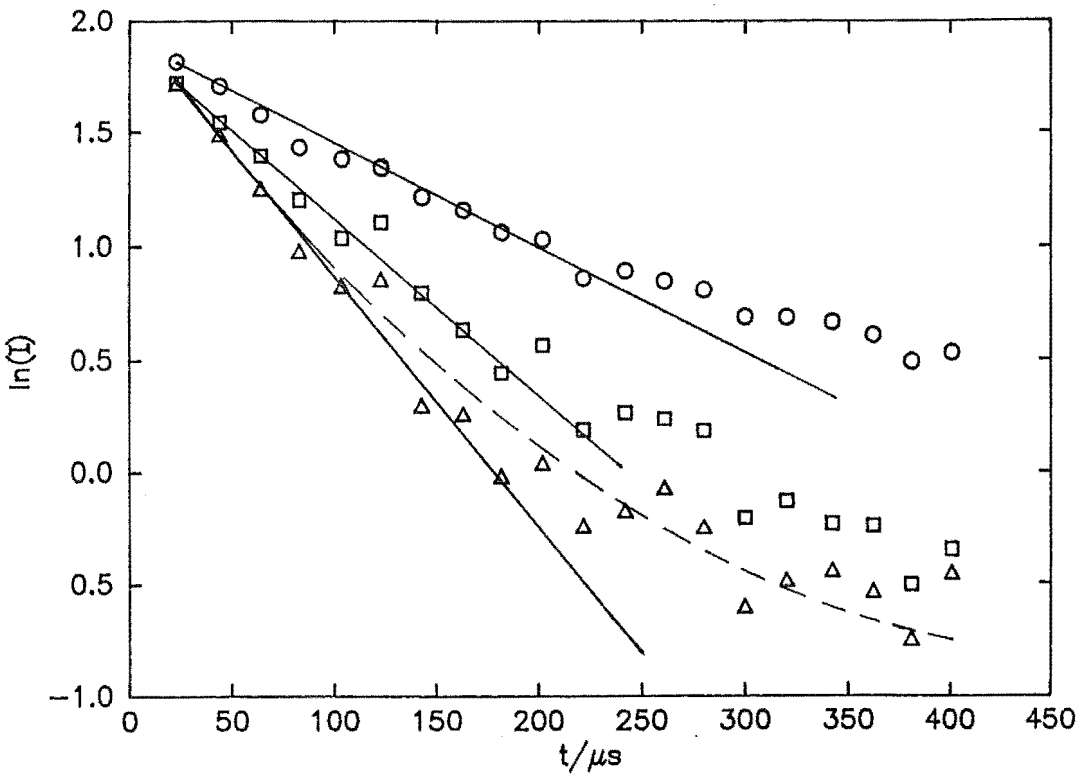

FIGURE 3.5: CN + N → N_2 + C: representative first-order decays of CN LIF intensity with time for long reaction times.

Note deviations from linearity beyond $t \approx 200$ - 300 μs. Circles, [N] = 0 cm^{-3}; squares, [N] = 2.5 x 10^{13} cm^{-3}; triangles, [N] = 7.8 x 10^{13} cm^{-3}. Broken curve is simulated decay for [N] = 7.8 x 10^{13} cm^{-3} with k_3 = 3 x 10^{-11} cm^3 s^{-1}.

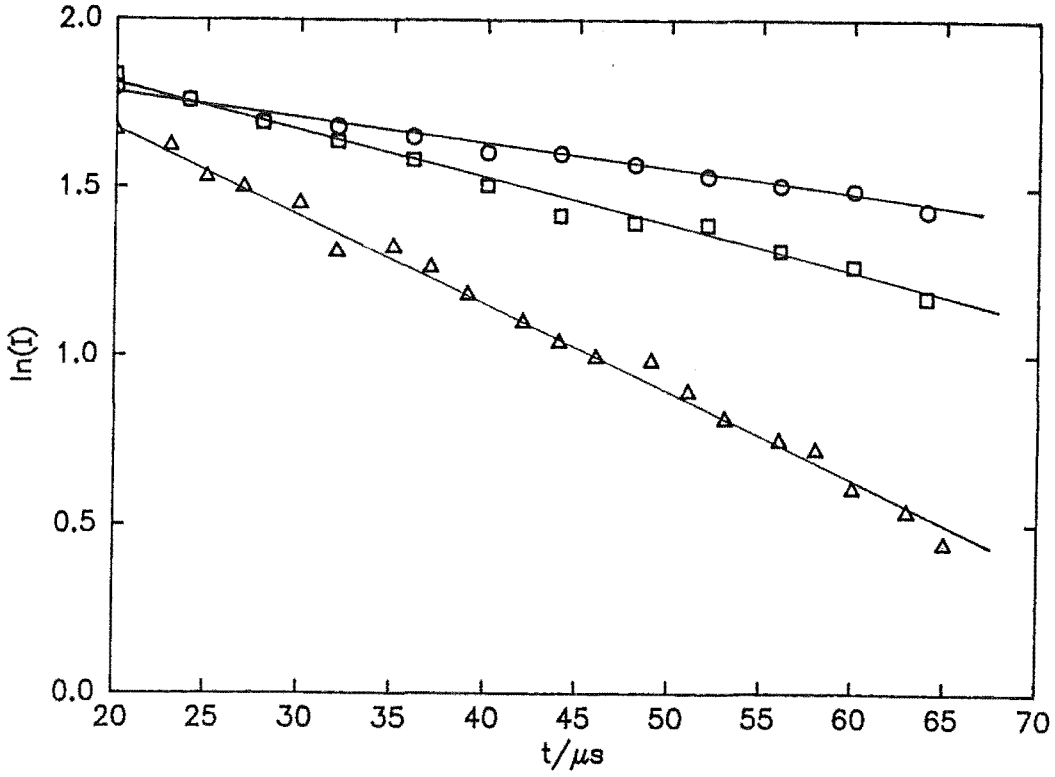

FIGURE 3.6: CN + N → N_2 + C: representative first-order decays of CN LIF intensity with time for short reaction times.

Circles, [N] = 0 cm^{-3}; squares, [N] = 0.92 x 10^{14} cm^{-3}; triangles, [N] = 2.06 x 10^{14} cm^{-3}.

A further restriction on the experimental conditions was imposed by the observation of a strong inverse dependence of the values of k_{2b} on the C_2N_2 concentration. This dependence appeared as a marked downward curvature of the k_1' - *vs* - [N] plot occurring at values of [N] greater than 1 x 10^{14} cm^{-3}, as shown in Fig. 3.7 for CN(v'' = 1). This effect could be readily explained in terms of a reaction between C_2N_2 and N atoms, occurring between the C_2N_2 inlet and the viewing region, which depleted the N atom concentration relative to that determined by the NO titrations which were performed with C_2N_2 absent. A series of measurements of k_{2b} made at varying C_2N_2 concentrations showed that for values of [C_2N_2] less than ca 1.5 x 10^{13} cm^{-3}, no curvature of the k_1' (or k_1) - *vs* - [N] plots occurred for N atom concentrations up to 2 x 10^{14} cm^{-3}. Thus by introducing low concentrations of C_2N_2 near to the viewing region the consumption of N atoms by the reaction

$$C_2N_2 + N \rightarrow \text{products} \qquad (7)$$

could be effectively suppressed and the value of k_{2b} could be obtained from plots such as Fig. 3.8 which contains data for both the $v'' = 0$ and $v'' = 1$ levels of CN.

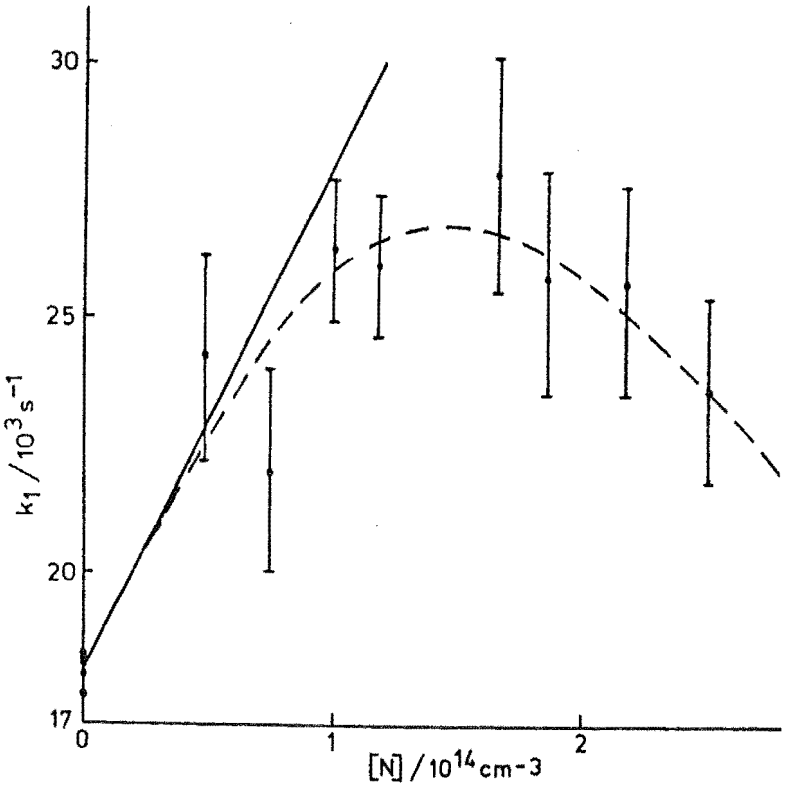

FIGURE 3.7: CN(v"=1) + N→ N_2 + C: plot of pseudo-first-order decay rate k_1 *vs.* [N] at high C_2N_2 concentration (2.5 x 10^{13} cm^{-3}).

Solid line, $k_{2b} = dk_1 / d[N] = 1.00 \times 10^{-10}$ cm^3 s^{-1}. Deviation at [N] > 10^{14} cm^{-3} is attributed to depletion of N atoms by reaction with C_2N_2.

The least squares regression analysis of this data gave k_{2b} ($v'' = 0$) = (9.92 ± 0.49) x 10^{-11} cm^3 s^{-1} and k_{2b} ($v'' = 1$) = (9.80 ± 0.62) x 10^{-11} cm^3 s^{-1}. A global fit to all the available data gave k_{2b} ($v'' = 0,1$) = (1.00 ± 0.05) x 10^{-10} cm^3 s^{-1}, the uncertainty being the 90 % confidence limit on the regression slope. Addition of an estimated ± 8 % for systematic uncertainties yields a final value of k_{2b} ($v'' = 0,1$) = (1.00 ± 0.13) x 10^{-10} cm^3 s^{-1} at 300 K.

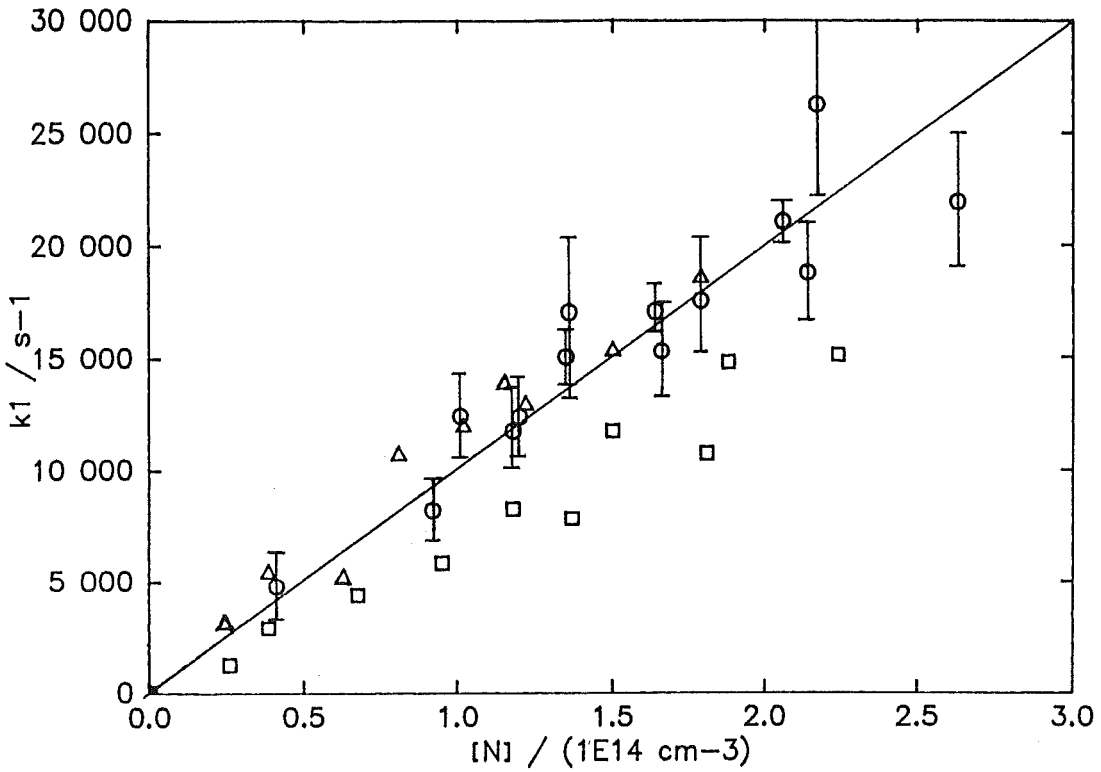

FIGURE 3.8: CN(υ") + N → N_2 + C: plot of pseudo-first-order decay rates k_1 *vs.* [N] to determine k_{2b} .

Circles, υ" = 0 data; triangles, υ" =1 data; squares υ" = 0 data obtained at $[C_2N_2] = 3 \times 10^{13}$ cm^{-3}, not included in regression analysis due to depletion of [N] by reaction with C_2N_2. Solid line is least-squares regression line for υ" = (0,1) data.

The only previous measurement of k_{2b} was obtained indirectly by Slack in a shock-tube study of the dissociation of CN [3.23]. These experiments spanned the temperature range from 4400 to 13000 K and revealed only a weak temperature dependence of k_{2b}. As this dependence could not be determined unambiguously by matching of numerically simulated CN concentration profiles to the time-resolved CN and C_2 emission data, an Arrhenius activation energy E_A was estimated at 38 kJ mol^{-1} using a semi-empirical method due to Hirschfelder [3.28], with the resulting expression

$$k_{2b} = (7.3 \pm 3.3) \times 10^{-10} \exp(\frac{-38000}{RT}) \qquad (8)$$

being preferred to a temperature-independent rate coefficient, particularly at temperatures outside the range covered by the shock-tube experiment. At 300 K, however, the rate coefficient predicted from equation (8) is lower, by a factor of almost 10^6, than the measured value of 1.00×10^{-10} cm^3 s^{-1}. However this discrepancy may not be as significant as it appears, in view of both the insensitivity of the calculated [CN] and [C_2] decay profiles in [3.23] to the choice of k_{2b}, and the uncertainty in the estimation of E_A. (For reactions of H atoms the calculated E_A's are larger than experimental values by as much as a factor of 2 [3.28]. However for the present reaction, greater deviations from the simple model may be expected as a result of the presence of multiple bonding, steric effects and the breakdown of the "constant percentage Coulombic interaction" assumption implicit in the method.) Using the present value of k_{2b} at 300 K together with values obtained from the limits of eq. (8) at 8000 K to calculate a new set of Arrhenius parameters gives

$$k_{2b} = 4.4 \times 10^{-10} \exp\left(\frac{-3700 \pm 1500}{RT}\right). \qquad (9)$$

This represents a ten-fold decrease in the barrier height relative to that obtained by Slack; the barrier height is now of the order of k_BT at 300 K within error. Such a low barrier would be expected if the reaction proceeds *via* a transient CNN (or NCN) complex.

In this case the absence of any effect of vibrational energy on k_{2b} is not surprising. On the other hand, if in fact E_A was as large as was estimated by Slack (and this must surely be an upper limit in view of the very low value of k_{2b} (300 K) predicted by eq. (8)), then the present observation of no vibrational enhancement of k_{2b} suggests an early barrier to the reaction, since 38 kJ mol^{-1} represents approximately 1.5 vibrational quanta for CN (ω_e = 2069 cm^{-1}). In this case the reaction would be the direct abstraction of N from CN, and would lead to the formation of vibrationally excited N_2 for which v' up to 6 would be energetically allowed for reaction of CN(v''=0) (see Fig. 3.9). However, since CNN and NCN are both strongly bound relative to N + CN and correlate with the products, formation of a complex would seem to be the preferred mode of CN removal.

Consideration of Fig. 3.9 also shows that there is no possibility of an additional product channel opening up at higher v'' levels as was suggested for the CN(v'') + O(^{3}P) reaction [3.10]. From the correlation diagram in Fig. 3.9 it can be seen that while reaction (2b) is exothermic for production of the C atom in both its ground and first excited states and a third channel becomes energetically allowed above the v'' = 3 level of CN, production of excited C atoms violates spin conservation so that these processes would be slow. An effect of increased vibrational energy on the A factor, *via*

the CN collision diameter, is also unlikely to be significant due to the small anharmonicity of the CN ground state [3.29].

In order to investigate the behaviour of the C_2N_2 - active nitrogen system at longer reaction times, a series of computer simulations were carried out by Professor L. F. Phillips. Numerical integration of the rate equations for a simple mechanism consisting of the three reactions (2b), (3) and (4) together with diffusive loss rates for the chain carriers CN and C was found to be sufficient to reproduce the curvature of $ln\ (I_f)$ - vs - time plots obtained using the 0.5 ms time scale as shown in Fig. 3.5. The diffusion rate of 3300 s^{-1} for CN loss from the viewing region was the experimentally observed value in 3.4 Torr of He buffer; this figure was scaled by a factor of $1.47 = (\frac{m_{CN}}{m_C})^{0.5}$ to obtain the corresponding value for C atoms. In these simulations the rate coefficient for reaction (4) was set equal to the measured value of k_{2b}. This value is likely to be appropriate for an exothermic reaction between radicals.

The full curve in Fig. 3.5 is the $ln\ (I_f)$ - vs - t profile calculated for the given values of $[C_2N_2]$ and [N], and an assumed initial CN concentration of 1×10^{11} cm^{-3}. The best fit to the long-time $ln\ (I_f)$ - vs - t data gave a value for k_3 of *ca.* 3×10^{-11} $cm^3\ s^{-1}$. Variation of k_3 by more than a factor of two in either direction gave a noticeably poorer fit to the measured [CN] profiles. ΔH_r for reaction (3) is calculated to be -35 ± 140 kJ mol^{-1}, the large uncertainty arising from the uncertainty in the estimated heat of formation for C_2N ($\Delta H_f = 556 \pm 126$ kJ mol^{-1}). The finding that reaction (3) is fast suggests a value for ΔH_f near the bottom of the indicated range.

3.4 **Summary**

The LP/LIF technique has been used to study the reactions of ground state CN with O_2 and N atoms. For the reaction with O_2, the measured bimolecular rate coefficients k_6 ($v'' = 0$) = $(1.35 \pm 0.20) \times 10^{-11}$ $cm^3\ s^{-1}$ and k_6 ($v'' = 1$) = $(1.25 \pm 0.32) \times 10^{-11}$ $cm^3\ s^{-1}$ are in good agreement with previous results obtained using similar techniques, although these values probably represent lower limits to k_6 due to the likely presence of cascade processes.

For the CN + N reaction, no effect of vibrational excitation of CN was observed on the rate coefficient, with k_{2b} ($v'' = 0,1$) = $(1.00 \pm 0.13) \times 10^{-10}$ $cm^3\ s^{-1}$. The Arrhenius expression $k_{2b} = 4.4 \times 10^{-10} \exp(\frac{-3700 \pm 1500}{RT})$ has been derived by combining the above result with a previous one obtained at a high temperature. The implications of these results have been discussed. The rate coefficient $k_3 \approx 3 \times 10^{-11}$

$cm^3\ s^{-1}$ has been estimated for the reaction between C atoms and C_2N_2 from computer modelling of the C_2N_2/active nitrogen system.

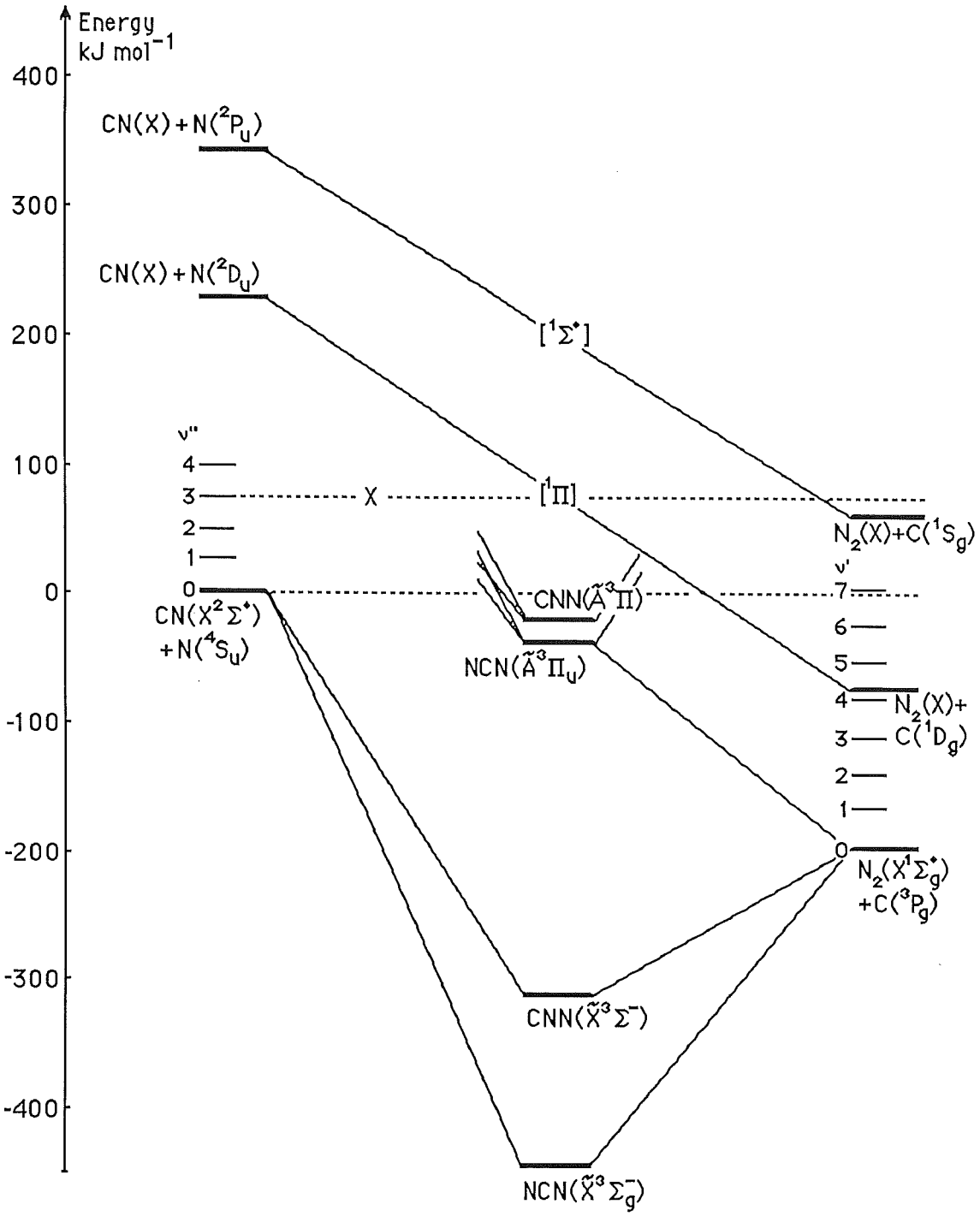

FIGURE 3.9: Correlation diagram for the reaction CN + N → N_2 + C.

(Relative energy data and electronic state assignments taken from references [3.38] - [3.40]).

3.5 Epilogue

Since the completion of this study several further investigations of the kinetics of the CN + O_2 reaction have been reported [3.11, 3.30 - 32]. The rate coefficients obtained in these studies are listed in Table 3-2.

The existence of a low activation barrier for reaction (6) was confirmed by the shock-tube measurements of Louge and Hanson [3.30] who obtained a value of k_6 = 8 (+7, -3) x 10^{-12} cm^3 s^{-1} at T = 2400 K. On the basis of a survey of previous results, they recommended a value of k_6 = 9.3 (+5.5, -2.7) x 10^{-12} cm^3 s^{-1} over the range $300 \leq T < 2400$ K.

Li and co-workers [3.11] have carried out a detailed study of the reactions of CN($v'' = 0,1$) with a variety of small molecules using an LP/LIF technique similar to the one used in this work. For the CN(v'') + O_2 reaction, values of (2.0 ± 0.1) x 10^{-11} and (2.4 ± 0.1) x 10^{-11} cm^3 s^{-1} were obtained for k_6 ($v'' = 0$) and k_6 ($v'' = 1$) at T = 303 K and total pressures between 5 and 25 Torr. These results were analysed with reference to the energy-gap law [3.33, 3.34] to separate the effects of vibrational quenching from chemical reaction. It was concluded that a measurable enhancement of the reaction rate occurred on going to $v'' = 1$, although the effect of the 4.2 kJ mol^{-1} activation barrier ($\approx \frac{1}{6}\omega_e$) was not completely negated, a result consistent with an early barrier reaction. The measured k_6 values were larger than previously reported ones (including the present one) by factors of 2 - 3. This discrepancy was explained in terms of the presence of cascade processes in earlier experiments. In view of the high pressures and low laser pulse energy (1 mJ) used in the study of Li *et al.*, this argument may account for the difference between their and earlier flash photolysis results but does not explain the difference between their values and the high-pressure pulse radiolysis results of Bullock and Cooper [3.24]. This disagreement may be a result of the much larger energies involved in the pulse radiolysis experiment.

A similar study to that of Li *et al.* has been described by Lichtin and Lin [3.31] who used a very low-intensity quadrupled Nd:YAG laser (266 nm) to dissociate ICN, the resulting CN($v'' = 0$ only) being detected by LIF from both the A-X and B-X transitions. The resulting value of k_6 = (2.5 ± 0.2) x 10^{-11} cm^3 s^{-1} agrees well with that of Li *et al.* The lower laser frequency and pulse energies (50 μJ) and the higher pressures (up to 50 Torr) used would tend to suppress cascading effects still further.

The ICN precursor would also be expected to give rise to CN in a different distribution of excited states to that produced by photolysis of C_2N_2. The 25 % increase in k_6 relative to the value obtained by Li and co-workers may reflect these considerations.

The most recent experiment to date on the CN + O_2 reaction have been reported by de Juan *et al.* [3.32]. These workers have used the LIF technique to follow the reactions of CN(υ'' = 0, 1) produced by visible-light photolysis of NCNO in the presence of H_2, O_2, NH_3 and hydrogen halides. For CN + O_2, no effect of vibrational energy was observed on the measured rate coefficient k_6 = $(1.9 \pm 0.1) \times 10^{-11}$ cm^3 s^{-1}. Full details of these experiments have yet to appear, however.

It is clear from the foregoing summary that the value of k_6 is still in some doubt, as is the true nature of such vibrational effects as have been observed. A thorough study of the important reaction (6) over a wide range of temperatures, pressures and vibrational states is still awaited. A similar situation applies in the case of the much less studied reaction between CN and N atoms. It is likely that the LP/LIF technique will be of considerable value in future work on both of these systems.

CHAPTER 4

REACTIONS OF NH_2 WITH N ATOMS, NO AND NO_2

4.1 Introduction

The potential significance of the amidogen (NH_2) radical in chemical systems of practical importance was foreshadowed nearly fifty years ago in the results of a study by Bamford [4.1] of the ultraviolet photolysis of ammonia/nitric oxide and hydrazine/nitric oxide mixtures. Since then NH_2 has been assigned important roles in a variety of combustion processes [4.2 - 8] as well as in atmospheric chemistry [4.9 -11]. In attempting to construct mechanistic models for these processes, researchers have suggested numerous elementary reactions of NH_2, at the same time making important assumptions about the temperature and pressure dependences of their rates. Yet in spite of the obvious need for kinetic data on such reactions, only a small number have been studied in detail, especially when comparison is made with the amount of information available on the reactions of the isoelectronic species OH and CH_3 (see e.g. [4.12, 4.13]).

Table 4-1 contains a summary of previous kinetic studies of NH_2 reactions, from which it can be seen that of the 20 reactions listed only five have been studied directly more than three times, and of those only three (NH_2 + NO, NO_2 and O_3) may be considered to have well-established rate coefficients. Even for these reactions the values obtained using different methods of radical generation (e.g. flash photolysis, discharge-flow or pulse radiolysis) may differ by a factor of two.

The reactions of NH_2 with atomic species in particular have received little attention in the past. The reaction

$$NH_2 + H + (M) \rightarrow \text{products} \qquad (1)$$

has been shown to be an important process for the removal of NH_2 in the pulse radiolysis of ammonia [4.14 - 16], while the reaction

$$NH_2 + O \rightarrow \text{products} \qquad (2)$$

is likely to be significant in combustion systems containing NH_3 or N_2H_4 and oxygen and also, possibly, in the stratosphere where large yields of O atoms are produced by the ultraviolet photolysis of ozone [4.17] and NH_2 is formed by the photodissociation of NH_3 [4.10, 4.18]. However, while rate coefficients for these processes have been

TABLE 4-1: Rate coefficients for reactions of NH_2 ($\tilde{X}^2B_1$).

Reactant	T (K)	k a) b) ($cm^3\ s^{-1}$)	Method c)	Reference
H	349	2.7 (-11)	PR/AS/CS	[4.16]
N	296	1.21± 0.14 (-10)	LP/LIF	This work
O	298	3.5 (-12)	FP-DF/AS	[4.19]
NH	349	1.2 (-10)	PR/AS/CS	[4.16]
OH	300	≤ 1 (-13)	-	[4.12]
$O_2(^3\Sigma_g^-)$ d)	298	< 3 (-18)	-	[4.12]
$O_2(^1\Delta_g)$	300	1.0 (-14)	DF/LIF	[4.39]
NO d)	297	1.81± 0.12 (-11)	LP/LIF	This work
NH_2 d)	349	2.7 (-11)	PR/AS/CS	[4.16]
HO_2	298	3.4 (-11)	-	[4.12]
O_3 d)	rt	1.5±0.3 (-13) (0) 1.5±0.4 (-12) (1,2)	LP/LIF	[4.35]
NO_2 d)	294	2.11± 0.18 (-11)	LP/LIF	This work
PH_3	218-456	$1.52\pm0.16\ (-12)\ \exp(\frac{-7.7}{RT})$ e)	FP/LIF	[4.50]
C_2H_2	241-459	$1.1\pm0.4\ (-13)\ \exp(\frac{-11}{RT})$ e)	FP/LIF	[4.51]
C_2H_4	250-465	$3.4\pm0.1\ (-14)\ \exp(\frac{-15.4}{RT})$ e)	FP/LIF	[4.51]
N_2H_4	298	9.0±1.5 (-11) (1)	LP/LIF	[4.45]
CH_3NH_2	298	7.7±0.9 (-11) (1)	LP/LIF	[4.45]
C_3H_4	rt	≤ 8 (-16)	DF/LIF	[4.31]
C_3H_6	rt	≤ 1 (-15)	DF/LIF	[4.31]
n-C_5H_{12}	300	3.3 (-17)	DF/LIF	[4.39]

a) rt - room temperature.

b) First parenthetical figure is base ten exponent. Second parenthetical figure, if present, is NH_2 bending mode quantum number v_2'' ; v_2'' = 0 otherwise.

c) DF - discharge-flow; FP - flash photolysis; LP - laser photolysis; PR - pulse radiolysis; AS - absorption spectroscopy; LIF - laser-induced fluorescence; CS - computer simulation.

d) Studied 3 or more times. e) Activation energy E_A in kJ mol^{-1}. R = 8.314 x 10^{-3} kJ K^{-1} mol^{-1}.

obtained (see Table 4-1), only the O atom reaction (2) has been studied directly [4.19], most of the recent determination of the rate coefficient k_1 having been made in kinetically complex pulse radiolysis experiments [4.14 - 16]. In these studies k_1 has generally been

derived by fitting concentration profiles computed from a more or less arbitrary model mechanism to the experimental data; so far no unique representation of either the temperature or the pressure dependence of k_1 has emerged (see discussions in [4.16] and [4.20]).

The reaction

$$NH_2 + N \rightarrow \text{products} \qquad (3)$$

is of interest from several points of view. Early work on the reaction of ammonia with active nitrogen [4.21] indicated that little or no consumption of N atoms occurred in spite of the appreciable observed decomposition of NH_3. Later, however, Back and Salahub [4.22] carried out a study using isotopically-substituted ammonia ($^{15}NH_3$), in which they found essentially complete ($\gtrsim$ 98 %) conversion of the nitrogen from the decomposed $^{15}NH_3$ into $^{14}N^{15}N$. This result was taken to indicate the operation of the reactions

$$NH_2 + N \rightarrow N_2 + 2H, \qquad \Delta H_r = -227\pm7 \text{ kJ mol}^{-1} \qquad (3a)$$

and

$$NH + N \rightarrow N_2 + H, \qquad -632\pm17 \text{ kJ mol}^{-1} \qquad (4)$$

where the NH_2 and NH radicals were postulated to arise from reactions such as

$$N_2^* + NH_3 \rightarrow NH_2 + H + N_2 \qquad (5a)$$

$$N_2^* + NH_3 \rightarrow NH + H_2 + N_2 \qquad (5b)$$

Direct reactions between N atoms and NH_3 could be ruled out on grounds of endothermicity or violation of spin-conservation, while a reaction of excited nitrogen molecules with $^{15}NH_3$ leading to ca. 100 % efficient isotopic exchange would be very unlikely.

The reactions

$$NH_2 + N \rightarrow 2NH, \qquad \Delta H_r = +91\pm41 \text{ kJ mol}^{-1} \qquad (3b)$$

$$NH_2 + N \rightarrow N_2 + H_2, \qquad -663\pm7 \text{ kJ mol}^{-1} \qquad (3c)$$

as well as reaction (4), were subsequently included in a mechanism proposed by Kaskan and Hughes [4.4] to account for their observations of the behaviour of NH_3, NH, OH and NO in ammonia/oxygen flames. NH_2 was not detectable in this system, a result which was explained in terms of rapid equilibration among NH_i species leading to NH_2 concentrations below the detection limit of the multiple-pass absorption experiment. The reaction system was modelled using an electrical analogue of the mechanism (reduced to a

set of first-order processes). For many of the 26 reactions involved, including reactions (3b), (3c) and (4), no previous experimental kinetic data existed. In these cases the required rate coefficients were either taken from a compilation of theoretical estimates [4.23] or adjusted to fit the measured concentration profiles in the flame. Unfortunately the values obtained in this way for k_3 and k_4 were not given in [4.4].

The rate coefficients for the disappearance of the isoelectronic OH and CH_3 radicals in the presence of oxygen atoms have been measured [4.12] and are at least an order of magnitude larger than the value of k_2 obtained by Gehring *et al.* [4.19] (see Table 4-2). Similarly the reaction of OH with N atoms has been shown to be fast [4.12], while an estimate of the rate coefficient for the analogous reaction between CH_3 and N [4.24], based on indirect measurements of the activation energy and steric factor [4.25], is comparable to that found for the fast reactions (6) and (7) discussed below. Thus it would be of interest to measure the rate of reaction (3) to obtain further information regarding the apparently low reactivity of NH_2 with atomic species, while an investigation of the products would give an indication of the relative importance of the pathways (3a) - (3c) and hence whether the reaction proceeds directly or *via* formation of a bound complex, since the direct reaction (3c) is spin-forbidden. The aim of the present work was to measure the overall rate for reaction (3) and to determine whether NH is a primary product.

TABLE 4-2: Rate coefficient for reactions of OH,NH_2 and CH_3 radicals with O and N atoms.

R	R + O → products				R + N → products			
	Products	ΔH_r (kJmol^{-1})	k_O(298 K) (10^{-11}cm^{3}s^{-1})	k_{rel}	Products	ΔH_r (kJmol^{-1})	k_O(298 K) (10^{-11}cm^{3}s^{-1})	a) k_{rel}
OH	O_2 + H	-70.2	3.3 b)	9.4	NO + H	-203.4	4.9 b)	0.4 (1.5)
NH_2	HNO+H	-107.3	0.35 c)	1	N_2 +2H	-227	12.1 d)	1 (35)
	NH+OH	-46.9			NH+NH N_2 +H_2	91 -663		
CH_3	HCOH+H	-292.7	13 b)	37	HCN+2H	-47.2	2.2 e)	0.2 (0.2)

a) Figures in parenthesis are values of k'_{rel}, where $k'_{rel} = \frac{k_N\ (298\ K)}{k_O\ (298\ K)}$ for each R.

b) Ref. [4.12]. c) Ref. [4.19]. d) This work. e) Ref. [4.24].

Since there had been no previous direct measurement of k_3, it was decided to test the reliability of the experiment by measuring the rate coefficients for the reactions

$$NH_2 + NO \rightarrow \text{products} \qquad (6)$$

and $$NH_2 + NO_2 \rightarrow \text{products} \qquad (7)$$

both of which have been studied previously. From Table 4-3 it may be seen that the room temperature rate coefficients k_6 and k_7 are established to within a factor of about two, the variation apparently being a function of the experimental method used; there is also disagreement over the precise form of the observed negative temperature dependence of k_6 (see, e.g., [4.26]).

The reaction between NH_2 and NO (6) is the most-studied of all amidogen reactions and is currently of considerable interest due to its acknowledged roles in a number of practically important chemical systems, notably the production or destruction of nitric oxide in the atmosphere [4.9 - 12] and the patented "Thermal deNO_x" process for the selective reduction of nitrogen oxides in the exhaust gases from large-scale industrial combustion processes [4.6 - 8]. (This process involves the addition of controlled amounts of ammonia to flue gases in a well-defined 'temperature window' and can result in conversion of up to 90 % of NO to N_2.) The related reaction (7) has received much less attention but is known to be slightly faster than (6), with a similar weak negative temperature dependence of its rate coefficient, *viz.*

$$\frac{k_7\ (298\ \text{K})}{k_7\ (500\ \text{K})} \approx 2 \approx \frac{k_6\ (298\ \text{K})}{k_6\ (480\ \text{K})}\ , \qquad [4.26, 4.27].$$

As a result reaction (7) may be of comparable importance to (6) in both of these situations. This point has been made earlier by Lesclaux *et al.* [4.27] in connection with tropospheric chemistry.

Reaction (6) is also of great theoretical interest, both as a target for quantum-chemical calculations of a complicated potential surface, leading to an evaluation of the relative importance of the numerous possible product channels, and as a test of current theories of chemical kinetics for the prediction of the pressure and temperature dependences of the rates of such multichannel processes. The application of such theories in a study of reaction (6) is the subject of Chapter 7 of this thesis, which includes a discussion of earlier experimental as well as theoretical work on this reaction. The present chapter is concerned only with the measurement of k_6 and k_7, as well as k_3, at room temperature. This work has previously been reported as reference [4.0].

4.2 Experimental

The apparatus and methods used in these experiments were similar to those described in the previous chapter. A diagram of the photolysis cell is given in Fig. 4.1. The windows were of magnesium fluoride and were demountable to allow the removal of appreciable amounts of a white solid (presumably ammonium nitrate) which built up gradually when either NO or NO_2 was present in the gas mixture.The stray-light baffles incorporated in the window arms were based on the design of Butler [4.28] but had rectangular rather than circular apertures to reduce losses.

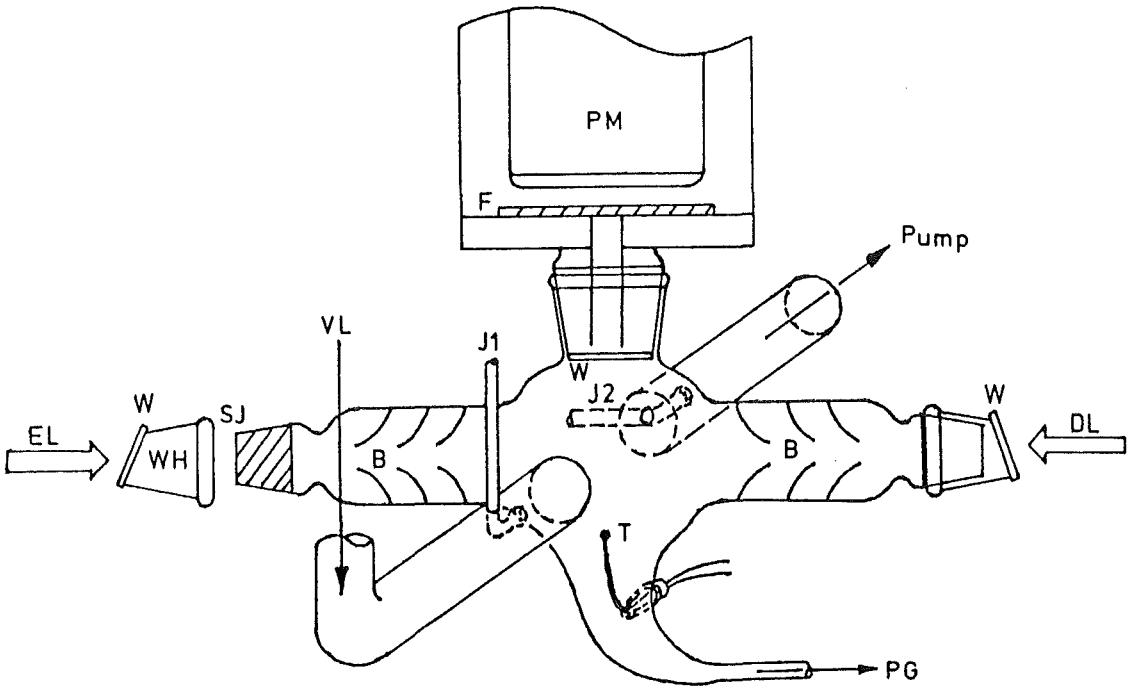

FIGURE 4.1:Schematic diagram of the photolysis cell.

Key: B - stray-light baffles; DL - dye laser beam; EL - excimer laser beam; F - filter; J1, J2 - NO inlet jets for photometric titration; PG - pressure gauge; PM - photomultiplier in housing; SJ - B24 standard-taper ground glass joint; T - thermocouple; VL - inlet from vacuum line; W - MgF_2 window; WH demountable window holder.

NH_2 radicals were generated by 193 nm excimer laser photolysis of mixtures of ammonia and the appropriate reactant (NO, NO_2 or N atoms) in a large excess of

either hydrogen or helium carrier gas. As in the previous study the mildly focussed photolysis pulses had effective energies near 50 mJ at the 28 Hz repetition rate used. To ensure thorough mixing of the gases, the ammonia and NO or NO_2 reactant gases were introduced well upstream from the cell. The N atoms were produced and their concentration monitored as described in Sections 2.1 E and 2.4 respectively. Typical concentration ratios in the mixture used were [M] : [R] : [NH_3] = 100 : 1 - 10 : 1 for carrier gas M and reactant R = NO or NO_2. In experiments on the much faster atom reaction the absolute value of [N] was reduced by a factor of 10. At total pressures between 1 and 2 Torr this resulted in NH_3 concentrations around 3 x 10^{14} cm^{-3} (0.01 Torr). This amount of NH_3 had no discernible effect on the endpoints of the NO titrations so the NH_3 was left flowing continuously. All gases used were purified by the methods given in Section 2.2.

NH_2 radicals were detected *via* LIF following dye laser excitation in an unresolved group of rotational lines in the intense Σ[(0,9,0) - (0,0,0)] vibronic sub-band of the ($\tilde{A}^2A_1$) - ($\tilde{X}^2B_1$) transition at 597.7 nm [4.29]. The dye used was a solution of Rhodamine 590 perchlorate in ethanol (see Table 2-2). The total fluorescent emission was observed with an EMI 9813QA photomultiplier tube, scattered light from the photolysis pulse being blocked by a CORNING CS 3-66 sharp-cut ultraviolet filter.

In experiments to detect NH radicals produced by reaction (3b), a mixture of R590 and Cresyl Violet 670 dyes in ethanol was used to generate an output at 672.2 nm which was frequency-doubled using the angle-tuned KDP crystal to excite fluorescence *via* absorption in the intense Q(0,0) branch of the ($A^3\Pi$) -$X^3\Sigma^-$) transition at 336.1 nm.For these experiments the EMI 9813QA photomultiplier tube was used with a CORNING CS7-54 filter to prevent interference from the undoubled probe beam.

The data-collection and signal-averaging parameters chosen were similar to those used in the CN study. All experiments were carried out at temperatures in the range 294 - 298 K as measured by a thermocouple situated in the gas stream just below the viewing region.

4.3 **Results and Discussion**

A. Rate Coefficients for the Reactions of NH_2 with N, NO and NO_2

A typical set of semilogarithmic LIF decay plots for the NH_2 + N reaction is shown in Fig. 4.2. These plots show the linearity expected for first-order radical removal. Corresponding plots for the NH_2 + NO and NH_2 + NO_2 reactions were of comparable

quality to those in Fig. 4.2. Fig. 4.3 shows the variation of the corrected pseudo-first-order decay rates k_1 (see Section 2.4) with reactant concentration for the three reactions studied. The least-squares regression analysis of these three plots gave second-order rate coefficients as follows:

k_6 (296 K) = (1.81 ± 0.12) x 10^{-11} cm^3 s^{-1}

k_7 (297 K) = (2.11 ± 0.18) x 10^{-11} cm^3 s^{-1}

and k_3 (294 K) = (1.21 ± 0.14) x 10^{-10} cm^3 s^{-1} .

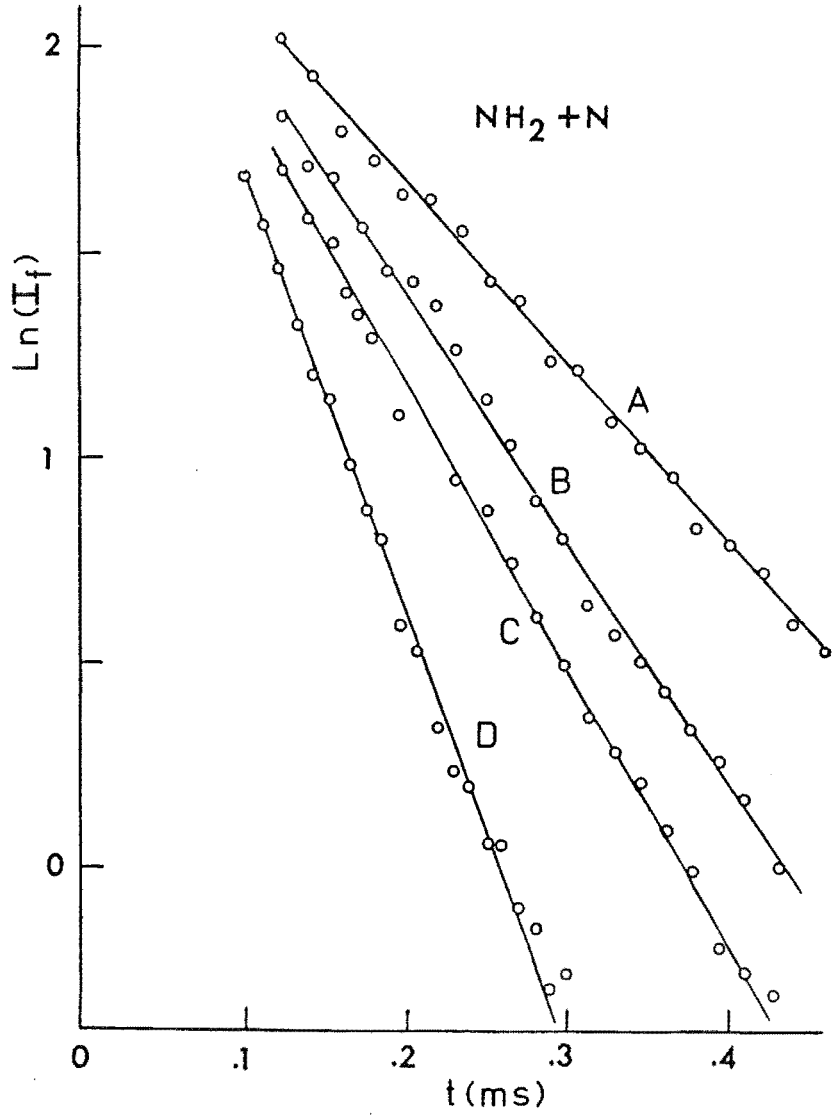

FIGURE 4.2: NH_2 + N → products: representative first-order decays of NH_2 LIF intensity with time at 296 K.

Curve A, [N] = 0 cm^{-3}; curve B, [N] = 1.5 x 10^{-13} cm^{-3}; curve C, [N] = 2.1 x $10^{-13}$$cm^{-3}$; curve D, [N] = 5.1 x 10^{-13} cm^{-3}.

The uncertainties quoted are the sum of 95 % confidence limits obtained from Student's t-testing of the regression results and estimated systematic uncertainties in the measurement of temperature, pressure, gas flow and boxcar timebase calibration. These estimates amounted to ± 4 % for NH_2 + NO, ± 5 % for NH_2 + NO_2 and ± 6 % for NH_2 + N, the last two figures being higher due to the inclusion of additional uncertainties associated with the NO_2 /N_2O_4 equilibrium correction and the photometric titration of N atoms, respectively.

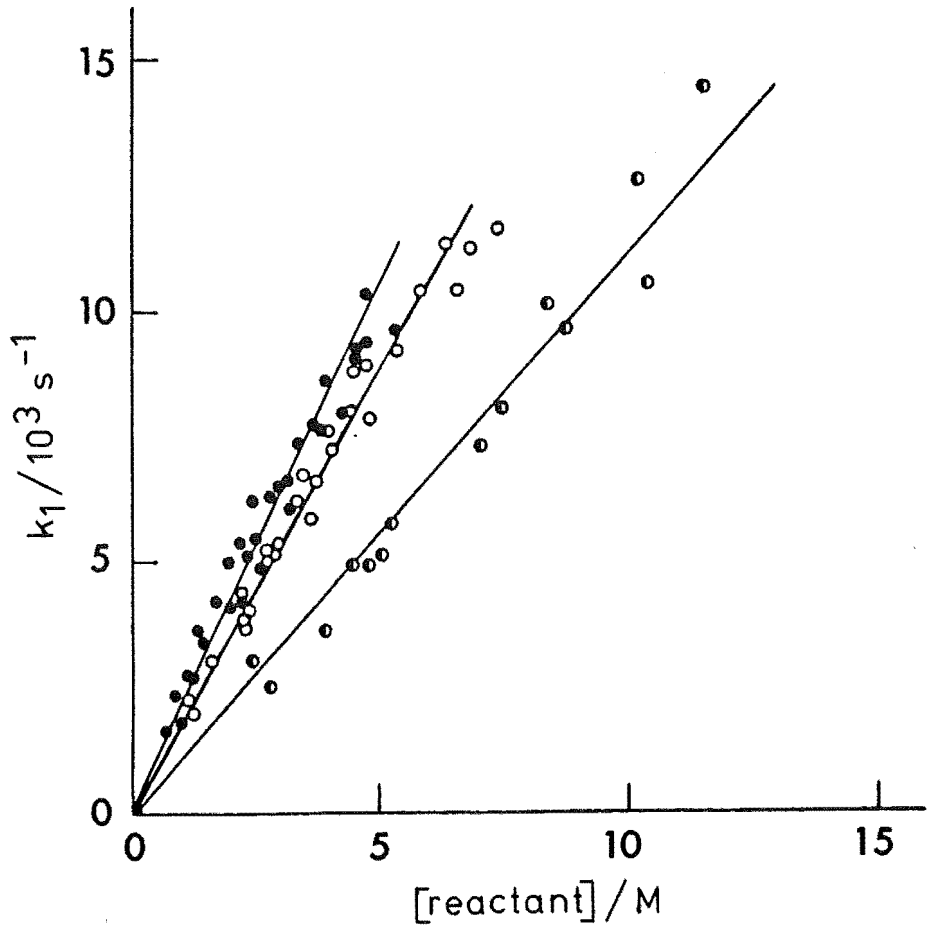

FIGURE 4.3: NH_2 + (N, NO, NO_2) → products: plots of pseudo-first-order decay rates k_1 [N], [NO] and [NO_2] to determine k_3, k_6 and k_7.

For NO (circles) and NO_2 (solid dots), the scale factor M = 10^{14} cm^{-3}. For N atoms as reactant (divided circles) M = 10^{13} cm^{-3}.

The value of k_7 should properly be regarded as a lower limit since the NO_2 concentration would be depleted with respect to the calculated value by photolysis at 193 nm. However, this effect is likely to have been small (< 2 % depletion at 50 mJ/pulse with σ (NO_2 ,193.3 nm) = 2.4 x 10^{-19} cm^2 [4.30]), and the high flow velocities used (*ca* . 200 cm s^{-1} , typically) ensured that the NO_2 concentration was restored between photolysis pulses.

A comparison of the present results for the reactions (6) and (7) with previous ones (see Table 4-3) reveals excellent agreement with earlier flash photolysis studies and confirms the above-mentioned discrepancy with the results of discharge-flow experiments. This variation may be explained in terms of the fate of a stable NH_2NO or NH_2NO_2 intermediate formed in the first step of the appropriate reaction. Such an addition complex was first suggested for the NH_2 + NO reaction (6) by Fenimore and Jones [4.3] in a study of low-pressure NH_3 /NO flames using probe-sampling mass spectroscopy. While nitrosamine (NH_2NO) was not observed directly, the authors argued that the drastic rearrangement involved in the formation of the observed major products N_2 and H_2O from NH_2 and NO necessitated the formation and subsequent isomerisation of such an adduct. More recently nitrosamine formation was confirmed by Hack *et al.* [4.31] who observed signals at m/e = 46 and m/e = 45 in time-of-flight mass spectrometry experiments on reaction (6) in a discharge-flow system. Although no observations of the analogous nitramine (NH_2NO_2) adduct have been reported in studies of reaction (7), such a complex might be expected to form at least as readily as NH_2NO under similar conditions in view of the larger dipole moment of NO_2 ($\mu = 0.32 \pm 0.01$ D) compared to that of NO ($\mu = 0.15 \pm 0.01$ D) [4.32]. Such adducts, once formed, may then either revert to reactants by unimolecular dissociation or undergo rearrangement(s) leading eventually to a variety of final products (see Chapter 7). The difference between the flash photolysis and discharge-flow results may then be a reflection of the lifetime of the complex, which may be sufficiently long-lived to diffuse out of the viewing region in a flash photolysis experiment, while in a discharge-flow system dissociation back to reactants may occur between the NO (or NO_2) inlet and the detection region downstream.

This behaviour might also account for the disagreement in the literature over the temperature dependence of reaction (6), although a comparison of the ratio k_6 (300 K)/k_6 (500 K) calculated from the expressions given in references [4.26, 4.31, 4.33, 4.34] does not indicate any clear correlation with the method used for radical production.

Reaction (3) is found to be extremely rapid, being faster than the isoelectronic OH + N and CH_3 + N reactions by factors of 2.5 and 5.5 respectively (see Table 4-2).

TABLE 4-3: Kinetic data for reactions of NH_2 radicals with NO, NO_2 and N atoms.

Year	T [a] (K)	p (Torr)	A [b] (cm^3s^{-1})	n [b]	E_A [b] (kJ mol^{-1})	k (rt) [c] ($10^{-11}cm^3s^{-1}$)	Method [d]	Reference
$NH_2 + NO \rightarrow$ products:								
1971	rt	250-100	-	-	-	2.7	PR/AS	[4.14]
1972	298	2.4	-	-	-	0.83±0.17	DF/AS,ES MS,ESR	[4.19]
1975	298	1	-	-	-	2.1 ± 0.2	FP/LIF	[4.52]
1975	300-500	2 - 700	2.09 (-8)	1.25	0	1.8 ± 0.3	FP/AS	[4.33]
1978	rt	0.1 - 1	-	-	-	1.7 ± 0.4	FP/LIF	[4.53]
1979	209-505	0.6 - 4	4.5 (-7)	1.85	0	1.2	DF/LIF	[4.31]
1982	294-1215	~ 1	4.4±.7(-5)	2.30	5.7±0.5	0.9	DF/LIF	[4.34]
1982	216-480	2.5 - 5	2.8±.9(-7)	1.67	0	2.1 ± 0.3	FP/LIF	[4.26]
1982	290-1150	0.04-38	-	-	-	1.7 ± 0.5	LP/RF, LIF,MS	[4.48]
1983	297	1 - 3	-	-	-	1.81 ± 0.12	LP/LIF	This work
1984	rt	0.5 - 5	-	-	-	0.9	LFR/LIF	[4.44]
1984	298	~ 2	-	-	-	1.4 ± 0.1 (0) 3.2 ± 0.2 (1)	LP/LIF	[4.45]
$NH_2 + NO_2 \rightarrow$ products:								
1979	298-505	3-10.5	3.8 (-8)	1.3	0	2.3 ± 0.2	FP/LIF	[4.27]
1979	250-503	1 - 2	3.2 (-4)	3.0	0	1.2	DF/LIF	[4.31]
1983	294	1 - 3	-	-	-	2.11 ± 0.18	LP/LIF	This work
1985	298	2 - 10	-	-	-	2.26 ± 0.08 (0) 1.73 ± 0.06 (1)	LP/LIF	[4.46]
$NH_2 + N \rightarrow$ products:								
1983	296	1 - 3	-	-	-	12.1 ± 1.4	LP/LIF	This work

a) rt - room temperature.

b) Temperature-dependent rate coefficient $k(T) = AT^{-n} exp(\frac{-E_A}{RT})$

c) Figure in parentheses, if present, is NH_2 bending mode quantum number v_2'' ; v_2'' = 0 otherwise.

d) DF - discharge-flow; FP - flash photolysis; LFR - laser flow reactor; LP - laser photolysis; PR - pulse radiolysis; AS - absorption spectroscopy; ES - emission spectroscopy; ESR - electron spin resonance; LIF - laser-induced fluorescence; MS - mass spectrometry; RF - resonance fluorescence.

This result is in marked contrast with that found in the analogous series of O atom reactions with OH, NH_2 and CH_3, in which the NH_2 reaction (2) is found to be the slowest of the three by at least an order of magnitude. From Table 4-2 it can be seen that there is no strong correlation between the rate coefficients and heats of reaction for the reactions of the three radicals with a given atomic species (i.e. vertical comparison in Table 4-2). This is not surprising in view of the different types of reactions represented (e.g. abstraction, atom exchange, substitution), for which considerably different potential surface geometries, and thus activation barriers, would be expected. In the case of the horizontal series in Table 4-2, however, where the possible reactions with atomic species are of essentially the same type for a given radical, so that similar activation barriers might be expected, some correlation is observed, the rate coefficients reflecting in a general way the exothermicities of the given reactions. It should be noted, though, that this trend depends heavily on positive identification of the specific product channels shown, whereas the source of the experimental kinetic data on the CH_3 and OH reactions in Table 4-2 [4.12] indicates that most of these reactions were studied by monitoring reactant concentrations, and the product channel assumed in references [4.24] and [4.25] for the CH_3 + N reaction is spin-forbidden.

The most striking feature of Table 4-2 is the 35-fold increase in the rate coefficient for the disappearance of NH_2 on going from O to N atoms as reactant, compared with the corresponding ratios of 1.5 and 0.2 for the reactions of OH and CH_3, respectively. This result is difficult to interpret due to the existence of several thermally- and spin-allowed product channels for both reactions (2) and (3) and the absence of branching coefficient data. Attempts to re-measure the overall rate coefficient k_2 for reaction (2) in the present system proved unsuccessful due to the large reduction in the NH_2 LIF signal which occurred on addition of even a small amount of O atoms. However, this result by itself suggests that reaction (2) may be much faster than was found by Gehring *et al.* [4.20].

If reaction (2) proceeds *via* formation of a stable H_2NO intermediate, similar to those postulated for reactions (6) and (7), a low value for k_2 might be expected to result from a discharge flow experiment, as discussed above. Such an adduct has been proposed as an important transient species in reactions of NH_2 with ozone studied in both discharge-flow and flash photolysis systems [4.35] as well as in the pulse radiolysis of NH_3 /O_2 mixtures [4.16], although no direct observation of H_2NO or its isomer NHOH has been reported. Secondary reactions producing NH_2 between the atom inlet and the viewing region in the discharge-flow reactor would also have contributed to a low result for k_2 in [4.19]. Clearly more work is required for a proper understanding of the kinetics and products of reaction (2).

B. Detection of NH Radicals in the NH_2 + N system

Although the reaction of NH_2 with nitrogen atoms to produce NH (3b) is endothermic, in the presence of excess N the highly exothermic reaction (4) may provide a driving force for the formation of NH as a primary product by competing with the reverse reaction

$$2NH \rightarrow NH_2 + N. \qquad (-3b)$$

This situation would lead to rapid equilibration between NH and NH_2 , with the concentration of NH at time t being given by the approximate relation

$$[NH]_t \approx 2\frac{k_{3b}}{k_4}[NH_2]_t \ . \qquad (8)$$

Unfortunately, poor signal-to-noise ratios were obtained in the LIF signals produced by excitation of NH at 336.1 nm, due both to the reduced intensity of the frequency-doubled probe beam and to the need to work at short delay times where the prompt emission following the photolysis pulse partly obscured the LIF signals; this prevented quantitative measurements on the behaviour of NH. However some qualitative observations could be made.

It was found that small NH signals could be detected at short delay times in the absence of N atoms. This was attributed to a small amount of multiphoton decomposition of NH_3 arising from the use of a long focal-length lens to steer the photolysis beam into the cell, and is in accord with a result of Donnelly *et al.* [4.36] who observed formation of NH in the photodissociation of NH_3 by an unfocussed ArF excimer laser at pulse energies near 30 mJ.

On addition of a small amount of N atoms, the NH signal observed at a fixed probe delay time increased, consistent with the operation of reaction (3b); increasing the N atom concentration resulted in a decrease in the signal. This behaviour was consistently observed over a range of delay times and NH_3 concentrations and was independent of the method of generation of N atoms. The variation in LIF intensity (i.e. in [NH]) with delay time appeared similar to that found in measurements of NH_2 , in accord with the prediction of equation (8), although this could not be confirmed.

From these observations it may be concluded that NH is a product of the NH_2 + N reaction, although it may not necessarily be a major one since other possible products (e.g. N_2 , H_2 , H) were not monitored.

The presence of NH among the products of reaction (3) at short reaction times, together with the high value obtained for k_3 , suggests that reaction (3) proceeds, at least in part, by a direct abstraction mechanism. This result appears to conflict with the endothermicity of reaction (3b). However it may be noted in this connection that the heats of formation of NH and NH_2 are not yet well-established , as can be seen from a comparison of the values given in [4.37, 4.38] and [4.39], and the possibility remains that reaction (3b) is close to thermoneutral as is suggested by the present findings at room temperature. However, it should be mentioned here that our subsequent observations indicate that reaction (3a) predominates over (3b) and (3c).

Elementary *ab initio* calculations using the CNDO method [4.40], performed by Dr. R. G. A. R. Maclagan of this University, have indicated that NH_2 may form quite strongly-bound adducts with NO and NO_2 , although since heats of formation obtained by this method are generally rather inaccurate [4.41] this result is only qualitative. Casewit and Goddard [4.42] have performed more accurate GVB-CI calculations on a series of isomers of formula H_2N_2O including nitrosamine, obtaining a value of ΔH_f = -128 kJ mol^{-1} for the complex-forming reaction

$$NH_2 + NO \rightarrow H_2N\text{-}NO. \qquad (9)$$

These workers have also studied the thermochemistry of 1,1-diazene (H_2NN) using the same computational methods [4.43]. They obtained a value of ΔH_f = 361 kJ mol^{-1} for H_2NN which, when combined with the known values of ΔH_f for NH_2 and N, leads to a heat of reaction ΔH_r = -302 kJ mol^{-1} for the association reaction

$$NH_2 + N \rightarrow H_2NN. \qquad (10)$$

Thus the possibility of rapid formation of an H_2NN complex followed by isomerisation to HNNH and subsequent dissociation on a microsecond timescale cannot be excluded by theory as a mode of formation of NH from reaction (3). A more detailed study of the products of this reaction is described in Chapter 5 of this thesis.

4.4 **Summary**

The LP/LIF technique has been used to study the reactions of NH_2 radicals with N atoms, NO and NO_2 at room temperature. The rate coefficients obtained were k_3 (296 K) = (1.21 ± 0.14) x 10^{-10} cm^3 s^{-1}, k_6 (297 K) = (1.81 ± 0.12) x 10^{-11} cm^3 s^{-1} and k_7 (296 K) = (2.11 ± 0.18) x 10^{-11} cm^3 s^{-1}, respectively. These values of k_6 and k_7 are in good agreement with the results of previous studies using flash photolysis to generate the NH_2 radical, but are higher by a factor of around two than corresponding

results obtained from discharge-flow experiments. This variation has been discussed in terms of the fate of a stable NH_2NO or NH_2NO_2 adduct.

The present measurement of k_3 represents the first quantitative kinetic study of reaction (3). The reaction is found to be very fast, as expected for a radical-atom reaction, and NH is observed among the primary products in the reaction system. These results have been compared to those found earlier for reactions of the isoelectronic species OH and CH_3 with atomic species, and their mechanistic and thermochemical implications have been discussed.

4.5 **Epilogue**

Since the completion of this work a number of further kinetic studies of the NO and NO_2 reactions (6) and (7) have been published. The measured rate coefficients are give in Table 4-3.

Reaction (6) was studied by Jeffries *et al.* [4.44] in a flow reactor using infra-red multiphoton dissociation (IRMPD) by a pulsed CO_2 laser to produce NH_2 radicals from hydrazine, the NH_2 concentration being followed by LIF. The reported value of $k_6 = 0.90 \times 10^{-11}$ cm^3 s^{-1} agrees well with previous measurements in discharge-flow experiments.

Gericke and co-workers [4.45] have performed the first investigation of the effect of vibrational excitation of the NH_2 radical on the rate of reaction (6), using an LP/LIF method similar to that used in the present work but with an infra-red rather than an ultraviolet photolysis source, and detecting NH_2 in the ground and first excited levels of the bending mode ν_2. They found $k_6\ (v_2'' = 0) = (1.4 \pm 0.1) \times 10^{-11}$ cm^3 s^{-1} which is intermediate between previously reported discharge-flow and flash photolysis results, and $k_6\ (v_2'' = 1) = (3.2 \pm 0.2) \times 10^{-11}$ cm^3 s^{-1}. This value includes the effect of vibrational relaxation of NH_2 (0,1,0) by NO, which was estimated to be an order of magnitude less efficient than chemical reaction for removal of NH_2 (0,1,0).

A similar study of the NO_2 reaction (7) in the same laboratory has also been reported [4.46]. In this case the measured rate coefficient $k_7(v_2'' = 0) = (2.26 \pm 0.08) \times 10^{-11}$ cm^3 s^{-1} agrees closely with previous flash photolysis results, while the corresponding value for vibrationally-excited NH_2 is less than that for the vibrational ground state, $k_7(v_2'' = 1) = (1.73 \pm 0.06) \times 10^{-11}$ cm^3 s^{-1}. This result was explained in terms of formation of a long-lived NH_2NO_2 intermediate from which the activation energy for product formation is less than the energy of the separated reactants, essentially

no barrier being assumed for the association of the NH_2 and NO_2 radicals. NO_2 was shown to be roughly twice as efficient as NO for collisional relaxation of NH_2 (0,1,0).

Very recently Hall and co-workers [4.47] have studied the product distribution from the NH_2 + NO reaction by infra-red kinetic spectroscopy, using an ArF excimer laser to generate NH_2 from ammonia. In the course of this work the overall rate coefficient for NH_2 decay was measured and was stated to be consistent with literature values, but no numerical value for k_6 was given. An appreciable yield of OH was observed in this system, in agreement with results of earlier workers [4.26, 4.34, 4.48]. However, there is evidence to suggest that this is due to a reaction of NH rather than NH_2 (see discussion in Section 6.3).

If the explanation given here for the observed discrepancy between flash photolysis and discharge-flow techniques is accepted, then the rate coefficients k_6 and k_7 for vibrational ground-state NH_2 may be considered to be well established at the values obtained in this and earlier studies using the former method. However the nature and distribution of the primary products and the detailed mechanisms for both reactions (6) and (7) are still uncertain. These matters are considered in Chapter 7 of this thesis.

No further work on the kinetics of the NH_2 + N reaction has appeared since the present study was completed. However an investigation of the products of reaction (3) in this laboratory has been reported [4.49]. This study is described in Chapter 5.

CHAPTER 5

PRODUCTS OF REACTION OF NH_2 WITH NITROGEN ATOMS

5.1 Introduction

In the previous chapter the results of a kinetic study of the reaction of NH_2 with N atoms, NO and NO_2 by the LP/LIF technique were presented. In that work the overall rate coefficient for the reaction

$$NH_2 + N \rightarrow \text{products} \qquad (1)$$

$k_1 = (1.21 \pm 0.14) \times 10^{-12}$ cm^3 s^{-1}, was found to be larger than the corresponding value for the NO and NO_2 reactions by factors of 6.7 and 5.7, respectively, and NH was detected as a product in the system containing N and NH_2. The results were interpreted in terms of a direct reaction occurring between NH_2 and N atoms, in contrast to the NO and NO_2 reaction systems in which the involvement of long-lived intermediate complexes is supported by previous observations of negative temperature dependences for both reactions, and by the extensive rearrangements required to generate the observed major products in each case [5.1 - 3]. However, because quantitative measurements of the NH yield were not made in the earlier study and other possible products from reaction (1), such as N_2, H_2 or H atoms were not monitored, no firm conclusion could be drawn regarding the importance of the channel leading to NH, and the possibility of a reaction between NH_2 and N occurring *via* formation and subsequent rearrangement of an intermediate H_2NN complex could not be ruled out in view of theoretical predictions of the stability of H_2NN [5.4].

The following product channels may be considered for reaction (1):

$$NH_2 + N \rightarrow N_2 + H_2, \quad \Delta H_r = -663 \pm 7 \text{ kJ mol}^{-1} \qquad (1a)$$

$$\rightarrow N_2 + H + H, \qquad -227 \pm 7 \text{ kJ mol}^{-1} \qquad (1b)$$

$$\rightarrow NH + NH, \qquad +91 \pm 41 \text{ kJ mol}^{-1} \qquad (1c)$$

$$\rightarrow N_2H + H, \qquad -208 \text{ kJ mol}^{-1} \qquad (1d)$$

Of these, reaction (1a) is spin-forbidden and would be expected to proceed only *via* an intermediate species having a sufficiently long lifetime for a spin change to occur. Reaction (1c) is apparently endothermic and so would not be expected to be fast at room

temperature. However , as was discussed in Chapter 4, the heat of formation of NH is still sufficiently uncertain that reaction (1c) could occur without an activation barrier [a]. In the presence of excess N atoms this reaction would be followed by the presumably fast reaction

$$NH + N \rightarrow N_2 + H, \quad \Delta H_r = -632 \pm 17 \text{ kJ mol}^{-1} \qquad (2)$$

so that the nett yields of H atoms from either reaction (1b) or (1c) followed by (2) should be similar.

Although N_2H has never been detected experimentally, there have been a number of *ab initio* theoretical predictions of its thermochemical properties and of the barrier to dissociation to N_2 + H [5.4, 5.7]. In the most recent of these studies Curtiss *et al.* [5.7] have used a large basis set and included electron correlation effects *via* fourth-order perturbation theory to calculate that N_2H is unstable with respect to N_2 + H by 82 kJ mol^{-1} at room temperature, and that the barrier to dissociation is probably less than 25 kJ mol^{-1}. A dissociation lifetime for N_2H of 2 x 10^{-9} s at 298 K was calculated using classical transition-state theory; this value falls to ca. 5 x 10^{-11} s when quantum mechanical tunnelling is included, so that reaction (1d) would be indistinguishable from (1b) on the microsecond timescale commonly used in kinetics experiments.

As mentioned in Section 4.1, all three of the pathways (1a) - (1c) have been postulated as being important in various chemical systems, e.g. the inclusion of reactions (1b) and (2) in the mechanism proposed by Back and Salahub [5.8] for the decomposition of NH_3 by active nitrogen, and the involvement of reactions (1a), (1c) and (2) in the modelling studies of NH_3 / O_2 flames near 2000 K by Kaskan and Hughes [5.9]. In view of the inconsistencies in these mechanisms related to the exothermicities of the various pathways, and of the large uncertainty in the heat of reaction for process (1c), it was considered desirable to determine directly the relative importance of channels (1a) - (1c) in the NH_2 + N reaction system. In the present study a resonance fluorescence technique has been used to measure the relative yields of H atoms produced by excimer laser photolysis of NH_3 in the presence and absence of N atoms, and the H atom concentration profiles measured at short times after the photolysis flash have been compared with simulated profiles calculated from simple model mechanisms for the pathways (1b) and (1c)+(2) to enable these processes to be distinguished. This work has previously been reported as reference [5.0].

---

[a] Recent measurements of ΔH_f (NH) = 361±9 kJ mol^{-1} [5.5] and 357±2 kJ mol^{-1} [5.6], and of ΔH_f (NH_2) = 192±2 kJ mol^{-1} [5.6] give values of ΔH_r = 59±25 and 50±6 kJ mol^{-1} for this reaction, based on the data of [5.5] and [5.6] respectively. Since 1979, values in the range 342 - 394 kJ mol^{-1} have been recommended for ΔH_f (NH) by various groups (see [5.5]).

5.2 Experimental

The experimental system used in this work was similar to that used in a previous study of O atom yields from the 308 nm XeCl excimer laser photolysis of HOCl [5.10]. The photolysis cell, shown in Fig. 5.1, consisted of a 29 cm length of DURAN glass tubing of rectangular (1.8 x 3.3 cm^2) cross-section, with SUPRASIL quartz windows at each end, the inlet and outlet being located close to the windows. The rectangular cross-section was intended to match the profile of the unfocussed photolysis beam and to reduce the amount of dead space in the cell. Mixtures of ammonia, nitrogen

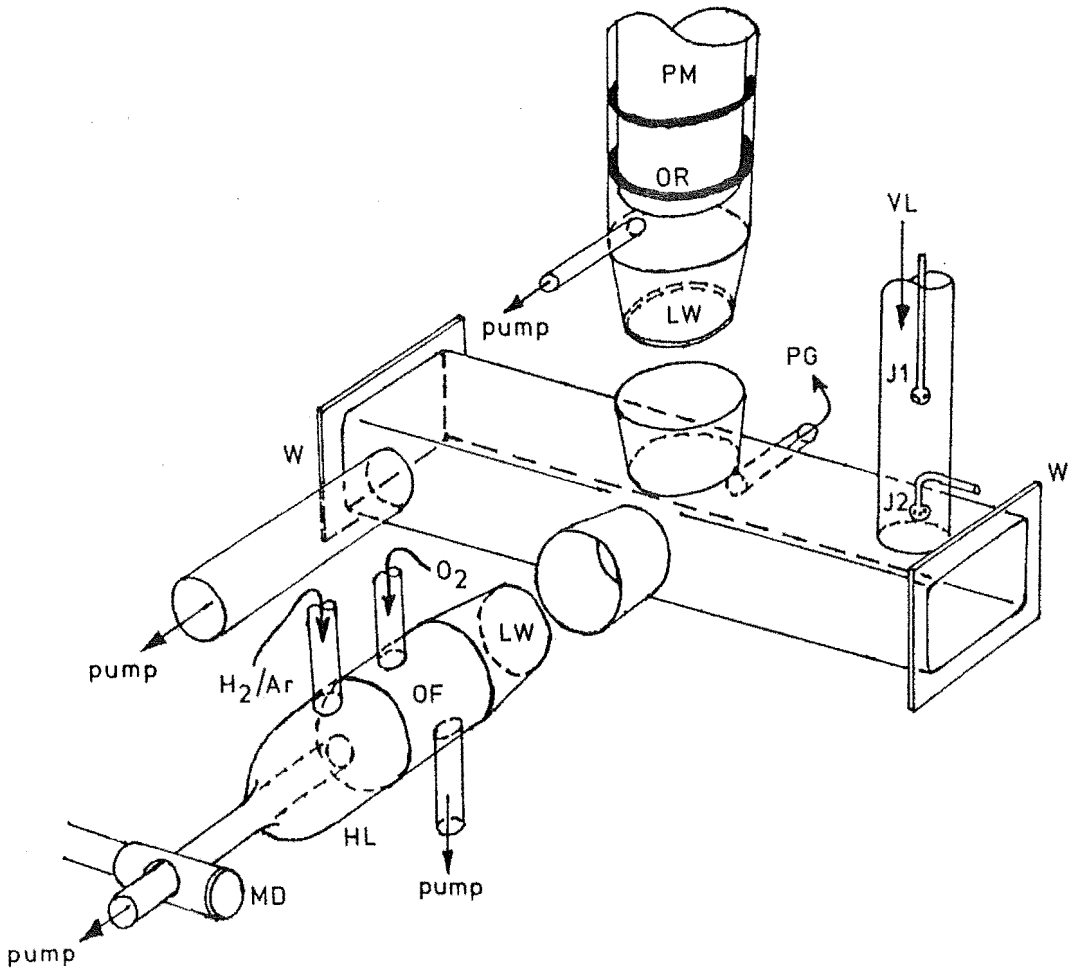

FIGURE 5.1: Schematic diagram of the photolysis cell. Cell, hydrogen lamp and photomultiplier housing all DURAN glass.

Key: HL - atomic hydrogen resonance lamp; J1 - NH_3 inlet jet; J2 - NO inlet jet (for photometric titrations): LW - lithium fluoride window; MD - microwave discharge head; OF - flowing oxygen filter; OR - O-ring seal; PG- pressure gauge; PM - photomultiplier in evacuable housing; VL - inlet from vacuum line including N atom source; W - SUPRASIL window.

and helium carrier, typically in the ratio NH_3 : N_2 : He = 1 : 20 : 120, were pumped through the cell at pressures in the range 1 - 3 Torr with flow velocities up to 600 cm s^{-1} . The ammonia was introduced to the carrier stream through a multiple-hole inlet jet placed a short distance above the inlet to the cell.

NH_3 was photolysed by the 193.3 nm ArF excimer laser operating at a repetition rate of 18 Hz and pulse energies between 0.5 and 30mJ, measured with the SCIENTECH Model 364 power-meter. Assuming only single-photon absorption by NH_3, for which $\sigma(NH_3, 193.3\ nm) = 4.5 \times 10^{-18}\ cm^2$ [5.11], it was estimated that 4 - 5 % of the NH_3 molecules within the beam could be dissociated to NH_2 + H by a 20 mJ pulse. However, experiments described below indicated that in fact multiphoton processes occurred to a significant extent at all except the lowest pulse energies used. This was confirmed in measurements of the absorption by NH_3 at 193.3 nm using the power-meter, in which the effective absorption cross-section was found to decrease with increasing pulse energy, falling from *ca.* $5 \times 10^{-17}\ cm^2$ 2 mJ/pulse to *ca.* $1 \times 10^{-17}\ cm^2$ at 20 mJ/pulse. These results were taken to indicate the saturation of one or more multiphoton absorption modes by "hot spots" in the unfocussed multi-mode laser beam (see Section 5.4), but it was not possible to determine whether these processes involved simultaneous or sequential absorption, nor whether the second photon was absorbed by excited NH_3 or an intermediate species such as NH_2. The latter seems more likely, in view of the observed unit quantum yield and short lifetime (0.1 - 1 ps) for predissociation of the first excited state of NH_3 ($\tilde{A}^1A_2''$) which is produced by absorption of one 193.3 nm photon [5.12, 5.13]. In this case NH_2 in either its ground or first excited electronic state would appear to be the most likely candidate for the intermediate [a], and the results indicate that it has a larger absorption cross-section than NH_3 at 193 nm.

Atomic hydrogen, formed by photolysis of NH_3 , or by reactions between N atoms and NH_2 or NH, was detected *via* resonance fluorescence at 121.6 nm (Lyman-α) excited by a lamp consisting of a microwave discharge in a flowing H_2 /He mixture, the discharge being modulated at the laser's repetition frequency to suppress a 50 Hz ripple which was present in the fluorescence signal, when the discharge ran continuously. The output of the lamp was passed through a flowing O_2 filter (pathlength 9.5 cm, pressure typically 65 Torr) to remove any component at 120 nm due to the presence of nitrogen-containing impurities in the lamp gases ($\sigma(O_2, 120\ nm) \approx 200\ \sigma(O_2, 121.6\ nm)$

a) Since the completion of this work the mechanism of formation of $NH(A^3\Pi_i)$ in the 193.3 nm photolysis of NH_3 has been studied in two-laser pump-and-probe experiments by Kenner, Rohrer and Stuhl [5.14]. These workers have concluded that sequential rather than simultaneous absorption is the major multiphoton process at 193.3 nm and that the NH_2 radical is "almost certainly" the intermediate state.

[5.15]). The fluorescence was observed perpendicular to both the laser beam and the lamp axis by an EMR 541-J photomultiplier in an evacuated housing. The photomultiplier was used unfiltered due to the low transmittance of available vacuum ultraviolet interference filters; the limited frequency response of the photomultiplier (11.3 % quantum efficiency at 121.6 nm decreasing to 1.7 % at 147 nm and 0.065 % at 180 nm) was relied upon to reject radiation at other wavelengths, and the large scattered signal due to the photolysis pulse was separated from the total signal at the data processing stage (see Section 5.3).

The instrumentation for control of the experiment and signal-processing was configured as shown in Fig.5.2. A single cycle of the experiment was initiated by a 10 V

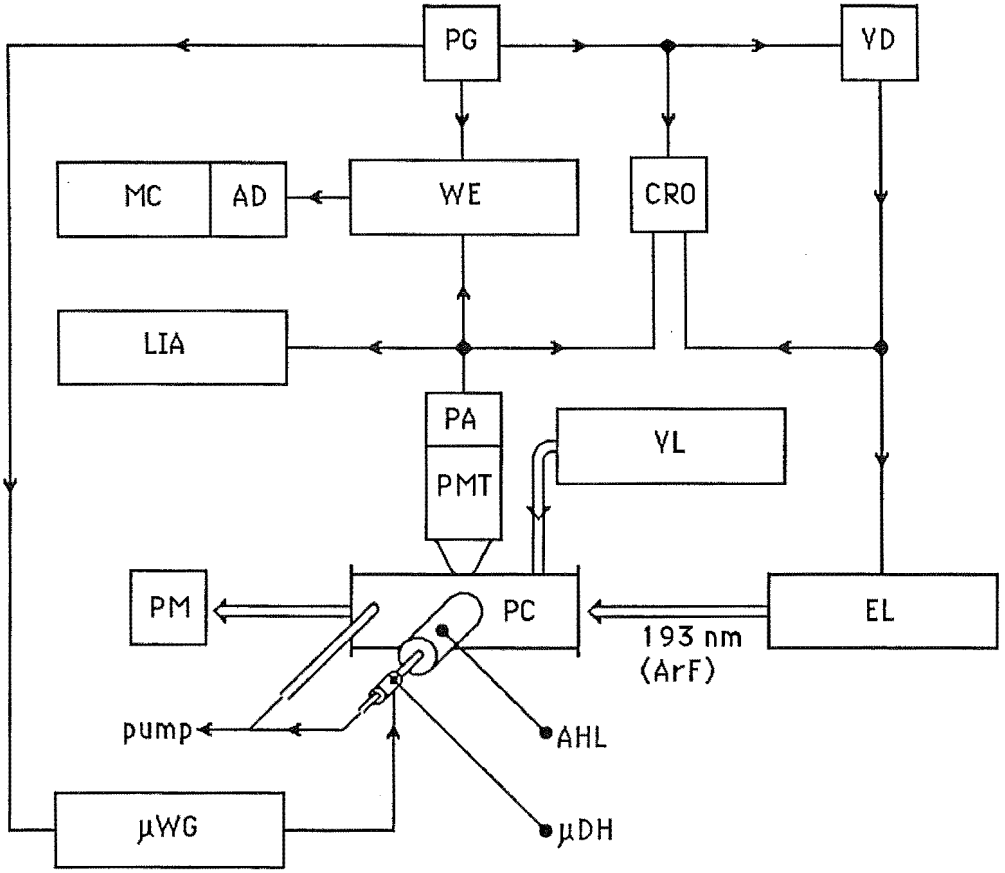

FIGURE 5.2. Experimental configuration for Lyman-α fluorescence resonance measurements.

Key: PG - pulse generator; VD - variable delay; MC - microcomputer; AD - analogue-digital interface; WE - waveform eductor; CRO - oscilloscope; LIA - losk-in amplifier; PA - preamplifier; PMT - photomultiplier tube; VL - vacuum line; PM - laser power meter; PC - photolysis cell; EL - excimer laser; AHL - O_2-filtered atomic hydrogen resonance lamp; μWG -microwave generator; μDH - microwave discharge head.

pulse (mark/space ratio = 9 : 1) provided by the variable frequency square-wave generator which turned on the microwave generator powering the resonance lamp, the excimer laser being fired after a preset delay of *ca* 20 ms. The H atom fluorescence signal was observed by the photomultiplier whose preamplified output was taken to the inputs of the PAR Model TDH-9 waveform eductor, a PAR Model HR-8 lock-in amplifier and to the TEKTRONIX oscilloscope for visual display.

The PAR Model TDH-9 waveform eductor (hereafter simply 'eductor') is a signal-averaging instrument which permits the recovery of the whole or part of a repetitive waveform from an otherwise noisy signal by sampling the input signal at 100 equally spaced points in each cycle, separately integrating each point to provide noise suppression (the average value of the noise component at any point of the input signal being zero) and storing the total integrated sample in an analogue memory comprising 100 low-leakage capacitors selected by FET switches. With repeated sampling the content of each memory element asymptotically approaches the value of the target waveform at the appropriate sample point. The contents of the memory are also made available at the output of the instrument in synchronisation with the averaging "sweep" at each repetition of the event under study. The instrument has a wide range of time constants and gain settings, and sweep periods ranging from 100 μs to 11 s are available. The start of the sweep may be delayed relative to an externally provided trigger pulse, allowing any desired portion of the target waveform to be 'educted'. The memory contents can also be read out slowly for display on a chart recorder or, as in the present case, for transfer to a microcomputer for subsequent processing and disk storage, *via* an A/D converter.

In the present experiments the eductor's internal delay and sweep period were adjusted such that a 30 ms sweep was initiated about 4 ms before the photolysis pulse in order to establish the background signal due to scattered light from the resonance lamp. The eductor's characteristic time constant was usually chosen to be either 50 or 100 s corresponding to an effective or observed time constant (OTC) of 93 or 185 s, which in turn required an analysis time of between 5 and 10 minutes per experimental run. Operation of the eductor under these conditions results in nominal signal-to-noise ratio improvement factors between 50 and 80. To increase the efficiency of these measurements the usual procedure adopted in this work was to monitor the eductor's output signal visually, using the oscilloscope; a run was terminated by stopping the eductor sweep when no further growth of the signal could be seen.

The lock-in amplifier (a type of phase-sensitive detector) was used to monitor the RMS value of the photomultiplier signal during each run, in order to check the stability of the experimental,conditions during a series of runs. Runs in which the HR-8

signal was noisy, signifying fluctuations in the resonance lamp output, gas flows or other variables, were discarded. At the end of each run the data was transferred to the DEC LSI 11/23 microcomputer for disk storage, using the program EDUCTR (see Table 2-3). For a given set of gas flow and pressure conditions, a set of experiments typically consisted of two or three runs with N atoms present, a similar number without N atoms, and a blank run in the absence of NH_3 to measure the effect of the large 'spike' signal caused by the photolysis pulse.

The N atoms were generated by a microwave discharge in the N_2 / He stream at a point 40 cm upstream from the NH_3 inlet. The removal of N atoms was accomplished either by shutting off the N_2 flow, in which case the discharge was left running, or by turning the discharge off without altering the N_2 flow. The concentration of N atoms was determined by the photometric NO titration method described in Section 2.1 E, the NO being added immediately above the entrance to the cell. The intensity of the nitrogen afterglow produced by N atom recombination was monitored throughout the photolysis experiments, using the photomultiplier/picoammeter combination described in Section 2.1 E to check that the N atom concentration was not significantly reduced by reactions with photolysis products. In experiments in which the NH_3 concentration was varied at a high laser power, the observed variations in the photocurrent I_{ag}, which is proportional to $[N]^2$, indicated that at high values of $[NH_3]$, over 60 % of the N atoms could be removed from a stream with an initial concentration near 3×10^{14} cm^{-3}. Such conditions were avoided in experiments carried out to examine the kinetics of the H atom production.

In this work the reproducibility of results was found to depend very strongly on the purity of the gases used. In particular it was necessary to exclude any trace of hydrogen-containing impurities from the nitrogen used in the N atom discharge to prevent absorption of the Lyman-α radiation between the input window and the viewing region. To this end the N_2 for the discharge was passed through a column of oxidised BASF catalyst at 140 °C followed by a silica gel trap at -117 °C (ethanol slush bath). Other gases were treated as described in Section 2.3 Gas flows, temperature and total pressure were measured as described in Chapter 2.

5.3 **Data Reduction Procedures**

Fig 5.3 shows a pair of Lyman-α fluorescence intensity - *vs* . - time plots obtained in the presence and absence of NH_3 . In these plots the whole of the excimer laser 'spike' at $t \approx 4$ ms is visible, but to improve the signal-to noise ratio for data in the post-flash region, the photomultiplier supply voltage was usually increased until the

signal immediately following the flash was close to the full scale of the eductor output, when most of the spike was lost through overloading of the fast preamplifier.

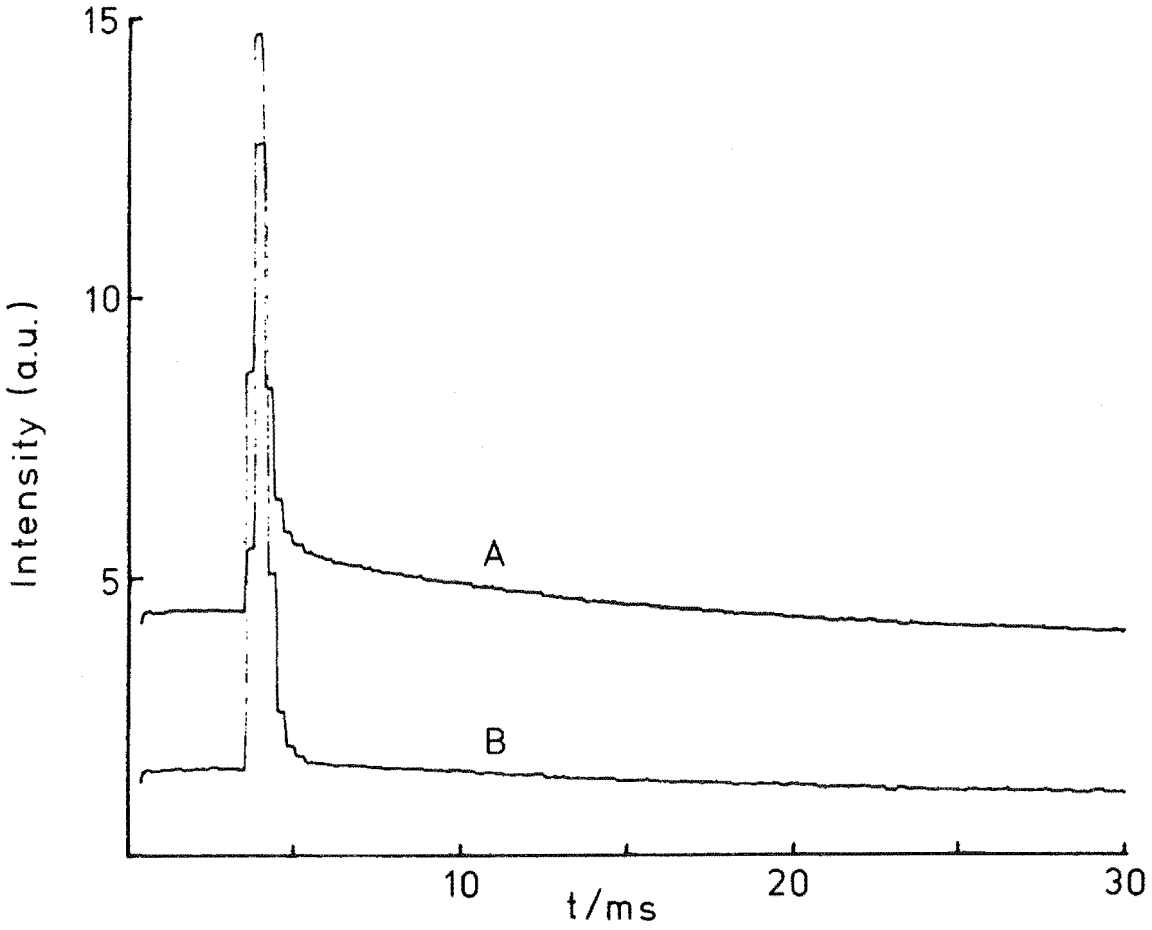

FIGURE 5.3: Waveform eductor output signals with NH_3 present (A) and without (B).

(Photomultiplier gain was reduced to show whole of laser spike.)

The first step in the processing of one of the 100-point data files produced by the data-transfer program EDUCTR (see Table 2.3) was the subtraction of the residual contribution from the laser spike obtained from the blank run, using the point-wise file subtraction routine of the program EDPROC (see Table 2.3). Next, the pre-flash data (usually points 1 - 11) were least-squares fitted to a straight line which was extrapolated over the full width of the sweep and then subtracted to provide a baseline correction for

the scattered light from the resonance lamp. Finally, the post-flash data (points 20 - 80 typically, due to the small S/N ratio at the tail of the decay) were least-squares fitted to an exponential decay curve, and the size of the increase or 'step' in the fluorescence signal at zero reaction time, proportional to the initial H atom concentration $[H]_0$, was obtained by extrapolation of the corresponding semilogarithmic decay plot to the time of the laser pulse. Step sizes obtained in this way from the data for different runs made under the same conditions generally agreed to within 10 %.

5.4 Results and Discussion

A. Measurements of Relative H Atom Yields from the NH_2 + N Reaction

The vacuum ultraviolet photolysis of NH_3 has been studied previously using both conventional and laser sources [5.15 - 18]. The major products of single-photon dissociation at wavelengths between 184.9 and 213.9 nm are known to be H atoms and NH_2, which is formed predominantly in its electronic ground state, although Donnelly *et al.* [5.16] have recently measured a quantum yield of *ca.* 2.5 % for the formation of NH_2 ($\tilde{A}^2A_1$) in experiments using an unfocussed ArF laser. These workers also detected NH in its $A^3\Pi_i$ and $b^1\Sigma^+$ states via emissions at 336.0 and 470.8 nm, respectively, the latter being very weak. Formation of either of these species together with H_2 or 2H requires energy in excess of that carried by a single 193.3 photon, but all four processes are energetically allowed for two-photon absorption. In view of the observed weak emission from NH ($b^1\Sigma^+$) and of the fact that the spin-forbidden process

$$NH_3\ (\tilde{X}^1A_1) \rightarrow NH\ (A^3\Pi_i) + H_2\ (X^1\Sigma^+_g)$$

has not been observed [5.16], it may be concluded that the process

$$NH_3\ (\tilde{X}) \rightarrow NH\ (A) + 2H$$

is likely to be the dominant pathway resulting from either simultaneous or sequential two-photon absorption by NH_3. At very high laser fluences the absorption of several 193.3 nm photons by NH_3 or its primary photolysis products could be expected to result in formation of NH at energies well above the dissociation limits of either the $A^3\Pi_i$ or $b^1\Sigma^+$ states, in which case the nett effect of photolysis would be the complete atomisation of NH_3.

Evidence for the occurrence of multiphoton processes in the present system is provided by the observed non-linear dependence of the size of the extrapolated signal step obtained without N atoms present on the concentration of NH_3. This effect is shown in Fig.5.4 for experiments carried out at fairly high laser pulse energies (*ca.* 15 mJ). The

deviation from linearity cannot be ascribed to absorption of the H atom fluorescence by NH_3 , since the absorption cross-section of NH_3 at Lyman-α (σ(NH_3 , 121.6 nm) = 7.5 x 10^{-18} cm^2 [5.11]) is such that even at the highest NH_3 concentration used in this work (*ca.* 6 x 10^{14} cm^{-3}) the fraction of fluorescent photons absorbed would be less than 5 x 10^{-3} cm^{-1} . Quenching of $H(^2P)$ by NH_3 can also be ruled out from a consideration of the Stern-Volmer relationship

$$\frac{\tau_r}{\tau} = 1 + k_Q \tau_r [Q] \qquad (3)$$

in which τ is the observed lifetime of the fluorescer in the presence of quencher Q, τ_r is the zero-pressure fluorescence lifetime and k_Q is the rate coefficient for fluorescence

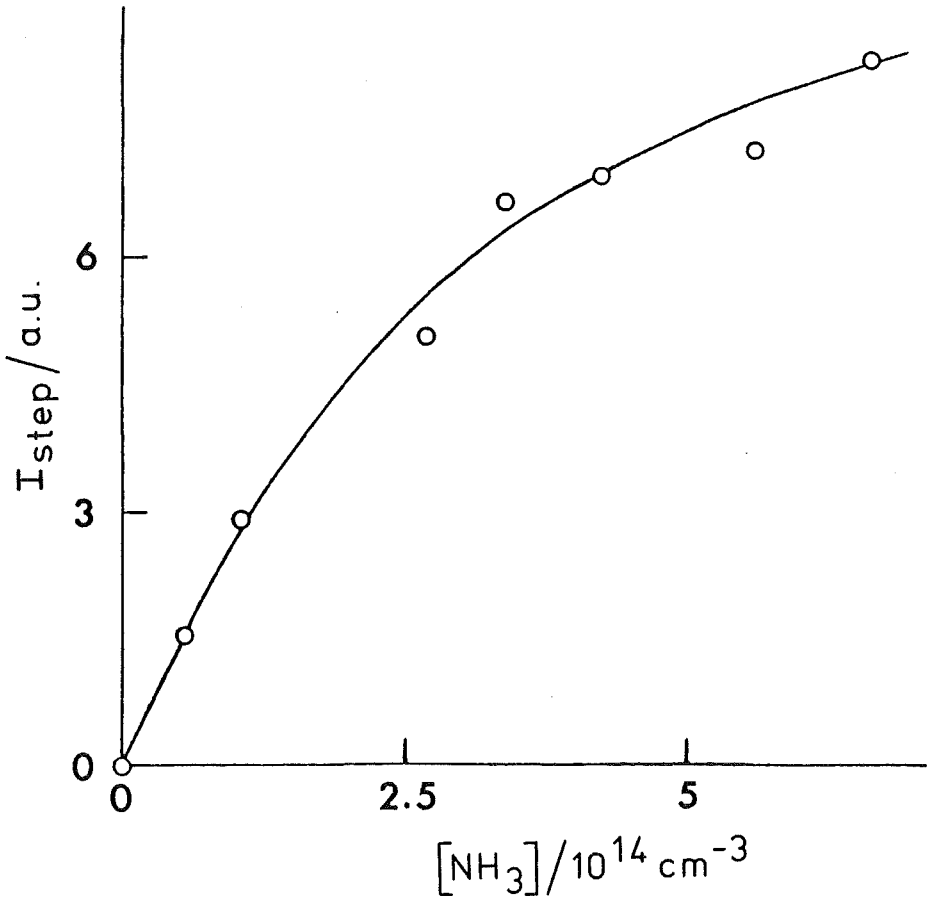

FIGURE 5.4: Variation of extrapolated step size at $t = 0$ with $[NH_3]$. Excimer laser pulse energy = 15 mJ.

quenching by Q. Taking $[NH_3]$ = 6×10^{14} cm^{-3} and assuming upper limits of 10^{-9} cm^3 s^{-1} and 10^{-8} s for k_{NH3} and τ_r ($H(^2P)$), equation (3) yields $\frac{\tau_r}{\tau}$ = 1.006 ≈ 1. Hence unless the fluorescence lifetime τ_r is significantly increased by some process such as radiation trapping the effect of quenching should be negligible. In view of the low H atom concentrations expected from the photolysis (10^{12} - 10^{13} cm^{-3}) and the short pathlength for reabsorption of fluorescence in the present cell, radiation trapping is unlikely to have been significant in these experiments.

Since the step size l_{step} in Fig. 5.4 is proportional to the concentration of H atoms formed in the photolysis event and so to the number of photons absorbed, the change in slope of the curve in Fig. 5.4 represents a decrease in the effective cross-section of NH_3 with increasing concentration, which is consistent with the saturation of some transition(s) contributing to the overall absorption. In view of the results of the direct measurements of the cross-section discussed in Section 5.2, which were made under conditions such that the single-photon absorption would not be expected to reach saturation except at the higher pulse energies, the present findings suggest that some higher-order absorption process is being saturated. It has been noted by Donovan [5.17] that such effects are common where sequential rather than simultaneous absorption occurs, as is likely for NH_3 . Spatial intensity variations ('hot spots') due to the multi-mode nature of the excimer laser's output [5.17] would appear to be a plausible cause of this behaviour.

Assuming that the relative importances of the processes described above vary more or less smoothly with the laser fluence or, equivalently, pulse energy, it is possible to make some predictions of the results to be expected from a comparison of the initial H atom yields in the presence and absence of excess N atoms. In the following arguments the N atom concentration is assumed to be sufficiently large that the fast reactions between N atoms and NH_2 or NH are essentially complete shortly after the photolysis pulse. The following cases may be considered:

Case 1: low laser fluence (single-photon absorption only),

$$NH_3 \rightarrow NH_2 + H$$

In this case the ratio R of initial H atoms yields (i.e. of the extrapolated Lyman-α fluorescence signal steps) obtained with and without N atoms should be either 1, if NH_2 is removed by reaction (1a) (no additional H atoms produced), or 3, if either process (1b) or (1c) + (2) occurs.

Case 2: intermediate laser fluence, $NH_3 \rightarrow NH + 2H$ predominantly.

Here the NH would be removed in the presence of N atoms by reaction (2) and R should be close to 3/2.

Case 3: high laser fluence, $NH_3 \rightarrow N + 3H$.

Addition of N atoms will have no effect on the initial H atom signal so that R should be 1.

In preliminary experiments the ratio R was measured over a range of NH_3 concentrations, total pressures and pulse energies, and quartz lenses were used to focus the photolysis beam to different extents. Values of [N] were typically in the range 10^{13} - 10^{14} cm^{-3} in these experiments, corresponding to pseudo-first-order lifetimes for reaction (1) in the 0.1 to 1 ms range. The observation of values of R close to 3 at the lowest available unfocussed laser pulse energies indicated that the spin-forbidden reaction (1a) is not a significant pathway for removal of NH_2 by reaction with N atoms. However, it was found that values of R close to 1.5 could be observed in experiments with the unfocussed laser operating at only slightly above its threshold level, indicating that two-photon and possibly higher order processes occur even at very low pulse energies. For this reason the excimer laser was used unfocussed in all subsequent experiments to determine the ratio R so that the value obtained in the limit of low pulse energies should correspond to predominantly single-photon absorption and thus be a true reflection of the mechanism of NH_2 removal. The results of these experiments are summarised in Fig. 5.5, in which R is plotted as a function of laser pulse energy for several NH_3 concentrations. As was indicated in the preliminary measurements, the value of R does in fact approach 3 at the low pulse energy limit, confirming that reaction (1a) is not an important pathway for the $NH_2 + N$ reaction. This result is expected in view of the high overall rate coefficient $k_1 = 1.21 \times 10^{-10}$ cm^3 s^{-1} and the violation of spin conservation required for reaction (1a) to proceed directly. R decreases with increasing pulse energy as expected, approaching the value of 1 predicted for total fragmentation of NH_3 at pulse energies of around 20 mJ. The apparent dominance of multiphoton processes at such low energies seems somewhat surprising in the light of the observations by Donnelly and co-workers [5.16] of $NH_2(\tilde{A}^2A_1)$ formation by single-photon processes at nominal pulse energies of 30 mJ. However it may be noted that absolute yields of NH_2 were not measured in [5.16] (the efficiency of formation of ground-state NH_2 was presumed to be 98 %) and that the Q(0,0) branch of the NH(A-X) system was observed to be very strong in emission, indicating that multiphoton effects were present to a significant extent. As has been noted by Donovan [5.17], rare gas/halide excimer lasers have multi-mode outputs; thus differences between the profiles of the excimer laser beams

used could be at least partly responsible for the apparent inconsistency between the present results and those of Donnelly *et al.*.

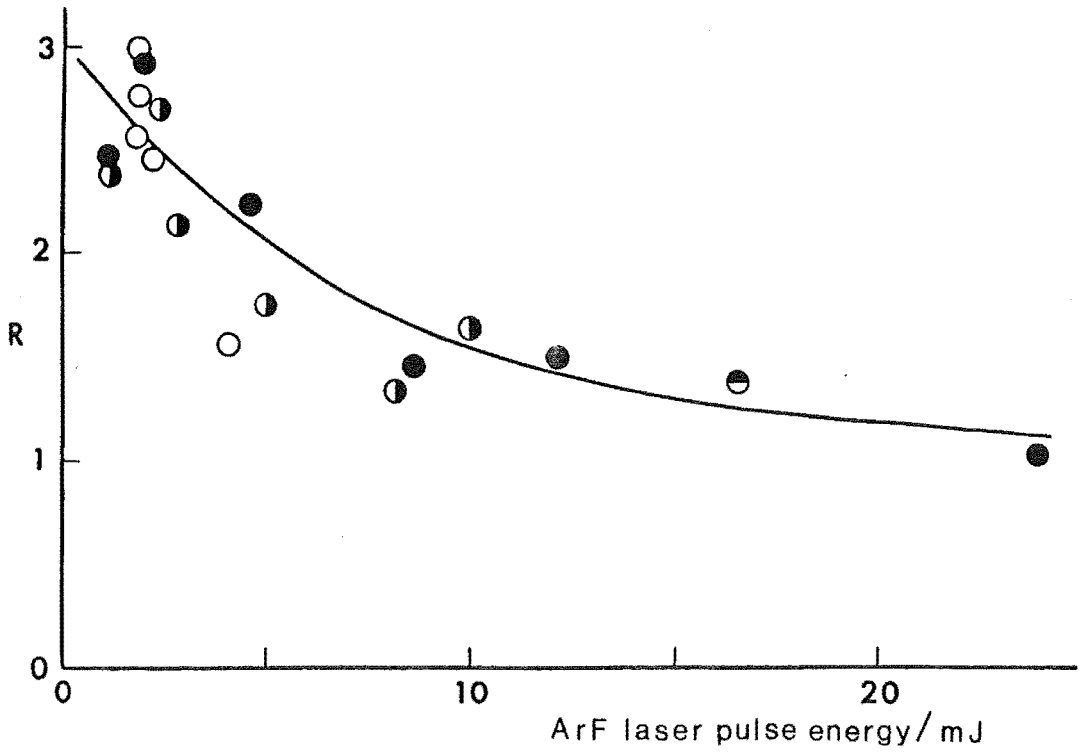

FIGURE 5.5: R (ratio of H atom signal step size with excess N atoms present to step size without N) *vs.* nominal laser pulse energy.

Circles, $[NH_3] = 4.7 \times 10^{14}$ cm^{-3} ; solid dots, $[NH_3] = 1.8 \times 10^{14}$ cm^{-3} ; vertically-divided circles, $[NH_3] = 3.2 \times 10^{14}$ cm^{-3} ; horizontally-divided circles, $[NH_3] = 5.8 \times 10^{14}$ cm^{-3} ;

The finding that the very exothermic reaction (1a) is unimportant at room temperature indicates that it would be unlikely to occur at very high temperatures as has been suggested by Kaskan and Hughes [5.9] in their study of NH_3 / O_2 flames. However it may be noted that the inclusion of reaction (1a) in their model mechanism was not considered to be crucial, so the present result probably does not invalidate any conclusions drawn in that work.

B. Analysis of H Atom Fluorescence - *vs* - Time Profiles.

In order to distinguish between the processes (1b) and (1c) + (2), the decay of the H atom fluorescence signal was studied at low laser pulse energies on the 30 ms timescale of the eductor sweep and the measured profiles were compared to ones calculated in numerical simulations of simple model mechanisms (see below). For these measurements it was necessary to work at N atom concentrations considerably lower than those used in the experiments described above; typical values of [N] were in the range 1×10^{12} - 3×10^{12} cm^{-3} . At these concentrations the pseudo-first-order lifetime for the NH_2 + N reaction (1) was 3 to 8 ms, so that low values of the ratio R were expected due to the incomplete formation of H atoms affecting the extrapolation of the semilogarithmic fluorescence decay plots to zero reaction time. Representative decay curves obtained under these conditions with and without N atoms present are shown in Fig. 5.6. The

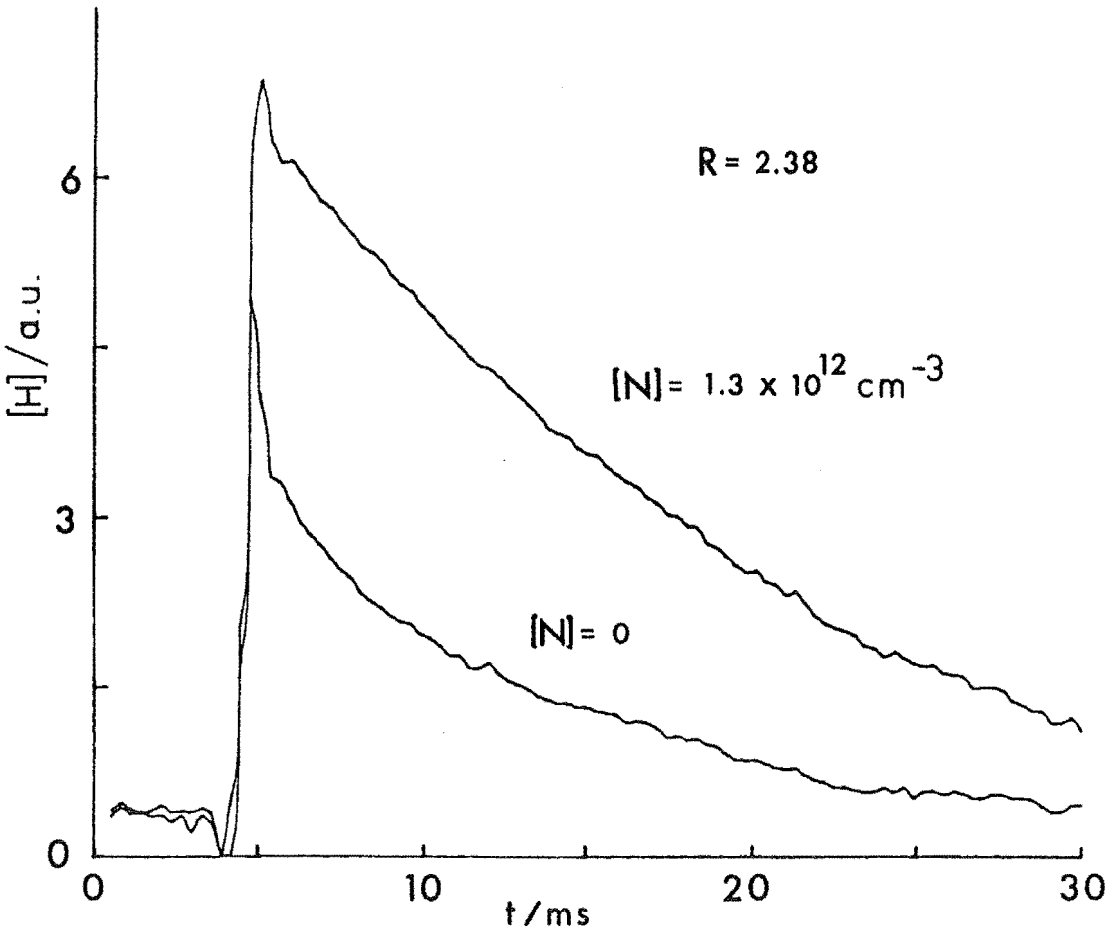

FIGURE 5.6: Time dependence of H atom concentration at low laser pulse energy (< 5 mJ).

R = ratio of extrapolated H atom signals at time of laser pulse.

sharp initial peak in each plot is due to the incomplete subtraction of the corresponding laser spike and was not included in the extrapolation to determine the step size. The value of R obtained from this pair of curves is 2.38, which is reasonable in view of the low N atom concentration in this run ([N] = 1.3 x 10^{12} cm^{-3}, $\tau \approx$ 6 ms).

The computer simulations of the fluorescence decay profiles were performed by Professor L. F. Phillips using the DEC LSI 11/23 microcomputer. In these simulations the photolysis of NH_3 was assumed to be the only process for NH_2 formation, which was taken to be complete at zero reaction time. From the experimental decay curves obtained in the absence of N atoms a first-order loss rate for H atoms could be calculated, this loss being primarily attributed to pumpout of the cell since the observed absence of any effect of pressure on the experimental results indicated that diffusion effects were negligible. The measured pumpout rates were typically in the range 50 - 150 s^{-1} and were assumed to apply to all of the radical species except N atoms, whose concentration was taken to be constant. The model mechanism then consisted of the first-order loss processes together with either reaction (1b) (Scheme I) or reaction (1c) followed by (2) (Scheme II).

Scheme I:

$$H, NH_2 \rightarrow \text{pump} \qquad (4)$$

$$NH_2 + N \rightarrow N_2 + H + H \qquad (1b)$$

Scheme II:

$$H, NH, NH_2 \rightarrow \text{pump} \qquad (4)$$

$$NH_2 + N \rightarrow 2NH \qquad (1c)$$

$$NH + N \rightarrow N_2 + H \qquad (2)$$

The rate equations for these schemes were integrated to give closed-form expressions for the time dependence of [H] in terms of the rate coefficients k_{1b} , k_{1c} and k_2 , the pumpout rate k_4 , and the initial concentration of N atoms. These expressions were incorporated in a simple BASIC program which generated 500 point [H] - *vs* . - t data files; these could then be processed in the usual way, using the program EDPROC to determine the initial concentration $[H]_0$ by extrapolation of the simulated curves to $t = 0$. The previously measured value of 1.21 x 10^{-10} cm^3 s^{-1} (see Chapter 4) was used for the rate coefficient k_{1b} or k_{1c} , while the experimentally unstudied reaction (2) was assumed to be similarly fast, estimates of k_2 between 1 x 10^{-10} and 5

x 10^{-10} cm^3 s^{-1} being used in these simulations. The value of [N] used were the appropriate experimental concentrations determined by photometric titration.

The results of such simulations carried out using the values of [N] and k_4 appropriate to the experimental decay plots in Fig. 5.6 are shown in Fig. 5.7. Curve D represents the decay of [H] due to pumpout only ([N] = 0, k_4 = 120 s^{-1}) and curve A is the profile calculated from Scheme I with [N] = 1.3 x 10^{12} cm^{-3} , while curves B and C were calculated from Scheme II with the same [N] and k_4 , and using values for k_2 of 5 x 10^{-10} and 1 x 10^{-10} cm^3 s^{-1} , respectively. The maxima in curves A and B represent the initial growth of [H] due to reactions (1b) and (2), respectively, and were not included in

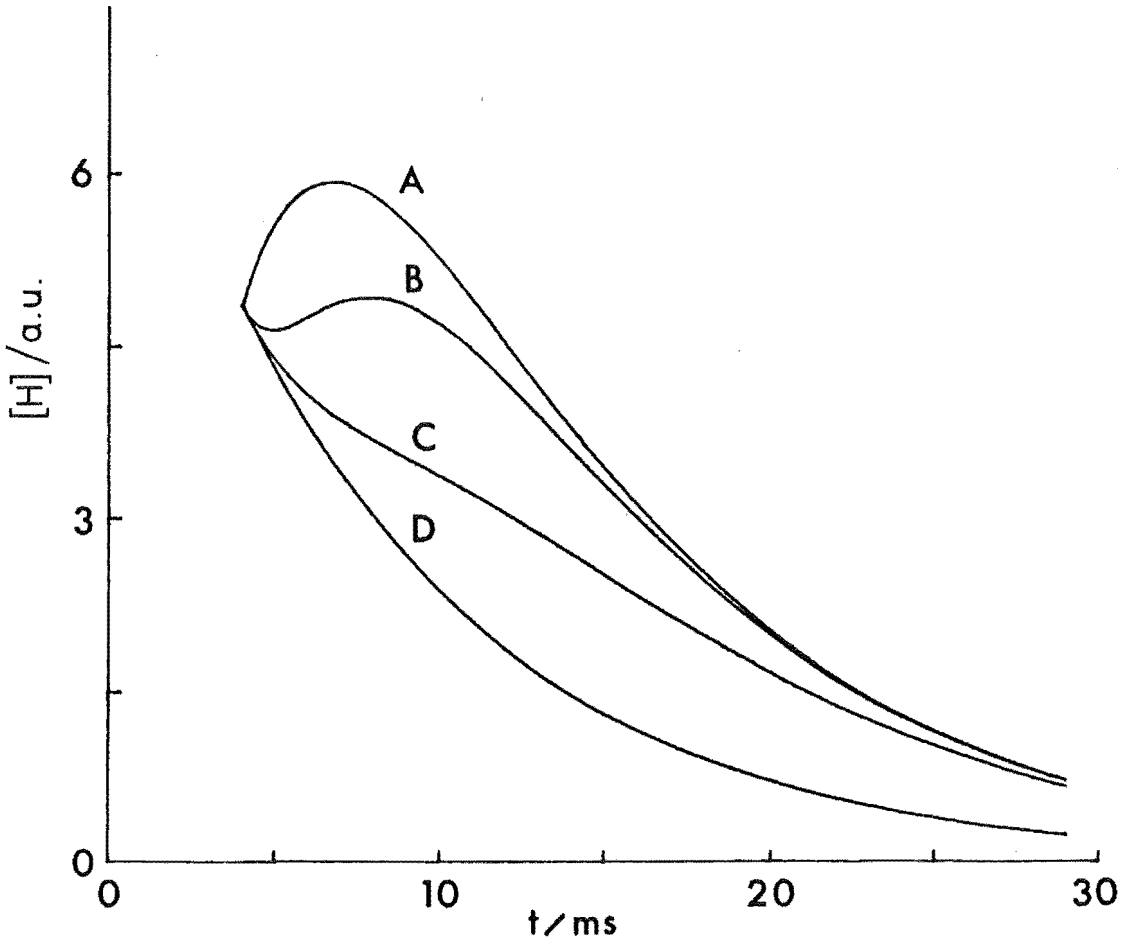

FIGURE 5.7: Simulated time dependence of [H].

A with [N] = 1.3 x 10^{12} cm^{-3} , H atoms produced by reaction (1b); B - same [N], H atoms produced by reactions (1c) and (2) with k_2 = 5 x 10^{-10} cm^3 s^{-1}; C - as for B but with k_2 = 1 x 10^{-10} cm^3 s^{-1}; D - [N] = 0 (pumpout rate = 120 s^{-1}, as for lower curve in Fig. 5.6).

the extrapolation to determine $[H]_0$. From curves A and D the calculated ratio R = $\frac{([H]_{0,A})}{([H]_{0,D})}$ was 2.46 if the extrapolation was based on points 200 - 500 (i.e. from t = 10 ms onward), falling to 2.18 if the extrapolation included all points beyond t = 5 ms. These results were in good agreement with the experimental ratio of 2.38 determined from the curves in Fig. 5.6. Since, qualitatively, these curves do not show the delayed maxima present in both curves B and C of Fig. 5.7, and as the very large value of k_2 used to calculate curve B can probably be regarded as an upper limit, it can be concluded that reaction (1b) is the major pathway for the NH_2 + N reaction, although in the absence of a measured value for k_2 no quantitative estimates of the branching coefficients for reactions (1b) and (1c) can be made.

This result is consistent with the heats of reaction for pathways (1b) and (1c) calculated using the most recent data for ΔH_f (NH) and ΔH_f (NH_2) (see footnote to page 62), while the observation of very small LIF signals at 336.0 nm in the earlier study of the NH_2 + N reaction (see Section 4.3) further supports the conclusion that reaction (1b) is of only minor importance for the removal of ground-state NH_2 at room temperature. It may, however, become significant at higher temperatures as has been suggested by Kaskan and Hughes [5.9]. Possible alternative sources of NH in the present system include the reactions of electronically and/or vibrationally excited NH_2 with N atoms. Donnelly *et al.* [5.16] have presented evidence for the production of NH_2 in its ground electronic state but with an inverted v_2'' vibrational population (v_2'' > 4) in the 193.3 nm photolysis of NH_3 , as well as observing the formation of a small amount of NH_2 in its first excited electronic state, as noted above. The fundamental frequency of the bending vibration v_2'' is 1498 cm^{-1} [5.19] or 17.9 kJ mol^{-1} , so that at most six quanta are required in v_2'' to render reaction (1b) thermoneutral, while the $\tilde{A}^2A_1$ state of NH_2 lies some 123 kJ mol^{-1} (10249 cm^{-1} , [5.20]) above the ground state. However, the measured average lifetime for NH_2 ($\tilde{A}^2A_1$) of 31 ± 4 μs and the rate coefficient for quenching by NH_3 (6 x 10^{-10} cm^3 s^{-1} [5.21]) are such that under the conditions of the earlier experiments ([NH_3] = 3 x 10^{14} cm^{-3} , [N] = 5 x 10^{13} cm^{-3} , 0.5 ms timescale, typically) the reaction between NH_2 ($\tilde{A}^2A_1$) and N atoms would have been negligible, assuming the same rate coefficient of 1.21 x 10^{-10} cm^3 s^{-1} for the reactions of both ground- and excited-state NH_2 .

C. Attempts to Detect H Atoms from the NH_2 + NO Reaction.

As has been noted earlier (Chapter 4) the reaction

NH_2 + NO → products (5)

has been subject of considerable interest over the last fifteen years due to its roles in atmospheric and combustion chemistry. However, although a large number of experimental studies have been made on this system (see Table 4-3), the nature and distribution of the primary products is not yet well characterised. It is generally accepted that N_2 and H_2O are the major products at room temperature, but the observations of significant yields of OH by several groups [5.1, 5.22, 5.23] has indicated that the alternative channels

$$NH_2 + NO \rightarrow N_2H + OH \qquad (5a)$$

$$\rightarrow N_2 + H + OH \qquad (5b)$$

may also be important. (Other product channels for reaction (5) have been ruled out either on energetic grounds or by experimental results, e.g. the non-observation of N_2O in the mass spectroscopy studies of Silver and Kolb [5.22] and Andresen *et al.* [5.23]. See [5.3] and [5.22] for further discussions.) These radical-forming processes have been invoked as key steps in the industrially important Thermal deNO_x process [5.24, 5.25] since they permit the observed temperature dependence of NO destruction in this system to be reproduced in modelling studies. In fact, Miller and co-workers [5.3] have suggested that reaction (5a) may be the dominant pathway throughout the temperature range 210 - 1500 K. Some evidence to support this proposal has since been provided by measurements of branching coefficients for OH production ranging from $\alpha < 0.22$ [5.1] to $\alpha = 0.7 \pm 0.2$ [5.23]. On the other hand, reaction (5b) now appears to be ruled out as a significant channel in this system in view of three separate reports of failures to detect H atoms in experiments using either electron spin resonance [5.26] or Lyman-α resonance fluorescence [5.22, 5.23].

The absence of the H atoms among the products of reaction (5) has been confirmed in the present study. The ratio of Lyman-α fluorescence steps at zero reaction time obtained with and without excess NO present was measured under conditions similar to those used in the earlier kinetics experiments on this reaction (see Chapter 4). At pressures near 1.4 Torr and NO concentrations between 5×10^{13} and 1.6×10^{14} cm^{-3} the mean value of R obtained at low laser pulse energies (*ca.* 5 mJ) was 0.99 ± 0.05, where the uncertainty is the standard error; the corresponding figure obtained in experiments at around 20 mJ/pulse was 0.98 ± 0.04. These results are in excellent agreement with those of Andresen *at al.* [5.23], who made similar measurements at three temperatures in the range 290 - 900 K, and Silver and Kolb [5.22]. Both of these groups reported branching coefficients for H atom production less than 0.05 at room temperature.

These findings, in conjunction with the observations of OH, would appear to support the suggestion of Miller *et al.* [5.3] that N_2H is produced in reaction (5). However, N_2H has never been observed directly and the calculations by Curtiss et al. [5.7] discussed in Section 5.1 predict that, even at room temperature, N_2H should dissociate to N_2 + H on a timescale much shorter (< 10^{-10} s) than that used in the present Lyman-α fluorescence experiments or any of the earlier studies [5.1, 5.22, 5.23]. Since H was not detected in any of these studies, either N_2H is not a product of reaction (5), or the barrier to dissociation of N_2H calculated by Curtiss *et al.* [5.7] is too low. The latter seems unlikely in view of the fact that similar calculations on the isoelectronic molecule HCO predicted a barrier to dissociation to H + CO of 31 kJ mol^{-1} which is 21 - 25 kJ mol^{-1} higher than the experimental value (see discussion in [5.7]).

The foregoing arguments appear to call into question the operation of channel (5a) in the NH_2 + NO system. It may be noted here that Stief *et al.* [5.1] have presented evidence to suggest that observations of OH by earlier workers may have been due to the presence of impurities such as H_2O, but the LP/LIF measurements of Andresen et al. [5.23] show unequivocally that OH is formed in reactions occurring after the photolysis flash. There is thus a severe conflict between the results of sophisticated experiments on the one hand, and state-of-the-art theoretical predictions on the other, as to the importance of reaction (5a). Resolution of this disagreement is provided by our conclusion (see Section 6.3) that the reaction of NH with NO gives OH (but not H) and the likelihood that the systems in which OH was detected contained NH as well as NH_2 , the reaction of NH with NO being faster than that of NH_2 by a factor of 3.

5.5 Summary

A resonance fluorescence technique has been used to investigate the relative importances of different product channels for the reaction between N atoms and NH_2 radicals produced by laser photolysis of NH_3 . Multiphoton effects have been found to be important in the latter process, even at very low laser pulse energies. Measurements of relative yields of atomic hydrogen indicate that the pathway leading to N_2 + H_2 as products is not significant. From a comparison of H atom concentration - *vs.* - time profiles, measured at short times after the photolysis flash, with simulated decay curves calculated from simple model mechanisms, it was concluded that the direct formation of N_2 + 2H predominates over the delayed production of H *via* the reaction NH_2 + N $\rightarrow$ 2NH followed by NH + N $\rightarrow$ N_2 + H.

Attempts to detect H atoms produced in the reaction between NH_2 and NO gave a negative result, in agreement with earlier work on this system. This result has been

discussed in the light of recent theoretical and experimental studies relating to the mechanism of the NH_2 + NO reaction.

5.6 Epilogue

Since the completion of this work no further studies of the NH_2 + N reaction itself have appeared but there have been several reports of work relating to the NH_2 + NO reaction (5); these are briefly summarised below.

Hall *et al.* [5.27] have studied reaction (5) using infrared laser spectroscopy to monitor several of the important species in this system. The most notable feature of this work was the low value of 0.13 ± 0.02 obtained for the branching coefficient for OH production. This is considerably less than the previous estimates of 0.4 ± 0.1 [5.22] and 0.7 ± 0.2 [5.23], and mitigates against reaction (5a) being the major product channel at room temperature as was suggested by Miller *et al.* [5.3]. Branching factor values of 0.66 ± 0.03 and 0.85 ± 0.09 were derived for the channel leading to formation of H_2O, corresponding to measurements of the ratio of H_2O produced to NH_3 photolysed for different pairs of absorption lines. These results represent an approximate "materials balance" for reaction (5) and appear to confirm the theory that other product channels are unimportant [5.22], however, the mechanism of the reaction was not discussed in detail.

A comprehensive modelling study of the Thermal deNO_x process has been presented by Kimball-Lynne and Hanson [5.28]. In this work the products of reaction (5) were taken to be either $N_2 + H_2O$ or $N_2H + OH$ following the work of Silver and Kolb [5.22] and Andresen and co-workers [5.23]. The proposed mechanism, which was based on that of Miller *et al.* [5.3], was considered to give reasonable agreement with experimental data for values of α between 0.48 and 1.0. However the height of the barrier to dissociation of N_2H used in this work was taken to be 117 kJ mol^{-1} which is almost 5 times larger than the value of *ca.* 25 kJ mol^{-1} predicted in both the *ab initio* study of Curtiss *et al.* [5.7] and the more recent calculations by Melius and Binkley [5.29]. The latter estimate was rejected by Kimball-Lynne and Hanson since it required the use of values of α around 0.2 in their model calculations, which they considered to be too low. It must be pointed out, though, that the value of α is far from well-established since there have now been four experimental determinations of α spanning the range 0.11 - 0.9 including uncertainties. A definitive experimental study of the NH_2 + NO system in which all of the potential reactants and products are monitored under well-controlled conditions is thus still awaited. (Although Andresen et al. [5.23] have alluded in passing to a study of OH formation in reaction (5) using crossed molecular beams, no quantitative results were given.) In the meantime, questions regarding the involvement of N_2H both as a product of reaction (5) and as a reactant in the Thermal deNO_x system

remain unresolved. As noted above, the most likely solution to the problem of the OH branching coefficient, involving the reaction of NH with NO, is discussed in Chapter 6 of this thesis.

CHAPTER 6

REACTIONS OF NH with NO and NO_2

6.1 Introduction

Our initial interest in the reactions of the NH radical was stimulated by the observation of NH in the NH_2 + N reaction system, as described in Chapters 4 and 5. There are, however, numerous other reasons why a study of the kinetics of NH reactions would be desirable; some of these are presented below.

The NH radical is well known to be an important species in many different types of flame, where its characteristic $A(^3\Pi_i)$ - $X(^3\Sigma^-)$ band system is observable in both emission and absorption at wavelengths between 300 and 400 nm [6.1, 6.2]. The reactions of NH might therefore be expected to be important in the chemistry of flames containing NH_3 , N_2H_4 or other nitrogenous fuels, or in hydrocarbon flames supported by nitrogen oxides. Thus, for example Kaskan and Hughes [6.3] have included the reactions between NH and H, N and O atoms, as well as NH, OH, NO and O_2 , in a mechanism proposed to account for the concentration profiles of NH, OH, NO and NH_3 which they observed in a lean NH_3 / O_2 flame near 2000 K.

Emission from NH has also been detected in the so-called 'atomic' flames arising from reactions between N_2H_4 (and, to a lesser extent, NH_3) and H or O atoms generated by microwave or electrical discharges in H_2 or O_2 [6.1], where the conditions of excess atoms would ensure that the presumably fast reactions

$$NH + H \rightarrow N + H_2 , \qquad \Delta H_r = -102 \pm 2 \text{ kJ mol}^{-1} \text{ a)} \qquad (1)$$

and $$NH + O \rightarrow \text{products} \qquad (2)$$

would occur to a significant extent. These reactions have also been included by Miller *et al.* [6.5] and Kimball-Lynne and Hanson [6.6] in model mechanisms for the Thermal deNO_x process mentioned in Section 4.1.

The reaction

$$NH + N \rightarrow N_2 + H, \qquad \Delta H_r = -611 \pm 2 \text{ kJ mol}^{-1} \qquad (3)$$

was proposed by Back and Salahub [6.7] to account for their observation of virtually complete conversion of the $^{15}NH_3$ decomposed in normal (i.e. ^{14}N) active nitrogen to

a) ΔH_f(NH) = 356.5 ± 1.7 kJ mol^{-1} and ΔH_f(NH_2) = 191.6 ± 1.3 kJ mol^{-1} [6.4] used in this chapter.

$^{14}N^{15}N$ (see Section 4.1). Similar behaviour might be expected in the N_2H_4 / active nitrogen system where NH could be formed in collisions between hydrazyl (N_2H_3) radicals and electronically-excited nitrogen molecules. Reaction (3)is also thought to be important step for the removal of N atoms in reactions of active nitrogen with hydrocarbons. However, while early workers [6.8] generally assumed reaction (3) to be very fast, the mechanism suggested by Safrany and Jaster [6.9] to account for many features of the behaviour of hydrocarbon / active nitrogen reactions requires this reaction to be slow, even in the presence of excess N atoms, while reaction (1) is assumed to be relatively efficient under similar conditions.

More recently, the ratio of rates for reactions (1) and (3) was considered by Yung and co-workers [6.10] to be a key assumption in their model for the photochemistry of the atmosphere of Titan, being a significant factor determining the rate of HCN formation in the thermosphere. In this work reaction (3) was assumed to predominate over (1). Reaction (3) was also suggested as part of a cyclic scheme for the catalytic dissociation of CH_4 in this model, the NH being generated by reactions of $N(^2D)$ produced by electron impact on N_2. NH is unlikely to be an important species in the Earth's atmosphere however, due to the low penetrating power of radiation of sufficiently short wavelength to produce NH from NH_3 , which is the only likely precursor, and the small quantum yields for these photodissociation processes [6.11, 6.12].

Very few experimental kinetic data yet exist for these reactions. Expressions giving room-temperature values for k_1 between 3×10^{-12} and 7×10^{-12} $cm^3\ s^{-1}$ have been used in modelling studies by several groups [6.5, 6.6, 6.10]. The origins of the expressions given in [6.5] and [6.6] are not apparent from the available literature, while that used by Yung *et al.* [6.10] was derived from calculations based on activated-complex theory at high temperatures.

For the reaction (2), two exothermic channels exist, namely

$$NH + O \rightarrow NO + H, \qquad \Delta H_r = -297 \pm 2 \text{ kJ mol}^{-1} \qquad (2a)$$

and

$$NH + O \rightarrow N + OH, \qquad -94 \pm 4 \text{ kJ mol}^{-1}. \qquad (2b)$$

The room temperature rate coefficients predicted using the expressions given by Miller *et al.* [6.5] and Kimball-Lynne and Hanson [6.6] differ by factors of 6×10^3 for reaction (2a) and 10^6 for reaction (2b), although the disagreements are much less serious at temperatures appropriate to the Thermal deNO_x process, factors of 10 and 40 arising for channels (2a) and (2b), respectively, at $T = 1250$ K.

For reaction (3) the expression $k_3 = 1.1 \times 10^{-11} T^{0.5}$ given by Yung *et al.* [6.10] predicts a room-temperature rate coefficient of 1.9×10^{-10} cm^3 s^{-1} . This high value is in accord with our earlier result for the reaction between NH_2 and N (see Chapter 4) and is consistent with values estimated for the reactions of the isoelectronic CH_2 radical with O and N atoms at room temperature (8.3×10^{-11} and 2.2×10^{-11} cm^3 s^{-1}, respectively [6.10]). Estimates of k_3 between 1×10^{-10} and 5×10^{-10} cm^3 s^{-1} were used in modelling studies of the N + NH_2 reaction system described in Section 5.4 of this thesis.

As far as reactions of NH with molecular species are concerned, the reactions of $NH(a^1\Delta)$, in both the gas and liquid phases, have attracted some attention due to their relationship to the reactions of the isoelectronic species $O(^1D)$ and CH_2 ($^1A_1$) [6.13]. The latter species and its substituted analogues, the carbenes, are very important in synthetic organic chemistry [6.14]. However, very few measurements on ground-state NH reactions have been reported, as can be seen from Table 6-1 in which the results of previous kinetic studies are summarised.

TABLE 6-1. Rate coefficients for reactions of $NH(X^3\Sigma^-)$.

Reactant	T [a] (K)	p (Torr)	k [b] (cm^3 s^{-1})	Method [c]	Reference
NO	300	30 - 700	4.7±1.2 (-11)	FP/RA	[6.25]
	300	5	4.8±0.2 (-11)	LP/LIF	[6.13]
	rt	250-1000	3.8 (-11)	PR/RA	[6.26]
$O_2(^3\Sigma_g^-)$	296	0.4 - 900	8.5±0.9 (-15)	FP/RA	[6.35]
	268-543	0.9 - 8	9.7 (-15)	DF/RA	[6.36]
	349	760	≤ 3.3 (-14)	PR/RA/CS	[6.37]
$O_2(^1\Delta_g)$	295	0.9 -8	1.0±0.16 (-15)	DF/RA	[6.36]
NH	349	760	1.2 (-10)	PR/RA/CS	[6.37]
HO_2	349	760	7.2 (-11)	PR/RA/CS	[6.37]
NH_2	349	760	1.2 (-10)	PR/RA/CS	[6.37]
NH_3	300	0.005-0.9	< 8 (-17)	FP/RF	[6.38]
		1013	< 2 (-15)	PR/RA	[6.39]
		760	< 3 (-16)	PR/RA	[6.40]
hydrocarbons	rt	?	<< 1 (-15)est.	?	[6.13]

a) rt = room temperature. b) Figure in parentheses is base ten exponent.

c) FP - flash photolysis; RA - resonance absorption; LP - laser photolysis; LIF - laser-induced fluorescence; PR - pulse radiolysis; DF - discharge flow; CS - computer simulation; RF - resonance fluorescence.

The reaction

$$NH + NO \rightarrow \text{products} \qquad (4)$$

is the fastest of those whose rate coefficients have been determined directly (i.e. without the use of numerical simulations based on a model mechanism). k_4 is found to be between two and three times larger than the rate coefficient for the corresponding reaction

$$NH_2 + NO \rightarrow \text{products}, \qquad (5)$$

for which $k = 1.8 \times 10^{-11}$ cm^3 s^{-1} (see Chapter 4). This suggests that NH may compete with NH_2 for NO in systems where both are present. Such a situation may apply in the Thermal deNO_x process. However, of the two major modelling studies of this system which have appeared, one [6.6] did not include reaction (4) in the proposed mechanism, while the earlier, more extensive scheme postulated by Miller *et al.* [6.5] included reaction (4) but with a weak, positive temperature dependence of the rate coefficient, which predicts a value of $k_4 \approx 3 \times 10^{-12}$ cm^3 s^{-1} in the temperature range of interest (1000 - 1500 K); this is an order of magnitude less than the measured value at room-temperature. The omission of reaction (4) from the model in [6.6] is puzzling since reactions (1), (2a) and (2b), whose rate coefficients at 1250 K are comparable to the experimental room-temperature value of k_4, were included. In view of the pivotal role attributed to the NH_2 + NO reaction (5) in both studies, such an omission would appear to be potentially serious. The expression for k_4 used in [6.5], which under-predicts k_4 at room-temperature by a factor of 45, is also clearly incorrect.

Reaction (4) is also interesting from a theoretical viewpoint. By analogy with current ideas on the mechanism of the corresponding NH_2 reaction (5) [6.5, 6.6, 6.15 - 6.17], reaction (4) may proceed *via* formation and subsequent rearrangement of a bound intermediate complex, in which case the rate coefficient based on the disappearance of NH would be expected to show both temperature and pressure dependences, although the latter is not a necessary condition for the operation of such a mechanism, as discussed in Chapter 7 of this thesis. Lately, several theoretical studies have appeared in the literature in which the mechanism of reaction (5) has been discussed in terms of various forms of unimolecular reaction rate theory [6.15, 6.16, 6.18]. Very recently, Phillips [6.19] has computed the rate coefficients for reactions (4) and (5) using a dynamical theory to calculate the rate of radical capture due to long-range (dipole-dipole) interactions and taking into account the effects of intramolecular vibrational relaxation (IVR) occurring within the centrifugal barrier on the potential surface for the reaction.

The application of such theories to investigations of the mechanism of reactions (4) and (5) requires a knowledge of the temperature and pressure dependences of the rate coefficients k_4 and k_5, of the detailed form of the potential surfaces for the reactions, and of the reaction products. Quantum-mechanical calculations of the thermochemical and physical properties (including the molecular structures and vibrational frequencies) of various stable and transient species occurring along the proposed reaction pathways have been presented for reactions (4) [6.17] and (5) [6.15, 6.17, 6.20, 6.21]. The nature of the possible products from these reactions has been discussed by many workers (see e.g. [6.5, 6.6, 6.15, 6.17, 6.18, 6.20, 6.22]).

In the present study we have measured the rates of reaction (4) and the analogous, previously unstudied reaction

$$NH + NO_2 \rightarrow \text{products} \qquad (6)$$

as functions of temperature in the range 269 - 377 K, and examined the effects of different inert carrier gases on the room-temperature values of k_4 and k_6. This work has previously been reported as reference [6.0].

6.2 **Experimental**

The experimental method used was similar to that described in Chapters 3 and 4. The variable -temperature photolysis cell is shown schematically in Fig. 6.1. The long window-arms, which bore SUPRASIL quartz windows, effectively eliminated stray-light interference and ensured prolonged contact between the flowing gas mixture and the surrounding thermal jacket, through which was circulated a glycol/water mixture from a thermostat. Temperatures between 265 and 380 K were measured to within ± 1 ° C by a copper-Constantan thermocouple in the gas stream, just below the viewing region. Accumulation of photolysis products in the probe window-arms was prevented by introducing part of the gas stream through a port close to the probe window.

NH radicals were generated by 248.5 nm photolysis (KrF, 75-100 mJ/pulse at 40 Hz) of mixtures of hydrazine and either NO or NO_2 in an excess of inert carrier gas. Initial experiments using the 193.3 nm ArF laser with both NH_3 and N_2H_4 precursors resulted in rate coefficients for the NH + NO reaction (4) which were lower than previously measured values by a factor of 10. This was attributed to unidentified secondary processes generating ground-state NH on the 0.5 ms timescale used for these measurements.

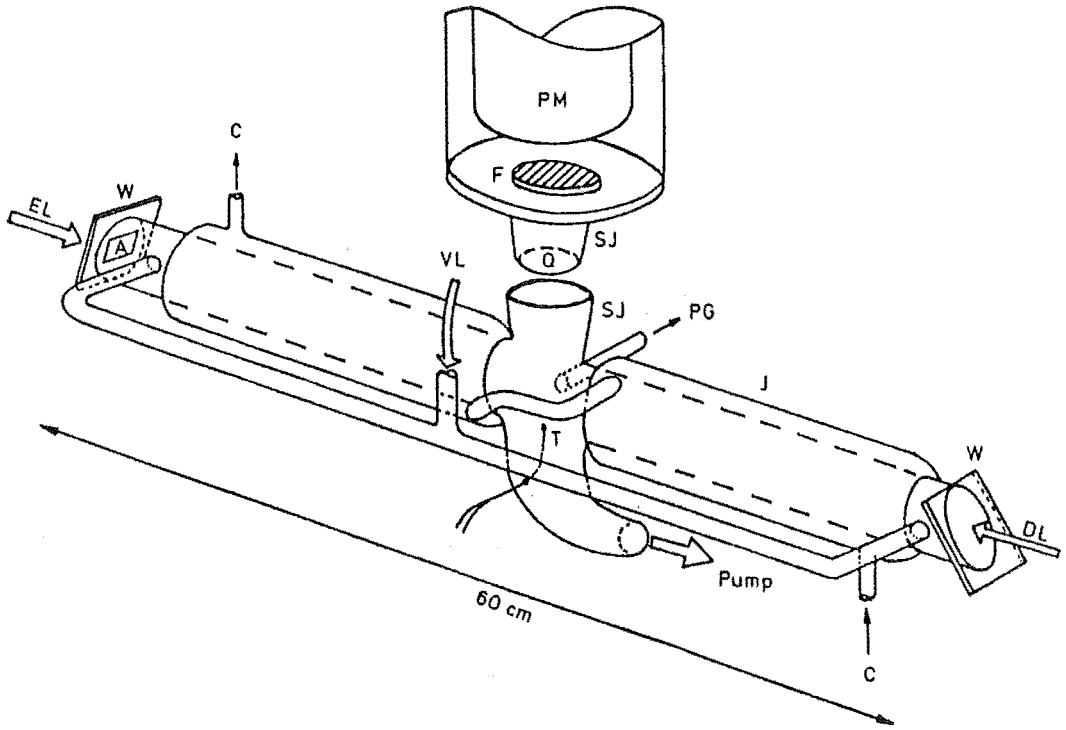

FIGURE 6.1: Schematic diagram of the photolysis cell.

Key: A - aperture; C - coolant; DL - dye laser beam; EL- excimer laser beam; F - interference filter; J - thermostatic jacket; PG - pressure gauge; PM - photomultiplier; Q - quartz window; SJ - standard-taper ground glass joint; T - thermocouple; VL - inlet from vacuum line; W - SUPRASIL window.

Typical concentration ratios in the cell were [M] : [N_2H_4] : [R] = 300 : 28 : 0 - 10 for M = Ar, He, N_2 or N_2O and R = NO or NO_2 , at total pressures between 0.9 and 1.1 Torr. Gases used were purified as described in Section 2.2; their concentrations were calculated as in Section 2.4. Hydrazine in the gas phase was obtained by passing a stream of the carrier gas at slightly less than atmospheric pressure through liquid hydrazine (anhydrous) in a saturator at room temperature. The final concentration of hydrazine was calculated from the measured temperature and saturator pressure (measured with the MKS Baratron gauge), using the vapour pressure data of Scott *et al.* [6.23].

In measurements of the transmitted laser power under normal experimental conditions, no absorption by N_2H_4 at the photolysis wavelength could be detected. From the estimated uncertainty in the power measurements, an upper limit of 5 x 10^{-19} cm^2 was

calculated for the absorption cross-section at 248.5 nm. The absorption spectrum of N_2H_4 between 210 and 260 nm has been measured by Willis *et al.* [6.24]. The single-photon cross-section at 248 nm was found to be 8.4 x 10^{-20} cm^2 ; this is consistent with the present result which likely represents both single- and multiphoton absorption by N_2H_4 , in view of the high pulse energies used.

As in the previous study of NH_2 radical reactions, NH was detected *via* LIF from the Q(0,0) branch of the $A(^3\Pi_i)$ - $X(^3\Sigma^-)$ transition at 336.1 nm, using a mixture of Cresyl Violet 670 and Rhodamine 590 dyes in ethanol and frequency-doubling the dye laser output at 672.2 nm with the angle-tuned KDP crystal. To avoid saturation of the EMI 9813QA photomultiplier tube by scattered photolysis radiation, it was necessary to use an interference filter (CORION INSTRUMENT CORPORATION, fwhm = 18 nm at 328 nm, 18 % transmittance at 336 nm) to isolate the LIF signal. Unfortunately the low filter transmittance, coupled with the low intensity of the frequency-doubled dye laser beam, resulted in rather small LIF signal levels which , in turn, led to difficulties in the initial establishment of the LIF signal. The latter problem was partly overcome by the use of an indirect method for initial tuning of the dye laser. This involved setting the 0.3 nm monochromator, with narrowed slits, to the intensity maximum in the NH(A-X) spectrum produced by a lamp consisting of a microwave discharge in argon flowing at 0.8 - 1 Torr pressure and containing a trace of N_2H_4 . For this procedure the wavelength-resolved emission was detected by an unfiltered EMI 9558QB photomultiplier connected to a KEITHLEY MODEL 417 picoammeter. The lamp spectrum shown in Fig. 6.2 is virtually identical to that obtained by Hansen and co-workers [6.25] from a similar lamp using NH_3 . The principle features are the Q-branches of the (0,0) and (1,1) vibrational bands at 336.1 and 337.3 nm, respectively, the very strong Q(0,0) branch appearing reversed in this spectrum due to absorption between the discharge region and the lamp window. The structure of the R- and P-branches of the (0,0) band due to the multiplet splitting in the $A(^3\Pi_i)$ upper state is clearly visible between 333 and 340 nm.

Once the monochromator wavelength had been set, the output from the 955QB photomultiplier was taken to the boxcar, the dye laser beam was diverted into the monochromator and the dye laser wavelength was optimised. Finally, the probe beam was returned to the cell and fine-tuning was carried out by very cautiously varying the due laser wavelength to obtain a maximum LIF signal under the conditions of the experiment, followed by optimisation of the aperture time and the variable delay between the boxcar gate and the dye laser pulse, as described in Section 2.3B.

Because of the low signal-to-noise ratios obtained in the LIF measurements, the number of individual samples of the boxcar output averaged at each point in the decay

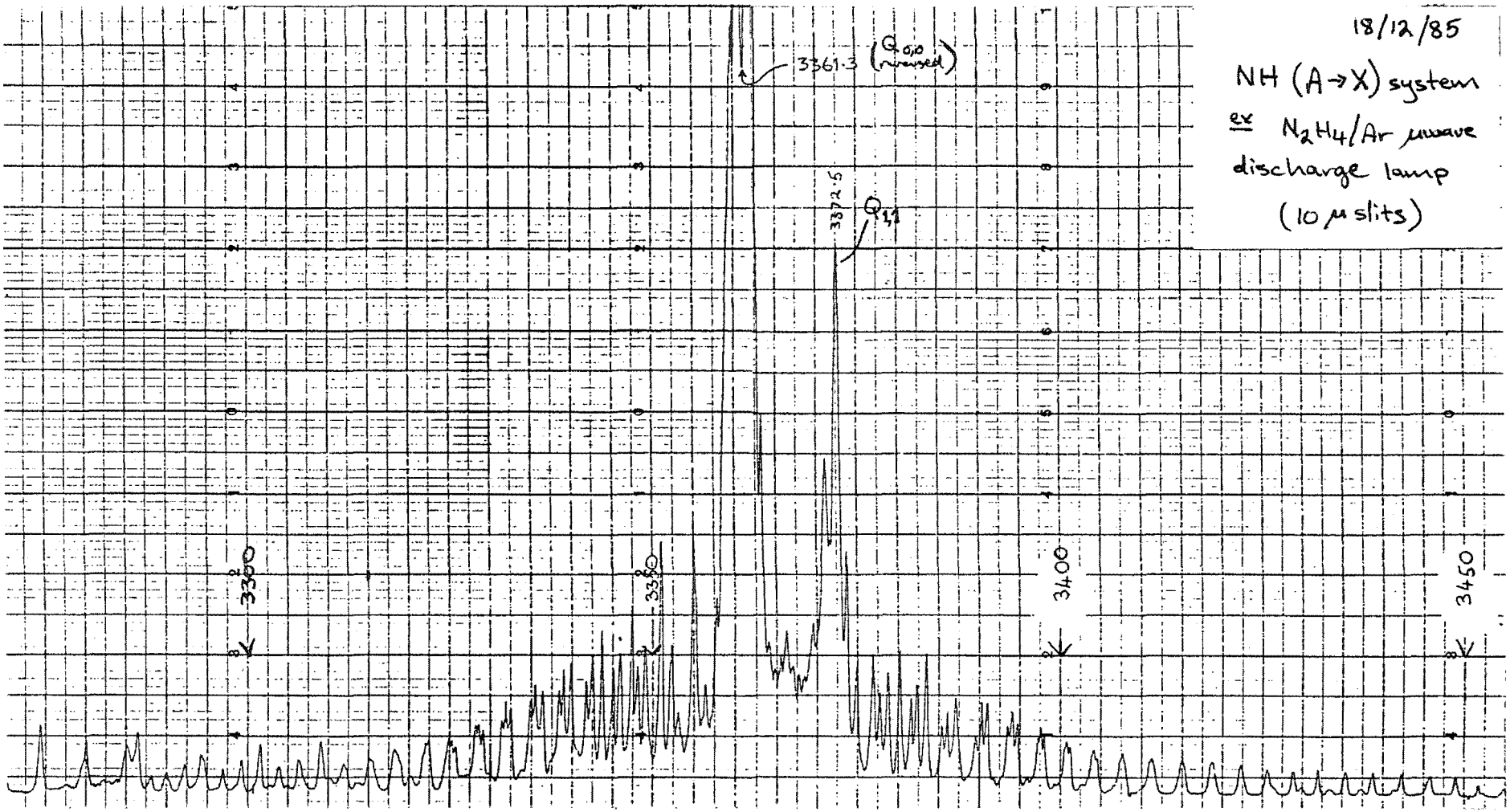

FIGURE 6.2: Spectrum of the N_2H_4 microwave discharge lamp between 325 and 340 nm.

curve for a given experiment was increased from 4 (as in the CN and NH_2 experiments) to 50. This was found to result in least-squares fits to the *ln* (I_f) - *vs* - *t* data of comparable quality to those in the previous studies, as measured by the RMS deviation of the points from the fitted line, despite the much-reduced signal levels.

6.3 **Results and Discussion**

A. Rate Coefficients for the Reactions of NH with NO and NO_2

Typical semilogarithmic plots of NH fluorescence intensity against probe laser delay time are shown in Fig. 6.3 for the NH + NO reaction. The linearity of these plots confirms that the reactant was present in excess, in spite of the relatively large concentration of hydrazine used, in agreement with our measurement of a small total absorption cross-section for N_2H_4 at 248.5 nm.

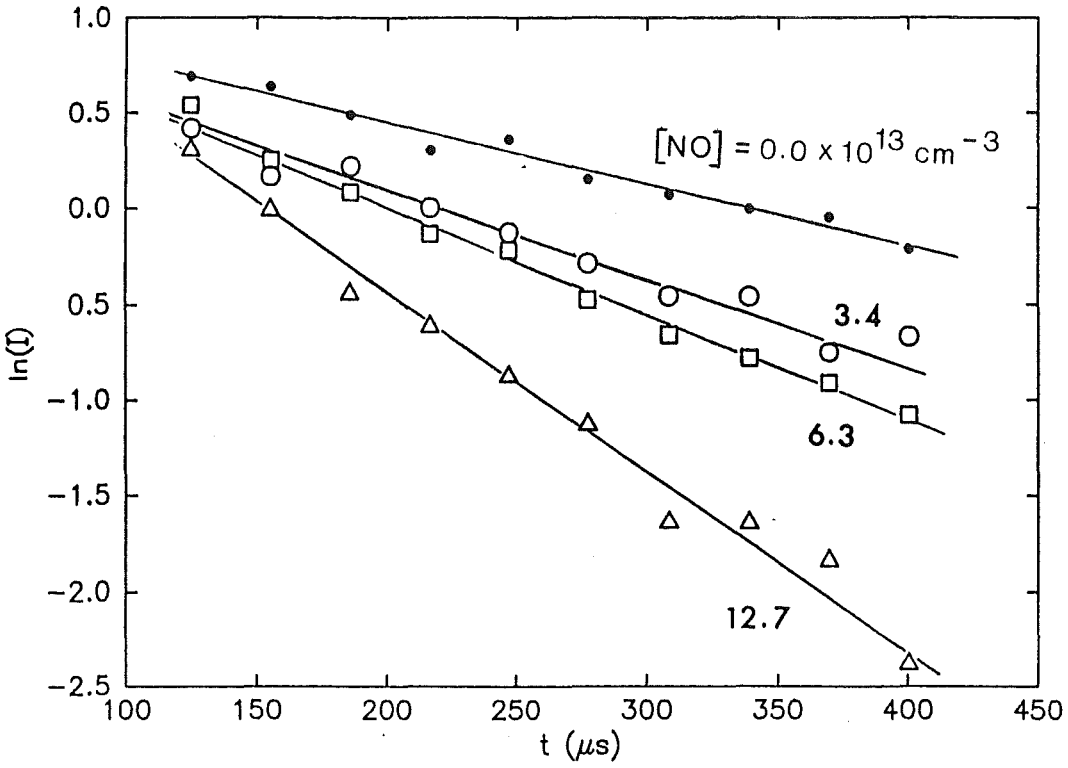

FIGURE 6.3: NH + NO → products: representative first-order decays of NH LIF intensity with time at T = 300 K, p = 1 Torr (Ar).

In Figs. 6.4 and 6.5 the room-temperature first-order decay rates k_1 (corrected for the effects of non-reactive removal of NH and a small component due to reaction with N_2H_4 ; see Section 6.5) are plotted as functions of the concentrations of NO and NO_2 , respectively. The different symbols used represent measurements performed using different carrier gases. Individual least-squares regression analyses of the data for each carrier yielded bimolecular rate coefficients k_2' which agreed with one another within their combined 95 % confidence limits, for both NO and NO_2 . Global fits using all of the room-temperature data for each reactant were therefore carried out; these yielded the rate coefficients k_4 (301±2 K) = 5.78 ± 0.64) x 10^{-11} cm^3 s^{-1} and k_6 (299±1 K) = 1.61 ± 0.14) x 10^{-11} cm^3 s^{-1} for the reactions of ground-state NH with NO and NO_2 , respectively. The uncertainty quoted in each case is the sum of the 95 % confidence limit on the regression slope from the k_1 - *vs* - [R] plot and the estimated ± 6 %

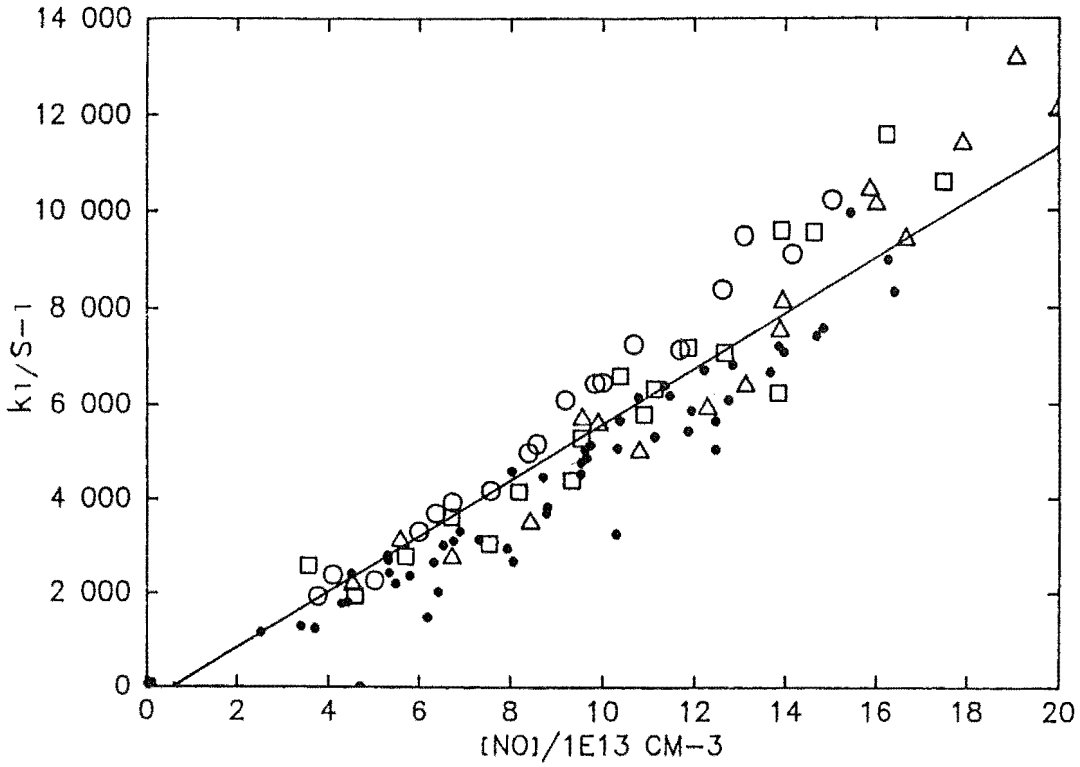

FIGURE 6.4: NH + NO → products: plot of pseudo-first-order decay rates k_1 *vs.* [NO] to determine k_4 at T = 299 ± 1 K.

Solid dots, Ar bath gas; circles, He; squares, N_2 ; triangles, N_2O. Solid line is least-squares regression line for all data.

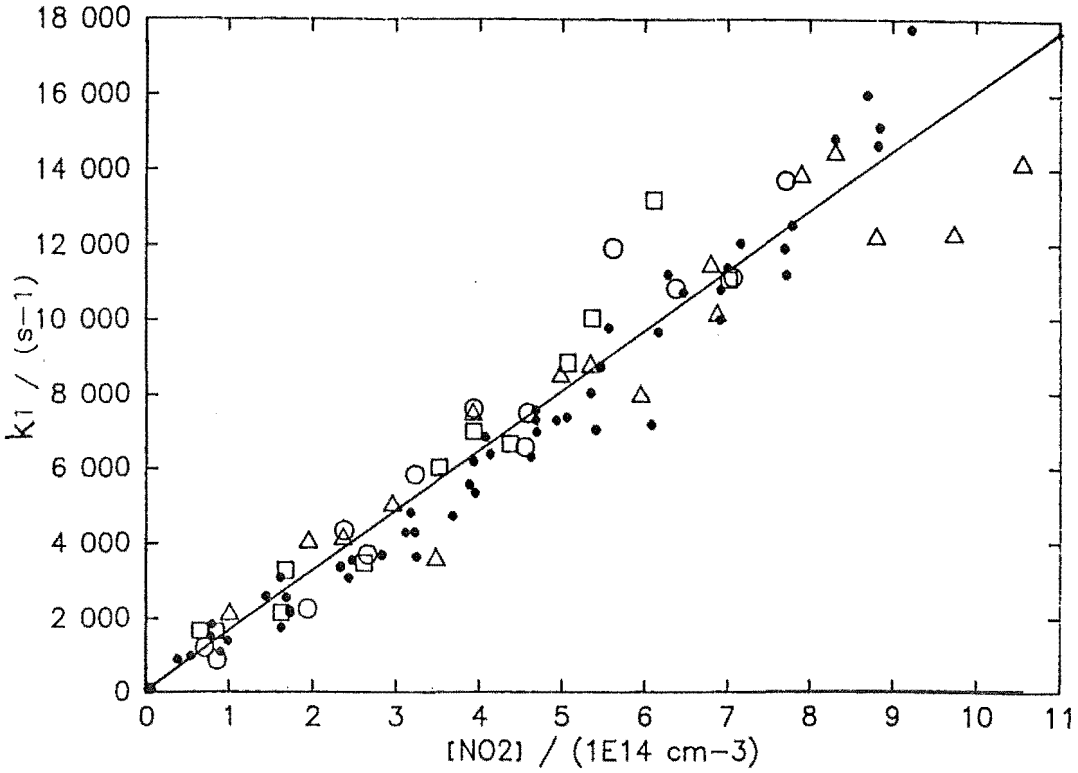

FIGURE 6.5: NH + NO_2 → products: plot of pseudo-first-order decay rates k_1 *vs.* [NO_2] to determine k_6 at $T = 301 \pm 2$ K.

Solid dots, Ar bath gas; circles, He; squares, N_2 ; triangles, N_2O. Solid line is least-squares regression line for all data.

systematic uncertainty resulting from the measurements of temperature, pressure, flow rate and delay time.

The absence of any distinct dependence of either k_4 or k_6 on the nature of the carrier gas used implies, in view of the variation in collision efficiencies among the carriers used, that both of these rate coefficients are pressure-independent in the region of 1 Torr. For the NO reaction (4) the pressure-independent regime may be extended by noting the reasonable agreement between the present value of k_4 at 300 K and the results obtained by Cox *et al.* [6.13] at 5 Torr and by Hansen *et al.* [6.25] between 30 and 700 Torr (see Table 6-1). The somewhat lower value measured by Gordon *et al.* [6.26] in pulse radiolysis experiments at pressures between 250 and 1000 Torr may have been due to the presence of secondary reactions or excited-state processes occurring as a result of the high energies associated with this technique.

The present work on the NH + NO_2 reaction (6) appears to be the first study of this system so no comparison of results is possible. However some comments on the relative values of k_4 and k_6 are made below.

The results of experiments to determine the temperature dependences of k_4 and k_6 in the presence of excess argon are summarised in Fig. 6.6, in which k_4 and k_6 are plotted directly against the temperature. Because smaller numbers of individual measurements of the pseudo-first-order decay rates were made at each of the elevated temperatures than at room temperature, the statistical analysis leading to each high temperature k_i - *vs* - [R] point was somewhat less precise. An approximate measure of the precision of these data was obtained by averaging the ratios $\Delta k_2 / k_2$ obtained at different temperatures, where Δk_2 was the calculated relative uncertainty in the bimolecular rate coefficient k_2, including both statistical and systematic contributions. This process yielded overall uncertainties of ± 15 % for both the NH + NO and NH + NO_2 data-sets; these uncertainties are included as error bars in Fig. 6.6.

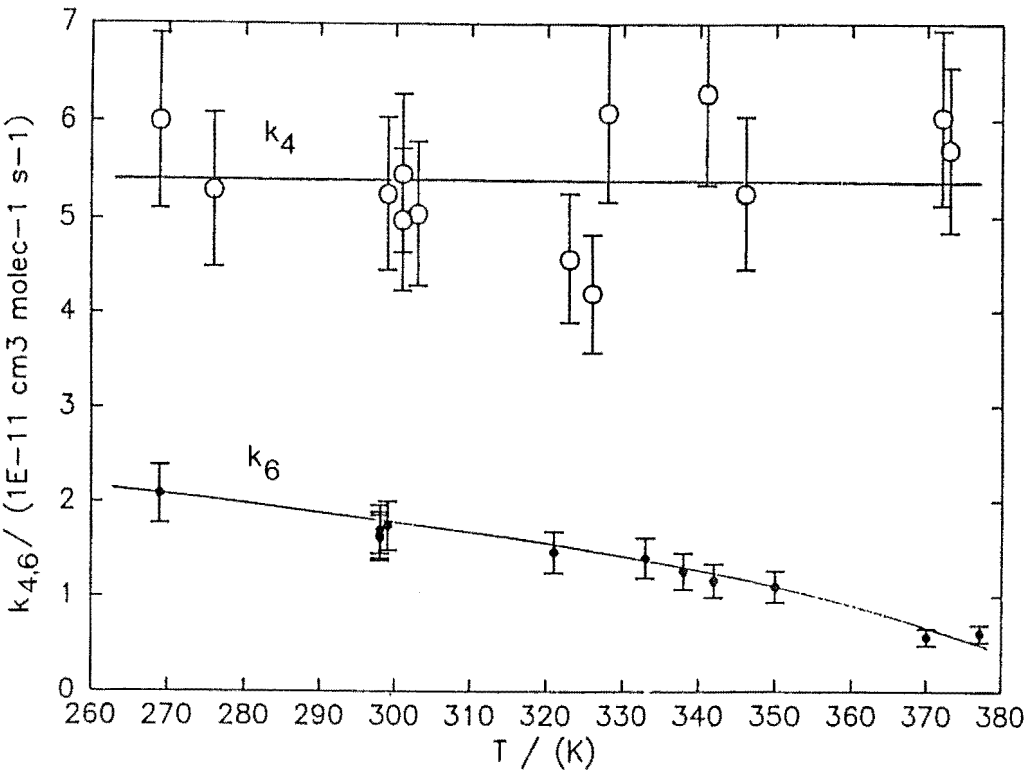

FIGURE 6.6: Temperature dependences of k_4 (NH+NO) and k_6 (NH+NO_2) measured in Ar bath gas. Error bars ± 15 %.

It may be seen from these plots that, within the given uncertainties, k_4 is essentially independent of temperature, while k_6 shows a small decrease with increasing temperature. Analysis of these data in terms of the usual Arrhenius expression

$$k = A \exp\left(\frac{-E_A}{RT}\right) \qquad (7)$$

gives activation energies of 0.4 ± 2.0 and -9.5 ± 3.2 kJ mol^{-1} for reactions (4) and (6) respectively (see Table 6.2). These values are consistent with the formation of adducts by association of the radical reactants, for which no activation barrier would be expected. The observation of pre-exponential factors which are less than the gas-kinetic limiting values typical for collisions between small molecules (10^{-10} to 10^{-9} cm^3 s^{-1}) could also be predicted on the basis of the orientational effects of the dominant dipole-dipole interactions. However, because the dynamics of complex formation are inadequately described by simple collision theory, not too much significance can be attached to such an analysis. In particular, no physical interpretation can be given to a negative activation energy.

TABLE 6-2. Analysis of k_1 - vs - T data for reactions of NH with NO and NO_2.

Reaction	$\ln k = \ln A - E_A/RT$			$\ln k = \ln A' - n \ln T$		
	$\ln A$	A (cm^3 s^{-1})	E_A (kJ mol^{-1})	$\ln A'$	A' (cm^3 s^{-1})	n
NH + NO (4)	-23.5 ± 0.8	6.2×10^{-11}	0.4 ± 2.0	-24.7 ± 4.4	1.9×10^{-11}	0.2 ± 0.8
NH + NO_2 (6)	-28.6 ± 1.2	3.8×10^{-13}	-9.5 ± 3.2	-4 ± 6	1.8×10^{-2}	-3.6 ± 1.1

The use of the alternative expression

$$k = A' T^n \qquad (8)$$

to analyse the temperature dependences of k_4 and k_6 is also unsatisfactory, due to the relatively small range of temperatures covered in the present experiments and to the presence of rather large uncertainties in the data. The failure of this treatment is best illustrated by the physically impossible value of the frequency factor A' predicted for reaction (6) (see Table 6-2.); the large regression error limits on $\ln A'$ indicate that the long extrapolation to $\ln T = 0$ is at least partly responsible for this result.

In view of these considerations, the present observations of the temperature dependences of k_4 and k_6 are probably best regarded as being consistent with, but not clear evidence for, the formation of intermediate complexes in reactions (4) and (6). A much wider range of temperatures than was available with the present experimental system needs to be covered in order to establish accurately the precise form of such weak temperature dependences.

B. The Mechanism and Possible Products of the Reactions of NH with NO and NO_2

Although the temperature dependences of reactions (4) and (6) are not unambiguously defined, it is still possible to make some comments regarding the mechanism of these reactions. The observation that the NO_2 reaction (6) is slower than that of NO (4) at all temperatures considered in this study, despite the larger dipole moment of NO_2 ($\mu = 0.32$ D *vs* $\mu = 0.15$ D for NO), is particularly suggestive. Since the rate of complex formation is determined by the strength of the dipole-dipole interaction between the approaching radicals, the formation of $HNNO_2$ must be faster than that of HNNO, which implies that the rearrangement of the complex is the rate-determining step, at least in the NO_2 reaction. At the same time, the observation of an approximately temperature-independent rate coefficient for reaction (4) suggests that the energy of the transition state leading to rearrangement of HNNO (TS1 in Fig. 6.7) is roughly equal to that of separated NH + NO, while the small, negative temperature dependence of k_6 indicates that the corresponding transition state for reaction (6) (TS2) lies slightly below the level of $NH + NO_2$. These factors, when combined with the observation that $k_6 < k_4$, imply that the binding energy of $HNNO_2$ with respect to separated NH and NO_2 is greater than that of HNNO relative to NH + NO, and that the barrier height for rearrangement of $HNNO_2$ lies between the binding energies of HNNO and $HNNO_2$ relative to their separated reactants, as shown in Fig. 6.7 in which the complexes HNNO and $HNNO_2$ are placed at the same energy for comparison purposes.

This argument is consistent with all of the present observations on the NH and NO reaction. However, the recent extensive *ab initio* calculations of Melius and Binkley [6.17] have indicated that the highest barrier to rearrangement of HNNO in an exothermic channel occurs in the pathway

$$NH + NO \rightarrow N_2 + OH, \quad \Delta H_r = -407 \pm 3 \text{ kJ mol}^{-1} \qquad (4a)$$

with the transition state lying some 79 kJ mol^{-1} below the energy of the separated reactants at 298 K. For the reaction

$$NH + NO \rightarrow N_2O + H, \quad \Delta H_r = -147 \pm 3 \text{ kJ mol}^{-1} \qquad (4b)$$

which these authors favoured as dominant pathway, the calculated barrier is lower than that for (4a) by a further 43 kJ mol^{-1} . On the basis of these results , a negative temperature dependence was predicted for k_4 , and reference was made to an unpublished study of H_2 /O_2 /Ar and H_2 /O_2 /Ar / pyridine flames in which such an effect was reportedly observed. However, the authors of [6.17] noted that the negative temperature coefficient obtained in this work was somewhat larger than would normally be expected.Thus, given the contrast between the relative simplicity of the present experimental technique and the difficulty of extracting reliable kinetic data for an isolated process from the complex reaction networks which occur in flames, this result may not be unequivocal.

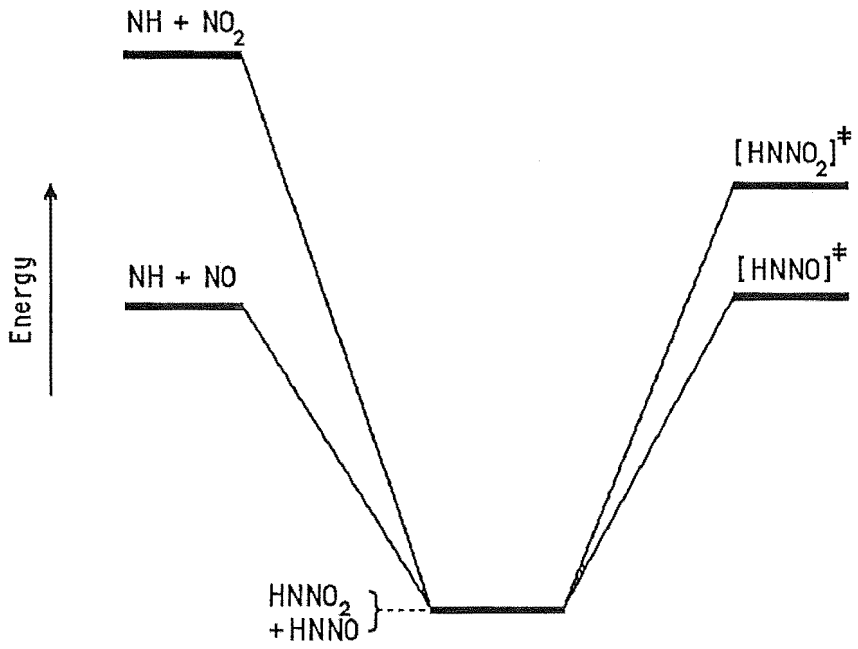

FIGURE 6.7: Relative energies of reactants, intermediates and transition states for rearrangement of intermediates in the NH + NO and NH + NO_2 reactions.

A knowledge of the product distributions from reactions (4) and (6) should provide valuable insight into the mechanisms of the reactions of both NH and NH_2 with NO and NO_2 . Information on the NH_2 + NO reaction (5), in particular, is of key significance for the successful modelling of the Thermal deNO_x process, as has been noted by Miller *et al.* [6.5] and Kimball-Lynne and Hanson [6.6]. It is generally accepted, following the work of Miller *et al.* that radical-forming channels for reaction (5) are required to account for the observed temperature dependence of NO destruction in this process, but the identity of these channels has not been clearly established, largely due to

conflicting reports of the importance of OH as a primary product of (5) (see discussions in [6.18], [6.22] and [6.27]). A consideration of the products of the analogous but simpler reaction (4) may help in resolving these issues.

The two processes (4a) and (4b) are the only exothermic channels for the reaction between NH and NO. Attempts to detect OH in the present system, *via* LIF from the $A(^2\Sigma^+)$ - $X(^2\Pi_i)$ transition excited at 306.4 nm, were unsuccessful. However , these were only preliminary experiments in which neither the excitation nor the detection system was fully optimised, so the operation of channel (4a) is not ruled out by this result. In fact, by analogy with the NH_2 + NO reaction (5) and in view of the large exothermicity involved, reaction (4a) leading to the formation of N_2 could be expected to be the major pathway. It may be noted that participation of this reaction to different extents in the NH_2 + NO systems studied by Silver and Kolb [6.28], Andresen *et al.* [6.27] and Hall *et al.* [6.22] could partly explain the widely varying yields of OH reported by these groups, all of which assumed OH to be a primary product of the NH_2 + NO reaction (5).

The operation of the alternative channel (4b) is counter-indicated by two earlier results. Mulvihill and Phillips [6.29] failed to detect N_2O in a hydrogen flame containing NH_3 and NO, while Whyte and Phillips [6.30] did not observe any change in the H atom yield from 193.3 nm photolysis of NH_3 on addition of NO at pulse energies such that NH would have been present due to multiphoton dissociation of NH_3 (see Chapter 5 of this thesis). On the other hand Melius and Binkley [6.17] have predicted that reaction (4b) should be the major product channel for the NH + NO reaction, in spite of its lower overall exothermicity, on the basis of their *ab initio* calculations of a lower barrier to rearrangement of the HNNO intermediate for this pathway than for reaction (4a). Although the identity of the major products from reaction (4) is so far unresolved, the general form of the potential energy surface derived by Melius and Binkley is supported by the recent semi-classical trajectory calculations of Phillips [6.19] which indicate, by the close agreement of the experimental reaction rate with the calculated dipole-capture rate, that all processes subsequent to the initial dipole-capture event (i.e. formation of HNNO) take place at energies at or below the energy of separated NH + NO.

For reaction (6) the following spin-allowed, exothermic channels are possible:

$$NH + NO_2 \rightarrow N_2 + HO_2, \quad \Delta H_r = -369 \pm 11 \text{ kJ mol}^{-1} \qquad (6a)$$

$$NH + NO_2 \rightarrow N_2O + OH, \qquad -269 \pm 4 \text{ kJ mol}^{-1} \qquad (6b)$$

and

$$NH + NO_2 \rightarrow NO + HNO, \qquad -200 \pm 3 \text{ kJ mol}^{-1}. \qquad (6c)$$

No previous experimental data exist for this reaction and, as for reaction (4), no OH was detected in the present study, although this observation was not conclusive. The observed temperature dependence of k_6 would tend to rule out the direct O-atom abstraction (6c), for which a positive activation energy, associated with the breaking of the O-NO bond, would be expected. Both the remaining pathways (6a) and (6b) are multicentre processes, which presumably would involve the initial formation of an $HNNO_2$ intermediate and are therefore consistent with the observed temperature dependence of k_6 . Of these, reaction (6b) seems to be the more likely in view of the simpler rearrangement required (a single 1,3 H-atom migration in the $HNNO_2$ complex followed by N-O bond fission, as opposed to the significant rearrangement of bonds in the NNO_2 skeleton required for elimination of N_2 after the initial H migration). Reaction (6b) also conforms to the pattern of N_2O formation observed in the corresponding reactions of N and NH_2 with NO_2 [6.31, 6.32].

The present observation of the negative temperature dependence of k_6 is the only existing experimental clue to the form of the potential energy surface for this reaction, and indicates that the barrier to rearrangement of the $HNNO_2$ intermediate lies below the energy of the separated reactants. However, the recent calculations of Phillips [6.19] predict a dipole-capture /IVR rate coefficient $k_{C,6}$ which is some four times larger than the measured value of k_6 at room-temperature, in contrast to the close agreement obtained between $k_{C,4}$ and k_4 for the NH + NO reaction. The reduction of k_6 relative to $k_{C,6}$ implies that the key factor controlling the rate of reaction (6) is the change of entropy occurring along the reaction coordinate rather than the corresponding enthalpy change, since the former contributes to the pre-exponential factor A in the transition-state theory (TST) expression for the rate coefficient k_6 and is thus consistent with both the reduced overall rate coefficient and the observed absence of a nett activation energy for reaction (6). (In TST, A is proportional to $\exp(\Delta S^{\neq}/R)$, in which the entropy of activation $\Delta S^{\neq}$ is associated with the structural changes which occur on passing from reactants to the transition state for the reaction, and R is the gas constant.) The finding that $k_{C,6} > k_6$ while $k_{C,4} \approx k_4$ then indicates a more negative entropy of activation, i.e. a 'tighter' transition state structure, for reaction (6) than for reaction (4). This argument also suggests that representations of potential energy surfaces based on free energies rather than enthalpies (as used in [6.17]) may be more useful for predicting the behaviour of these complex processes.

A careful study of both reactions (4) and (6), in which both reactant and product species are monitored on the same timescale over a wide temperature range, is clearly required to elucidate the mechanism of these reactions. Mass spectroscopic detection of N_2O would appear to be the simplest method of distinguishing unequivocally

between the pairs of reactions (4a) / (4b) and (6a) / (6b). An *ab initio* quantum-chemical study of these reactions is presently being carried out by Dr. G. A. R. Maclagan and Mr. J. A. Harrison of this Department in conjunction with the author [6.33]. Preliminary results indicate that the inclusion of electron correlation effects *via* perturbation theory is very important for an accurate representation of the HNNO and $HNNO_2$ intermediates, these being essentially unbound relative to reactants at the Hartree-Fock (single-determinant) level of theory. It is hoped that the results of this study may be useful in further studies of the reaction mechanisms using the RRKM-master equation formalism of unimolecular decay rate theory, similar to those described in Chapter 7 of this thesis for the NH_2 + NO reaction.

6.4 **Summary**

The LP/LIF method has been used to study the reactions of ground-state NH radicals with NO and NO_2 . At room temperature the rate coefficients k_4 = (5.78 ± 0.64) x 10^{-11} cm^3 s^{-1} and k_6 = (1.61 ± 0.14) x 10^{-11} cm^3 s^{-1} , respectively, were found to be independent of the nature of the carrier gas used in the experiment, implying pressure independence of both rate coefficients in the vicinity of 1 Torr pressure. The value obtained for k_4 is in reasonable agreement with the results of previous studies using similar techniques. The temperature dependences of k_4 and k_6 were studied at temperatures between 269 and 377 K: k_4 showed virtually no effect of temperature in this range, while a small negative temperature dependence was observed for k_6 . The implications of these results have been discussed with regard to the mechanisms and possible products of the reactions.

6.5 **Epilogue**

Since the completion of this work the rate of the reaction

$$NH + N_2H_4 \rightarrow \text{products} \qquad (9)$$

has been studied by Mr. J. A. Harrison of this Department in the same experimental system used for the present study. The effect of varying the N_2H_4 concentration upon the pseudo-first-order rate for NH removal was found to be very small, values of k = (3.6 ± 2.2) x 10^{-15} and (3.0 ± 2.5) x 10^{-15} cm^3 s^{-1} being obtained at 301 and 362 K, respectively. These very low values, which are close to the limit available using the present technique as indicated by the large uncertainties, presumably reflect a high barrier to the formation of an additional radical species in a process such as

$$NH + N_2H_4 \rightarrow NH_2 + N_2H_3\ ,\ \Delta H_r = -65 \pm 25\ kJ\ mol^{-1}\ ^{a)} \qquad (9a)$$

An attempt by Mr. Harrison to study the reaction between NH and N atoms (3) was unsuccessful due to the pronounced quenching of the active nitrogen afterglow which occurred on addition of even small amounts of N_2H_4 . This observation may imply the occurrence of a rapid reaction between N_2H_4 and N atoms which presumably proceeds through the formation of an intermediate complex, since the direct abstraction reaction

$$N + N_2H_4 \rightarrow NH + N_2H_3\ ,\ \Delta H_r = -16 \pm 25\ kJ\ mol^{-1} \qquad (10)$$

would be likely to have an appreciable activation energy, while the spin-forbidden process

$$N + N_2H_4 \rightarrow N_2 + H_2 + NH_2\ ,\ \Delta H_r = -376 \pm 3\ kJ\ mol^{-1} \qquad (11)$$

could conceivably occur with only small barriers to rearrangement of an N_3H_4 intermediate e.g. by dissociation of N_3H_4 to $H_2NN + NH_2$ followed by dissociation of 1,1-diazene. Energy transfer between excited N_2 molecules and N_2H_4 , folowed by relaxation or dissociation of N_2H_4* to give, e.g., NH_2 radicals, would also explain the observed quenching.

---

a) $\Delta H_f(N_2H_3) = 195\ kJ\ mol^{-1}$ taken from [6.34] , with an arbitrary estimate of $\pm 20\ kJ\ mol^{-1}$ for the uncertainty.

CHAPTER 7

THEORETICAL STUDIES OF THE NH_2 + NO REACTION MECHANISM

7.1 Introduction

As has been noted earlier (see Chapters 4, 5 and 6), the reaction

$$NH_2 + NO \rightarrow \text{products} \qquad (1)$$

has been the subject of considerable interest since the early 1970s. This interest was initially due to suggestions that reaction (1) could be important both in determining the fate of atmospheric NO [7.1, 7.2] and in combustion systems, notably the Thermal deNO_x process developed by Lyon and co-workers [7.3, 7.4] for the control of NO_x emissions from industrial combustion systems. More recently, though, this reaction has provided a considerable challenge to current theories of both chemical kinetics and molecular electronic structure (i.e. *ab initio* quantum-chemical theory). In this section recent applications of kinetic theories in studies of reaction (1) are discussed in order to provide the motivation for the *ab initio* investigation of the potential energy surface for the NH_2 + NO reaction described in Section 7.5. In the course of this discussion references will be made to concepts from statistical rate theories,in particular the transition-state or activated-complex theory (TST) and the Rice-Ramsperger-Kassel (RRK) and Rice-Ramsperger-Kassel-Marcus (RRKM) theories which are developments of TST applicable to unimolecular reactions. These theories have been the subject of many books and review articles, notably [7.5, 7.6] for TST and [7.7] for RRK and RRKM theories, hence only those details which are immediately relevant to the present discussion will be given in this section, together with appropriate references. A summary of the concepts and methods used in the *ab initio* calculations will be presented in Section 7.2. Before proceeding with the discussion of earlier theoretical work on reaction (1) it will be useful to review briefly the principal results of previous experimental studies of this system.

A. Experimental Results for the NH_2 + NO Reaction

Early work on reaction (1) was primarily concerned with determining the reaction products in order to explain the observed results of the ultraviolet photolysis of NH_3 in the presence of NO. Bamford [7.8] suggested that N_2 and H_2O were the only products and this was apparently confirmed in later studies [7.9 - 11]. Similar findings were reported by Fenimore and Jones [7.12] who studied the decomposition of NH_3 in a variety of low pressure flames. These workers were the first to propose that reaction (1)

might involve the formation and subsequent isomerisation of an intermediate addition complex; this process was tentatively represented by the reaction

$$NH_2 + NO \rightarrow H_2NNO \rightarrow HN{=}NOH \rightarrow N_2 + H_2O \qquad (2)$$

Support for this hypothesis was later provided by the results of Gehring *et al.* [7.13] who studied reaction (1) in a discharge flow system, using both time-of-flight mass spectrometry and absorption spectroscopy to detect reactant and product species. Both N_2 and vibrationally excited H_2O were observed among the products and evidence for the formation of an adduct species was found in the observation of MS signals at $m/e = 46$ and $m/e = 45$ at a reaction time of 5 ms.

The finding by McConnell [7.1] and Stuhl [7.2] in 1973 that the $NH_2 + NO$ reaction was a potentially important process in the regulation of atmospheric ozone levels and the development of the Thermal deNO_x process by Lyon and co-workers [7.3, 7.4] between 1973 and 1976 stimulated considerable interest in the kinetic behaviour of reaction (1). The nett result of this interest was that by early 1982 some eight studies of the rate of (1) had been reported, effectively spanning temperature and pressure ranges of 210 to 1215 K and 0.1 to 700 Torr, respectively. Attempts to detect alternative products such as H atoms, OH, HNO, N_2H, N_2O and HNNO had also been made using a variety of methods including LIF, emission and absorption spectroscopy, mass spectrometry and ESR (see Table 4-3). The combined results of these studies could be summarised as follows:

(i) Reaction (1) is fast, having a room-temperature rate coefficient $k_1 \approx 2 \times 10^{-11}$ cm^3 s^{-1} [a] which represents reaction on one in every 15 - 20 collisions;

(ii) k_1 shows a small negative temperature dependence, values of n in the range -1.85 to - 1.25 being reported by different groups following analysis of their k_1 - *vs* - temperature data by means of the expression $k_1 = A' T^n$;

(iii) k_1 is essentially independent of pressure in the range given above, and

(iv) only three product channels need to be considered, namely

$$NH_2 + NO \rightarrow N_2 + H_2O\,, \quad \Delta H_r = -524 \pm 2 \text{ kJ mol}^{-1} \qquad (1a)$$

---

[a] The value given here is that obtained in experiments using flash photolysis to generate the NH_2 radicals, and is roughly twice the value obtained in discharge-flow experiments. A rationale for this discrepancy is given in Section 4.3.

$\rightarrow N_2H + OH$, $57 \pm ?$ kJ mol^{-1} [a] (1b)

and $\rightarrow N_2 + H + OH$, -24 ± 2 kJ mol^{-1} (1c)

although the importance of the channels leading to OH production was not well established (see Section 5.4).

B. Studies of the NH_2 + NO System by Means of Statistical Rate Theories

The first attempt to predict the rate of reaction (1) from standard kinetic theories was reported in 1982 by Stief *et al.* [7.14]. In this work the possibility of a concerted mechanism leading directly to products was ruled out since, although a standard TST treatment for a radical recombination occurring with no activation barrier predicts zero pressure dependence and a temperature coefficient $n = -1.5$ in agreement with the experimental results for reaction (1), the requirement of a tight transition state for the extensive rearrangement involved would be expected to lead to low absolute values of k_1 (2 - 3 orders of magnitude less than gas-kinetic), due to the negative entropy of activation which arises from the increased normal mode frequencies at the transition state. Instead the reaction was proposed to proceed through a vibrationally excited-collision complex, and the absence of any pronounced pressure dependence of k_1 was taken to indicate that the lifetime of the complex is short relative to the mean time between collisions at the pressures normally used in discharge-flow or flash photolysis experiments, i.e. that rearrangement of the complex to form products competes effectively with collisional stabilisation. The mechanism was formulated as follows:

$$NH_2 + NO \underset{k_b}{\overset{k_{ad}}{\rightleftharpoons}} NH_2NO^* \xrightarrow{k_f} \text{products}, \quad (3)$$

$$NH_2NO^* \xrightarrow{\omega} NH_2NO$$

thermal decomposition of stabilised nitrosamine being considered unimportant, and the steady state approximation for $[NH_2NO^*]$ gave the observed rate coefficient as

$$k_1 = \frac{k_{ad}(k_f + \omega)}{k_b + k_f + \omega}, \quad (4)$$

---

[a] Calculated using $\Delta Hf(N_2H) \approx 300$ kJ mol^{-1} derived from data in [7.15] and experimental $\Delta Hf(H) = 218$ kJ mol^{-1} [7.16].

in which ω is the rate of collisions between the excited complex and bath gas molecules. This expression was evaluated within the framework of microcanonical transition state theory (μTST) [7.5], in which reaction is constrained to occur on a constant energy hypersurface in phase space [a]; this is equivalent to defining an energy-dependent rate coefficient $k_1(E)$. The observed or thermal rate coefficient k_1 at a given temperature T is then obtained by averaging $k_1(E)$ over an appropriate distribution of energies at that temperature. In the present case the resulting expression for k_1 was

$$k_1(T) = k_{ad} \int_0^\infty \frac{k_f(E) + \omega}{k_b(E) + k_f(E) + \omega} f(E)\, dE \qquad (5)$$

in which $k_f(E)$ and $k_b(E)$ are the energy-dependent rate coefficients for rearrangement and redissociation of the collision complex at energies between E and $E + dE$, and $f(E)$ is the chemical activation distribution [7.7] given by

$$f(E) = \frac{k_b(E)\, P(E) dE}{\int_0^\infty k_b(E)\, P(E)\, dE}$$

in which $P(E)$ is the Boltzmann distribution function.

The rate coefficient for complex formation, k_{ad}, was calculated from ordinary TST. No activation barrier was assumed for this process and the structure at the transition state was taken to be that of a weakly bound, Lennard-Jones-type complex. Such a loose transition state, which led to large values of k_{ad} (ca. 5×10^{-11} cm^3 s^{-1}), had to be invoked to allow the calculated values of k_1 to approach the experimental ones.

The rate coefficients $k_f(E)$ and $k_b(E)$, as well as $f(E)$, were calculated within the classical RRK approximation of unimolecular reaction rate theory [7.5, 7.7] . In this approximation the active internal modes of the reactant species are treated as a set of s

---

[a] This terminology arises from the classical mechanical formulation of μTST in which a reaction is represented by certain specified motions (trajectories) of points in a multidimensional space whose dimensions are the conjugate coordinates and momenta of all the degrees of freedom of the reacting system apart from overall translation.

identical harmonic oscillators, each having a frequency ν, and the microscopic rate coefficient $k(E)$ for a generalised unimolecular process occurring with a critical energy E_0 is given by

$$k(E) = \nu \left(1 - \frac{E}{E_0}\right)^{s-1}, \quad E > E_0 \qquad (6)$$

$$= 0 \qquad , \quad E \leq E_0$$

The frequency ν in this expression can be identified with the Arrhenius pre-exponential factor A and can thus be calculated from a knowledge of the structures of the reactant molecule in both its stable and transition state configurations, while the number of active oscillators s is generally treated as an adjustable parameter and is commonly taken to be half the number of internal modes of the reactant.

For the two channel mechanism given above, the planar structure I [a] for the nitrosamine molecule was taken from *ab initio* study by Casewit and Goddard [7.17] of the structures and energetics of several stable isomers of formula N_2H_2O. (This study is further discussed in Section 7.3.) The $k_b(E)$ values were calculated assuming the same transition state structure for the re-dissociation as was used to calculate k_{ad} ; the critical energy for this process was taken to be 128 kJ mol^{-1} following Casewit and Goddard. The forward rearrangement was assumed to lead directly to the formation of $N_2 + H_2O$ as products *via* an activated complex having the pyramidal structure II. The critical energy for this process was taken to be 42 kJ mol^{-1} . The possibility of rearrangement to hydroxydiimide HN=NOH *via* migration of an H atom, which had first been suggested by Fenimore and Jones [7.12] and later considered in some detail from a thermochemical point of view by Miller *et al.* [7.18], was rejected by Stief and co-workers [7.14] in view of the high barriers to both 1,2 and 1,3 H atom migrations which had been calculated for the isoelectronic nitrosomethane (CH_3NO) system [7.19]. Since the relationship among the stable species on the CH_3NO potential energy surface is very similar to that found for the NH_2NO system [7.17] it was thought that similarly high barriers to the rearrangement of nitrosamine could also be expected.

On the basis of these considerations Stief *et al.* [7.19] were able to reproduce the observed temperature dependence of k_1 quite closely, obtaining a value of $n = -1.73$, while the absolute values of $k_1(T)$ were some 60 % larger than the corresponding experimental values. In addition, the values of $k_f(E)$ and $k_b(E)$ obtained from equation

---

a) All molecular structures referred to in this chapter are shown in Fig. 7.1 on the foldout page at the end of this thesis (p. 164).

(6) were found to exceed the collision rate ω by 1 - 3 orders of magnitude, apparently confirming that collisional relaxation of NH_2NO^* is not important, and in agreement with the experimental pressure independence of k_1. However it should be noted that this treatment embodied several major assumptions and has been overtaken by subsequent developments. In particular the assumption made in [7.14] regarding the critical energy and structure of the activated complex leading to products have been shown to be erroneous (see Section 7.5 A).

A second study of reaction (1), involving both *ab initio* calculations of the potential energy surface and analysis of a proposed mechanism *via* statistical rate theory, was conducted by Abou-Rachid and co-workers [7.20]. From the *ab initio* calculations were obtained the structures, energies and vibrational frequencies of several stable and transient species occurring along each of two possible pathways, both of which involved initial formation of planar nitrosamine (I) followed by rearrangement of hydroxydiimide. The experimentally observed final products of the reaction can be formed from this species by 1,2 elimination of H_2O across the NN bond, corresponding to pathway (1a), or by appropriate bond fissions to produce either $N_2H + OH$ (1b) or $N_2 + H + OH$ (1c). The results of this study, which are further discussed in Section 7.5 B, indicated that while a pathway leading to hydroxydiimide *via* two successive 1,2 migrations of a hydrogen atom would have a significant nett activation energy, the transition state for a rearrangement *via* a 1,3 H atom shift lies at essentially the same energy as the separated reactants so that no activation barrier would be expected for this process. This result is in contrast with the findings of Adeney *et al.* [7.19] for the $CH_3 + NO$ system mentioned above and agrees with the earlier prediction made by Miller *et al.* [7.18] on mainly thermochemical grounds.

On the basis of these results the following mechanism was proposed for reaction (1):

$$NH_2 + NO \underset{k_{-1}}{\overset{k_1}{\rightleftharpoons}} NH_2NO^* \xrightarrow[1,3\ \text{shift}]{k_2} HNNOH \longrightarrow \text{products}, \qquad (7)$$

$$NH_2NO^* \xrightarrow{k_3} NH_2NO$$

in which the last step represents the combination of conformational changes in the initially formed hydroxydiimide which are necessary to permit ready formation of the observed products, and the appropriate bond fissions. The barriers to these conformational changes

were calculated to be much lower than that for the initial H atom migration. The observed rate coefficient was expressed in the form

$$k_{global} = \frac{k_1' k_2}{k_{-1} + k_2}, \qquad (8)$$

collisional stabilisation effects being neglected in view of the experimental zero pressure dependence of k_1.

A kinetic study of the reaction was then carried out using a similar approach to that of Stief *et al.* [7.14]. A Lennard-Jones-type structure was again assumed for the transition state for the association reaction and k_1' was calculated from ordinary TST at temperatures between 200 and 1500 K, the unimolecular rate coefficients k_{-1} and k_2 being obtained from "semiclassical RRKM" (i.e. RRK) theory. The transition state structure and frequencies used in the calculation of the RRK pre-factor for k_2 (see equation (6)) were those obtained in the *ab initio* study of the 1,3 migration pathway. The activation energy for this process was corrected for the effects of quantum-mechanical tunnelling; this brought the energy at the transition state just below that of separated NH_2 + NO. k_{-1} and k_2 were calculated explicitly at each temperature in the range studied, in contrast to the overall averaging procedure employed by Stief *et al.* (equation (5)).

The results of this study were considered to be in very good agreement with experimental results, in terms of both the absolute values of k_{global} obtained and the prediction of a negative temperature dependence for k_{global} in the range 200 - 700 K. However this agreement is marred by a serious arithmetic error in the tabulated values for k_{global}, the quantity given in Table 8 of [7.20] being in fact $\frac{k_1'}{k_{-1} + k_2}$ rather than $\frac{k_1' k_2}{k_{-1} + k_2}$ as required by equation (8). If the latter quantity is calculated from the given values of k_1', k_2 and k_{-1}, the resulting k_{global} values are larger than the experimental ones of Stief *et al.* [7.14] by factors of up to 2.5 and the predicted temperature dependence is significantly weaker than that observed in experiments, e.g. compare the calculated ratio k_{global} (298 K) / k_{global} (500 K) $\approx$ 1.2 with the experimental value of around 2.

The two studies described above suffer from a number of deficiencies. The first and most serious of these is the use of the classical RRK formalism in both cases for calculation of the unimolecular rate coefficients k_b and k_f (k_{-1} and k_2). The principal weaknesses of RRK theory are the inadequate treatment given to the internal modes of the reactant molecule and the activated complex for a unimolecular process, and the use of the

strong collision assumption which is inherent in this theory. The representation of the internal modes as a set of classical harmonic oscillators is physically unrealistic and is certainly a serious oversimplification for a loosely-structured species such as the activated complex for dissociation of NH_2NO, since this species will certainly posses torsional modes which are better approximated as hindered internal rotations. At the same time, high frequency vibrations such as the N-H stretching modes cannot be properly represented by a classical treatment. The use of values of s substantially less than the number of internal modes of the reactant is likewise unrealistic and, further, there is no *a priori* way of determining s for any given reaction. It may be noted that the prediction of no pressure dependence of k_1 in [7.14] was at least partly due to the low value of s used in calculations of $k_b(E)$ and $k_f(E)$.

The strong collision assumption, which asserts in essence that large amounts of energy are transferred in collisions or, alternatively, that a single collision is sufficient to transport an activated molecule below the threshold for reaction, is now known to be physically incorrect also; this is especially so for the case of chemically-activated systems, of which reaction (1) is an example, since the collision complex may be formed at energies much greater than those available in the case of thermal (i.e. collisional) activation only.

The use of RRK theory by Stief *et al.* [7.14] can be understood in view of the paucity of potential energy surface information then available, but it is more difficult to rationalise in the case of [7.20], especially in view of the fact that an extensive investigation of the potential surface had been carried out as part of the same study although, as will be shown in Section 7.5, some of the results of that investigation are open to question, including the structure and vibrational frequencies of nitrosamine itself.

A second problem is the question of the pressure independence of k_1, the prediction of which by Stief and co-workers was partly due to the use of the RRK theory, and which was simply assumed by Abou-Rachid *et al.* [7.20]. A thorough theoretical treatment of reaction (1) should be able to predict this result *a priori*. Finally, a comparison of the values of the association rate coefficients obtained in these two studies reveals that the predicted temperature dependence of k_1 is strongly dependent on the structure assumed for the transition state for the association of NH_2 and NO. In particular, it may be noted that in [7.14] where the transition state was assumed to have properties similar to those of separated reactants, k_{ad} was found to be only weakly temperature dependent, whereas in [7.20] the transition state was considered to resemble more closely the stable nitrosamine molecule, and the explicit inclusion of vibrational partition functions in the calculation of k_1' led to a considerably greater temperature

variation of this quantity than was found in [7.14]. It should also be pointed out that the *ab initio* calculations in [7.20] revealed no evidence for the existence of such a species. In fact the problem of describing the transition state for reactions which occur without appreciable activation energy is a major one which has received much study recently (see, e.g. [7.21 - 23]).

The first two problems mentioned above have recently been addressed in a study of reaction (1) by Gilbert, Whyte and Phillips [7.24]. In this work attention was focussed on an important feature of the potential energy surface for this system, namely the presence of significant anharmonicity, which arises from the extensive change in the bonding that occurs in passing from NH_2 + NO to the major products N_2 + H_2O. (Reaction (1) and others like it, in which such a major rearrangement of bonds takes place in an intermediate complex, might be termed 'bond-switching' reactions.) This anharmonicity can be viewed as a consequence of the existence of multiple minima in the potential energy surface, which thus cannot be adequately represented by a harmonic force field and which must also be non-separable in terms of normal modes at the energies at which the recombination occurs since regions of the surface corresponding to widely different geometries (e.g. compare I and III) are known to be connected by barriers lying at or below the energy of the separated reactants. (This may be deduced from the observed negative temperature dependence of k_1 .) These low barriers to rearrangement result in a high mobility of the H atoms in the collision complex and effectively render the complex very loose. It will be shown below that the pressure independence of k_1 can be directly attributed to the effects of these factors. The principal result of this work was the development of two relatively simple criteria for predicting whether the overall rate coefficient for a bond-switching reaction is likely to be pressure-independent. The derivations of these criteria are outlined below.

The mechanism of reaction (1) may be written as

$$NH_2 + NO \underset{k_{-s}[M]}{\overset{k_i}{\rightleftharpoons}} NH_2NO^* \xrightarrow{k_r} HNNOH \longrightarrow \text{products}, \quad (9)$$

$$k_s[M] \uparrow\downarrow NH_2NO$$

This is qualitatively similar to the mechanism treated by Abou-Rachid *et al.* [7.20] but differs from it in that both collisional stabilisation and activation steps, represented by k_{-s} [M] and k_s [M] respectively, are included. ([M] is the concentration of bath gas.) The

rearrangement of NH_2NO^*, symbolised by k_r, is assumed to lead irreversibly to final products *via* hydroxydiimide. The usual steady state treatment gives

$$k_1 = \frac{k_r k_i + k_r k_{-s} \dfrac{[M][NH_2NO]}{[NH_2][NO]}}{k + k_r + k_s[M]} \qquad (10)$$

for the observed rate coefficient k_1. The form of equation (10) is identical to that obtained by Patrick and co-workers [7.25] in their study of another bond-switching reaction, namely the disproportionation of HO_2 radicals to produce $H_2O_2 + O_2$. From calculations based on strong-collision RRKM theory (see below), these workers were able to reproduce the observed negative temperature dependence and small positive pressure dependence of the rate coefficient as well as its absolute value only by assuming the intermediate species H_2O_4 to have a high vibrational entropy, i.e. low vibrational frequencies. Similar results were obtained by Kircher and Sander [7.26] who also studied the $HO_2 + HO_2$ system by means of RRKM theory, although these workers neglected collisional activation effects. The treatment applied by Gilbert *et al.* [7.24] to reaction (1) was similar to that of Patrick *et al.* but featured an improved treatment of collisional effects through the use of a master equation formalism, thereby avoiding the strong collision hypothesis, as well as taking account of the anharmonicity effects described above.

The master equation for a given reaction system relates the time evolution of the system to the microscopic rate coefficients for the various contributing processes, e.g. chemical reactions, collisional activation and deactivation and/or radiative energy transfer. The basic theory of master equations is discussed in [7.7] and [7.27]; a more detailed treatment is given in [7.28]. If the mechanism in equation (9) is rewritten in general terms as

$$\begin{array}{ccccc} & & k_i & & k_r \\ A + B & \rightleftharpoons & AB^* & \longrightarrow & \text{products}, \\ & & {\scriptstyle k} \;\; {\scriptstyle k_s[M]} \big\downarrow \big\uparrow {\scriptstyle k_{-s}[M]} & & \\ & & AB & & \end{array} \qquad (11)$$

then, by analogy with equation (10), we obtain

$$k_1 = \frac{k_r k_i + k_r k_{-s} \dfrac{[M][AB]}{[A][B]}}{k + k_r + k_s[M]} \qquad (12)$$

and the following microcanonical master equation may be written:

$$\frac{\partial g(E,t)}{\partial t} = \omega \int_0^\infty [P(E,E')\, g(E') - P(E',E)\, g(E)]\, dE'$$

$$- k(E)\, g(E) - k_r(E)\, g(E) + k_i(E) \qquad (13)$$

Here $g(E,t) \equiv g(E)$ is the population of complex molecules (both AB and AB*) having internal energy E at time t, ω is the pressure dependent rate of collisions between AB and M, and $P(E,E')$ is the normalised probability distribution function for transfer of AB from energy E' to energy E by collision with M. The collisional energy transfer rates $\omega \int P(E,E')\, g(E')\, dE'$ and $\omega \int P(E',E)\, g(E)\, dE'$ correspond to the rates k_{-s} [M] and k_s [M], respectively, in equation (12); the rate coefficient $k_i(E)$ represents recombination of A and B to give AB with internal energy E. Assuming that a steady state concentration of AB is rapidly established, (13) reduces to

$$\omega \int_0^\infty [P(E,E')\, g(E') - P(E',E)\, g(E)]\, dE' - k(E)\, g(E)$$

$$- k_r(E)\, g(E) + k_i(E) = 0 \qquad (14)$$

For each energy E_i considered in a given range there will be a similar equation; taken together they constitute a set of coupled integral equations, the solutions to which are the populations $g(E)$. Given appropriate values of $k(E)$, $k_r(E)$ and $k_i(E)$ and the functional form of $P(E,E')$, such a system can be solved numerically using iterative matrix techniques, and the observed rate coefficient for product formation is then obtained as a weighted average of the microscopic rate coefficients at each energy level

$$k_{obsd} = \frac{\int_{E_{0,r}}^\infty k_r(E)\, g(E)\, dE}{\int_0^\infty g(E)\, dE} \qquad (15)$$

where $E_{0,r}$ is the critical energy for the rearrangement process. Alternatively, the corresponding quantities $k(E)$ and $E_{0,d}$ for the redissociation of AB to A + B can be used in (15) to obtain the overall rate coefficient for this process, k_{uni}, and the rate coefficient k_{rec} for the disappearance of A or B can be calculated from the microscopic reversibility relationship

$$k_{rec} = k_{uni} \frac{Q_{AB}}{Q_A Q_B} \exp\left(\frac{\Delta H^\circ (0\ \mathrm{K})}{RT}\right) \qquad (16)$$

in which Q_X is the total partition function for species X, calculated relative to its zero-point energy, and ΔH° (0 K) is the difference between the zero-point energies of A + B and AB. The criteria mentioned above for deciding whether the overall rate coefficient for the process illustrated in (11) should be pressure-dependent were obtained by considering the solution to equation (14) in the limits of long and short lifetimes for the collision complex AB. The former case arises when the rate of rearrangement to products is small, i.e. when $k_r << k + k_s$ [M] in equation (11), while the latter situation arises when rearrangement is fast, i.e. $k_r >> k + k_s$ [M]; this is the situation which was believed by Stief *et al.* [7.14] and Abou-Rachid *et al.* [7.20] to hold for reaction (1). These two cases are briefly discussed below.

Case 1: Slow Internal Rearrangement, Long-Lived Complex

In this case a pressure dependence of the overall reaction rate is possible through the effects of collisions on the population $g(E)$ which is governed by the relative rates of recombination, redissociation and collisional energy transfer. Since the first two of these processes are related by microscopic reversibility (equation (16)), the time development of $g(E)$ may be described by the master equation for unimolecular dissociation

$$\frac{dg(E)}{dt} \equiv -k_{uni}\, g(E) = \omega \int_0^\infty [P(E,E')\, g(E') - P(E',E)\, g(E)]\, dE'$$

$$- k(E)\, g(E). \qquad (17)$$

Solution of this eigenvalue problem by matrix methods yields the unimolecular rate coefficient k_{uni} directly, as well as the populations $g(E)$. If k_{uni} is pressure dependent (determined by varying $\omega = Z_{LJ}\, p$, where Z_{LJ} is the Lennard-Jones collision frequency) then so is the population $g(E)$. This results in the so-called fall-off behaviour characteristic of unimolecular reactions, which appears as a decrease in the observed rate coefficient with decreasing pressure. This happens because the decreased rate of collisional redistribution of the population of AB at low pressure is no longer sufficient to maintain an invariant (Boltzmann) distribution over the available energy levels, each level above $E_{0,d}$ being depleted by reactive loss which occurs with the rate coefficient $k(E)$. Many gas phase dissociation reactions and their reverse recombination processes are found to show this behaviour in the pressure range at which reaction (1) has been studied (mainly between 1 and 10 Torr). However, if for some reason the values of $k(E)$

are very low, then the competition between reactive loss and collisional redistribution will not become significant until much lower pressures than normal are reached, so that the overall rate coefficient k_{uni} , and hence also k_{rec} , reaches its high-pressure limiting value at a relatively low pressure. In the case of radical recombination occurring with no activation energy *via* a loose activated complex this value will approach the gas-kinetic collision rate, as is found for reaction (1).

Case 2: Rapid Internal Rearrangement, Short-Lived Complex

In this case a sufficient condition for the pressure independence of k_{obsd} was derived by considering the competition between rearrangement and collisional stabilisation of the excited AB molecule. This led to the development of the following expression for the probability P_r of a molecule undergoing rearrangement with a rate coefficient $k_r(E)$ before being de-energised by collisions:

$$P_r = 1 - \exp\left[-\frac{1}{\omega \langle \Delta E \rangle} \int_0^{E_{init}} k_r(E)\, dE \right] \qquad (18)$$

Here E_{init} is the initial energy with which the reactants A and B recombine, and $\langle \Delta E \rangle$ is the average energy transferred per collision. $\langle \Delta E \rangle$ can be calculated from the assumed form of $P(E,E')$ (see below). Thus given $P(E,E')$ and $k_r(E)$, P_r may be calculated from (18); if P_r is close to 1 at a given pressure then the observed rate coefficient will be pressure independent.

Either of the two conditions described above, namely pressure independence of k_{uni} as determined from the solution of equation (17) or a value of P_r close to 1, is sufficient to ensure that the observed rate coefficient will be pressure independent. If neither conditions holds then the pressure dependence of k_{obsd} must be determined from the full solution of equations (14) and (15).

As noted above the application of these tests requires a knowledge of the microscopic rate coefficients $k(E)$ and $k_r(E)$, as well as the collisional energy transfer probability distribution function $P(E,E')$. In fact the results of master equation calculations of thermal rate coefficients in the fall off region are generally found not to be very sensitive to the precise form of $P(E,E')$ [7.29] and in the program used to calculate k_{uni} [7.30] a commonly used exponential form was assumed for this function.

The microscopic unimolecular rate coefficients $k(E)$ and $k_r(E)$ may be calculated from RRKM theory [7.5, 7.7]. This is a variant of microcanonical TST in which a much more realistic treatment than those in the earlier RRK theories is afforded to

the internal modes of the species AB (these may include free and/or hindered internal rotations as well as vibrations) and in which effects such as anharmonicity and angular momentum conservation can be taken into account at varying levels of approximation. The fundamental equation of RRKM theory gives $k(E)$ for a general unimolecular process occurring with critical energy E_0 as

$$k(E) = \frac{\int_{E_0}^{E} \rho^{\dagger}(E')\, dE'}{h\rho(E)} \qquad (19)$$

in which $\rho(E)$ is the density of internal energy states of AB at energy E, $\rho^{\dagger}(E)$ is the density of states of AB at the configuration of the transition state for the reaction, and h is Planck's constant. The total density of states $\rho(E)$ represents a convolution of the densities for the individual internal modes of AB. A number of methods exist for the calculation of $\rho(E)$; in the present work a version of the very efficient Beyer-Swinehart algorithm [7.31] for direct counting of vibrational-rotational states was used to obtain both sums and densities of states (numerator and denominator in (19) respectively).

The calculation of $\rho(E)$ requires a knowledge of the vibrational frequencies and moments of inertia of internal rotations, the latter, in turn, requiring information on the structures of the species AB and of the activated complex for the reaction. For stable molecules experimentally observed frequencies are used where possible,but for species which have not been positively identified spectroscopically, harmonic frequencies calculated from the curvature of the potential energy surface by *ab initio* methods are commonly used. However in the case of NH_2NO such calculations are unlikely to be reliable due to the presence of significant anharmonicity. While there exist various methods for correction of the density of states for the effect of anharmonicity, e.g. those of Haarhof [7.32] and Troe [7.33], these cannot be used in the present case since the former requires detailed information on the form of the potential surface (in particular the dissociation energies of individual oscillators are required) while the latter assumes no coupling between oscillators, which will not be the case for the NH_2 + NO surface at the energies at which recombination of NH_2 and NO occurs. At this point it may be noted that the general effect of anharmonicity is to increase the density of states at a given energy. A simple illustration of this is provided by a comparison of the vibrational state pattern for a single harmonic oscillator with that of a Morse oscillator at the same energy. Thus it may be seen from equation (19) that the presence of significant anharmonicity in the species AB will greatly reduce $k(E)$; in the limit of slow rearrangement (Case 1 above), this will result in the high-pressure regime for k_{obsd} extending to lower than normal pressures. In calculations on the NH_2 + NO reaction, the effects of anharmonicity and of

the presence of mobile H atoms in the collision complex on the density of states of NH_2NO were included in an approximate manner by treating the motion of the two H atoms as a free internal rotation and using reduced frequencies of vibration for the remaining internal modes. Although the choice of absolute values for these frequencies and for the properties of the internal rotor in this model was necessarily rather arbitrary, in the absence of reliable vibrational frequencies, e.g. from infrared spectroscopy, the resulting increase in the density of states was considered to be at least qualitatively equivalent to that expected to arise from the significant anharmonicity of this species.

The structure and frequencies of the activated complex for dissociation to NH_2 + NO, required for the calculation of $k(E)$, were determined using the well-known Gorin or restricted rotor model for a simple fission process producing two free radicals [7.21, 7.22]. In this model the incipient product radicals are treated as being independent at the transition state with a separation distance r^+ given by the location of the centrifugal barrier in the dissociation potential. This maximum, which occurs as a result of the requirement that the total energy and angular momentum of the system be conserved throughout the dissociation process, may be thought of as arising from the superposition of a repulsive 'centrifugal potential' on the attractive interaction potential between the two radical moieties. The geometries of these moieties are taken to be those of the totally separated molecules. The internal modes of the activated complex are represented by the vibrational frequencies of the isolated product radicals together with internal rotations of the two fragments; these rotations will be free or hindered depending on the value of r^+ , which may be obtained as the value which gives the correct high pressure limiting rate coefficient k_{rec}^{∞} , as calculated from equations (19), (15) and (16). (Note that the value of r^+ determines the overall moment of inertia of the activated complex and thus affects the density of states $\rho^+(E)$.) The effects of steric hindrance to the internal rotations may be accounted for by the use of effective (i.e. reduced) moments of inertia; this is equivalent to the inclusion of a steric factor in the overall high pressure rate coefficient k_{uni}^{∞} [7.21, 7.22].

The $k_r(E)$ for the rearrangement process were calculated by assuming a tight planar transition state intermediate in structure between nitrosamine (I) and hydroxydiimide (III), with frequencies similar to those assumed for I. The critical energies $E_{0,d}$ and $E_{0,r}$ were taken to be equal to the energy of separated NO + NH_2 (164 kJ mol^{-1}) following Abou-Rachid *et al.* [7.20].

Calculations [a] of the overall rate coefficient for reaction (1) from equations (17) and (16) (i.e. in Case 1 where $k_1 = k_{rec}$) over a wide range of pressures predicted that at 300 K, k_1 should indeed be close to its high pressure limit and only weakly dependent on pressure at pressures above 1.5 Torr (see Fig. 7.2), while at higher temperatures a pronounced pressure effect might be observable. These calculations also yielded a temperature coefficient of around -1.5 for k_1 at 3.5 Torr, in good agreement

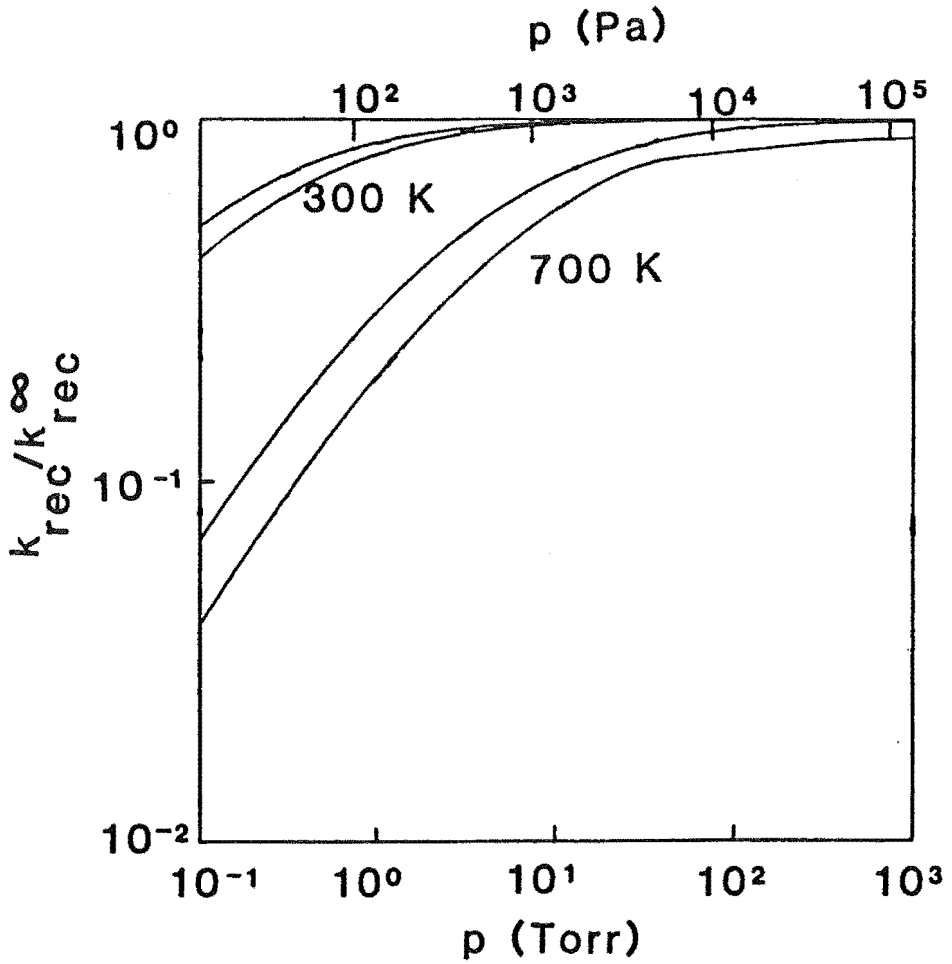

FIGURE 7.2: Calculated fall-off curves for at 300 K and 700 K.

Upper curve for each temperature is for $\langle \Delta E_{down} \rangle = 500$ cm^{-1}; lower curve for $\langle \Delta E_{down} \rangle = 300$ cm^{-1}. (Taken from reference [7.20]. k^{∞}_{rec} is the high pressure limiting value of k_{rec} calculated from k^{∞}_{uni} using equation (16), where k^{∞}_{uni} is a Boltzmann average of the $k(E)$.)

[a] These calculations were carried out by Professor R. G. Gilbert of the University of Sydney, Sydney, Australia.

with experimental results. At a temperature of 700 K, where appreciable pressure dependence of k_1 below 100 Torr was not ruled out in Case 1, a Case 2 calculation using equation (18) indicated that P_r does not fall significantly below unity until sufficiently high pressures are reached that the rate coefficient k_{rec} for the recombination reaction is already at its high pressure limit (i.e. $k_{rec} / k_{rec}^{\infty} \geq 0.5$; see Fig. 7.3). Hence no significant fall-off behaviour is to be expected for reaction (1) at T = 700K. In the absence of experimental data on the variation of k_1 with pressure at elevated temperatures, however, this prediction could not be tested.

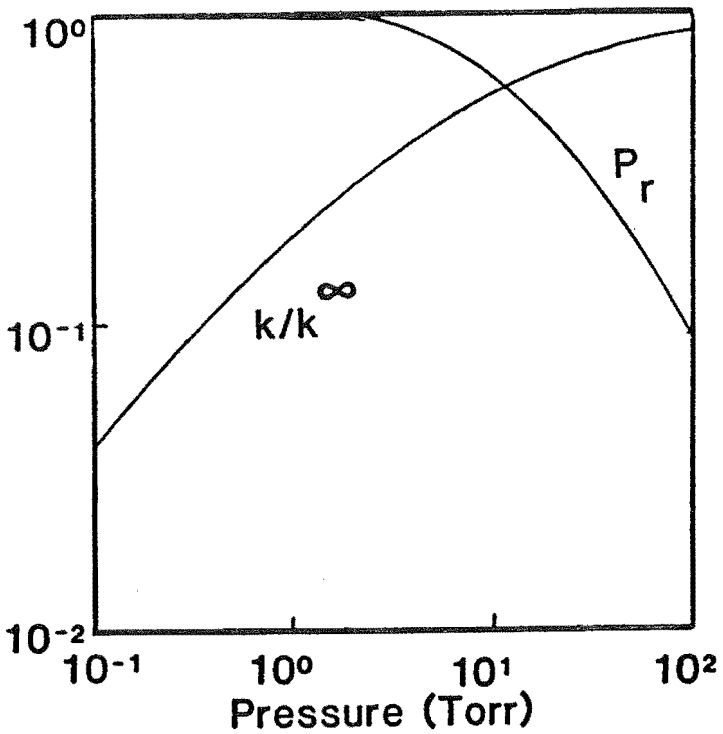

FIGURE 7.3: For NO + NH_2 → N_2 + H_2O: Pressure dependence of P_r, the probability of reacting when only rearrangement and collisional energy relaxation of the complex are considered, calculated from equation (18).

Results are for the NO + NH_2 reaction at 700 K, assuming $\langle \Delta E_{down} \rangle$ = 300 cm^{-1}. Pressure dependence of corresponding $k_{rec} / k_{rec}^{\infty}$ from Fig. 7.2 is also reproduced.

It was not possible to decide from the results of this study whether the lifetime of the NH_2NO complex was long or short. The arguments presented in Section 4.3

regarding the discrepancy between the results of flash photolysis and discharge-flow experiments on reaction (1) are consistent with a long-lived complex, as is the reported mass-spectrometric observation of this species by Gehring *et al.* [7.13]. However, the recent trajectory calculations of Phillips [7.34] indicate that the lifetime is in fact very short (< 1 ns). An unequivocal solution to this problem is thus still awaited.

The preceding discussion illuminates several aspects of the NH_2 + NO system which require further study. On the experimental front these include measurements of k_1 as a function of pressure at high temperatures and studies of the corresponding deuterated system. The latter should clearly reveal whether the hydrogen migration mechanisms examined in [7.14], [7.18] and [7.20] are realistic; in particular the importance ofquantum-mechanical tunnelling could be determined.[a)] Direct measurements of the vibrational frequencies of NH_2NO would also be of considerable value and, in fact, matrix isolation FTIR experiments on NH_2NO, as well as ND_2NO and $^{15}NH_2NO$, have very recently been performed although the results have not yet been published [7.36].

From the theoretical point of view, the most obvious need is for more detailed information on the form of the potential energy surface for reaction (1). Points of particular interest would include information on possible alternative rearrangement channels, including structural parameters for the stable species and transition states involved and the associated barrier heights. Harmonic vibrational frequencies calculated from the curvature of the potential energy surface at stationary points would be useful for the assignment of future infra-red spectroscopic data.

Very recently Miller *et al.* [7.37] have reported the results of a study of the O +HCN reaction in which potential energy surface data obtained from high quality *ab initio* calculations was used in a detailed analysis of the kinetics of this multiple-channel system by means of RRKM theory, with specific inclusion of angular momentum conservation and tunnelling effects. The predicted temperature dependences of the overall rate coefficient and the branching coefficient for the channel leading to NH + CO were in very good agreement with experimental results, illustrating that accurate predictions of kinetic parameters by such methods are possible for systems where the potential energy

a) Attempts by the author to study the ND_2 +NO reaction by the LP/LIF technique were unsuccessful due to repeated failures to detect an LIF signal at 538 nm (ND_2 (A-X) system, (0,15,0) - (0,0,0)). This was tentatively attributed to an isotopic shift of the ND_3 absorption spectrum leading to weak absorption of the 193 nm photolysis radiation. Although the absorption coefficient of ND_3 at this wavelength appears not to have been measured, this argument is supported by the observation of a significant shift (580 cm^{-1}) of the (0,0) band origin in the ($\tilde{A}$-$\tilde{X}$) system near 215 nm and larger shifts for bands of the ($\tilde{B}$-$\tilde{X}$) and ($\tilde{C}$-$\tilde{X}$) systems at shorter wavelengths [7.35].

surface is well characterised. It should be pointed out that formation of the initial HOCN collision complex involves a significant activation energy and that the transition state for the 1,2 H- atom migration leading to NH + CO also lies well above the energy of the separated reactants. Hence the problems due to anharmonicity of the collision complex and to the difficulty in describing the transition state for the former process, which are prominent features of the NH_2 + NO system, are much less significant in this case. Nonetheless, it should be possible to give an improved treatment of the more complicated reaction (1), along the lines of that in [7.37], given more information on the form of the NH_2 + NO potential energy surface. In particular, predictions of the temperature dependence of the branching factors for the reaction channels (1a) - (1c) (as given in [7.37] for the O + HCN reaction) could assist in rationalising the conflicting experimental data on OH yields from reaction (1) which were discussed in Section 5.4 C. An *ab initio* quantum-chemical study of this surface is described in the subsequent sections of this chapter.

7.2 *Ab Initio* Potential Energy Surface Calculations: A Summary of Basic Principles [a)]

A. Definition of the Potential Energy Surface

The potential energy surface for a chemical reaction (hereafter abbreviated to PES) represents the dependence of the total potential energy of the system on the relative positions of its constituent nuclei. For a reaction between two atoms the potential energy is a function only of the internuclear distance and can thus be represented in two dimensions by the familiar diatomic potential energy curve. For a general N- atomic system however, the potential energy depends on the $3N$ - 6 ($3N$ - 5 for a linear polyatomic) internal degrees of freedom of the molecule, so that the PES is a multidimensional hypersurface. For such system the PES is commonly represented by a reaction coordinate diagram in which the potential energy is plotted against a reaction coordinate which is usually taken to be a minimum energy pathway connecting the various stable configurations of atoms representing reactant, intermediate and product species which correspond to local minima on the PES. These minima are separated by potential barriers which correspond to saddle points on the hypersurface (local maxima along the reaction coordinate) and which represent transition states for the reactions that lead from one stable configuration to another. Hence calculations of the relative energies of stable and transient species occurring along two or more alternative pathways for a given reaction can be useful in determining the relative importance of these channels.

---

a) The material in this section is primarily based on the excellent texts by Szabo and Ostlund [7.38] and Levine [7.39].

Such calculations are possible within the framework of molecular quantum mechanics, in which the energy of a given configuration of a polyatomic system is obtained by solving the Schrödinger equation

$$\hat{H}\,\Psi = E\,\Psi$$

in which $\hat{H}$ is the Hamiltonian operator for the system comprising N nuclei and M electrons, Ψ is the total wavefunction for the system and E is the total energy. The Hamiltonian $\hat{H}$ contains terms representing the kinetic energies of the electrons and nuclei and potential energy terms corresponding to the pairwise electron-electron and nuclear-nuclear repulsions and the pairwise electron-nuclear attractions. However within the Born-Oppenheimer approximation, in which the electronic motions are considered to occur in the field of fixed nuclei by virtue of the large difference between electron and nuclear masses, the nuclear kinetic energy terms may be neglected and the internuclear repulsion terms become constant for a given nuclear configuration. This gives rise to the so-called 'electronic problem' which is described by the electronic Schrödinger equation

$$\hat{H}_{el}\,\Psi_{el} = E_{el}\,\Psi_{el} \qquad (20)$$

in which the electronic Hamiltonian $\hat{H}_{el}$ is given (in atomic units [7.40]) by

$$\hat{H}_{el} = -\frac{1}{2}\sum_{i=1}^{M}\nabla_i^2 - \sum_{i=1}^{M}\sum_{A=1}^{N}\frac{Z_a}{r_{ia}} + \sum_{i=1}^{M}\sum_{j>1}^{M}\frac{1}{r_{ij}} \qquad (21)$$

where ∇_i^2 is the Laplacian operator for electron i, Z_A is the atomic number of nucleus A, r_{iA} is the distance between electron i and nucleus A and r_{ij} is the distance between the i th and j th electrons. The electronic wavefunction Ψ_{el} depends explicitly on the electronic coordinates and parametrically on the nuclear coordinates, as does the electronic energy E_{el}. The total energy of a given nuclear configuration is then given by

$$U \equiv U(\{q_A\}) = E_{el} + V_{NN} \qquad (22)$$

where the $\{q_A\}$ are the nuclear coordinates and

$$V_{NN} = \sum_{A=1}^{N}\sum_{B>A}^{N}\frac{Z_A Z_B}{R_{AB}} \qquad (23)$$

is the internuclear repulsion energy with R_{AB} being the distance between the A th and B th nuclei. Within the Born-Oppenheimer approximation of adiabatic electron motion U functions as the potential energy of nuclear motion. Since the various stable and transient intermediates occurring along a given reaction pathway correspond to distinct

configurations of the component nuclei, the investigation of the PES for this process becomes equivalent to the solution of the electronic problem (20) for each such species, the total energy U being calculated from the known configuration at each stationary point by means of equations (22) and (23).

B. The Hartree-Fock Self-Consistent Field Molecular Orbital Theory

The electronic problem for an N-atom, M-electron molecule may be solved at varying levels of approximation within the framework of molecular orbital theory. The simplest such approximation is the Hartree-Fock (HF) self-consistent field (SCF) theory in which the wave function Ψ_{el} is represented by a fixed linear combination of products of one-electron wavefunctions called molecular orbitals (MOs), each of which depends on both the spatial coordinates and the spin of the electron it describes. The linear combination, which is chosen such that the overall wavefunction Ψ_{el} obeys the Pauli antisymmetry principle and is normalised, is called a Slater determinant. The solution of the electronic problem within the HF approximation consists of choosing a set of M MOs such that the energy E_{el} is minimised. The MOs are the solutions to a set of M coupled integrodifferential equations (the HF equations) and are, in principle, infinite in number. For practical computational purposes it is necessary to use a finite set of MOs; these are obtained by expanding each MO as a linear combination of a finite number ($\geq M$) of known basis functions. These functions constitute the basis set for a HF calculation and are commonly chosen to be approximate atomic orbitals (AOs) of the N component atoms of the molecule. This procedure defines the linear combination of atomic orbitals or LCAO-MO approximation in which each MO is described by the expansion coefficients in the corresponding LCAO. The use of a finite basis set results in a set of algebraic eigenvalue equations [a] which may be solved by matrix methods to give the eigen-functions (MOs) and eigenvalues (orbital energies) of the operator associated with the HF equations (the Fock operator). The Fock operator depends on its eigenfunctions (the MOs), hence the HF equations are non-linear and must be solved iteratively. The HF procedure involves repeated solution of the HF equations starting with an initial 'guess' at the wavefunction and modifying the MOs until successive iterations produce a sufficiently small change in the average value of the expansion coefficients, hence the term self-consistent field (SCF). The HF ground state wavefunction Φ_0 is then constructed from the M MOs having the lowest orbital energies [b] and the HF or SCF energy is given by

$$<\Phi_0 \mid \hat{H} \mid \Phi_0> = E_0 \qquad (24)$$

where the well-known Dirac bra-ket notation has been used. Since the HF procedure is variational in terms of the expansion coefficients in the LCAO, E_0 is an upper bound to the true ground state energy E_{el}°. Once the MOs are known the electronic state of the

molecule may be determined and properties such as the ionisation potentials, dipole moment and charge distribution may be calculated.

C. Restricted and Unrestricted Hartree-Fock Theory

In a closed-shell species all electrons are spin-paired and the MOs describing each member of a pair have the same dependence on spatial coordinates. A Slater determinant formed from such MOs is termed a restricted determinant and represents a pure singlet state of the species. HF theory applied to closed-shell restricted determinants is termed restricted HF theory (RHF). An open-shell species containing one or more unpaired electrons may be described by an unrestricted determinant in which the MOs for electrons with different spins have different spatial parts. Unrestricted determinants do not represent pure spin states but in general an unrestricted determinant for a species with one (two, three,...) unpaired electron(s) is approximately a doublet (triplet, quartet,...) wavefunction, this wavefunction being mixed with those for states of higher spin multiplicity. Although the presence of such spin contamination makes the unrestricted determinant a less accurate approximation to the true wavefunction for an open-shell species than is the restricted determinant for a closed-shell molecule, this drawback is generally offset by the fact that unrestricted determinants lead to lower energies in the HF approximation (UHF) than do restricted determinants. This is due to the greater flexibility of the unrestricted determinant in accommodating the differential polarisation of doubly-occupied orbitals by the unpaired electrons, which in turn occurs because in a single determinant wavefunction only the motions of electrons with parallel spins are correlated.

D. Geometry Optimisation and Calculation of Vibrational Frequencies

The forces acting on the constituent nuclei of the molecule may be calculated as the first derivatives of the energy U with respect to a set of internal coordinates which are commonly taken to be the internuclear distances and angles of the molecule. This leads to the possibility of geometry optimisation, which is accomplished by seeking that configuration of the molecule in which the internal coordinate forces are minimised. At this equilibrium geometry the second derivatives of the energy represent the harmonic force constant for motions in the internal coordinates. These force constants may be used in a normal coordinate analysis to calculate the harmonic vibrational frequencies of the normal modes of the molecule. This analysis, which involves solution of the equations of

---

a) These are the Roothaan equations in restricted HF theory, or the Pople-Nesbet equations in unrestricted HF theory (see Section 7.2 C).

b) The calculation of wavefunctions and energies for excited electronic states is not considered here.

motion of the N-particle system, is carried out *via* a matrix method originally due to Wilson *et al.* [7.41] and yields a set of $3N$ -6 eigenvalues λ_i which are related to the frequencies ν_i by equations of the form

$$\lambda_i = 4\pi^2 \nu_i^2 \quad . \tag{25}$$

At a local minimum on the PES corresponding to a bound state of the system, the PES is convex in all the normal coordinates and all λ_i are positive. For a transition state species, however, the PES is concave in one coordinate (the reaction coordinate) and there will be one negative eigenvalue, leading to an imaginary frequency for motion in the reaction coordinate. Once the energy, structure and vibrational frequencies (i.e. the zero-point energy) of the molecule are known, thermodynamic properties such as enthalpies, entropies and free energies may be calculated as functions of temperature from standard statistical mechanical relationships based on the molecular partition function [7.42].

E. AO Basis Sets for MO Theory Calculations

The most commonly used AO basis functions are the Slater and Gaussian functions given by

$$\phi_S(\zeta,r) = N_S(\zeta)\, F_S(x,y,z)\, exp(-\zeta r) \tag{26}$$

and

$$\phi_G(\alpha,r) = N_G(\alpha)\, F_g(x,y,z)\, exp(-\alpha r^2)\,, \tag{26}$$

respectively, where r is the distance between the electron and the expansion centre ($r^2 = x^2 + y^2 + z^2$), ζ and α are the Slater and Gaussian orbital exponents, $N_S(\zeta)$ and $N_G(\alpha)$ are normalisation factors and $F_S(x,y,z)$ and $F_G(x,y,z)$ are polynomials in x, y and z. The type of orbital (1s, 2p, etc.) represented by $\phi_{S,G}$ is determined by the form of $F_{S,G}$. Slater functions give a better representation of atomic wavefunctions than do Gaussians principally due to differences in their behaviour at $r = 0$ and $r = \infty$, and in general a Slater basis contains fewer functions than a Gaussian basis of comparable quality. On the other hand,the computer evaluation of molecular integrals is more efficient for Gaussians. Currently, the most widely used AO basis sets consist of functions which are linear combinations (contractions) of Gaussians (primitives), the contraction coefficients and orbital exponents of the primitives being fixed for atoms of different elements. The number of primitives used in a contraction, called the contraction length, is usually less than six.

The simplest basis set for an MO calculation of the type described above contains one basis function per occupied AO in each of the atoms comprising the molecule under study. Such a basis set is termed minimal and the SCF energy obtained with such a

set will normally be significantly above the true energy. The results of minimal basis set calculations are usually only qualitatively correct at best, although such calculations are capable of predicting trends in molecular properties. In the widely used near-minimal STO-3G basis set each basis function is a contraction of three Gaussians which has been least-squares fitted to the appropriate Slater function or Slater-type orbital. In a double-zeta (DZ) basis set the number of basis functions is twice that in the corresponding minimal basis, with each function from the minimal basis set occurring with two different orbital exponents in the DZ basis set. In the related split-valence basis sets, the inner shell functions are not doubled since in general the chemical properties of a molecule depend primarily on the valence electronic structure. Such bases are denoted L-MNG, where L is the contraction length for the unsplit inner shell functions, M and N are contraction lengths for the valence shell basis functions and G stands for Gaussian. Examples are the 4-31G and 6-31G basis sets developed by Pople and co-workers [7.43, 7.44]. DZ and split-valence bases may be further extended by the addition of polarisation functions, which allow account to be taken of the anisotropy of the electric field within a molecule and its effects on the charge distributions about polarisable atoms. These functions are usually chosen to be atomic orbitals having angular momentum quantum numbers one greater than the highest valence orbital in each atom. Thus for hydrogen a set of 2p functions is added to the AO basis set, while for first-row elements a set of six 3d-type functions is added. The resulting basis sets are generically termed double-zeta-plus-polarisation (DZP) bases. A split-valence basis set with only 'heavy-atom' polarisation functions included is denoted L-MNG*; L-MNG** indicates the presence of both heavy atom and hydrogen polarisation functions.

F. Post-Hartree-Fock Theories

The HF theory contains two principal approximations, namely (i) the use of a single Slater determinant to describe the wavefunction and (ii) the representation of instantaneous interelectronic repulsion (i.e. correlation effects) by an average field seen by each electron, this approximation being implicit in the HF equations. As a result the SCF energy is bounded below by a limiting value, the HF limit E_{HF}, which would be attained if a complete (i.e. infinite) basis set was used in a HF calculation. In order to go beyond the HF level it is necessary to include more than one determinant in the wavefunction, which allows account to be taken of the effects of mixing between the ground and excited states of the molecule, and to improve the treatment of electron-electron interactions. The two most common post-HF formalisms are based on the techniques of configuration interaction (CI) and perturbation theory.

In the basic CI method the wavefunction is expressed as a linear combination of determinants Φ_i , including the HF ground state wavefunction Φ_0 together with excited determinants corresponding to the electron configurations obtained by raising one or more electrons from occupied orbitals in Φ_0 to previously unoccupied or virtual orbitals within the set of MOs spanned by the finite basis set

$$\Psi_{CI} = \sum_i c_i \Phi_i \ . \qquad (28)$$

The expansion coefficients c_i are then varied to obtain a minimum energy. If all possible such excitations, corresponding to 1, 2, ..., M-tuply excited states, are included in the wavefunction, then the procedure is termed full CI and the CI energy E_{CI} is exact within the space spanned by the chosen basis set. Hence full CI provides a reference to which more approximate methods may be compared. However, full CI is computationally very demanding and is commonly performed only for small molecules. More often a restricted form of CI, e.g. including only all double excitations (CID) or all single and double excitations (CISD), is performed. With a well-chosen basis set an appreciable fraction of the correlation energy

$$E_{corr} = E_{CI} - E_{HF} \qquad (29)$$

may be obtained by such methods since, in general, the importance of contributions from excited determinants decreases with the level of excitation. In more sophisticated CI methods, orbitals other than the HF MOs are used in the CI wavefunction in order to reduce the size of the CI expansion and improve the rate of convergence of the wavefunction. In the multiconfiguration SCF (MCSCF) methods, for example, both the CI coefficients c_i and the orbitals used to construct the Φ_i in equation (28) are optimised; in the generalised valence bond (GVB) method of Goddard and co-workers [7.45] these orbitals are approximate valence AOs (rather than MOs) which are in turn constructed from a known basis set and whose form is determined by a variational SCF technique.

In perturbation theories the true electronic Hamiltonian $\hat{H}_{el}$ of equation (20) is expressed as the sum of a zeroth-order Hamiltonian $\hat{H}_0$, whose eigenfunctions Ψ_i° and eigenvalues E_i° are known, and a perturbation $\hat{V} = \hat{H}_{el} - \hat{H}_0$. The standard Rayleigh-Schrödinger perturbation treatment [7.38, 7.39] leads to expressions for Ψ_{el} and E_{el} as infinite sums of the form

$$E_{el} = E^{(0)} + E^{(1)} + E^{(2)} + ... \quad (30)$$

$$\Psi_{el} = \Psi^{(0)} + \Psi^{(1)} + \Psi^{(2)} + ..., \quad (31)$$

the n-th terms of which are called nth-order energy and wavefunction, respectively. In general, if the kth-order wavefunction is known then the energy to order 2k+1 is determined and may be derived in terms of the known E°_{i} and Ψ°_{i}. In a commonly used form of perturbation theory known as Møller-Plesset perturbation theory (MPPT), the unperturbed Hamiltonian $\hat{H}_0$ is taken to be the sum of the Fock operators for all M electrons of the molecule. The eigenfunctions Ψ°_{i} and energies E°_{i} are then the MOs and orbital energies obtained by solution of the HF equations and the SCF energy is the sum of the zeroth- and first-order energies, with second- and higher-order terms representing contributions to the correlation energy E_{corr}. For computational reasons the infinite series (30) and (31) are terminated at some finite order n (usually $2 \leq n \leq 4$); the resulting nth-order MPPT is usually symbolised as MPn. Post-HF calculations of molecular properties such as equilibrium geometries are often found to be accurate within the limits of experimental uncertainty.

7.3 Previous *Ab Initio* Studies of the NH_2 + NO Reaction PES

The earliest *ab initio* calculations on N_2H_2O species appear to be those of Pople and co-workers [7.46, 7.47] who reported HF energies for nitrosamine (I) and four geometrical isomers of hydroxydiimide (III - VI), calculated using STO-3G and 4-31G basis sets. Geometries were not optimised in this study, all of these molecules being assumed to be planar with typical bond lengths and angles. The first equilibrium geometry calculations on these species, as well as the monomethyl- and dimethyl-substituted analogues of I, were carried out by Thomson and co-workers [7.48] as part of a study of chemical carcinogenesis by N-alkylnitrosamines. These workers also studied the rearrangement pathway I → III → IV (1,3 migration of H_1 followed by rotation about the OH bond in III) by a partial optimisation technique in which one or two internal coordinates were varied while the remainder were kept fixed at average values. The barrier to H atom migration was found to be *ca.* 380 kJ mol^{-1} but in view of the many approximations and the small basis set (STO-4G) used in this study, no significance may be attached to this value which has since been shown to be grossly overestimated.

In a systematic investigation of the properties of stable species occurring on the N_2H_2O PES, Casewit and Goddard [7.17] obtained structural and thermochemical data for nine isomers of formula H_2H_2O including I and III - VI. In this study the

geometries were optimised at the HF/4-31G [a)] level, planar structures being obtained for all the species being examined. However, these workers did not determine the barrier heights for the interconversions between isomers, nor did they calculate vibrational frequencies. The thermochemical data were derived using total energies obtained from GVB-CI calculations performed at the HF geometry with a DZP basis set, together with vibrational frequencies estimated from model compounds.

The structure of nitrosamine was also studied by Ha *et al.* [7.49] at the HF level using both 3-21G and 6-31G* basis sets. The reported equilibrium geometry was planar in each case, however, the possibility of a non-planar structure for H_2NNO appears not to have been considered in this work.

The first calculations on transient as well as stable species on the NH_2 + NO PES were performed by Abou-Rachid *et al.* [7.20] who obtained HF/4-31G energies and geometries for reactants, products, stable intermediates and some transition state species occurring along pathways corresponding to reactions (1a) - (1c). Nitrosamine was again found to have the planar structure I. Barrier heights were calculated by a CI method and thermodynamic properties were derived using the CI energies together with vibrational frequencies obtained from a normal mode analysis. As was noted in Section 7.1 B, these calculations showed that the most likely pathway involves a 1, 3 shift of a hydrogen atom in I to generate the NN-trans, NO-cis hydroxydiimide III *via* a transition state of the form VII, followed by a series of isomerisations to give the (cis, trans) structure VI, from which the products corresponding to reactions (1a) - (1c) may most readily be formed. This pathway was shown not to possess any nett activation barrier relative to NH_2 + NO, consistent with the experimental negative temperature coefficient of the rate constant for reaction (1). An alternative pathway, involving two successive 1,2 shifts of H_2 to give VI *via* the diimide N-oxide VIII, was eliminated due to the high barriers found for the processes I $\rightarrow$ VIII and VIII $\rightarrow$ VI. The structures and vibrational frequencies obtained in this study for nitrosamine and the activated complex VII were used in statistical rate theory calculations to predict the absolute values and temperature dependences of the rate coefficient for the NH_2 + NO reaction (see discussion in Section 7.1 B).

A similar investigation to that of Abou-Rachid *et al.* [7.20] was carried out by Melius and Binkley [7.50], who also studied the related NH + NO reaction. Using their BAC-MP4 (bond additivity corrections with fourth-order MPPT) method, they calculated

---

[a)] This is a convenient notation in which the level of theory and basis set for an *ab initio* calculation may be compactly expressed, e.g. MP2/6-31G**, CID/DZP, etc.

heats of formation and free energies at 0 and 298 K for a large set of reactants, products, intermediates and activated complexes occurring in each of these reaction systems; these data were then used in a discussion of possible reaction mechanisms. The BAC-MP4 method involves calculation of the equilibrium geometry and vibrational frequencies of each species at the HF level of theory, followed by calculation of the MP4 energy at the HF geometry. (For the calculations reported in [7.50] the 6-31G* basis set was used.) The MP4 energy is then corrected by application of empirical bond additivity corrections. Although details of the BAC method have yet to be published, these calculations are the most sophisticated performed on the NH_2 + NO system to date, being comparable to large-scale CI calculations. (The perturbation expansion for the fourth-order contribution to the correlation energy includes up to quadruple substitutions relative to the HF wavefunction.) However, Melius and Binkley presented only the thermochemical data for the reactions studied; they did not report structural parameters or individual vibrational frequencies for any of the species involved. Since these data are of fundamental importance for any further statistical rate theory calculations, it was decided to carry out an *ab initio* investigation of the NH_2 + NO reaction pathways which lead to experimentally observable products, i.e. channels (1a) - (1c), with emphasis on determining the structures and vibrational frequencies of both the stable and transition state species involved, in particular those of nitrosamine. The results of this study, presented in Section 7.5, have previously been reported as reference [7.0a] and [7.0b].

7.4 **Details of Calculations**

All calculations were done using the GAUSSIAN 82 computer program package developed by J. A. Pople and co-workers [7.51] which was installed on the DIGITAL EQUIPMENT CORP. VAX 11/750 computer in the Civil Engineering Department of this University. This powerful system permits MO calculations to be performed at levels ranging from HF to MP4SDQ and CISD. A range of standard basis sets is provided, including both minimal and extended sets, the latter being predominantly of the split-valence type with various polarisation options. Other features of GAUSSIAN 82 include automatic geometry optimisation at both HF and post-HF levels, including optimisation to a transition state, normal coordinate vibrational analysis and calculation of thermodynamic functions. Most of the present calculations used the 6-31G* split-valence-plus-polarisation basis set [7.52] which has recently been shown by de Frees and McLean [7.53] to give reliable results in calculations of harmonic vibrational frequencies and which has been widely used for equilibrium geometry predictions at both the HF and MP2 levels [7.54, 7.55]. In this work all geometry optimisations were performed at the HF level unless otherwise specified. An extension of the notation introduced in Section 7.3 is used to indicate a single-point post-HF energy calculation at the equilibrium

geometry obtained in a previous calculation, thus MP2/6-31G*//HF/6-31G* represents a calculation of the first perturbational contribution to the correlation energy at the HF/6-31G* equilibrium geometry. In investigations of the structure of nitrosamine, the variation of the equilibrium geometry with changes in the basis set was also determined, using basis sets ranging from STO-3G to the triple-split-valence 6-311G** set.

7.5 **Results and Discussion**

A. The Structure of Nitrosamine

The geometry of nitrosamine (H_2NNO) was initially optimised at the HF/STO-3G level with the set of HF/4-31G structural parameters obtained by Casewit and Goddard [7.17] being used as the starting point for the calculation and the molecule being held planar throughout (i.e. constrained or partial optimisation). However a calculation of the vibrational frequencies yielded one imaginary frequency [a)], indicating that the stationary point found was a saddle point on the PES. An unconstrained optimisation at the same level, commencing with both H_1 and H_2 out of the plane defined by N_1, N_2 and O resulted in the non-planar structure IX which gave nine real frequencies. Similar results were obtained using the 6-31G* basis set but an unconstrained HF/4-31G optimisation reproduced CG's [b)] planar geometry precisely, indicating that the inclusion of polarisation functions is of considerable importance for the accurate description of the structure of nitrosamine. This result is in accord with the finding that calculations using either minimal or DZP basis sets predict a pyramidal structure for NH_3 whereas use of a DZ basis set without polarisation functions results in a trigonal planar conformation [7.56, 7.57]. Since CG did not calculate vibrational frequencies the transition-state character of the planar structure would not have been immediately apparent. On the other hand ARPC did calculate harmonic force constants based on the planar HF/4-31G structure and obtained nine real frequencies although one was very low (83 cm^{-1}, unassigned). These workers also tested for the effect of polarisation functions on the equilibrium geometry, reporting that the results confirmed the 'quasi-planar' nature of nitrosamine. However, as no details of the SCF technique used were given, the reasons for the discrepancy between their results and the present ones are not clear.

The properties of the non-planar structure IX were investigated using basis sets ranging from STO-3G to 6-311G**. The results given in Table 7-1 show that the shift from STO-3G to split-valence basis sets leads to significant changes in both the equilibrium geometry and the energy, but that changes to the basis set within the split-

---

a) The calculations of vibrational frequencies for various N_2H_2O isomers are discussed in Section 7.5 C.

b) For the sake of brevity the authors of references [7.17], [7.20] and [7.50], and the references themselves, will hereafter be referred to as CG, ARPC and MB, respectively.

valence approximation result in only relatively small variations in the structural parameters, except in the case of the dihedral angles where the inclusion of d polarisation functions has a pronounced effect as described above. The variations in bond lengths and angles among the split-valence basis set results are generally less than 1%. The HF/6-31G* energy given in Table 7-1 is some 13 kJ mol^{-1} lower that that reported by Ha and co-workers [7.49]. The corresponding bond lengths also differ slightly, probably reflecting differences in the SCF procedure as well as the constrained optimisation used in [7.49]. The effects of changes in the basis set on the total energy of IX at both the HF and MP2 levels are more pronounced. Most of the decrease on going from the 4-31G to the 6-31G* basis set can be attributed to the presence of d functions on the N and O atoms in the 6-31G* basis set, with a smaller contribution arising from the improved description of the inner shell orbitals. The addition of 2p functions to the hydrogen atoms results in a much smaller change, while introduction of a triple split in the valence shell (6-311G**) produces a larger change at the HF level than at MP2.

The difference in energy between the planar and non-planar structures is very small (< 1 kJ mol^{-1}) and varies both with the basis set and with the level of theory used. At the HF level the non-planar structure is lower for all of the split-valence-plus-polarisation sets (see Table 7-1) while at the MP2/6-31G*//HF/6-31G* and MP2/6-31G**//HF/6-31G** levels this trend is reversed, although the difference is less than 20 J mol^{-1} . At a higher level of theory (MP4SDQ/6-31G**//HF/6-31G**) the non-planar structure is again lower in energy (by 0.33 kJ mol^{-1}).

In order to test the effects of electron correlation on the H_2NNO structure a geometry optimisation was performed at the MP2/6-31G** level of theory, in which the contributions of inner shell electrons to the correlation energy were neglected. This 'frozen core' approximation has been shown to have essentially no effect on equilibrium geometries [7.55]. As can be seen from Table 7-1 the only significant changes occurred in the NN and NO bond lengths which increased by 2 % and 4 % respectively. These increases parallel those observed for N_2H_4 and HNO in a comparison by De Frees *et al.* [7.55] of MP2/6-31G* and HF/6-31G* equilibrium geometries of 23 two-heavy-atom molecules. In that study it was found that the HF and MP2 results for multiple bond lengths usually bracket experimental values and also that bond lengths and angles involving hydrogen atoms are virtually unaffected. The changes in the dihedral angles in H_2NNO were negligible, indicating that correlation effects do not lead to a planar structure for this species.

TABLE 7-1. Optimised geometrical parameters, SCF, MP2 and relative energies for nitrosamine IX.

	STO-3G	4-31G (I)	6-31G*	6-31G** a)	6-311G**
$R(N_1 - N_2)$ (Å)	1.450	1.312	1.316	1.312 (1.340)	1.313
$R(N_2 - O)$	1.230	1.212	1.184	1.185 (1.236)	1.176
$R(N_1 - H_1)$	1.036	0.995	1.0001	0.998 (1.012)	0.999
$R(N_1 - H_2)$	1.033	0.987	0.994	0.991 (1.004)	0.991
$\angle(N_1N_2O)°$	110.9	115.4	114.5	114.5 (112.9)	114.8
$\angle(N_2N_1H_1)$	110.3	119.9	117.3	118.3 (118.2)	118.3
$\angle(N_2N_1H_2)$	107.5	117.3	115.4	116.4 (116.3)	116.2
$\omega(ON_2N_1H_1)°$ b)	- 28.0	0.0	- 13.4	- 8.9 (- 8.8)	- 10.2
$\omega(ON_2N_1H_2)$	212.6	180.0	195.2	190.5 (190.2)	190.9
E_{SCF} (hartree) c)	-182.393920	-184.538659	-184.826480	-184.834480	-184.881969
E_{MP2}	-182.571920	-184.897633	-185.337296	-185.356473	-185.485622
ΔE_{SCF} (kJ mol^{-1})	17.31	0.0	0.51	0.07	0.23
ΔE_{MP2}	26.15	0.0	-0.024	-0.016	-

a) Figures in parentheses are optimised parameters at the MP2/6-31G* level.
b) $\omega(ON_2N_1H_1)$ is the dihedral angle between the plane containing O, N_2 and N_1 and that containing N_2, N_1 and H_1 .
c) 1 hartree = 2625.5 kJ mol^{-1}.

Calculations were also performed at the HF/6-31G* level for two other conformers of nitrosamine, namely the cis and trans structures II and X, respectively. The optimised geometries as well as the absolute and relative SCF and MP2 energies of the four conformers I, II, IX and X are given in Table 7-2. Comparison of structures I and IX shows that the bond lengths and the NNO bond angles are slightly larger in the planar structure. The structures II and X, which result from an internal rotation about the NN bond in IX, are much higher in energy than I and IX at both the HF and MP2 levels and they have significantly longer NN bonds, comparable to a reported experimental NN bond length in hydrazine (1.447 Å) [7.55]. These observations are consistent with the existence of a resonance canonical form such as XI which lowers the energy of the non-planar structure IX but is lost when internal rotation occurs. This idea is further supported by the observed shortening of the NO bond and the observation that the MP2/6-31G*//HF/6-31G* barrier heights ΔE_{MP2} for the rotation are somewhat less than the observed 105 kJ mol^{-1} barrier in dimethylnitrosamine [7.58]. The barrier to rotation in the unsubstituted molecule could be expected to be lower overall for steric reasons, and the cis structure should be higher in energy than the trans as was found in these calculations.

The finding of larger NNO and NNH bond angles in II than in X supports the notion of a steric contribution to the rotational barrier at the cis configuration.

TABLE 7-2. HF/6-31G* geometries, SCF, MP2 and relative energies of nitrosamine conformers.

	I (planar)	IX (non-planar)	II (cis)	X (trans)
$R(N_1 - N_2)$ (Å)	1.307	1.316	1.439	1.438
$R(N_2 - O)$	1.186	1.184	1.164	1.160
$R(N_1 - H_1)$	0.999	1.000	1.008	1.008
$R(N_1 - H_2)$	0.992	0.994	1.008	1.008
$\angle(N_1N_2O)^\circ$	114.6	114.5	113.6	111.5
$\angle(N_2N_1H_1)$	119.4	117.3	105.7	104.0
$\angle(N_2N_1H_2)$	117.4	115.4	105.7	104.0
$\omega(ON_2N_1H_1)^\circ$	180.0	- 13.4	55.8	125.6
$\omega(ON_2N_1H_2)$	0.0	195.2	55.8	125.6
E_{SCF} (hartree)	-184.826285	-184.826480	-184.795820	-184.798065
E_{MP2}	-185.337305	-185.337296	-185.303000	-184.305093
ΔE_{SCF} (kJ mol^{-1})	0.51	0.00	80.50	74.60
ΔE_{MP2}	- 0.02	0.00	90.04	84.55
ΔH_{rel} a)	- 2.0	0.00	87.8	90.0

a) ΔH_{rel} calculated from ΔE_{MP2} with inclusion of zero-point energies from HF/6-31G* vibrational frequencies (Table 7-5). Imaginary frequencies not included.

Both the structures II and X were found to possess a single imaginary frequency in calculations at the HF/6-31G* geometry, confirming their transition state character. As was noted in Section 7.1 B, the cis structure II was chosen by Stief *et al.* [7.14] for the activated complex leading to direct formation of $N_2 + H_2O$ in the $NH_2 +$ NO reaction, for which a barrier height of 42 kJ mol^{-1} was assumed. This value is less than 50 % of that calculated at the MP2 level of theory in this work. Additional calculations in which the NO and NH bond lengths in II were lengthened simultaneously showed that the direct dissociation of H_2NNO to form $N_2 + H_2O$ involves a substantially greater activation energy than the rearrangement pathways discussed below.

B. The NH_2 + NO Reaction PES

The pathway considered in this study is essentially the same as that suggested by ARPC and subsequently examined in more detail by MB, differing in that the trans-cis isomerisations and internal rotations linking various hydroxydiimide conformers are

explicitly included. The two pathways presented in the reaction coordinate diagram Fig. 7.4 are equivalent apart from the order of the trans-cis conversions and internal rotations which convert trans, cis hydroxydiimide (III) to the cis, trans form (VI). The structures of the intermediates and transition states are shown in Fig.7.1. The optimised HF/6-31G* geometrical parameters are listed in Table 7-3 together with those of the reactants and products corresponding to reactions (1a) - (1c).

The geometrical parameters of the hydroxydiimides III - VI are in good agreement with those obtained at the HF/4-31G level by CG and ARPC apart from the shortening of *ca.* 0.5 Å in the NO bond length and decreases of 2 - 4 ° in the NOH and HNN bond angles. These effects are primarily due to the presence of d polarisation functions on the nitrogen and oxygen atoms, changes in the inner shell structure generally having little effect on calculated geometries at the HF level [7.38]. As would be expected, rather larger and less systematic deviations are observed in a comparison of the present structures with those calculated by Thomson and co-workers [7.48] using the minimal STO-4G basis set at the HF level. The NO and NN bonds in all of the hydroxydiimides are longer and shorter, respectively, than those in nitrosamine, consistent with the shift of the formal double bond from N=O to N=N.

The transition state VII is intermediate in structure between nitrosamine IX and trans, cis hydroxydiimide III, apart from the NNO bond angle which is *ca* 10 ° smaller than that in either IX or III. The HF/6-31G* structure is very similar to the 4-31G structure [ARPC], apart from the expected decrease (0.06 Å) in the NO distance, but is significantly different to the partly optimised HF/STO-4G structure of Thomson *et al.* [7.48]. In each of the transition states XII - XV, which link pairs of hydroxydiimide conformers, the NO bond is longer than that in either of the appropriate intermediates whereas the NNO bond angles lie between those of the intermediates.

The absolute and relative energies of each stationary point on the PES shown in Fig. 7.4 are given in Table 7-4 together with barrier heights $\Delta H^{\neq}$ (0 K) for each rearrangement. The absolute energies for nitrosamine (IX) and the hydroxydiimides (III - VI) at the MP2/6-31G*//HF/6-31G* level are below the GVB-CI energies reported by CG. The MP2 energies of IX and VI are also substantially lower than the CI values of ARPC. Thus the MP2 method, which includes all double substitutions relative to the HF wavefunction, appears to be superior to the limited CI techniques when comparable basis sets are used.

TABLE 7-3. HF/6-31G* optimised geometrical parameters for N_2H_2O species on the PES of Fig. 7.4.

	NH_2, NO [a]	H_2NNO [b] IX	HNNOH III trans, cis	HNNOH IV trans, trans	HNNOH V cis, cis
$R(N_1 - N_2)$ (Å)		1.316	1.206	1.203	1.202
$R(N_1 - H_1)$	1.013	1.000	-	-	-
$R(N_1 - H_2)$	1.013	0.994	1.007	1.008	1.020
$R(N_2 - O)$	1.127	1.184	1.334	1.351	1.347
$R(O - H_1)$		-	0.958	0.949	0.957
$\angle(N_2N_1H_1)°$		117.3	-	-	-
$\angle(N_2N_1H_2)$		115.4	107.0	106.0	113.4
$\angle(N_1N_2O)$		114.5	112.8	110.4	118.6
$\angle(N_2OH_1)$		-	107.5	104.6	110.8
	HNNOH VI cis, trans	N_2, H_2O [c]	N_2, H, OH	TS VII [d] (IX → III)	TS XII [e] (III → IV)
$R(N_1 - N_2)$	1.199	1.078	1.179	1.240	1.201
$R(N_1 - H_1)$	-			1.002	1.011
$R(N_1 - H_2)$	-		1.029	1.638	-
$R(N_2 - O)$	1.366			1.260	1.383
$R(O - H_1)$	0.949	0.947	0.958	1.327	0.951
$\angle(N_2N_1H_1)$	-				
$\angle(N_2N_1H_2)$	111.0		113.0	118.6	106.0
$\angle(N_1N_2H_1)$				50.8	-
$\angle(N_1N_2H_2)$				-	-
$\angle(N_1N_2O)$	112.8			103.3	110.6
$\angle(N_2OH_1)$	105.4			78.5	106.3
	TS XIII (III → V)	TS XIV [f] (V → VI)	TS XV IV → VI)	TS XVI [g]	TS N_2 + H
$R(N_1 - N_2)$	1.179	1.199	1.172	1.128	1.119
$R(N_1 - H_2)$	0.982	1.017	0.981	1.140	1.386
$R(N_2 - H_1)$	-	-	-	-	-
$R(N_2 - H_2)$	-	-	-	1.724	-
$R(N_2 - O)$	1.380	1.391	1.406	1.837	-
$R(O - H_1)$	0.956	0.953	0.950	0.953	
$\angle(N_2N_1H_2)$	179.9	111.9	176.9	98.9	113.3
$\angle(N_1N_2H_1)$	-	-	-	-	
$\angle(N_1N_2H_2)$	-	-	-	40.8	
$\angle(N_1N_2O)$	115.2	114.8	111.7	90.0	
$\angle(N_2OH_1)$	107.4	107.8	103.9	139.8	

a) $\angle(H_1NH_2) = 104.3$ b) $\omega(ON_2N_1H_1) = -13.4$; $\omega(ON_2N_1H_2) = 195.2$ c) $\angle(H_1OH_2) = 105.5$
d) $R(N_1\text{-}H_1) = 1.285$; $\angle(N_2N_1H_1) = 80.8$ e) $\omega(N_1N_2OH_1) = 8.75$ f) $\omega(N_1N_2OH_1) = 65.0$
g) $\angle(H_1OH_2) = 158.7$; $R(O\text{-}H_2) = 1.485$.

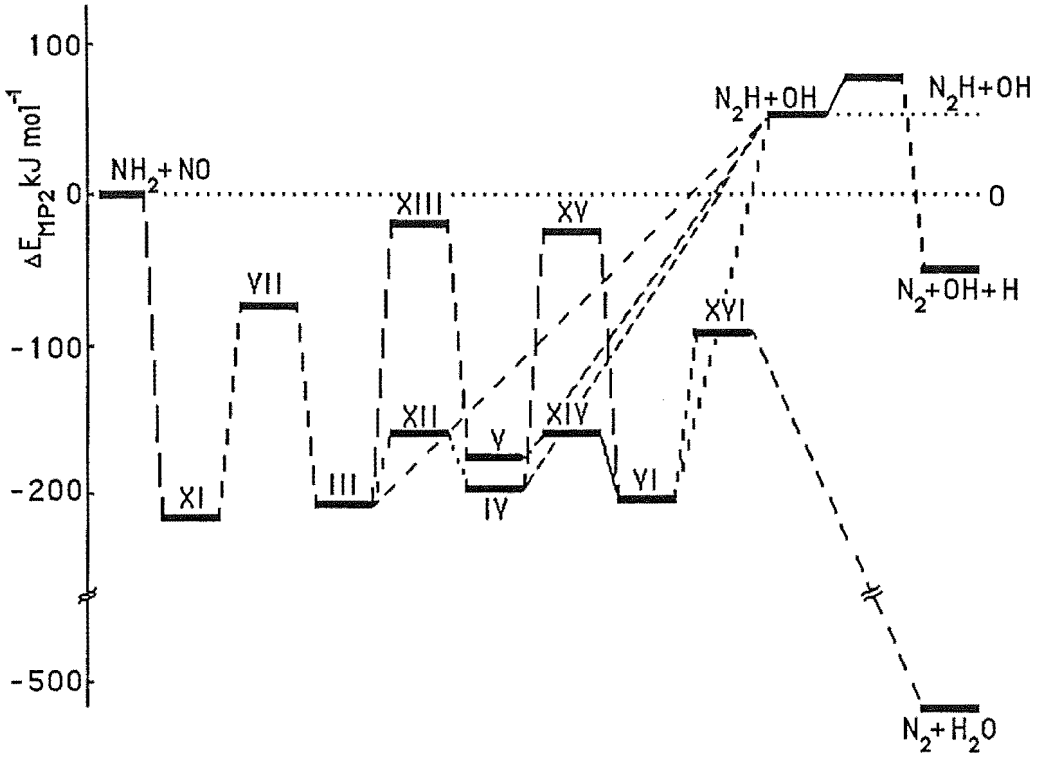

FIGURE 7.4: Schematic representation of the NH_2 + NO PES.

MP2/6-31G* energies of N_2H_2O species relative to the energy of reactants ($E_{MP2}(NH_2 + NO) \equiv 0$) for reactions (1a) - (1c). See Fig. 7.1 for structures.

At the HF level all but two of the transition states lie well above the energy of separated NH_2 + NO. From the data in Table 7-4 it can be seen that the inclusion of electron correlation lowers the relative energies of the stable intermediates in a fairly uniform way but that the effects on the transition states are considerably more varied. The intermediate energies are lowered by between 152 and 162 kJ mol^{-1} while the decreases in the transition state energies range from 146 to 234 kJ mol^{-1} , the largest changes occurring for structures VII and XIV. The reasons for the latter effects are not clear but they probably partly reflect the deficiencies of the HF theory in treating molecules containing multiple bonds between electronegative atoms, which were noted by De Frees *et al.* [7.55]. For example, there may be similar problems associated with the representation of the multicentre bonding in VII and XVI within the HF approximation.

The calculated enthalpy of nitrosamine, relative to that of separated NH_2 + NO is 16 kJ mol^{-1} above the value reported by MP (D_0(N-N) = 201.3 kJ mol^{-1}) but is lower than the CI values obtained by CG and ARPC by 64 and 44 kJ mol^{-1} respectively. The NN bond energy in nitrosamine is therefore still very uncertain. The present value of D_0 = 185 kJ mol^{-1} is very close to that obtained by averaging the NN bond energies of

isoelectronic molecules HONO and CH_3NO (163 and 209 kJ mol^{-1} , respectively [7.59]). For the hydroxydiimides the present relative enthalpies are ca. 25 kJ mol^{-1} above the corresponding BAC-MP4 values [MB] and 35 - 45 kJ mol^{-1} below the CI values [CG, ARPC].

TABLE 7-4. Total and relative energies of N_2H_2O species

	- E_{SCF} a)	- E_{MP2} a)	ΔE_{SCF} b)	ΔE_{MP2} b)	ΔH_{rel} b,c)	$\Delta H^{\neq}$ b,d)
N_2 + NO	184.805586	185.256365	0.0	0.0	0.0	
IX H_2NNO	184.826480	185.337296	-54.9	-212.5	-185.1	
HNNOH						
III trans, cis	184.825151	185.334729	-51.4	-205.7	-175.1	
IV trans, trans	184.822464	185.331126	-44.3	-196.3	-165.9	
V cis, cis	184.810008	185.322680	-11.6	-174.1	-146.3	
VI cis, trans	184.822198	185.333654	-43.6	-202.9	-173.3	
TS VII	184.747581	185.284015	+152.3	-72.6	-57.9	127.2
TS XII	184.809332	185.315552	-9.8	-155.4	-129.4	45.7
TS XIII	184.744409	185.262915	+160.6	-17.2	+1.9	177.0
TS XIV	184.804977	185.315405	+1.6	-155.0	-130.1	16.2
TS XV	184.746270	185.264672	+155.7	-21.8	-2.5	163.4
TS XVI	184.750187	185.289940	+145.5	-88.2	-81.5	91.8
TS(N_2+H+OH)	184.786185	185.226567	+50.9	+78.2	+52.9	6.1
N_2H + OH	184.807677	185.236141	+5.5	+53.1	+46.8	
N_2+H+OH	184.825503	185.276760	-52.3	-53.5	-80.4	
N_2+H_2O	184.954696	185.453037	-391.5	-516.4	-506.9	

a) E_{SCF} and E_{MP2} in hartrees. b) ΔE and ΔH in kJ mol^{-1} .

c) Calculated from E_{MP2} with inclusion of zero-point energies from HF/6-31G* vibrational frequencies (Table 7-5). Imaginary frequencies not included.

d) Barrier heights calculated from appropriate ΔH_{rel} values.

The calculated barrier heights at the transition states VII, XV and XVI agree with the BAC-MP4 results of MB to within their estimated 12 kJ mol^{-1} uncertainty but in the absence of information on the BAC method no detailed comparison of these results is possible. The highest barrier in the pathway leading to N_2 + H_2O as products is that associated with the in-plane migration of a hydrogen atom in either of the processes III → XIII → V or IV → XV → VI. This result agrees with the finding of MB but is in contrast with the earlier suggestion by ARPC that the initial 1,3 H atom migration (IX → VII → III) was the rate-limiting step for rearrangement of NH_2NO to products. The fact that the latter idea was a key assumption in the RRK and RRKM calculations by ARPC and Gilbert *et al.* [7.24], respectively, reinforces the need for reliable PES data for use in such calculations and indicates that a detailed analysis of the rates of the individual

barrier-crossing processes would be required for a truly *a priori* calculations of the overall rate coefficient of reaction (1).

Calculations at the MP2 level of theory of the total enthalpy of N_2H + OH relative to that of NH_2 + NO showed that the production of N_2H + OH is *ca.* 47 kJ mol^{-1} endothermic, implying a nett positive activation energy for reaction (1b) of at least this magnitude. CG reported a very similar value (50 kJ mol^{-1}) while ARPC and MB found reaction (1b) to be nearly thermoneutral, reporting ΔH_f values of -15 and 10 ± 12 kJ mol^{-1} , respectively. Reaction (1c) on the other hand was found to be exothermic by 80 kJ mol^{-1} in close agreement with the result of ARPC (ΔH_f = - 83 kJ mol^{-1}) but 57 kJ mol^{-1} below the value of -23.4 kJ mol^{-1} reported by CG. The absence of consistent trends among the results of the four studies considered here prevents meaningful conclusions from being drawn from the above comparison. Factors contributing to the observed variation would include differences in the *ab initio* techniques and basis sets used and, possibly, the use of the UHF formalism to describe the doublet ground state of N_2H in the three MO theory studies. As was pointed out by Curtiss *et al.* [7.15], the UHF wavefunction for this molecule is appreciably spin-contaminated, a value of $<S^2>$ = 0.879 being found in the present work compared to the pure doublet value of 0.75. Hence larger uncertainties would be expected in the energy data calculated for processes involving N_2H than in data for other processes since UHF wavefunctions for other doublet species such as NH_2 , NO and OH were generally well-behaved. MB have noted that the use of spin-contaminated wavefunctions in post-HF calculations may also lead to significant uncertainties in barrier heights.

In regard to the importance of reactions (1b) and (1c) relative to that of reaction (1a) leading to N_2 +H_2O, it can be seen from Fig. 7.4 that the latter pathway is clearly favoured since it involves no nett activation barrier and is highly exothermic. Thus it would be expected to be fast and its rate coefficient should show a negative temperature coefficient, as is found experimentally for the NH_2 + NO reaction. The present finding that reaction (1b) is endothermic therefore indicates that it will be at most a minor reaction channel at room temperature, possibly becoming more important at higher temperatures. It is clear from Fig. 7.4 that the formation of N_2H + OH from any of the hydroxydiimides will involve a much larger activation barrier than any of the rearrangements shown. Such a process could occur *via* a transition state similar to XVI in which H_2 is still quite strongly bound to N_1 as is shown by the relatively small extension of the N_1H_2 bond compared to its length in structure VI.

The overall reaction (1c) could occur by a number of mechanisms. A concerted process involving simultaneous breaking of both the NH and NO bonds in any

of the hydroxydiimides seems unlikely due to the constraints this would impose on the vibrational phases of the parent molecule. MB have shown that the formation of HNNO + H is highly endothermic with respect to reactants and that the rearrangement of HNNO to form unstable NNOH requires significant activation energy. A process involving initial formation of N_2H + OH followed by dissociation of N_2H appears to be ruled out at room temperature by the arguments given above, as well as by the fact that the N_2H dissociation itself requires a finite activation energy. The calculated barrier height of 6 kJ mol^{-1} for this process is less than the value obtained in the MP4-level calculations of Curtiss *et al.* [7.15] (24 kJ mol^{-1}) and MB (26 kJ mol^{-1}).

Experimental results regarding the importance of reaction (1b) at room temperature are thus far inconclusive, with reported branching coefficients for OH production ranging from 0.13 to 0.7, although three recent experiments [7.14, 7.60, 7.61] have favoured the bottom of this range. At higher temperatures reaction (1b) could become more significant but the predicted low barrier to dissociation of N_2H means that the lifetime of N_2H at elevated temperatures is likely to be very short, particularly if quantum-mechanical tunnelling is taken into account. In fact, a tunnelling-rate calculation by Curtiss *et al.* [7.15], mentioned in Section 5.1, predicted a room temperature lifetime for N_2H of only about 5 x 10^{-11} s. Hence the participation of N_2H formed by reaction (1b) in secondary reactions with combustion products at temperatures above 1000 K, as required in model mechanism [7.18, 7.62] for the Thermal deNO_x process, seems unlikely. The short lifetime of N_2H also implies that H atoms should be generated if reaction (1b) occurs. However four experimental groups have failed to detect any H atom production in the NH_2 +NO system at either room [7.13, 7.63 - 65] or elevated temperatures [7.64]. These results also virtually rule out the operation of reaction (1c). Several alternative explanations for the observations of OH in this system have been offered. These include the formation of OH from (i) H_2O impurities in the experimental apparatus [7.14], (ii) the decomposition of vibrationally excited H_2O produced in reaction (1a) [7.61], and (iii) the reaction of NH with NO, since NH is a likely by-product of NH_2 generation in both flash photolysis and discharge-flow systems (see Section 6.3). Since both (i) and (ii) would also yield H atoms, the latter explanation seems the most plausible. Overall, experimental results to date support the general conclusion of this study that the channel (1a) leading to N_2 +H_2O is the major, if not the only pathway for the NH_2 + NO reaction.

C. Vibrational Frequencies of the N_2H_2O Species

In Table 7-5 are listed the harmonic vibrational frequencies of the four conformers of nitrosamine discussed in Section 7.5 A, together with those of all

reactants, intermediates, transition states and products involved in the NH_2 + NO reaction. These frequencies were determined from force constants calculated at the HF/6–31G* equilibrium geometries. The 6-31G* basis set has recently been shown by De Frees and McLean [7.53] to give good agreement between the calculated and experimental values of 165 frequencies of first-row molecules when the former are scaled by a factor of 0.89. They obtained a mean absolute error of 49 cm^{-1} with 92 % of the scaled frequencies being within 100 cm^{-1} of experiment. The scale factor represents corrections for the neglect of anharmonicity and for the inherent tendency of SCF theories to overestimate harmonic frequencies. In the present work a comparison of the calculated and experimental frequencies of N_2, NO, NH_2 and H_2O suggested the use of a scale factor 0.88 which gave a mean absolute error of 41 cm^{-1}. With a scale factor of 0.89 the corresponding error was 50 cm^{-1}. It should be noted that the deficiency of HF theory in treating molecules containing bonds between electronegative elements [7.55] also extends to the calculation of harmonic frequencies for such molecules. In the present case this means that the frequencies of NN and NO stretching modes are likely to be somewhat overestimated as is the frequency of inversion motions about N. In general, however, the scaled frequencies should be at least as accurate as estimates based on model compounds. In particular the calculated frequencies of non-planar nitrosamine (IX), for which a vibrational assignment is given in Table 7-5, represent an improvement on the values obtained by ARPC since the planar species I, on which their calculations were based, has now been shown to be a transition state rather than a true minimum on the PES. Calculations of the frequencies of IX using the 6-31G** and 6-311G** basis sets indicated that the true unscaled NH_2 wagging frequency (which corresponds to inversion about N_1) is close to 200 cm^{-1}. In view of the flat profile of the PES along the inversion coordinate, indicated by the closeness in energy of structures I and IX, the harmonic approximation is likely to be very poor for this mode. (At the HF/6-311G** level of theory the calculated barrier to inversion is only 20 cm^{-1} , an order of magnitude less than ν_9.) Similar considerations apply to the lowest frequency of structure XVI but the higher frequencies, once scaled, should serve as a useful basis for the assignment of any spectroscopic data which become available for N_2H_2O species.

7.6 **Summary**

The potential energy surface for the reaction between NH_2 and NO has been studied by the methods of *ab initio* molecular orbital theory in order to determine the structural parameters and vibrational frequencies of the various stable and transient species occurring along the reaction coordinate for the principal reaction channel which was found to be that yielding $N_2 + H_2O$ as final products (1a). A non-planar structure was calculated for the initially-formed nitrosamine intermediate, in contrast to the results

of previous studies in which planar geometry was proposed. The planar species was shown to represent a transition state on a very flat inversion coordinate, the energy separation between the two structures being very small and strongly dependent on the

TABLE 7-5: HF/6-31G* vibrational frequencies of species on the NH_2 + NO reaction PES. [a]

NH_2 (C_{2v}) NO ($C_{\infty v}$)	H_2NNO IX (C_1)	HNNOH III (C_s)	HNNOH IV (C_s)	HNNOH V (C_s)
	370 (NH_2 wag)	A" 668	A" 498	A" 475
	690 (NH_2 rock)	A' 738	A' 735	A' 761
	744 ((NH_2 torsion)	A" 1080	A" 1096	A" 1089
	1251 (NNH_2b/NN str)	A' 1136	A' 1107	A' 1100
	1392 (NNH_1b/NNH_2b)	A' 1547	A' 1510	A' 1455
A_1 1712	1781 (NH_2 sci)	A' 1618	A' 1618	A' 1635
Σ^+ 2221	1882 (NO str/NNH_2b)	A' 1925	A' 1966	A' 1937
A_1 3605	3772 (NH s-str)	A' 3710	A' 3692	A' 3505
B_2 3705	3955 (NH a-str)	A' 3953	A' 4108	A' 3946

HNNOH VI (C_s)	N_2 ($D_{\infty h}$) H_2O (C_{2v})	N_2H (C_s) OH ($C_{\infty v}$)	TS VII (C_s)	TS XII (C_1)	TS XIII (C_s)
A" 475			A' 2444i	539i	A' 1561i
A' 711			A" 705	746	A" 544
A' 1060			A' 1058	1066	A" 613
A" 1147			A" 1282	1074	A' 727
A' 1477			A' 1343	1462	A' 971
A' 1607	A_1 1827	A' 1264	A' 1507	1592	A' 1508
A' 1975	Σ_g^+ 2758	A' 1661	A' 1693	1939	A' 2001
A' 3576	A_1 4070	A' 3276	A' 2316	3663	A' 3976
A' 4101	B_2 4189	Σ^+ 3997	A' 3811	4058	A' 4103

TS XV (C_1)	TS XIV (C_s)	TS XVI (C_s)	TS N_2+H (C_s)	H_2NNO I (C_s) [b]	H_2NNO II (C_s) [b]	H_2NNO X (C_s) [b]
461i	A' 1554i	A' 1615i	A' 1919i	A' 268i	A' 548i	A' 421i
725	A' 500	A" 91		A' 706	A' 717	A' 738
1030	A" 631	A' 616		A" 759	A' 1028	A' 1016
1103	A' 717	A' 859		A' 1264	A' 1244	A' 1235
1441	A' 898	A" 1139		A' 1372	A" 1300	A" 1279
1585	A' 1482	A' 1184		A' 1769	A' 1773	A' 1795
1943	A' 2036	A' 2122		A' 1862	A' 1988	A' 2025
3559	A' 4088	A' 2326	A' 896	A' 3788	A' 3657	A' 3666
4035	A' 4120	A' 4048	A' 2136	A' 3984	A" 3753	A' 3746

a) Unscaled frequencies in cm^{-1}. Recommended scale factor 0.88 (see text).

b) Unstable conformers of nitrosamine (see Section 7.5 A for discussion).

properties of the basis set used in the calculations. Once formed, nitrosamine can undergo a series of rearrangements leading ultimately to the formation of a hydroxydiimide conformer from which the major products are formed by 1,2 elimination across the NN double bond. This process can occur with no nett activation energy relative to the reactants, in accordance with the experimentally observed negative temperature dependence of the overall rate coefficient. The highest individual barrier in the rearrangement pathway was shown to correspond to a trans-cis isomerisation of hydroxydiimide, rather than to the initial 1,3 migration of a hydrogen atom in nitrosamine as was believed earlier. Alternative reaction channels producing either N_2H + OH (1b) or N_2 + H + OH (1c) were found to involve positive activation energies with respect to the reactants, the former process being endothermic overall, implying that they are not important at room temperature. Their operation at higher temperatures is also counter-indicated by recent experimental data on the yields of OH and H atoms from reaction (1).

Harmonic vibrational frequencies have been calculated for all of the N_2H_2O isomers involved, using a well characterised basis set (6-31G*). Apart from two very low frequencies these results should be sufficiently reliable for use in statistical rate theory calculations and for the assignment of vibrational spectra once a scale factor of 0.88 has been applied.

7.7 Epilogue

Since the completion of this work a number of similar studies of related reaction systems have been commenced in this laboratory. These include studies of the NH + NO and BH + NO reactions and calculations of the energies of the N_2H_2O intermediates and transition states in the NH_2 + NO system at the MP4/6-31G*//HF/6-31G* level of theory. The latter calculations may provide insight into the reasons for the previously observed differential effects of electron correlation on the energies of the transition states, as well as giving an indication of the magnitude of the bond additivity corrections applied by MB in their calculations of heats of formation. Possible future work in this area includes studies of the related reactions of NH_2, NH and BH with NO_2.

A preliminary report of matrix isolation infra-red spectroscopic studies of the NH_2 + NO reaction by Sodeau [7.36] has lead to calculations (by Dr. R. G. A. R. Maclagan and Dr. B. G. Williamson of this University) of the vibrational frequencies of the isotopically substituted ND_2NO, $^{15}NH_2NO$ and $^{15}ND_2NO$ molecules. These calculations were performed using the FG-matrix method of Wilson *et al.* [7.41] with

internal coordinate force constants obtained for NH_2NO and with appropriate changes to the mass factors which appear in the G matrix.

Very recently Phillips [7.34] has performed *a priori* calculations of the temperature dependence of the rate coefficient for reaction (1) in which RRKM rates for the crossing of the barriers on the PES were calculated using the frequencies obtained in this work, together with the MP4 barrier heights given by MB. The barrier-crossing rates were combined with a calculated rate for the initial formation of NH_2NO based on the rates of dipole capture and intramolecular vibrational relaxation to obtain the overall rate coefficient for reaction (1). The calculated temperature dependence of k_1 was in good agreement with experimental results at temperatures above 300 K.

CHAPTER 8

CONCLUSIONS

The principal aim of this work was to study the rates of reactions of photofragment species produced in the gas phase by laser photolysis of stable precursor molecules. We have focussed attention on reactions of the CN, NH_2, and NH radicals, which are important species in combustion and/or atmospheric chemistry. First measurements of rate coefficients for three reactions, (namely $CN + N \rightarrow N_2 + C$, $NH_2 + N \rightarrow$ products and $NH + NO_2 \rightarrow$ products) are reported, together with several re-evaluations of previously measured rate coefficients. Questions arising in the course of the rate studies and the existence of some unresolved problems in the literature have led to additional studies of the nature of the products of the $NH_2 + N$ reaction, and to a theoretical investigation, by means of molecular orbital theory, of the form of the potential energy surface for the reaction $NH_2 + NO \rightarrow$ products. The results of each of these studies have been discussed with regard to their implications concerning the appropriate reaction mechanisms in particular, and to the role of those reactions in larger chemical systems. In this chapter we briefly summarise conclusions which may be drawn from each of these studies.

In Chapter 3, the first direct measurement of the rate coefficient for the reaction

$$CN + N \rightarrow N_2 + C \qquad (1)$$

is described. The rate coefficient k_1 was found to be $(1.00 \pm 0.05) \times 10^{-10}$ cm^3 s^{-1} at 300 K and around 1 Torr pressure, for reaction of both the $\upsilon'' = 0$ and $\upsilon'' = 1$ vibrational levels of CN in its electronic ground state. The measurements of pseudo-first-order decay rates, on which were based the determinations of k_1, were made over short reaction times. This was necessary in order to avoid apparent deviations from first-order behaviour at longer times, which were caused by secondary generation of CN, either by cascade processes or by secondary reactions such as

$$C + C_2N_2 \rightarrow C_2N + CN \qquad (2)$$

and

$$N + C_2N \rightarrow 2\,CN. \qquad (3)$$

Simple numerical simulation of this behaviour, based on a minimal model mechanism, led to an estimate of 3×10^{-11} cm^3 s^{-1} for k_2, with the assumption that $k_3 = k_1$. This result for k_2 suggests that the heat of formation of C_2N is near the low end of the range $430 \leq \Delta H_f(C_2N) \leq 682$ kJ mol^{-1} [8.1]. Reaction (1) appears to have a very low

activation energy (*ca.* 4 kJ mol^{-1}) consistent with formation of an intermediate CN_2 species. The absence of an effect of vibrational excitation of CN upon the rate of its disappearance is therefore unsurprising. However, the estimation of E_A for reaction (1) relies on a number of approximations and should not be regarded as reliable. Measurements of k_1 over a range of temperatures, with detection of products as well as reactants and possibly CNN or NCN, will be necessary for the elucidation of the detailed mechanism of reaction (1).

The rate coefficient for the reaction

$$CN(\upsilon'') + O_2 \rightarrow \text{products} \qquad (\upsilon'' = 0, 1) \qquad (4)$$

was also determined in this study. Values of k_4 ($\upsilon''=0$) = (1.35 ± 0.20) x 10^{-11} cm^3 s^{-1} and k_4 ($\upsilon''=1$) = (1.25 ± 0.32) x 10^{-11} cm^3 s^{-1} were found at 300 K and pressures near 1 Torr. These results were in reasonable agreement with those of earlier workers using flash photolysis to generate CN; however, measurements made by other workers since the completion of this study indicate that the measurements of k_4 for $\upsilon'' > 0$ may be considerably affected by cascade processes.

In Chapter 4 the first measurement is reported of the rate coefficient for the reaction

$$NH_2 + N \rightarrow \text{products.} \qquad (5)$$

This reaction is considered to be important in the decomposition of ammonia in active nitrogen and in the flame oxidation of NH_3. The rate coefficient was found to be (1.21 ± 0.14) x 10^{-10} cm^3 s^{-1}; this is some 35 times greater than the rate coefficient for the analogous reaction between NH_2 and O atoms. This result is consistent with the different exothermicities of the two reactions, but the situation is not entirely clear, since neither the products nor the mechanisms are well characterised for either reaction. Small concentrations of NH were detected by LIF at short reaction times in the NH_2 + N system, indicating the operation of the channel leading to NH + NH as products by direct H atom abstraction. However the possibility of formation of a short-lived H_2NN intermediate could not be ruled out, since signal-to-noise problems in the detection of NH prevented a detailed examination of the behaviour of this species. Determination of the temperature coefficient of k_5 would aid in the resolution of this question.

Rate coefficients for the reactions

$$NH_2 + NO \rightarrow \text{products} \qquad (6)$$

and $NH_2 + NO_2 \rightarrow$ products (7)

were also measured in this work. The values of $k_6 = (1.81 \pm 0.12) \times 10^{-11}$ cm^3 s^{-1} and $k_7 = (2.11 \pm 0.18) \times 10^{-11}$ cm^3 s^{-1} obtained were in very good agreement with those found in previous flash- or laser photolysis studies, but were a factor of two larger than the corresponding values obtained by means of discharge-flow experiments. A rationale for this discrepancy was proposed, based on the idea of formation of a collision complex whose lifetime was sufficiently long to permit diffusion away from the viewing region in a flash photolysis experiment, but which may revert to reactants before reaching the detection region in a flow system. Such a complex has been suggested for the $NH_2 + O$ reaction; this could partly explain the discrepancy between the rates of this process and reaction (5). Spectroscopic measurements of the lifetimes of these complexes would be very valuable in establishing the cause of the flash/flow discrepancy; as the electronic spectra of nitrosamine (H_2NNO) and nitramine (H_2NNO_2) have not yet been observed there is scope for further work in this area.

An investigation of the nature of the products of the $NH_2 + N$ reaction (5), motivated by the work reported in Chapter 4, is described in Chapter 5. In this study a resonance fluorescence technique was used to measure the yields of product H atoms; these measurements showed clearly that formation of N_2 and H_2 as products does not occur. The observed time dependence of the H atom concentration following excimer laser photolysis of NH_3/ N-atom mixtures was compared with [H] *vs.* time profiles calculated by numerical simulation of simple model mechanisms corresponding to various product pathways. These comparisons showed that the major product channel is that leading to direct formation of N_2 and two H atoms, rather than the initial formation of NH followed by reaction of this species with N atoms. These results are consistent with the observation of small NH LIF signals in this system, as reported in Chapter 4, and with the endothermicity of the reaction $NH_2 + N \rightarrow 2$ NH, but they contradict the assertion by Kaskan and Hughes [8.2] that both the ($N_2 + H_2$) and (NH + NH) product channels operate in the flame oxidation of ammonia near 2000 K. However, the conclusions drawn in that study are not likely to be materially affected by the present findings. Measurements of the branching coefficient for the various pathways as functions of temperature, with direct detection of the products, would be of considerable value for future modelling studies of systems in which reaction (5) is likely to be important, e. g., combustion systems containing nitrogenous fuels or support gases.

The variation of the H atom fluorescence signal with NH_3 concentration at moderate laser pulse energies, together with the observation of exalted absorption cross-sections for NH_3 at 193 nm, indicates the occurrence of multiple-photon processes in the

photolysis at even relatively low pulse energies (*ca.* 20 mJ). These observations are consistent with previous spectroscopic measurements on NH_3 and its photolysis products. The most likely candidate for the intermediate state in these processes is NH_2 in either its ground or first excited electronic state.

The H atom resonance fluorescence technique has also been used to establish that H atoms are not produced in the NH_2 + NO reaction (6), as found by earlier workers. In view of the predicted instability of N_2H toward dissociation to N_2 + H, this result has serious consequences for previous modelling studies [8.3, 8.4] of the Thermal deNO_x process, in which N_2H and OH have been proposed as the major products at temperatures around 1250 K (see below).

Measurements of the temperature dependences of the rate coefficients for the reactions

$$NH + NO \rightarrow \text{products} \qquad (8)$$

and

$$NH + NO_2 \rightarrow \text{products} \qquad (9)$$

are described in Chapter 6. The rate coefficients $k_8 = (5.78 \pm 0.64) \times 10^{-11}$ cm^3 s^{-1} and $k_9 = (1.61 \pm 0.14) \times 10^{-11}$ cm^3 s^{-1} were obtained at 300 K and 1 Torr of pressure. Several different bath gases were used in these experiments (Ar, He, N_2, N_2O); the absence of any pronounced dependence of k_8 or k_9 on the nature of the bath gas was taken to indicate that the rate coefficients were pressure-independent near 1 Torr. k_8 was also found to be virtually independent of temperature in the range 269 - 377 K, while k_9 showed a small negative temperature dependence. This behaviour is consistent with formation of an intermediate complex as the first step in either reaction (8) or (9). For reaction (8) this suggestion is confirmed by the results of *ab initio* quantum chemical calculations [8.5]. Some speculations regarding the nature of the potential energy surfaces and products of these reactions have been offered. These are based on the present results for k_8 and k_9, previous, related experimental results and the analogy between the reactions of NH and NH_2 with NO and NO_2. We suggest that N_2 and OH are likely to be the major products of reaction (8); N_2O and OH are postulated as major products of reaction (9). If indeed OH is produced in reaction (8), then the conflict in the literature regarding the importance of OH-producing channels for reaction (6) could be resolved if NH could be shown to have been present along with NH_2 in the systems studied.

Potential future work related to these reactions could include a comprehensive study of the pressure and temperature dependences of their rate coefficients over wider temperature and pressure ranges than were available in the present work, with detection

of OH by LIF and of N_2O by mass spectroscopy; attempts to detect HNNO or $HNNO_2$ by spectroscopic means; and further theoretical studies of the potential energy surfaces for the reactions. It should be noted that the pressure independence of k_8 at pressures as low as 1 Torr may indicate that reaction (8) is a 'fast, bond-switching' reaction, of the type described in Section 7.1; thus it may be suitable system for further testing of the theory developed in reference [8.6] for prediction of such behaviour.

In Chapter 7 are reported the results of an investigation of the potential energy surface (PES) for reaction (6) by means of *ab initio* molecular orbital theory. This study was motivated by the need for accurate PES information for use in the application of statistical rate theories in calculations of the pressure and temperature dependences of k_6. The nature of a proposed model for the mechanism of reaction (6), which involves rapid migration of H atoms in a series of intermediate complexes, suggests that experimental and theoretical studies of the corresponding deuterated system (ND_2 + NO) could be very valuable.

Previous *ab initio* studies of reaction (6) have focussed attention on various aspects of the PES such as thermochemistry, structures of intermediates or relative energies, as well as on more technical points concerning choice of basis set, method of calculation etc., However, there has been no comprehensive and consistent study of this system in which all such areas have been covered; the present work was an attempt to remedy this situation.

The principal results of this work are (1) the identification of a non-planar geometry for nitrosamine (H_2NNO) and the finding that the planar structure is in fact a transition state for inversion about the amine N atom, a result which calls into question previous calculations of harmonic vibrational frequencies for the planar species; (2) the calculation of molecular geometries for the intermediates and transition states on the multiple-minimum PES; (3) the calculation of barrier heights for the interconversions between various N_2H_2O isomers; (4) the finding that the highest barriers on the PES are associated with trans-cis isomerisation about the N–N bond in hydroxydiimide (HNNOH), rather than with the initial 1, 3 H atom migration which forms this species from nitrosamine; (5) the calculation of vibrational frequencies for N_2H_2O intermediates, which may be useful for identification of infrared spectra; and (6) our conclusion that N_2H, OH and H atoms are only minor products of the NH_2 +NO reaction. Significantly, the formation of N_2H in reaction (6) is considered to be a key step in model mechanisms for the Thermal deNO_x process at temperatures between 1000 and 1500 K [8.3, 8.4]. However the present work, in conjunction with recent measurements of OH and H yields from reaction (6) and other *ab initio* calculations on N_2H (see Chapters 4 - 6), indicates

that this cannot be the case. It appears that further work on modelling of this important process is required.

APPENDIX: Estimated Experimental Uncertainties

Cell temperature	= ± 1 K	(including drifts and thermocouple calibrations)
Cell pressure	= ± 1 %	(TEXAS INSTRUMENTS gauge)
NO_2/N_2O_4 pressure and N_2H_4 saturator pressure	< ± 1 %	(MKS BARATRON gauge)
Individual flow rates	= ± 1 - 3 %	(Low values for high capacity flowmeters)
Flowmeter calibration factors	< ± 1 %	(from bubble-meter measurements)
Reproducibility of photometric nitrogen atom titration	= ± 2 %	
NO_2/N_2O_4 heat capacity correction factor	= ± 2 %	
Boxcar integrator timebase calibration	< ± 0.2 %	

REFERENCES

Chapter 1:

1.1 W. Demtröder, "Laser Spectroscopy", Springer Series in Chemical Physiscs, Vol. 5, Springer-Verlag, Berlin, 1982.

1.2 O. Svelto, "Principles of Lasers", Heyden, London, 1976.

1.3 C. B. Moore (ed.), "Chemical and Biochemical Applications of Lasers", Vol.s 1 - 4, Academic Press, New York, 1974 - 1979.

1.4 A. K. Levine (ed.), "Lasers: A Series of Advances", Vol.s 1 - 3, Marcel Dekker, New York, 1966 - 1971.

1.5 M. Bass, T.F. Deutsch and M. J. Weber, in Vol. 3 of [1.4], p. 269.

1.6 S. R. Leone and C. B. Moore, in Vol. 1 of [1.3], p. 1.

1.7 F. P. Schaefer, "Dye Lasers", 2nd Ed., Springer-Verlag, Berlin, 1977.

1.8 M. D. Levenson, "Introduction to Non-Linear Laser Spectroscopy", Academic Press, New York, 1982.

1.9 S. Druet and J.-P. Taran, in Vol 4 of [1.3], p. 187.

1.10 J. F. Verdieck, R. J. Hall, J. A. Shirley and A. C. Eckbreth, J. Chem. Ed., 59 (1982) 456.

1.11 D. M. Friedrich, J. Chem. Ed., 59 (1982) 472.

1.12 R. W. Terhune and P. D. Maker, in Vol. 2 of [1.4], p. 295.

1.13 M. J. Shaw, Prog. Quant. Electron., 6 (1979) 3.

1.14 V. Evtuhov and J. K. Neeland, in Vol. 1 of [1.4], p. 1.

1.15 L. F. Johnson, in Vol. 1 of [1.4], p. 137.

1.16 E. Snitzer and C. G. Young, in Vol. 2 of [1.4], p. 191.

1.17 M. T. Macpherson and R. F. Barrow, Annu. Rep. Prog. Chem., Sect. C, 78 (1981) 221.

1.18 M. N. R. Ashfold and G. Hancock, in "Gas Kinetics and Energy Transfer", Vol. 4, ed. P. G. Ashmore and R. J. Donovan (Specialist Periodical Reports), The Royal Society of Chemistry, London, 1981, p. 73.

1.19 M. C. Lin and J. R. McDonald, in "Reactive Intermediates in the Gas Phase", ed. D. W. Setser, Academic Press, New York, 1979, p. 233.

1.20 R. J. Donovan, in "Gas Kinetics and Energy Transfer", Vol. 4, ed. P. G. Ashmore and R. J. Donovan (Specialist Periodical Reports), The Royal Society of Chemistry, London, 1981, p. 117.

1.21 H. M. Gillespie and R. J. Donovan, Annu. Rep. Prog. Chem., Sect. C, 77 (1980) 173.

1.22 G. Duxbury, Annu. Rep. Prog. Chem., Sect. C, 78 (1981) 31.

1.23 A. H. Zewail (ed.), "Advances in Laser Chemistry", Springer Series in Chemical Physics, Vol. 3, Springer-Verlag, Berlin, 1978.

1.24 K. L. Kompa and S. D. Smith (ed.s), "Laser-Induced Processes in Molecules", Springer Series in Chemical Physics, Vol. 6, Springer-Verlag, Berlin, 1979.

1.25 J. I. Steinfeld (ed.), "Laser-Induced Chemical Processes", Plenum, New York, 1981.

1.26 M. A. A. Clyne, in "Physical Chemistry of Fast Reactions", Vol. 1, ed. B. P. Levitt, Plenum, London, 1973, p. 245.

1.27 M. A. A. Clyne and W. S. Nip, in "Reactive Intermediates in the Gas Phase", ed. D. W. Setser, Academic Press, New York, 1979, p. 2.

1.28 C. J. Howard, J. Phys. Chem., 83 (1979) 3.

1.29 L. M. Dorfman and M. C. Saver, in "Investigation of Rates and Mechanisms of Reactions", Part 1, 4th ed., ed. C. F. Bernasconi, John Wiley, New York, 1986, p. 493.

1.30 C. T. Bowman and R. K. Hanson, J. Phys. Chem., 83 (1979) 757.

1.31 See for example: M. A. Kimball-Lynne and R. K. Hanson, Combustion and Flame, 64 (1986) 337.

1.32 G. Porter and M. A. West, in "Techniques of Chemistry", Vol. 6, Part 2, 3rd ed., ed. G.G. Hammes, John Wiley, New York, 1974, p. 367.

1.33 M. T. Macpherson and R. F. Barrow, Annu. Rep. Prog. Chem., Sect. C, 76 (1979) 51.

1.34 J. Wolfrum, in "Physical Chemistry: An Advanced Treatise", Vol. 6B, ed.s H. Eyring, D. Henderson and W. Jost, Academic press, New York, 1975, p. 629.

1.35 K. S. Chen and N. Hirota, in "Techniques of Chemistry", Vol. 6, Part 2, 3rd ed., ed. G.G. Hammes, John Wiley, New York, 1974, p. 565.

1.36 J. E. Baggott and M. J. Pilling, Annu. Rep. Prog. Chem., Sect. C, 76 (1979) 199.

1.37 W. M. Fairbank Jr., T. W. Hänsch and A. L. Schawlow, J. Opt. Soc. Am., 65 (1975) 199.

1.38 B. A. Thrush, Acc. Chem Res., 14 (1981) 116.

1.39 P. B. Davies, J. Phys. Chem., 85 (1981) 2599.

1.40 M. A. West, in "Investigation of Rates and Mechanisms of Reactions", Part 1, 4th ed., ed. C. F. Bernasconi, John Wiley, New York, 1986, p. 391.

Chapter 2:

2.1 M. J. Shaw, Prog. Quant. Electron., 6 (1979) 3.

2.2 W. Demtröder, "Laser Spectroscopy", Springer Series in Chemical Physiscs, Vol. 5, Springer-Verlag, Berlin, 1982.

2.3 J. E. Butler, Appl. Opt., 21 (1982) 3617.

2.4 A. N. Wright and C. A. Winkler, "Active Nitrogen", Academic Press, New York, 1968, pp. 258-264 and 382-387.

2.5 Instruction Manual, Series TE 861-T Excimer Laser, Lumonics Inc.

2.6 L. F. Phillips and A. M. Fergusson, in "Physical Methods of Chemistry", Vol. 1, ed. B. W. Rossiter, John Wiley, New York, 1986.

2.7 Instruction Manual, Model 160 Boxcar Integrator, Princeton Applied Research, Princeton, 1969.

2.8 D. L. Baulch, D. D. Drysdale, D. G. Horne and A. C. Lloyd, "Evaluated Kinetic Data for High Temperature Reactions", Vol. 2, Butterworths, London, 1973.

2.9 M. W. Chase Jr., J. L. Curncutt, J. R. Downey Jr., R. A. McDonald, A. N. Syverud and E. A. Valenzuela, JANAF Thermochemical Tables, 1982, Supplement, J. Phys. Chem. Ref. Data, 11 (1982) 695, and earlier collections referenced therein.

Chapter 3:

3.0 A. R. Whyte and L. F. Phillips, Chem Phys. Lett., 98 (1983) 590.

3.1 W.S. Adams, Astrophys. J., 109 (1949) 354.

3.2 B. E. Turner and R. H. Gammon, Astrophys. J., 198 (1975) 71.

3.3 A. P. C. Mann and D. A. Williams, Nature, 283 (1980) 721.

3.4 C. P. Fenimore, 13th Symp. (Int.) Combust., 1971, p. 373.

3.5 D. Iverach, K. S. Basden and N. Y. Kirov, 14th Symp. (Int.) Combust., 1973, p. 767.

3.6 B. S. Haynes,D. Iverach and N. Y. Kirov, 15th Symp. (Int.) Combust., 1975, p. 1103.

3.7 E. L. Merryman and A. Levy, 15th Symp. (Int.) Combust., 1975, p. 1073.

3.8 J. N. Mulvihill and L. F. Phillips, 15th Symp. (Int.) Combust., 1975, p. 1113.

3.9 L. F. Phillips, Combustion and Flame, 26 (1976) 379.

3.10 H. Schacke, K. J. Schmatjko and J. Wolfrum, Ber. Bunsenges. Phys. Chem., 77 (1973) 248.

3.11 X. Li, N. Sayah and W. M. Jackson, J. Chem. Phys., 81 (1984) 833.

3.12 X. Li, N. Sayah and W. M. Jackson, J. Chem. Phys., 83 (1985) 616.

3.13 J. C. Boden and B. A. Thrush, Proc. Royal Soc., A305 (1968) 107.

3.14 K. J. Schmatjko and J. Wolfrum, Ber. Bunsenges. Phys. Chem., 79 (1975) 696.

3.15 K. J. Schmatjko and J. Wolfrum, Ber. Bunsenges. Phys. Chem., 82 (1978) 419.

3.16 E. A. Albers, K. Hoyermann, H. Schacke, K. J. Schmatjko, H. G. Wagner and J. Wolfrum, 15th Symp. (Int.) Combust., 1975, p. 765.

3.17 I. M. Campbell and B. A. Thrush, Proc. Chem Soc., (1964) 410.

3.18 K. D. Bayes, Can. J. Chem., 39 (1961) 1074.

3.19 D. R. Safrany and W. Jaster, J. Phys. Chem., 72 (1968) 3305.

3.20 D. R. Safrany and W. Jaster, J. Phys. Chem., 72 (1968) 3318.

3.21 D. Kley, N. Washida, K. H. Becker and W. Groth, Chem. Phys. Lett., 15 (1972) 45.

3.22 A. R. Fairburn, J. Chem. Phys., 51 (1969) 972.

3.23 M. W. Slack, J. Chem. Phys., 64 (1976) 228.

3.24 G. E. Bullock and R. Cooper, J. Chem Soc., Faraday Trans. 1, 68 (1972) 2175.

3.25 R. W. B. Pearse and A. G. Gaydon, "The Identification of Molecular Spectra", 4th ed., Chapman and Hall, London, 1976.

3.26 F. J. LeBlanc, J. Chem. Phys., 48 (1968) 1980.

3.27 W. M. Jackson and J. B. Halpern, J. Chem. Phys., 70 (1979) 2373.

3.28 J. O. Hirschfelder, J. Chem. Phys., 9 (1941) 645.

3.29 K. P. Huber and G. Herzberg, " Molecular Spectra and Molecular Structure", Vol. 4, Constants of Diatomic Molecules, van Nostrand Reinhold, New York, 1979, p. 154.

3.30 M. Y. Louge and R. K. Hanson, Int. J. Chem. Kin., 16 (1984) 231.

3.31 D. A. Lichtin and M. C. Lin, Chem. Phys., 96 (1985) 473.

3.32 J. de Juan, I. W. M. Smith and B. Veyret, paper presented at XVIIth Informal Conference on Photochemistry, University of Colorado, Boulder, Colorado, June 22-26, 1986.

3.33 J. D. Lambert, Chem. Soc. Quart. Rev., 21 (1967) 67.

3.34 R. N. Schwartz, Z. I. Slawsky and K. F. Herzfeld, J. Chem. Phys., 20 (1952) 1591.

3.35 D. E. Paul and F. W. Dalby, J. Chem. Phys., 37 (1962) 592.

3.36 G. E. Bullock and R. Cooper, Trans. Faraday Soc., 67 (1971) 3258.

3.37 N. Basco, Proc. Roy. Soc., A 283 (1965) 302.

3.38 D. R. Stull and H. Prophet, Project Directors, JANAF Thermochemical Tables, 2nd. ed., U. S. Natl. Bur. Stds. Publ. NSRDS-NBS 37, Washington, 1971.

3.39 M. E. Jacox, J. Mol. Spect., 72 (1978) 26.

3.40 R. N. Perutz, Chem. Rev., 85 (1985) 97.

Chapter 4:

4.0 A. R. Whyte and L. F. Phillips, Chem. Phys. Lett., 102 (1983) 451.

4.1 C. H. Bamford, Trans. Faraday Soc., 35 (1939) 568.

4.2 G. K. Adams, W. G. Parker and H. G. Wolfhard, Disc. Faraday Soc., 14 (1953) 97.

4.3 C. P. Fenimore and G. W. Jones, J. Phys. Chem., 65 (1961) 298.

4.4 W. E. Kaskan and D. E. Hughes, Combustion and Flame, 20 (1973) 381.

4.5 A. G. Gaydon and H. G. Wolfhard, "Flames: Their Structure, Radiation and Temperature", 3rd ed., Chapman and Hall, London, 1970.

4.6 R. K. Lyon, Int. J. Chem. Kin., 8 (1976) 315.

4.7 R. K. Lyon and D. Benn, 17th Symp. (Int.) Combust., 1979, p. 601.

4.8 J. A. Miller, M. C. Branch and R. J. Kee, Combustion and Flame, 43 (1981) 81.

4.9 F. Stuhl, J. Chem. Phys., 59 (1973) 635.

4.10 J. C. McConnell, J. Geophys. Res., 78 (1973) 7812.

4.11 J. A. Logan, M. J. Prather, S. C. Wofsy and M. B. McElroy, J. Geophys. Res., 86 C (1981) 7210.

4.12 CODATA Task Group on Chemical Kinetics, D. L. Baulch, R. A. Cox, R. F. Hampson Jr., J. A. Kerr, J. Troe and R. T. Watson, J. Phys. Chem. Ref. Data, 13 (1984) 1259 and earlier collections referenced therein.

4.13 D. L. Baulch, D. D. Drysdale, D. G. Horne and A. C. Lloyd, "Evaluated Kinetic Data for High Temperature Reactions", Vol. 2, Butterworths, London, 1973.

4.14 S. Gordon, W. Mulac and P. Nangia, J. Phys. Chem., 75 (1971) 2087.

4.15 A. W. Boyd, C. Willis and O. A. Miller, Can. J. Chem., 49 (1971) 2283.

4.16 P. B. Pagsberg, J. Eriksen and H. C. Christensen, J. Phys. Chem., 83 (1979) 582.

4.17 M. J. McEwan and L. F. Phillips, "Chemistry of the Atmosphere", Edward Arnold, London, 1975, p. 27.

4.18 H. Okabe,"Photochemistry of Small Molecules", John Wiley, New York, 1978, p. 269 -272.

4.19 M. Gehring, K. Hoyermann, H. Schacke and J. Wolfrum, 14th Symp. (Int.) Combust., 1972, p. 99.

4.20 P. V. Khê, J. C. Soulignac and R. Lesclaux, J. Phys. Chem., 81 (1977) 210.

4.21 A. N. Wright and C. A. Winkler, "Active Nitrogen", Academic Press, New York, 1968, pp. 375 - 380.

4.22 R. A. Back and D. R. Salahub, Can. J. Chem., 45 (1967) 851.

4.23 Reference 11 in [4.4].

4.24 Y. L. Yung, M. Allen and J. P. Pinto, Astrophys. J. Suppl., 55 (1984) 465.

4.25 D. A. Armstrong and C. A. Winkler, Can. J. Chem., 33 (1955) 1649.

4.26 L. J. Stief, W. D. Brobst, D. F. Nava, R. P. Borkowski and J. V. Michael, J. Chem. Soc. Faraday Trans. 2, 78 (1982) 1391.

4.27 H. Kurasawa and R. Lesclaux, Chem. Phys. Lett., 66 (1979) 602.

4.28 J. E. Butler, Appl. Opt., 21 (1982) 3617.

4.29 K. Dressler and D. A. Ramsey, Phil. Trans. Royal Soc., A 251 (1959) 553.

4.30 A. M. Bass, A. E. Ledford and A. H. Laufer, U. S. Natl. Bur. Stds. J. Res., 80A (1976) 143.

4.31 W. Hack, H. Schacke, M. Schröter and H. G. Wagner, 17th Symp. (Int.) Combust., 1979, p. 505.

4.32 "CRC Handbook of Chemistry and Physics", 64th ed., ed. R. C. Weast, Chemical Rubber Publ., Boca Raton, 1985.

4.33 R. Lesclaux, P. V. Khê, P. Dezazier and J. C. Solignac, Chem. Phys. Lett., 35 (1975) 493.

4.34 J. A. Silver and C. E. Kolb, J. Phys. Chem., 86 (1982) 3240.

4.35 S. G. Cheskis, A. A. Iogansen, O. M. Sarkisov and A.A. Titov, Chem. Phys. Lett., 120 (1985) 45.

4.36 V. M. Donnelly, A. P. Baronavski and J. R. McDonald, Chem. Phys., 43 (1979) 271.

4.37 D. R. Stull and H. Prophet, Project Directors, JANAF Thermochemical Tables, 2nd. ed., U. S. Natl. Bur. Stds. Publ. NSRDS-NBS 37, Washington, 1971.

4.38 M. W. Chase Jr., J. L. Curncutt, J. R. Downey Jr., R. A. McDonald, A. N. Syverud and E. A. Valenzuela, JANAF Thermochemical Tables, 1982, Supplement, J. Phys. Chem. Ref. Data, 11 (1982) 695.

4.39 W. Hack and H. Kurzke, Ber. Bunsenges. Phys. Chem., 89 (1985) 86.

4.40 J. A. Pople and D. L. Beveridge,"Approximate Molecular Orbital Theory", McGraw Hill, New York, 1970.

4.41 I. N. Levine, "Quantum Chemistry", Allyn and Bacon, Boston, 1974.

4.42 C. J. Casewit and W. A. Goddard III, J. Am. Chem. Soc., 104 (1982) 3280.

4.43 C. J. Casewit and W. A. Goddard III, J. Am. Chem. Soc., 102 (1980) 4057.

4.44 J. B. Jeffries, J. A. McCauley and F. Kaufman, Chem. Phys. Lett., 106 (1984) 111.

4.45 K.-H. Gericke, L. M. Torres and W. A. Guillory, J. Chem. Phys., 80 (1984) 6134.

4.46 T.-X. Xiang, L. M. Torres and W. A. Guillory, J. Chem. Phys., 83 (1985) 1623.

4.47 J. L. Hall, D. Zeitz, J. W. Stephens, J. V. V. Kaspar, G. P. Glass, R. F. Curl and F. K. Tittel, J. Phys Chem., 90 (1986) 2501.

4.48 P.A. Andresen, A. Jacobs, C. Kleinermanns and J. Wolfrum, 19th Symp. (Int.) Combust., 1982, p. 11.

4.49 A. R. Whyte and L. F. Phillips, J. Phys. Chem., 88 (1984) 5670.

4.50 S. R. Bosco, W. D. Brobst, D. F. Nava and L. J. Stief, J. Geophys. Res., 88C, (1983) 8543.

4.51 S. R. Bosco, D. F. Nava, W. D. Brobst, and L. J. Stief, J. Chem. Phys., 81 (1984) 3505.

4.52 G. Hancock, W. Lange, M. Lenzi and K. H. Welge, Chem. Phys. Lett., 33 (1975) 168.

4.53 O. M. Sarkisov, S. G. Cheskis and E. A. Sviridenkov, Izv. Akad. Nauk SSSR, Ser. Khim., 27 (1978) 2612.

Chapter 5:

5.0 A. R. Whyte and L. F. Phillips, J. Phys. Chem., 88 (1984) 5670.

5.1 L. J. Stief, W. D. Brobst, D. F. Nava, R. P. Borkowski and J. V. Michael, J. Chem. Soc. Faraday Trans. 2, 78 (1982) 1391.

5.2 H. Kurasawa and R. Lesclaux, Chem. Phys. Lett., 66 (1979) 602.

5.3 J. A. Miller, M. C. Branch and R. J. Kee, Combustion and Flame, 43 (1981) 81.

5.4 C. J. Casewit and W. A. Goddard III, J. Am. Chem. Soc., 102 (1980) 4057.

5.5 A. Hofzumahaus and F. Stuhl, J. Chem Phys., 82 (1985) 5519.

5.6 S. T. Gibson, J. P. Greene and J. Berkowitz, J. Chem. Phys., 83 (1985) 4319.

5.7 L. A. Curtiss, D. L. Drapcho and J. A. Pople, Chem. Phys. Lett., 103 (1984) 437.

5.8 R. A. Back and D. R. Salahub, Can. J. Chem., 45 (1967) 851.

5.9 W. E. Kaskan and D. E. Hughes, Combustion and Flame, 20 (1973) 381.

5.10 P. J. D. Butler and L. F. Phillips, J. Phys. Chem., 87 (1983) 183.

5.11 M. Suto and L. C. Lee, J. Chem. Phys., 78 (1983) 4515.

5.12 H. Shinohara, J. Chem. Phys., 79 (1983) 1732.

5.13 S. Coda and R. A. Back, Can. J. Chem., 55 (1977) 1380.

5.14 R. D. Kenner, F. Rohrer and F. Stuhl, Chem. Phys. Lett., 116 (1985) 374.

5.15 M. J. McEwan and L. F. Phillips, "Chemistry of the Atmosphere", Edward Arnold, London, 1975, p. 26.

5.16 V. M. Donnelly, A. P. Baronavski and J. R. McDonald, Chem. Phys., 43 (1979) 271.

5.17 R. J. Donovan, in "Gas Kinetics and Energy Transfer", Vol. 4, ed. P. G. Ashmore and R. J. Donovan (Specialist Periodical Reports), The Royal Society of Chemistry, London, 1981, p. 117.

5.18 H. Okabe,"Photochemistry of Small Molecules", John Wiley, New York, 1978, pp. 269 -272.

5.19 G. Herzberg, " Molecular Spectra and Molecular Structure", Vol. 3, Electronic Spectra and Electronic Structure of Polyatomic Molecules, van Nostrand Reinhold, New York, 1966.

5.20 K. Dressler and D. A. Ramsey, Phil. Trans. Roy. Soc., A 251 (1959) 553.

5.21 V. M. Donnelly, A. P. Baronavski and J. R. McDonald, Chem. Phys., 43 (1979) 283.

5.22 J. A. Silver and C. E. Kolb, J. Phys. Chem., 86 (1982) 3240.

5.23 P.A. Andresen, A. Jacobs, C. Kleinermanns and J. Wolfrum, 19th Symp. (Int.) Combust., 1982, p. 11.

5.24 R. K. Lyon, Int. J. Chem. Kin., 8 (1976) 315.

5.25 R. K. Lyon and D. Benn, 17th Symp. (Int.) Combust., 1979, p. 601.

5.26 M. Gehring, K. Hoyermann, H. Schacke and J. Wolfrum, 14th Symp. (Int.) Combust., 1972, p. 99.

5.27 J. L. Hall, D. Zeitz, J. W. Stephens, J. V. V. Kaspar, G. P. Glass, R. F. Curl and F. K. Tittel, J. Phys. Chem., 90 (1986) 2501.

5.28 M. A. Kimball-Lynne and R. K. Hanson, Combustion and Flame, 64 (1986) 337.

5.29 C. F. Melius and J. S. Binkley, 20th Symp. (Int.) Combust., 1984, p. 575.

Chapter 6:

6.0 J. A. Harrison, A. R. Whyte and L.F. Phillips,Chem. Phys. Lett., 129 (1986) 346.

6.1 A. G. Gaydon, "The Spectroscopy of Flames", Chapman and Hall, London, 1957.

6.2 A. G. Gaydon and H. G. Wolfhard, "Flames: Their Structure, Radiation and Temperature", 3rd ed., Chapman and Hall, London, 1970.

6.3 W. E. Kaskan and D. E. Hughes, Combustion and Flame, 20 (1973) 381.

6.4 S. T. Gibson, J. P. Greene and J. Berkowitz, J. Chem. Phys., 83 (1985) 4319.

6.5 J. A. Miller, M. C. Branch and R. J. Kee, Combustion and Flame, 43 (1981) 81.

6.6 M. A. Kimball-Lynne and R. K. Hanson, Combustion and Flame, 64 (1986) 337.

6.7 R. A. Back and D. R. Salahub, Can. J. Chem., 45 (1967) 851.

6.8 A. N. Wright and C. A. Winkler, "Active Nitrogen", Academic Press, New York, 1968, pp. 427 - 432.

6.9 D. R. Safrany and W. Jaster, J. Phys. Chem., 72 (1968) 518.

6.10 Y. L. Yung, M. Allen and J. P. Pinto, Astrophys. J. Suppl., 55 (1984) 465.

6.11 J. C. McConnell, J. Geophys. Res., 78 (1973) 7812.

6.12 H. Okabe,"Photochemistry of Small Molecules", John Wiley, New York, 1978, pp. 269 -272.

6.13 J. W. Cox, H. H. Nelson and J. R. McDonald, Chem. Phys., 96 (1985) 175.

6.14 J. March, "Advanced Organic Chemistry", 3rd. ed., John Wiley, New York, 1985.

6.15 H. Abou-Rachid, C. Pouchan and M. Chaillet, Chem. Phys., 90 (1984) 243.

6.16 R. G. Gilbert, A. R. Whyte and L. F. Phillips, Int. J. Chem. Kin., 18 (1986) 721.

6.17 C. F. Melius and J. S. Binkley, 20th Symp. (Int.) Combust., 1984, p. 575.

6.18 L. J. Stief, W. D. Brobst, D. F. Nava, R. P. Borkowski and J. V. Michael, NASA Technical Memorandum 83928, 1982.

6.19 L. F. Phillips, J. Chem. Soc., Faraday Trans. 2, 83 (1987) 857.

6.20 C. J. Casewit and W. A. Goddard III, J. Am. Chem. Soc., 104 (1982) 3280.

6.21 J. A. Harrison, A. R. Whyte and R. G. A. R. Maclagan, Chem. Phys. Lett., 130 (1986) 98.

6.22 J. L. Hall, D. Zeitz, J. W. Stephens, J. V. V. Kaspar, G. P. Glass, R. F. Curl and F. K. Tittel, J. Phys. Chem., 90 (1986) 2501.

6.23 D. W. Scott, G. D. Oliver, M. E. Gross, W. N. Hubbard and H. M. Huffman, J. Am. Chem. Soc., 71 (1949) 2293.

6.24 C. Willis, R. A. Back and J. G. Purdon, Int. J. Chem. Kin., 9 (1977) 787.

6.25 I. Hansen, K. Hoinghaus, C. Zetzsch and F. Stuhl, Chem. Phys. Lett., 42 (1976) 370.

6.26 S. Gordon, W. Mulac and P. Nangia, J. Phys. Chem., 75 (1971) 2087.

6.27 P.A. Andresen, A. Jacobs, C. Kleinermanns and J. Wolfrum, 19th Symp. (Int.) Combust., 1982, p. 11.

6.28 J. A. Silver and C. E. Kolb, J. Phys. Chem., 86 (1982) 3240.

6.29 J. N. Mulvihill and L. F. Phillips, Chem. Phys. Lett., 35 (1975) 327.

6.30 A. R. Whyte and L. F. Phillips, J. Phys. Chem., 88 (1984) 5670.

6.31 CODATA Task Group on Chemical Kinetics, D. L. Baulch, R. A. Cox, R. F. Hampson Jr., J. A. Kerr, J. Troe and R. T. Watson, J. Phys. Chem. Ref. Data, 13 (1984) 1259.

6.32 W. Hack, H. Schacke, M. Schröter and H. G. Wagner, 17th Symp. (Int.) Combust., 1979, p. 505.

6.33 J. A. Harrison, A. R. Whyte and R. G. A. R. Maclagan, to be published.

6.34 V. H. Dibeler, J. L. Franklin and R. M. Reese, J. Am. Chem. Soc., 81 (1959) 68.

6.35 C. Zetzsch and I. Hansen, Ber. Bunsenges. Phys. Chem., 82 (1978) 830.

6.36 W. Hack, H. Kurzke and H. G. Wagner, J. Chem. Soc., Faraday Trans. 2, 81 (1985) 949.

6.37 P. B. Pagsberg, J. Eriksen and H. C. Christensen, J. Phys. Chem., 83 (1979) p. 582.

6.38 C. Zetzsch and F. Stuhl, Ber. Bunsenges., Phys. Chem., 85 (1981) 564.

6.39 G. M. Meaburn and S. Gordon, J. Phys. Chem., 72 (1968) 1592.

6.40 M. Clerc, M. Schmidt, J. Hagege-Temman and J. Belloni, J. Phys. Chem., 75 (1971) 2908.

Chapter 7:

7.0 a J. A. Harrison, R. G. A. R. Maclagan and A. R. Whyte, Chem. Phys. Lett., 130 (1986) 98.

7.0 b J. A. Harrison, R. G. A. R. Maclagan and A. R. Whyte, J. Phys. Chem., 91 (1987) 6683.

7.1 J. C. McConnell, J. Geophys. Res., 78 (1973) 7812.

7.2 F. Stuhl, J. Chem. Phys., 59 (1973) 635.

7.3 R. K. Lyon, Int. J. Chem. Kin., 8 (1976) 315.

7.4 R. K. Lyon and D. Benn, 17th Symp. (Int.) Combust., 1979, p. 601.

7.5 I. W. M. Smith, "Kinetics and Dynamics of Elementary Gas Reactions, Butterworths, London, 1980.

7.6 H. S. Johnston, "Gas Phase Reaction Rate Theory", Ronald, New York, 1966.

7.7 P. J. Robinson and K. A. Holbrook, " Unimolecular Reactions", Wiley - Interscience, London, 1972.

7.8 C. H. Bamford, Trans. Faraday Soc., 35 (1939) 568.

7.9 A. Serewicz and W. A. Noyes Jr., J. Phys. Chem., 63 (1959) 843.

7.10 R. Srinivasan, J. Phys. Chem., 64 (1960) 6796.

7.11 R. K. M. Jayanti, M. Simonaitis and J. Heicklen, J. Phys. Chem., 80 (1976) 433.

7.12 C. P. Fenimore and G. W. Jones, J. Phys. Chem., 65 (1961) 298.

7.13 M. Gehring, K. Hoyermann, H. Schacke and J. Wolfrum, 14th Symp. (Int.) Combust., 1972, p. 99.

7.14 L. J. Stief, W. D. Brobst, D. F. Nava, R. P. Borkowski and J. V. Michael, NASA Technical Memorandum 83928, 1982.

7.15 L. A. Curtiss, D. L. Drapcho and J. A. Pople, Chem. Phys., Lett., 103 (1984) 437.

7.16 M. W. Chase Jr., J. L. Curncutt, J. R. Downey Jr., R. A. McDonald, A. N. Syverud and E. A. Valenzuela, JANAF Thermochemical Tables, 1982, Supplement, J. Phys. Chem. Ref. Data, 11 (1982) 695.

7.17 C. J. Casewit and W. A. Goddard III, J. Am. Chem. Soc., 104 (1982) 3280.

7.18 J. A. Miller, M. C. Branch and R. J. Kee, Combustion and Flame, 43 (1981) 81.

7.19 P. D. Adeney, W. J. Bouma, L. Radom and W. R. Rodwell, J. Am. Chem. Soc., 102 (1980) 4069.

7.20 H. Abou-Rachid, C. Pouchan and M. Chaillet, Chem. Phys., 90 (1984) 243.

7.21 S. W. Benson, "Thermochemical Kinetics", 2nd ed., John Wiley, New York, 1976.

7.22 S. W. Benson, Can. J. Chem., 61 (1983) 881.

7.23 P. G. Greenhill and R. G. Gilbert, J. Phys. Chem., 90 (1986) 3104.

7.24 R. G. Gilbert, A. R. Whyte and L. F. Phillips, Int. J. Chem. Kin., 18 (1986) 721.

7.25 R. Patrick, J. R. Barker and D. M. Golden, J. Phys. Chem., 88 (1984) 128.

7.26 C. C. Kircher and S. P. Sander, J. Phys. Chem., 88 (1984) 2082.

7.27 R.G. Gilbert and M. J. McEwan, Aust. J. Chem., 38 (1985) 231.

7.28 D. C. Tardy and B. S. Rabinovitch, Chem. Rev., 77 (1977) 369.

7.29 R. G. Gilbert, Chem Phys. Lett., 96 (1983) 259.

7.30 R. G. Gilbert, Program Package FALLOFF, Quantum Chemistry Program Exchange, 3 (1983) 64.

7.31 T. Beyer and D. F. Swinehart, Comm. Assoc. Comput. Machines, 16 (1973) 379.

7.32 P. C. Haarhof, Mol. Phys., 7 (1963) 101.

7.33 J. Troe, J. Chem. Phys. , 66 (1977) 4758.

7.34 L. F. Phillips, Chem Phys. Lett., 135 (1987) 269.

7.35 A.E. Douglas, Disc. Faraday Soc., 35 (1963) 158.

7.36 J. R. Sodeau, private communication.

7.37 J. A. Miller, C. Parrish and N. J. Brown, J. Phys. Chem., 90 (1986) 3339.

7.38 A. Szabo and N. S. Ostlund, "Modern Quantum Chemistry", Macmillan, New York, 1982.

7.39 I. N. Levine, "Quantum Chemistry", 2nd ed., Allyn and Bacon, Boston, 1974.

7.40 H. Shull and G. G. Hall, Nature, 184 (1959) 1559.

7.41 E. B. Wilson Jr., J. C. Decius and P. C. Cross, "Molecular Vibrations", McGraw Hill, New York, 1955.

7.42 D. A. McQuarrie, "Statistical Mechanics", Harper and Row, New York, 1976.

7.43 R. Ditchfield, W. J. Hehre and J. A. Pople, J. Chem. Phys., 54 (1971) 724.

7.44 W. J. Hehre, R. Ditchfield and J. A. Pople, J. Chem. Phys., 56 (1972) 2257.

7.45 F. W. Bobrowicz and W. A. Goddard III, in "Modern Theoretical Chemistry: Methods of Electronic Structure Theory", Vol. 3, ed. H. F. Schaefer III, Plenum, New York, 1977, p. 79.

7.46 L. Radom, W. J. Hehre and J. A. Pople, J. Chem Soc., A (1971) 2299.

7.47 L. Radom, W. J. Hehre and J. A. Pople, J. Am. Chem Soc., 93 (1971) 289.

7.48 C. Thompson, D. Provan and S. Clark, Int. J. Quant. Chem., Quant. Biol. Symp., 4 (1977) 205.

7.49 T.-K. Ha, M. T. Nguyen and P. Ruelle, J. Mol. Struct., 109 (1984) 339.

7.50 C. F. Melius and J. S. Binkley, 20th Symp. (Int.) Combust., 1984, p. 575.

7.51 J. S. Binkley, M. J. Frisch, D. J. DeFrees, K. Raghavachari, R. A. Whiteside, H. B. Schlegel, E. M. Fluder and J. A. Pople, "GAUSSIAN 82", Carnegie-Mellon University, Pittsburgh, 1983.

7.52 P. C. Hariharan and J. A. Pople, Theor. Chim. Acta, 28 (1973) 213.

7.53 D. J. DeFrees and A. D. McLean, J. Chem. Phys., 82 (1985) 333.

7.54 D. Poppinger, L. Radom and J. A. Pople, J. Am. Chem. Soc., 99 (1977) 7806.

7.55 D. J. DeFrees, B. A. Levi, S. K. Pollack, W. J. Hehre, J. S. Binkley and J. A. Pople, J. Am. Chem. Soc., 101 (1979) 4085.

7.56 U. Kaldor and I. Shavitt, J. Chem. Phys., 45 (1966) 888.

7.57 R. M. Stevens, J. Chem. Phys., 55 (1971) 1725.

7.58 S. M. Glidewell, Spectrochim. Acta A, 33A (1977) 361.

7.59 L. Batt and R.T. Milne, Int. J. Chem. Kin., 5 (1973) 1067.

7.60 J. L. Hall, D. Zeitz, J. W. Stephens, J. V. V. Kaspar, G. P. Glass, R. F. Curl and F. K. Tittel, J. Phys. Chem., 90 (1986) 2501.

7.61 D. A. Dolson, J. Phys. Chem.,90 (1986) 6714.

7.62 M. A. Kimball-Lynne and R. K. Hanson, Combustion and Flame, 64 (1986) 337.

7.63 J. A. Silver and C. E. Kolb, J. Phys. Chem., 86 (1982) 3240.

7.64 P.A. Andresen, A. Jacobs, C. Kleinermanns and J. Wolfrum, 19th Symp. (Int.) Combust., 1982, p. 11.

7.65 A. R. Whyte and L. F. Phillips, J. Phys. Chem., 88 (1984) 5670.

Chapter 8:

8.1 D. R. Stull and H. Prophet, Project Directors, JANAF Thermochemical Tables, 2nd. ed., U. S. Natl. Bur. Stds. Publ. NSRDS-NBS 37, Washington, 1971.

8.2 W. E. Kaskan and D. E. Hughes, Combustion and Flame, 20 (1973) 381.

8.3 J. A. Miller, M. C. Branch and R. J. Kee, Combustion and Flame, 43 (1981) 81.

8.4 M. A. Kimball-Lynne and R. K. Hanson, Combustion and Flame, 64 (1986) 337.

8.5 C. F. Melius and J. S. Binkley, 20th Symp. (Int.) Combust., 1984, p. 575.

8.6 R. G. Gilbert, A. R. Whyte and L. F. Phillips, Int. J. Chem. Kin., 18 (1986) 721.

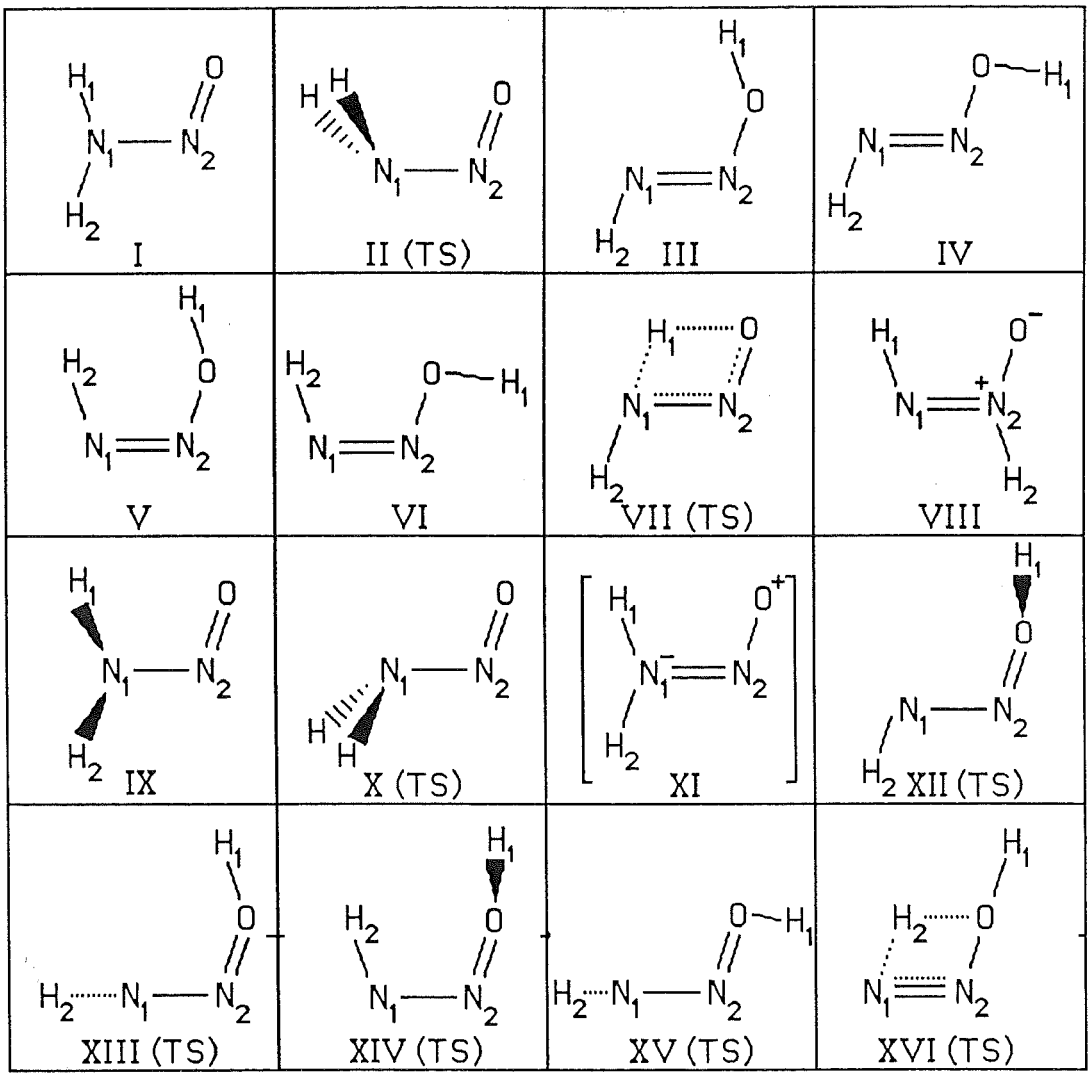

FIGURE 7.1: Structures of N_2H_2O intermediates and transition states (TS).